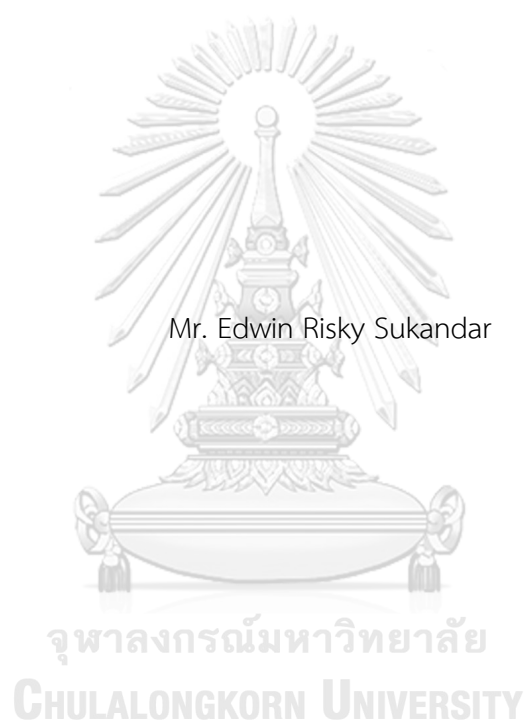


CHEMICAL CONSTITUENTS FROM THE STEMS OF *Garcinia cylindrocarpa* AND THE  
STEM BARK OF *Garcinia picrorhiza* AND *Garcinia tetrandra*



A Dissertation Submitted in Partial Fulfillment of the Requirements  
for the Degree of Doctor of Philosophy in Chemistry

Department of Chemistry

FACULTY OF SCIENCE

Chulalongkorn University

Academic Year 2019

Copyright of Chulalongkorn University

องค์ประกอบทางเคมีจากลำต้น *Garcinia cylindrocarpa* เปลือกลำต้น *Garcinia picrorhiza* และ  
*Garcinia tetrandra*



วิทยานิพนธ์นี้เป็นส่วนหนึ่งของการศึกษาตามหลักสูตรปริญญาวิทยาศาสตรดุษฎีบัณฑิต  
สาขาวิชาเคมี ภาควิชาเคมี  
คณะวิทยาศาสตร์ จุฬาลงกรณ์มหาวิทยาลัย  
ปีการศึกษา 2562  
ลิขสิทธิ์ของจุฬาลงกรณ์มหาวิทยาลัย



เอ็ดวิน ริสกี ชูกานดา : องค์ประกอบทางเคมีจากลำต้น *Garcinia cylindrocarpa*  
เปลือกลำต้น *Garcinia picrorhiza* และ *Garcinia tetrandra*. ( CHEMICAL  
CONSTITUENTS FROM THE STEMS OF *Garcinia cylindrocarpa* AND THE  
STEM BARK OF *Garcinia picrorhiza* AND *Garcinia tetrandra*) อ.ที่ปรึกษาหลัก :  
รศ. ดร.สันติ ทิพยางค์

เพื่อการค้นหาสารออกฤทธิ์ทางชีวภาพชนิดใหม่ จากพืชสกุล *Garcinia* จึงได้เลือกทำการศึกษาองค์ประกอบทางเคมี และฤทธิ์ทางชีวภาพจากพืชสกุล *Garcinia* 3 ชนิด และทำการเก็บตัวอย่างพืชเหล่านี้จากประเทศอินโดนีเซีย สำหรับการแยกองค์ประกอบทางเคมีจากพืชสกุล *Garcinia* ให้บริสุทธิ์ จะต้องอาศัยเทคนิคทางโครมาโทกราฟี และในการพิสูจน์ทราบเอกลักษณ์ทางโครงสร้างของสารบริสุทธิ์ ต้องอาศัยการวิเคราะห์ข้อมูลทางสเปกโทรสโกปี จากนั้นสารบริสุทธิ์ทั้งหมดที่แยกได้จะถูกนำไปทดสอบความเป็นพิษต่อเซลล์มะเร็ง 5 ชนิด (HeLa S3, Hep G2, HT-29, MCF-7 และ KB) ด้วยวิธี MTT assay สาร xanthones ชนิดใหม่ 4 ชนิด ชื่อ cylindroxanthones D–G และสาร biphenyls ชนิดใหม่ 2 ชนิด ชื่อ cylindrobiphenyls A และ B รวมทั้งสารที่เคยมีการรายงานมาแล้วอีก 28 ชนิด ถูกแยกได้จากลำต้น ของ *G. cylindrocarpa* สาร xanthones ชนิดใหม่ 9 ชนิด ชื่อ tetrandraxanthones A–I และสารที่เคยมีการรายงานมาแล้วอีก 22 ชนิด ถูกแยกได้จากเปลือกลำต้น ของ *G. tetrandra* สาร polyprenylated benzoylphloroglucinols (PPBPs) ชนิดใหม่ 8 ชนิด ชื่อ picrorhizones A–H และสารที่เคยมีการรายงานมาแล้วอีก 4 ชนิด ถูกแยกได้จากเปลือกลำต้น ของ *G. picrorhiza* ผลจากการทดสอบพบว่า สาร 9-hydroxycalabaxanthone มีความเป็นพิษต่อเซลล์มะเร็งทั้ง 5 ชนิด โดยมีค่า  $IC_{50}$  ในช่วง 1.6–3.4  $\mu$ M ในขณะที่สาร 2-deprenylrheediaxanthone B และ picrorhizone F มีความเป็นพิษต่อเซลล์มะเร็งทั้ง 4 ชนิด ยกเว้นเซลล์มะเร็ง HT-29 โดยมีค่า  $IC_{50}$  ในช่วง 2.2 ถึง 9.4  $\mu$ M

สาขาวิชา เคมี  
ปีการศึกษา 2562

ลายมือชื่อนิสิต .....  
ลายมือชื่อ อ.ที่ปรึกษาหลัก .....



# # 6072836923 : MAJOR CHEMISTRY

KEYWORD:    *Garcinia*, xanthone, biphenyl, polyprenylated benzoylphloroglucinol,  
                  cytotoxic

Edwin Risky Sukandar : CHEMICAL CONSTITUENTS FROM THE STEMS OF  
*Garcinia cylindrocarpa* AND THE STEM BARK OF *Garcinia picrorhiza* AND  
*Garcinia tetrandra*. Advisor: Assoc. Prof. Dr. SANTI TIP-PYANG

Aiming to discover novel bioactive secondary metabolites from genus *Garcinia*, we performed phytochemical and biological investigations of three *Garcinia* species collected from Indonesia. A series of chromatographic techniques and spectroscopic data analysis were used to isolate and characterize the *Garcinia* phytochemicals. The cytotoxicity of the isolated compounds was evaluated against five human cancer cell lines (HeLa S3, Hep G2, HT-29, MCF-7, and KB) using MTT assay. Four new xanthenes, cylindroxanthenes D–G, and two new biphenyls, cylindrobiphenyls A and B, together with 28 known compounds were successfully isolated from *G. cylindrocarpa* stems. From the stem bark of *G. tetrandra*, nine new xanthenes, tetrandraxanthenes A–I, were identified along with 22 previously described analogues. Eight new polyprenylated benzoylphloroglucinols (PPBPs), picrorhizones A–H, and four known analogues were reported from the stem bark of *G. picrorhiza*. Among the tested compounds, 9-hydroxycalabaxanthone showed significant cytotoxicity against five human cancer cell lines with  $IC_{50}$  values in the range of 1.6–3.4  $\mu\text{M}$ , while 2-deprenylrheediaxanthone B and picrorhizone F were active against four cancer cells, except HT-29, with  $IC_{50}$  values ranging from 2.2 to 9.4  $\mu\text{M}$ .

Field of Study:    Chemistry

Student's Signature .....

Academic Year:   2019

Advisor's Signature .....

## ACKNOWLEDGEMENTS

I am deeply grateful to my advisor, Prof. Santi Tip-pyang, for his advice throughout my Ph.D journey. He gave me the freedom to work whatever I wanted and, at the same time, continuously guided and encouraged me to make this thesis possible. ขอขอบคุณมากครับอาจารย์

My sincerely thank to Prof. Thammarat Aree for his help in single crystal X-ray diffraction and ECD calculation analysis. I also take this opportunity to thank for his big help revising our manuscript. I am indebted to my former advisor, Prof. Taslim Ersam, who inspire me to work in natural product field. Thanks to him for providing me three Garcinia plant extracts. I would like to thank Prof. Rudolf Bauer and his lab member (Huyen, Shanshan, Pia, Eva, Nadine, Volker, Teresa, Timo, Khalil, and others) from University of Graz, Austria for the fruitful discussion and great experience during my research stay (June-December 2019). I truly appreciate Dr. Pongpun Siripong and Ms. Kitiya Rassamee from National Cancer Institute, Thailand for their continuous help in MTT assay.

I am very thankful to Santi&Preecha lab members (P'Kao, P'Moo, Shinta, and Pee) and Indonesian group at CENP Chula (Mbak Devi, Mbak Ibey, Mbak Rita, Mas Ade) for amazing friendship and help. In particular, P'Noom (Dr. Sutin Kaennakam) and P'Yok (Dr. Wisuttaya Worawalai) have always been generous to provide technical support in lab.

I wish to express my gratitude to my Ph.D thesis committees, Prof. Vudhichai Parasuk, Prof. Worawan Bhanthumnavin, Prof. Aroonsiri Shitangkoon, and Prof. Jongkolnee Jongaramruong, for their valuable comments and suggestion. I gratefully acknowledge Chulalongkorn University for The Doctoral Scholarship Program for ASEAN Countries. My projects were funded by The 90th Anniversary of Chulalongkorn University Scholarship and Overseas Research Experience Scholarship Program from the Graduate School.

Finally, I owe deepest thanks to my mom and dad for their unconditional love and care. My dad always support me for everything I have decided for my future and my mom always text and call me almost everyday, especially during this COVID-19 pandemic, just to make sure I am alright. "Our love for you will never end", she says.

Edwin Risky Sukandar

## TABLE OF CONTENTS

	Page
.....	iii
ABSTRACT (THAI).....	iii
.....	iv
ABSTRACT (ENGLISH).....	iv
ACKNOWLEDGEMENTS.....	v
TABLE OF CONTENTS.....	vi
LIST OF FIGURES.....	x
LIST OF TABLES.....	xii
LIST OF ABBREVIATIONS.....	xiv
Chapter I.....	1
Introduction.....	1
1.1. Genus <i>Garcinia</i> : botanical aspect, distribution, and beneficial uses.....	3
1.2. Biosynthesis of <i>Garcinia</i> secondary metabolites.....	4
1.3. Diverse structures of <i>Garcinia</i> secondary metabolites.....	8
1.3.1. Xanthones.....	9
1.3.2. Depsidones.....	14
1.3.3. Biphenyls.....	16
1.3.4. Benzophenones.....	18
1.3.5. Flavonoids and biflavonoids.....	21
1.3.6. Terpenoid quinones.....	25
1.3.7. Phloroglucinols.....	27

1.3.8. Triterpenoids .....	28
1.3.9. Miscellaneous compounds.....	31
1.4. Cytotoxic evaluation of natural products for preliminary anticancer screening	33
1.5. Anti-inflammatory evaluation of natural products on COX enzymes inhibition	34
1.6. Objectives of the research.....	36
Chapter II.....	37
Phytochemical and biological investigation of the stems of <i>Garcinia cylindrocarpa</i> ..	37
2.1. Botanical and chemical aspects of <i>G. cylindrocarpa</i> .....	37
2.2. Experimental.....	38
2.2.1. General Experiment Procedures.....	38
2.2.2. Plant Material.....	39
2.2.3. Extraction and Isolation.....	39
2.2.4. Cytotoxicity Assay.....	41
2.3. Results and discussion.....	42
2.3.1. Structural elucidation of compound GC1 .....	43
2.3.2. Structural elucidation of compound GC2 .....	44
2.3.3. Structural elucidation of compound GC3 .....	45
2.3.4. Structural elucidation of compound GC4 .....	46
2.3.5. Structural elucidation of compound GC5 .....	46
2.3.6. Structural elucidation of compound GC6 .....	47
2.3.7. Cytotoxic activities of the isolated compounds .....	52
Chapter III .....	55
Phytochemical and biological investigation of the stem bark of <i>Garcinia tetrandra</i> ..	55
3.1. Botanical and chemical aspects of <i>G. tetrandra</i> .....	55

3.2. Experimental.....	57
3.2.1. General Experimental Procedures .....	57
3.2.2. Plant Material .....	57
3.2.3. Extraction and Isolation.....	57
3.2.4. Cytotoxicity Assay.....	59
3.3. Results and discussion.....	59
3.3.1. Structural elucidation of compound GT1 .....	60
3.3.2. Structural elucidation of compound GT2 .....	62
3.3.3. Structural elucidation of compound GT3 .....	62
3.3.4. Structural elucidation of compound GT4 .....	63
3.3.5. Structural elucidation of compound GT5 .....	64
3.3.6. Structural elucidation of compound GT6 .....	64
3.3.7. Structural elucidation of compound GT7 .....	65
3.3.8. Structural elucidation of compound GT8 .....	66
3.3.9. Structural elucidation of compound GT9 .....	67
3.3.10. Cytotoxic activities of the isolated compounds.....	74
Chapter IV.....	77
Phytochemical and biological investigation of the stem bark of <i>Garcinia picrorhiza</i> ..	77
4.1. Botanical and chemical aspects of <i>G. picrorhiza</i> .....	77
4.2. Experimental.....	79
4.2.1. General Experimental Procedures .....	79
4.2.2. Plant Material .....	79
4.2.3. Extraction and Isolation.....	79
4.2.4. X-ray crystallography of GP9.....	80

4.2.5. ECD calculation of GP6 and GP9.....	81
4.2.6. Cytotoxicity Assay.....	81
4.2.7. Cyclooxygenase-1 and -2 Inhibition Assays.....	82
4.3. Results and discussion.....	82
4.3.1. Structural elucidation of compound GP1 .....	83
4.3.2. Structural elucidation of compound GP2 and GP3.....	86
4.3.3. Structural elucidation of compound GP4 .....	87
4.3.4. Structural elucidation of compound GP5 .....	88
4.3.5. Structural elucidation of compound GP6 .....	91
4.3.6. Structural elucidation of compound GP7 .....	91
4.3.7. Structural elucidation of compound GP8 .....	92
4.3.8. Determining relative and absolute configurations of GP1–GP9 .....	95
4.3.9. Cytotoxic and anti-inflammatory activities of the isolated compounds ..	99
4.4. Chemotaxonomic study.....	101
Chapter V.....	103
Conclusion .....	103
REFERENCES .....	104
APPENDIX.....	120
VITA.....	211

## LIST OF FIGURES

	Page
Figure 1.1. Natural product-derived compounds as anticancer agents.....	2
Figure 1.2. Biosynthesis of biphenyl, xanthone, and depsidone in plant. ....	6
Figure 1.3. Biosynthesis of polyprenylated benzophenone in plant. ....	7
Figure 1.4. Biosynthesis of isocoumarin, flavonoid, and biflavonoid in plant. ....	8
Figure 1.5. Simple oxygenated and prenylated xanthenes (1.5–1.19) from <i>Garcinia</i> plants. ....	9
Figure 1.6. Xanthenes with extended prenyl units (1.20–1.25) from <i>Garcinia</i> plants. ....	11
Figure 1.7. Rearranged polyprenylated and caged xanthenes (1.26–1.34) from <i>Garcinia</i> plants. ....	12
Figure 1.8. Unusual substituted xanthenes (1.35–1.39) from <i>Garcinia</i> plants. ....	14
Figure 1.9. Depsidones and its derivatives (1.40–1.51) from <i>Garcinia</i> plants. ....	15
Figure 1.10. Biphenyls (1.52–1.67) from <i>Garcinia</i> plants. ....	17
Figure 1.11. Simple benzophenones (1.68–1.73) from <i>Garcinia</i> plants. ....	19
Figure 1.12. Polyprenylated benzophenones (1.74–1.82) from <i>Garcinia</i> plants. ....	20
Figure 1.13. Flavonoids (1.83–1.95) from <i>Garcinia</i> plants. ....	22
Figure 1.14. Flavonoid dimers and trimers (1.96–1.104) from <i>Garcinia</i> plants. ....	24
Figure 1.15. Terpenoid quinone derivatives (1.105–1.113) from <i>Garcinia</i> plants. ....	26
Figure 1.16. Phloroglucinol derivatives (1.114–1.127) from <i>Garcinia</i> plants. ....	28
Figure 1.17. Tetracyclic triterpenoids (1.128–1.138) from <i>Garcinia</i> plants. ....	29
Figure 1.18. Pentacyclic triterpenoids (1.139–1.143) from <i>Garcinia</i> plants. ....	30
Figure 1.19. Miscellaneous compounds (1.144–1.156) from <i>Garcinia</i> plants. ....	32

Figure 1.20. Formazan formation through NADH-catalyzed MTT reduction.....	33
Figure 1.21. Prostaglandins production via arachidonic acid metabolism and a strategy in COX activity inhibition.....	35
Figure 1.22. Reaction between <i>p</i> NPP and alkaline phosphatase enzyme to produce <i>p</i> -nitrophenol.....	36
Figure 2.1. The whole plant, leaves, and fruit of <i>Garcinia cylindrocarpa</i> .....	37
Figure 2.2. Cyliandroxanthones A–C ( <b>2.1–2.3</b> ) from <i>G. cylindrocarpa</i> stem bark.....	38
Figure 2.3. Isolated compounds ( <b>GC1–GC34</b> ) from the stems of <i>G. cylindrocarpa</i> ... ..	48
Figure 2.4. Key COSY and HMBC correlations of <b>GC1–GC6</b> .....	52
Figure 3.1. The whole plant, stem, and stem bark of <i>Garcinia tetrandra</i> .....	55
Figure 3.2. Isolated compounds ( <b>3.1–3.8</b> ) from the stem bark of <i>G. tetrandra</i> .....	56
Figure 3.3. Structures of isolated xanthones ( <b>GT1–GT31</b> ) from <i>G. tetrandra</i> stem bark.....	60
Figure 3.4. Key $^1\text{H} - ^1\text{H}$ COSY (blue line) and HMBC (red arrow) correlations of tetrandraxanthones A–I ( <b>GT1–GT9</b> ).....	73
Figure 4.1. The whole plant, branches, and leaves of <i>Garcinia picrorhiza</i> .....	77
Figure 4.2. Isolated compounds ( <b>4.1–4.6</b> ) from the roots and the stem bark of <i>G. picrorhiza</i> .....	78
Figure 4.3. Benzoylphloroglucinols ( <b>GP1–GP12</b> ) from <i>G. picrorhiza</i> stem bark.....	83
Figure 4.4. Key COSY (blue line) and HMBC (red arrow) correlations of picrorhizones A–H ( <b>GP1–GP8</b> ).....	93
Figure 4.5. Key NOE correlations (blue dashed line) of compounds <b>GP1</b> and <b>GP6</b> . ....	97
Figure 4.6. (a) ORTEP diagram for compound <b>GP9</b> ; (b) Comparison of calculated ( <b>GP9a</b> , <b>GP9a enantiomer</b> , <b>GP6a</b> ) and experimental ( <b>GP1</b> , <b>GP6</b> , <b>GP9</b> ) ECD spectra; (c,d) experimental ECD spectra for <b>GP2–GP8</b> .....	98



## LIST OF TABLES

	Page
Table 2.1. $^1\text{H}$ (400 MHz) and $^{13}\text{C}$ (100 MHz) spectroscopic data of <b>GC1–GC3</b> in acetone- $d_6$ (in ppm) and <b>GC4</b> in $\text{CDCl}_3$ ( $\delta$ in ppm).....	49
Table 2.2. $^1\text{H}$ (400 MHz) and $^{13}\text{C}$ (100 MHz) spectroscopic data of compounds <b>GC5</b> and <b>GC6</b> .....	51
Table 2.3. <i>In vitro</i> cytotoxicity of compounds <b>GC1–GC34</b> .....	53
Table 3.1. $^1\text{H}$ NMR spectroscopic data (400 MHz) of compounds <b>GT1–GT9</b> ( $\delta$ in ppm, $J$ in Hz) .....	68
Table 3.2. $^{13}\text{C}$ NMR spectroscopic data (100 MHz) of compounds <b>GT1–GT9</b> ( $\delta$ in ppm) .....	71
Table 3.3. Cytotoxicity data of compounds <b>GT1–GT31</b> .....	75
Table 4.1. $^1\text{H}$ (400 MHz) and $^{13}\text{C}$ (100 MHz) NMR spectroscopic data of compounds <b>GP1– GP3</b> ( $\delta$ in ppm) .....	85
Table 4.2. $^1\text{H}$ (400 MHz) and $^{13}\text{C}$ (100 MHz) NMR spectroscopic data of compounds <b>GP4</b> and <b>GP5</b> ( $\delta$ in ppm) .....	89
Table 4.3. $^1\text{H}$ (400 MHz) and $^{13}\text{C}$ (100 MHz) NMR spectroscopic data of compounds <b>GP6– GP8</b> ( $\delta$ in ppm) .....	94
Table 4.4. Cytotoxic activity of compounds <b>GP1, GP3, GP5, GP6, and GP8–GP11</b> after 72 h of treatment .....	100
Table 4.5. COX-1 and COX-2 inhibitory activity of compounds <b>GP1–GP11</b> .....	101

## LIST OF ABBREVIATIONS

HR-ESI-MS	High Resolution Electrospray Ionization Mass Spectroscopy
ECD	Electronic Circular Dichroism
$^1\text{H}$ NMR	Proton Nuclear Magnetic Resonance
$^{13}\text{C}$ NMR	Carbon-13 Nuclear Magnetic Resonance
1D-NMR	One-Dimensional Nuclear Magnetic Resonance
2D-NMR	Two-Dimensional Nuclear Magnetic Resonance
COSY	$^1\text{H}$ – $^1\text{H}$ Correlation Spectroscopy
HSQC	Heteronuclear Single Quantum Correlation
HMBC	Heteronuclear Multiple Bond Correlation
NOESY	Nuclear Overhauser Effect Spectroscopy
$m/z$	mass per charge number of ions (Mass Spectroscopy)
$\delta_{\text{H}}$	chemical shift of proton (NMR)
$\delta_{\text{C}}$	chemical shift of carbon (NMR)
$J$	coupling constant (NMR)
s	singlet (NMR)
d	doublet (NMR)
t	triplet (NMR)
m	multiplet (NMR)
brs	broad singlet (NMR)
dd	doublet of doublets (NMR)
tt	triplet of triplets (NMR)
DMSO- $d_6$	deuterated dimethyl sulfoxide

CDCl <sub>3</sub>	deuterated chloroform
Acetone-d <sub>6</sub>	deuterated acetone
MeOH-d <sub>6</sub>	deuterated methanol
calcd.	calculated
m.p	melting point
TLC	Thin Layer Chromatography
MTPA	$\alpha$ -methoxy- $\alpha$ -trifluoromethylphenylacetic acid in Mosher's method
PPBP	polyprenylated benzoylphloroglucinol
iNOS	inducible nitric oxide synthase
COX	cyclooxygenase enzyme
MTT	3-(4,5-dimethylthiazol-2-yl)-2,5-diphenyltetrazolium bromide, a reagent in cytotoxic assay
EC <sub>50</sub>	the molar concentration of an agonist that produces 50% of the maximal possible effect of that agonist
IC <sub>50</sub>	the molar concentration of an antagonist that reduces the response to an agonist by 50%
CC <sub>50</sub>	the concentration of a compound required for the reduction of cell viability by 50%

## Chapter I

### Introduction

Cancer remains one of serious health problems across the world and caused over nine million deaths in 2018. In general, cancer arise from alteration of genes which control cell functions, especially in cell growth and division [1]. As the result, cells with certain genetic changes will divide out of control. These abnormal and malignant cells become invasive by spreading into surrounding tissues and inducing normal cells to form blood vessels for their oxygen and nutrients supply. In many cases, metastasis also occurs where cancer cells are able to travel through blood or lymph vessels to other parts of the body and form other cancerous tumors [2, 3]. Several effective cancer treatments have been developed, including chemotherapy, in which drugs having anticancer properties are used to inhibit growth of cancer cells and its metastasis, restrict cancer invasion, and increase cancer cells death [4]. Recent advance of chemotherapy has been developed by targeting specific enzymes and growth factor receptors involved in carcinogenesis as many previous chemotherapeutic drugs had broad spectrum of cells destruction causing numerous side effects [5].

Natural products play a pivotal role in an attempt to discover potential chemotherapeutic agents and over 60% of current anticancer drugs are bioactive substances originally produced by terrestrial plants, marine invertebrates (e.g. mollusks, sponges, echinoderms, cnidarians, and tunicates), and microorganisms (e.g. bacterial and fungal cultures) [6]. The secondary metabolites are produced in a limited number and used by specific living organisms as response to protect and adapt in various environmental conditions. Their roles in nature provide an insight to explore those bioactive compounds for human health benefit with the major use in cancer therapy [7]. Due to relatively ease to access in sample collection and

preparation, medicinal plants or herbs are frequently targeted to find potential anticancer candidates and a million of phytochemicals has been hitherto isolated and pharmacologically screened [8].

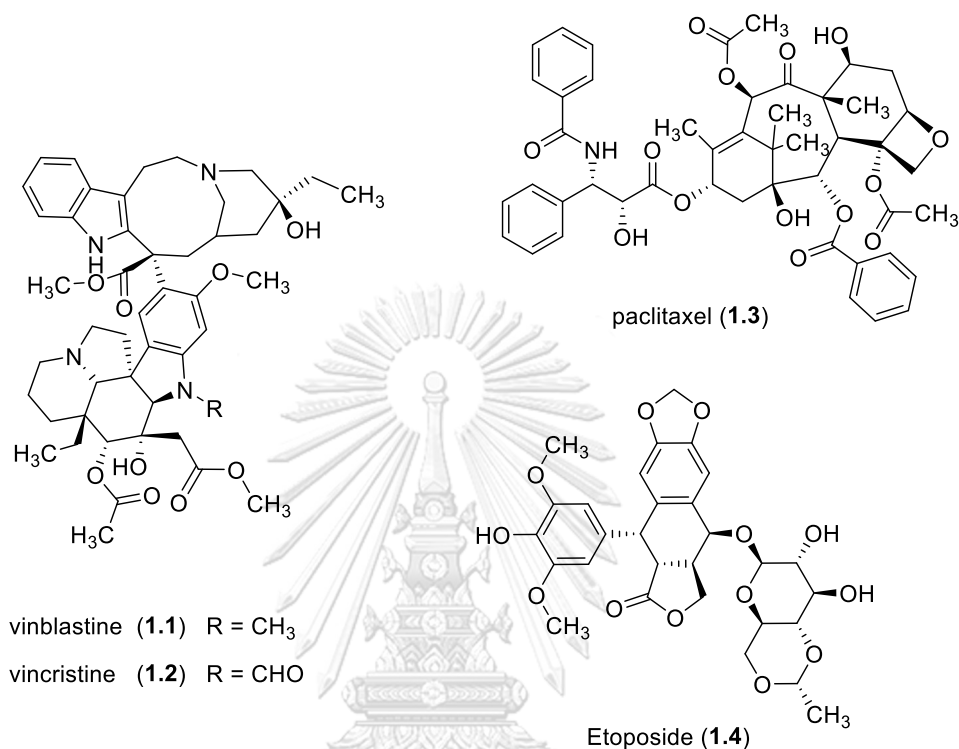


Figure 1.1. Natural product-derived compounds as anticancer agents.

Vinblastine (1.1) and vincristine (1.2), two vinca alkaloids originally isolated from *Catharanthus roseus* G. Don. (common name: Madagascar periwinkle), were the first introduced anticancer drugs prescribed to combat childhood leukemia, Hodgkin's lymphoma, and testicular teratoma. An extensive research revealed that both compounds were capable to destabilize microtubules and obstruct cancer cells during metaphase stage causing the cells apoptosis [9, 10]. Later, the discovery of paclitaxel (Taxol<sup>®</sup>) (1.3), a bioactive constituent isolated from the bark of *Taxus brevifolia* Nutt. (common name: Pacific yew), became one of great breakthroughs in cancer research area. This clinically effective chemotherapeutic drug was found to be active against a variety of human cancers, including ovarian, non-small cell lung,

breast, and Kaposi's sarcoma by promoting tubulin heterodimers polymerization and suppressing dynamic changes in microtubules leading to mitotic obstruction [9]. Several structural modifications of the above natural product-based anticancer agents were also carried out to overcome clinical trials limitation, such as low solubility which affect drug delivery process, high toxicity causing several side effects, and drug resistance associated with the current drugs. Etoposide (**1.4**), a synthetic analog of podophyllotoxin isolated *Podophyllum peltatum* L. (common name: American mandrake/mayapple), was approved for ovarian, lymphoma, testicular teratoma, small-cell lung cancers treatment. The latter anticancer agent was found to have different mode of action to kill cancer cells via topoisomerase II inhibition and give higher efficacy than its precursor [7, 9].

The above-mentioned data illustrate a potency of natural products as chemotherapeutic agents and exploration of bioactive secondary metabolites, especially from medicinal plants, is highly recommended to be done. This research will focus on the phytochemical and biological investigation *Garcinia* plants which have been reported previously to contain many pharmacologically active substances.

### 1.1. Genus *Garcinia*: botanical aspect, distribution, and beneficial uses

The genus *Garcinia*, one of the largest genera to the family Clusiaceae, is widely distributed in tropical rain forests of Southeast Asia, South America, and West and Central Africa. This genus is pantropical and comprise high level of species diversity with more than 250 species of evergreen, lactiferous, dioecious, and small shrubs to medium-sized trees [11, 12]. There are approximately 77 species of this genus distributed throughout Indonesia, with the main population in Sumatera, Kalimantan, and Papua Islands [13]. In its natural habitat, *Garcinia* species can be found along rivers, swamps, and streams as wild plants or cultivated in garden and widely grow on sandy, clay, chalk, silt, peat, and loam soils [14, 15].

Some *Garcinia* plants have been consumed traditionally by local people as Indonesian dishes and herbal medicines to prevent and treat several health problems. The fruits of *G. mangostana* (local name: manggis), well known as mangosteen, have mixed sweet and sour taste and become one of potential commodities in market. The pericarps of mangosteen are extracted for additive in herbal soap and food [12, 15]. *G. atroviridis* fruits (local name: Gelugur) are edible with sour taste and used for food spices after drying and grinding process and its leaves are prepared for food salad. In medical aspect, the infusion of the leaves of *G. atroviridis* and *G. parvifolia* (local name: Kandis) is consumed for stomach pain remedy associated with pregnancy. The latex of *G. mangostana* is topically applied for oral ulcer treatment, while the decoction of its inner bark is consumed to treat dysentery [15, 16]. The pericarps of *G. mangostana* are prepared as a gargling solution for oral hygiene protection [17]. Moreover, the pericarps of *G. mangostana* and *G. cambogia* are formulated as a herbal supplement for weight loss and natural antioxidant [18].

## 1.2. Biosynthesis of *Garcinia* secondary metabolites

Phytochemical investigation of the genus *Garcinia* resulted in the isolation of structurally diverse secondary metabolites, especially phenolic compounds, such as xanthenes, biphenyls, polyprenylated benzoylphloroglucinols, isocoumarins, depsidones, and biflavonoids. Biosynthetically, amino acids L-phenylalanine or L-tyrosine, derived from shikimate pathway, act as a  $C_6C_3$  building block and precursor for the phenolic metabolites. Plant employs phenylalanine ammonia lyase (PAL) enzyme to eliminate ammonia of the amino acids and produce cinnamic acid (Figure 1.2). The hydration of cinnamic acid via coenzyme A ester substrate (cinnamoyl-CoA) and oxidation of the hydrated intermediate generate a  $\beta$ -ketoester and subsequently lose acetyl-CoA through reverse Claisen rearrangement to introduce a CoA-ester of

benzoic acid. The chain elongation of benzoyl-CoA with three malonyl-CoA derived from acetate pathway generates a shikimate-acetate intermediate I, which is involved later in an intramolecular cyclization to yield several *Garcinia* phenolics [19]. Claisen condensation of intermediate I catalyzed by benzophenone synthase (BPS), a type III polyketide synthase, afford a benzophenone, 2,4,6-trihydroxybenzophenone. This metabolite is oxidized by benzophenone 3'-hydroxylase (B3'H) to give 2,4,6,3'-tetrahydroxybenzophenone and converted to xanthenes by 1,3,5-/1,3,7-trihydroxyxanthone synthases (TXSs) via intramolecular oxidative C-O coupling reaction [20]. Further oxidation of xanthenes via Baeyer-Villiger rearrangement by specific enzymes gives a depsidone, which is rarely found in higher plants. In general, depsidones are well known as lichen secondary metabolites derived polyketide biosynthesis pathway [21]. A biphenyl-type compound, 3,5-dihydroxybiphenyl, is constructed through aldol condensation and enolization of the intermediate I by biphenyl synthase (BIS) [22].

As depicted in Figure 1.3, a simple benzophenone can be converted to more complex structure, so-called polyprenylated benzophenone (PPB)/benzoylphloroglucinol (PPBP), via polyprenylation which utilize plant enzymes and DMAPP (dimethylallyl pyrophosphate), a C<sub>5</sub>-building block from mevalonate pathway [23]. Multiple prenylation of benzophenone generate two type-D PPB intermediates and different attacking position at phloroglucinol A-ring results various type of PPBs. A C-5 enol attack to the double bond of prenyl unit at C-1 generates type-C PPB, while C-1 and C-3 attacking position to a prenyl moiety at C-5 introduce type-A and -B PPBs, respectively. Such enzyme-catalyzed modifications afford various PPBs with a high degree of complexity [24].



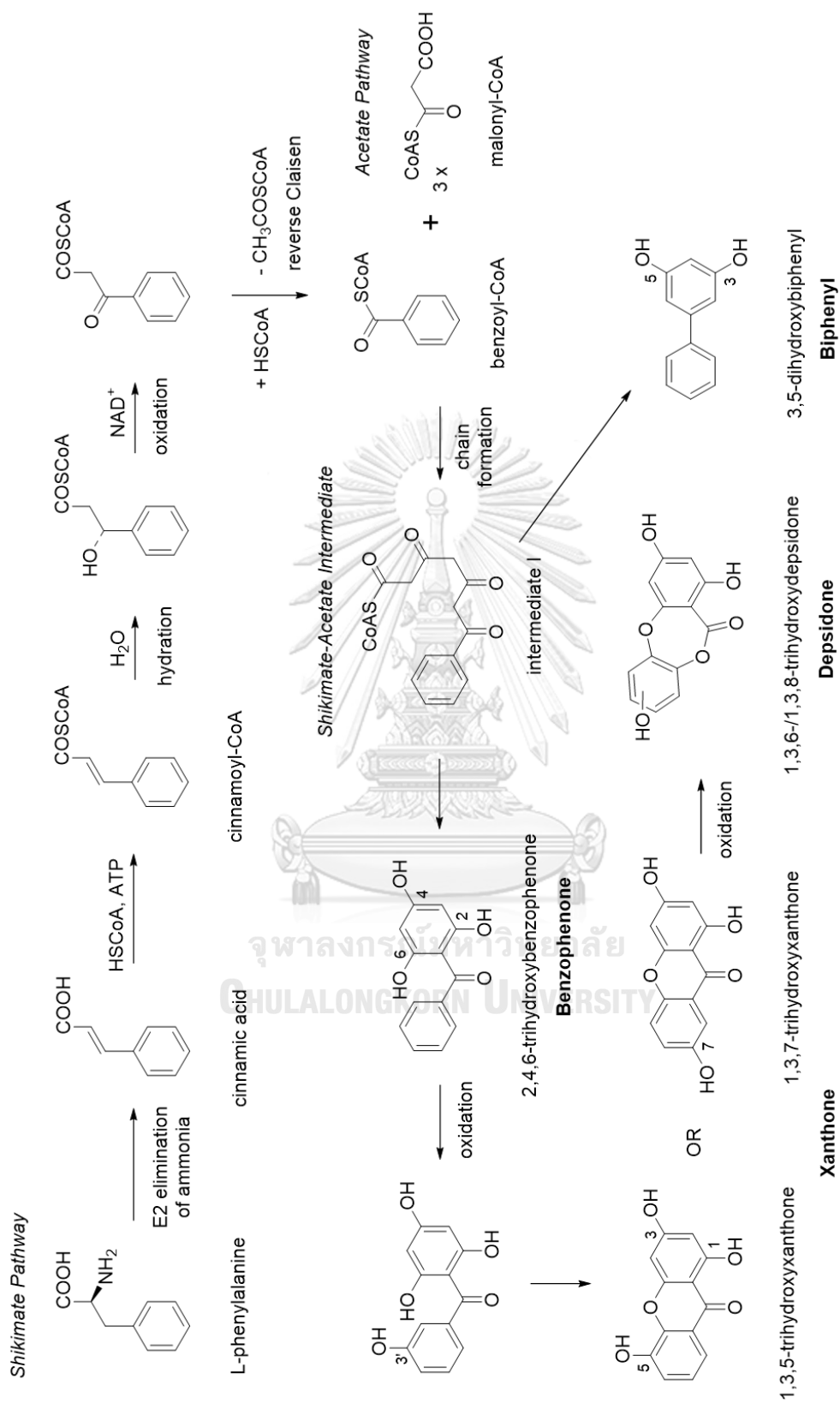


Figure 1.2. Biosynthesis of biphenyl, xanthone, and depsidone in plant.

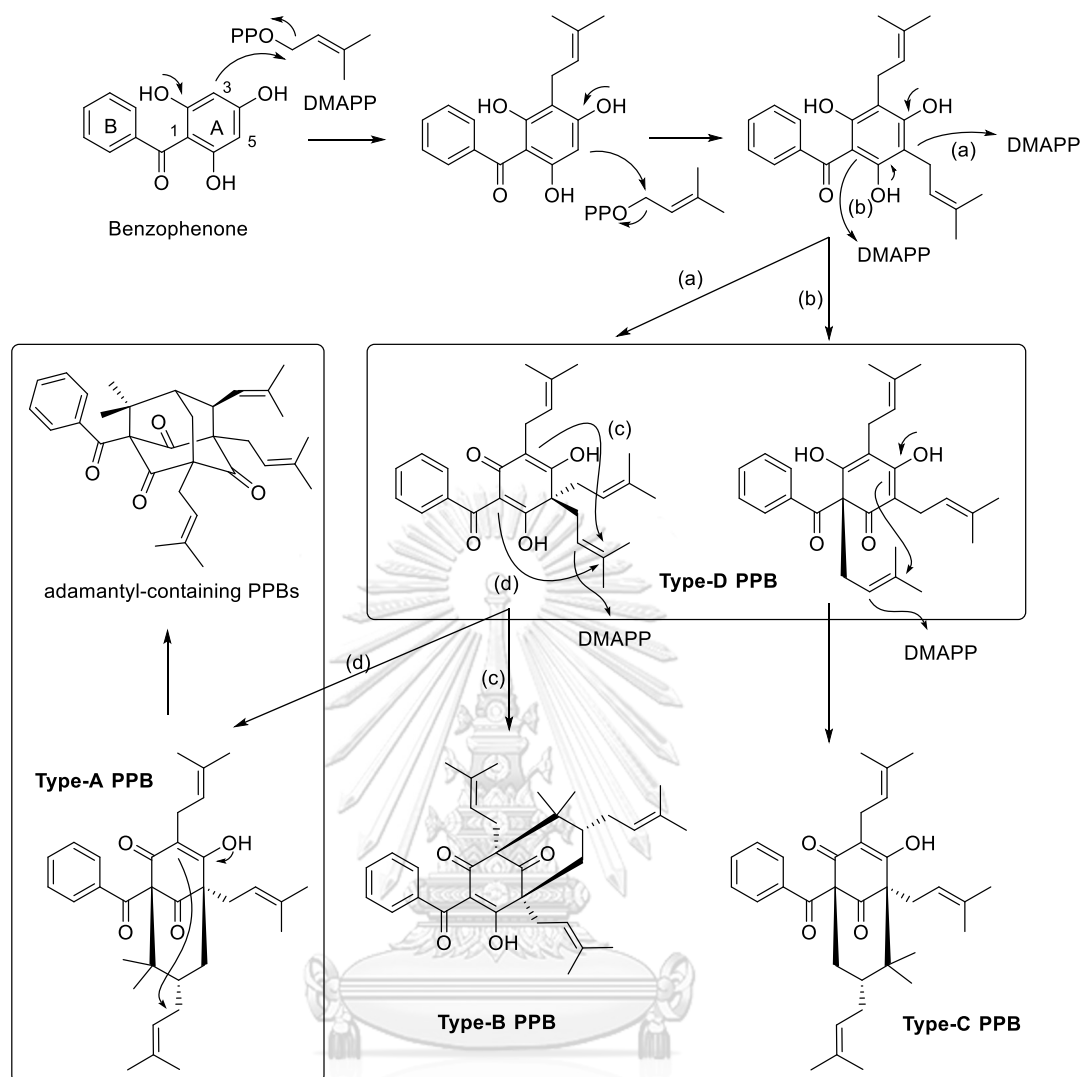


Figure 1.3. Biosynthesis of polyprenylated benzophenone in plant.

The biosynthesis of flavonoid and isocoumarin lie to the precursor CoA-ester of cinnamic acid with three malonyl-CoA which give intermediate II with chain extension, as described in Figure 1.4. Later, this intermediate is cyclized via Claisen condensation, followed by enolization to form naringenin, a flavonoid-type secondary metabolite. Intermolecular oxidative C-C and C-O coupling reaction initiated by specific plant enzymes (e.g. peroxidase) produce biflavonoid structures [19]. The aldol condensation and enolization of intermediate II give intermediate III which is subsequently hydrated and lactonized to generate an isocoumarin [25].

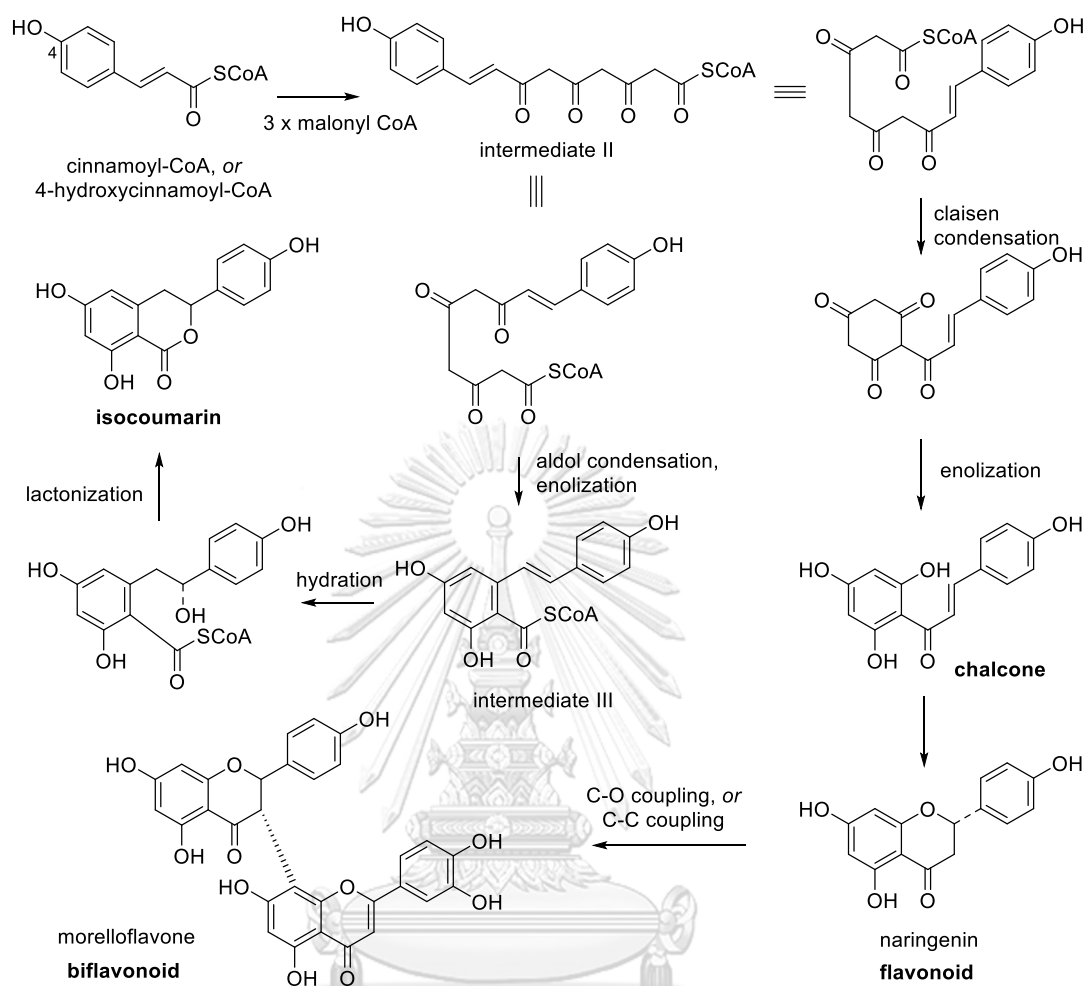


Figure 1.4. Biosynthesis of isocoumarin, flavonoid, and biflavonoid in plant.

### 1.3. Diverse structures of *Garcinia* secondary metabolites

In this section, several secondary metabolites which have been reported previously are briefly reviewed based on the core structures and substituent modifications. The biological and pharmacological results of the isolated compounds are also described and restricted to those having potent activities, particularly in anticancer study. This is due to the fact that *Garcinia* phytochemicals, particularly xanthone and benzophenone derivatives, are well recognized to exhibit significant effects on cancer growth inhibition, such as  $\alpha$ -mangostin (1.8), gambogic acid (1.32),

and garcinol (**1.76**), wherein detailed mechanism of action of those compounds against cancer cells are described below.

### 1.3.1. Xanthenes

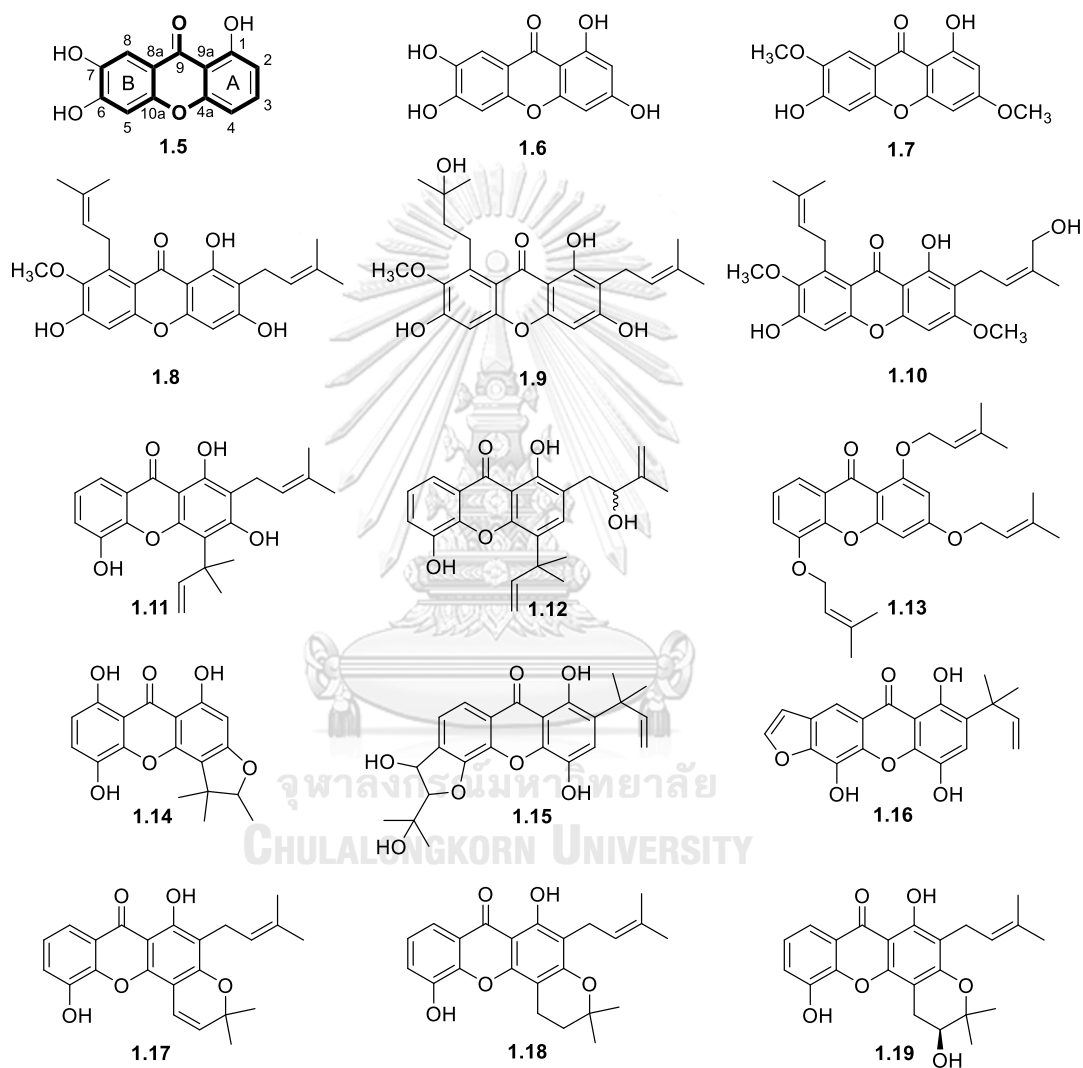


Figure 1.5. Simple oxygenated and prenylated xanthenes (**1.5–1.19**) from *Garcinia* plants.

Xanthone is an oxygenated heterocyclic compound bearing dibenzo- $\gamma$ -pyrone skeleton and derived biosynthetically from shikimate-acetate pathway, as described

in Figure 1.2. Xanthone derivatives can be found in higher plants, microorganisms, marine sources, and lichens, while they are isolated as a chemotaxonomic marker and major component of the genus *Garcinia* with high chemical diversity [26].

Most common xanthenes found in *Garcinia* plants bear oxygenated functional groups such as hydroxy and methoxy substituents, as well as prenyl and geranyl side chains (Figure 1.5). For example, three tri- and tetra-oxygenated xanthenes, 1,3,6,7-tetrahydroxyxanthone (**1.5**), 1,6-dihydroxy-7-methoxyxanthone (**1.6**), and 1,6-dihydroxy-3,7-dimethoxyxanthone (**1.7**), were obtained from the leaves and twigs of *G. multiflora* [27]. Another phytochemical investigation led to the isolation of prenylated xanthone  $\alpha$ -mangostin (**1.8**) and its analogues, garcinone D (**1.9**) and fuscaxanthone D (**1.10**), with hydrated and hydroxylated prenyl side chains from the roots of *G. cowa* and all compounds showed moderate cytotoxicity against KB and HeLa cancer cells with  $IC_{50}$  values ranging from 11.7 to 33.5  $\mu$ M. Moreover,  $\alpha$ -mangostin, originally isolated from the pericarps of mangosteen (*G. mangostana*), had a cytostatic effect on colon cancer cells by inducing G1 cell cycle arrest and promote the suppression of breast tumor growth *in vivo* [28]. Xanthenes with modified prenyl moieties were found in the leaves of *G. bracteata* and *G. polyantha*, such as allaxanthone A (**1.11**) and bracteaxanthone VIII (**1.12**) bearing a dimethylallyl unit and *O*-prenylated polyanxanthone A (**1.13**) [29, 30].

Three furanoxanthenes were obtained from the roots of *G. fusca* and the stem bark of *G. dulcis*, including garbogiol (**1.14**), garciniaxanthone D (**1.15**), and subelliptenone C (**1.16**), whereas three pyranoxanthenes, ananixanthone (**1.17**) and nigrolineaxanthenes Q and X (**1.18** and **1.19**), were isolated from the leaves of *G. nigrolineata* [31-33]. The five- and six-membered ring moieties of the six xanthenes are formed from cyclization of prenyl unit and its adjacent hydroxy group (Figure 1.5). Compound **1.14** was found to inhibit  $\alpha$ -glucosidase enzyme with  $IC_{50}$  value of 21.2

$\mu\text{M}$ , while **1.18** exhibited antibacterial activity against *Micrococcus luteus* with MIC value of  $8 \mu\text{g}/\text{mL}$ .

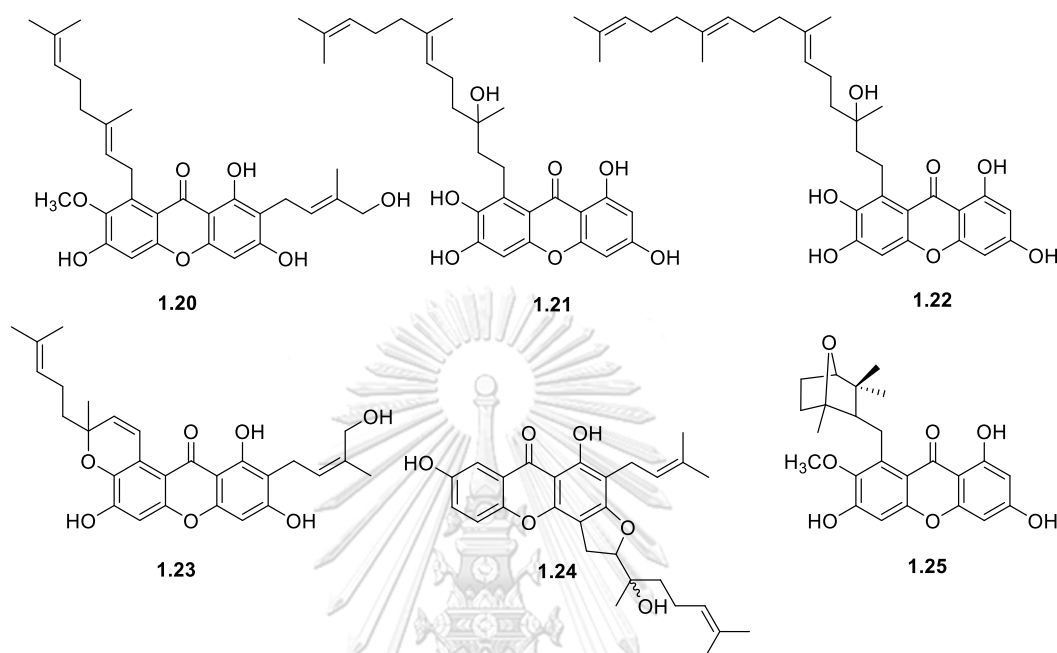


Figure 1.6. Xanthones with extended prenyl units (**1.20–1.25**) from *Garcinia* plants.

The extension of  $\text{C}_5$ -prenyl side chain on a xanthone skeleton was found in the extracts of *Garcinia* species, such as cowanol (**1.20**) with a  $\text{C}_{10}$ -geranyl substituent, garciniacowone H (**1.21**) bearing a  $\text{C}_{15}$ -farnesyl unit, and garciniacowone I (**1.22**) substituted by a  $\text{C}_{20}$ -geranylgeranyl side chain (Figure 1.6) [34]. The three phytochemicals were obtained from fractionation of the acetone extract of *G. cowa* leaves and they demonstrated NO (nitric oxide) production inhibition in LPS-induced RAW 263.7 macrophage cells and  $\alpha$ -glucosidase inhibition with  $\text{IC}_{50}$  values in the range of  $5.8\text{--}13.4 \mu\text{M}$  and  $15.4\text{--}28.7 \mu\text{M}$ , respectively. Modification of a geranyl functionality was observed in kaennacowanol B (**1.23**) and fuscaxanthone J (**1.24**) isolated from *G. cowa* and *G. fusca* roots via intramolecular cyclization to give furan and pyran rings [31, 35], while a metabolite with an uncommon 7-oxo-[2.2.1]-bicyclic

system, parvixanthone I (**1.25**), was obtained from the bark of *G. parvifolia* (Figure 1.6) [36].

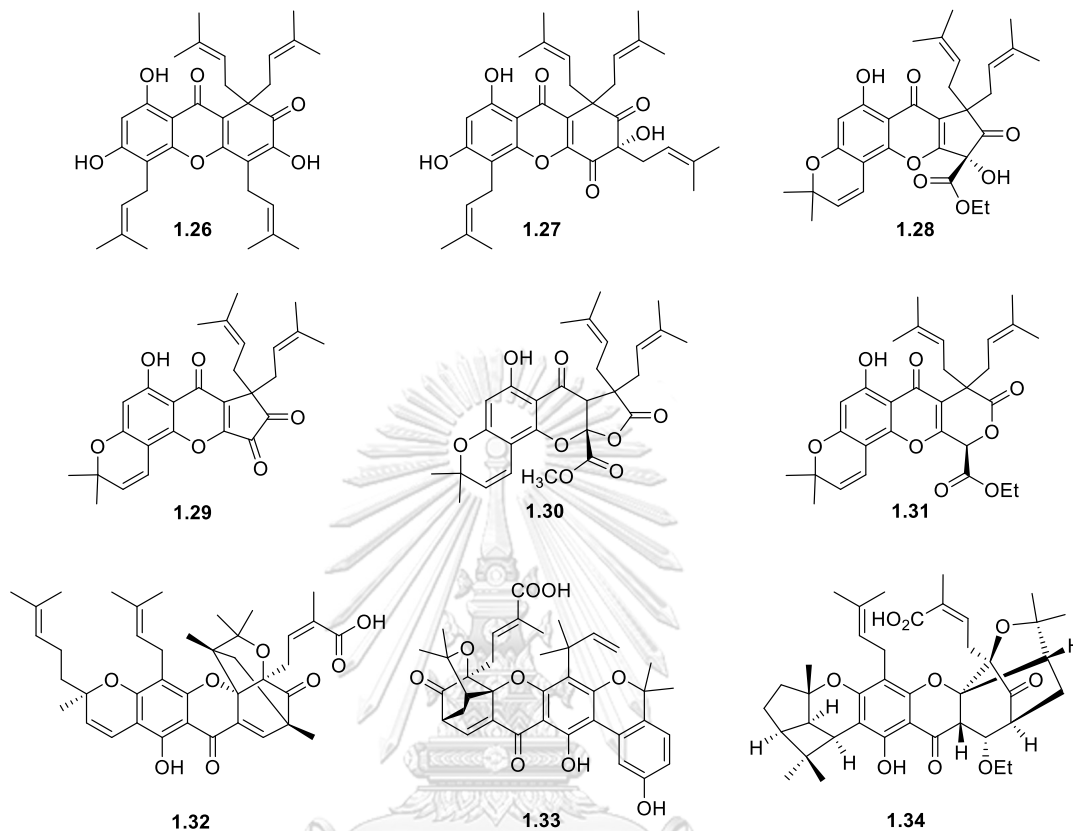


Figure 1.7. Rearranged polyprenylated and caged xanthenes (**1.26–1.34**) from *Garcinia* plants.

Extensive phytochemical studies on the leaves and twigs of *G. oligantha* resulted in discovery of unique xanthenes, including dihydro and tetrahydroxanthenes garoliganthin I (**1.26**) and garoliganthin H (**1.27**), as well as (–)-garoliganthin F (**1.28**), (–)-garoliganthin G (**1.29**), (+)-oliganthin T (**1.30**), and (–)-garoliganthin B (**1.31**) featuring structurally rearranged xanthenone cores (Figure 1.7). The formation of such unprecedented scaffolds in the ring A of **1.28–1.31** was biosynthetically proposed by pinacol rearrangement to form **1.28** and **1.29** and an oxidative ring cleavage followed by a series of enzyme-catalyzed oxidation and hydration reactions and intramolecular cyclization to achieve **1.30** and **1.31** [37, 38].

Gambogic acid (**1.32**), gaudichaudiic acid (**1.33**), and epi-gambogic acid C (**1.34**), originally exist in *G. hanburyi* and *G. gaudichaudii*, represent another class of complex modified xanthenes with 4-oxo-tricyclo[4.3.1.0<sup>3,7</sup>]dec-8-en-2-one ring system containing a highly substituted tetrahydrofuran moiety, so-called caged xanthenes [28, 39, 40]. Additionally, compound **1.34** also bears a bridged tricyclic ring moiety which is derived from an unusual cyclization of geranyl functionality at the xanthone skeleton (Figure 1.7). Cytotoxic evaluation showed that **1.33** was active against P388/DOC and Messa cell lines with IC<sub>50</sub> values of 3.4 and 3.8  $\mu\text{g/mL}$ . Moreover, pharmacological study revealed that **1.32** was capable to induce apoptosis, reverse multidrug resistance of cancer cells, inhibit cell proliferation, and anti-angiogenic activities and it has been completed a phase IIa clinical trial in China for patients with lung, colon, and renal cancers.

A xanthone possessing an unusual  $\alpha,\beta$ -unsaturated- $\gamma$ -lactone unit, garcinexanthone F (**1.35**), was obtained from *G. xanthochymus* bark with its scavenging potential against DPPH and OH radical at IC<sub>50</sub> values of 22.3 and 1.2  $\mu\text{M}$  [41]. Garciduol A (**1.36**), isolated from the stem bark of *G. dulcis*, was found to be a trioxygenated xanthone connected with 2,4,6-trihydroxybenzophenone [33]. The isolation of schomburgkixanthone (**1.37**) from *G. schomburgkiana* twigs and garmoxanthone (**1.38**) and garcinoxanthone B (**1.39**) from the bark and pericarps of *G. mangostana* revealed the existence of bixanthone structures, the coupled xanthenes via C—C or C—O bond formation (Figure 1.8) [42-44]. Compound **1.38** significantly inhibited the growth of MRSA ATCC 43300 and CGMCC 1.12409 strains with MIC values of 3.9  $\mu\text{g/mL}$  and was moderately active against *Vibrio* strains with MIC values in the range of 15.6–31.2  $\mu\text{g/mL}$ , whereas **1.39** showed NO production inhibition at IC<sub>50</sub> value of 11.3  $\mu\text{M}$  and suppressed *iNOS* expression in a concentration-dependent curve.



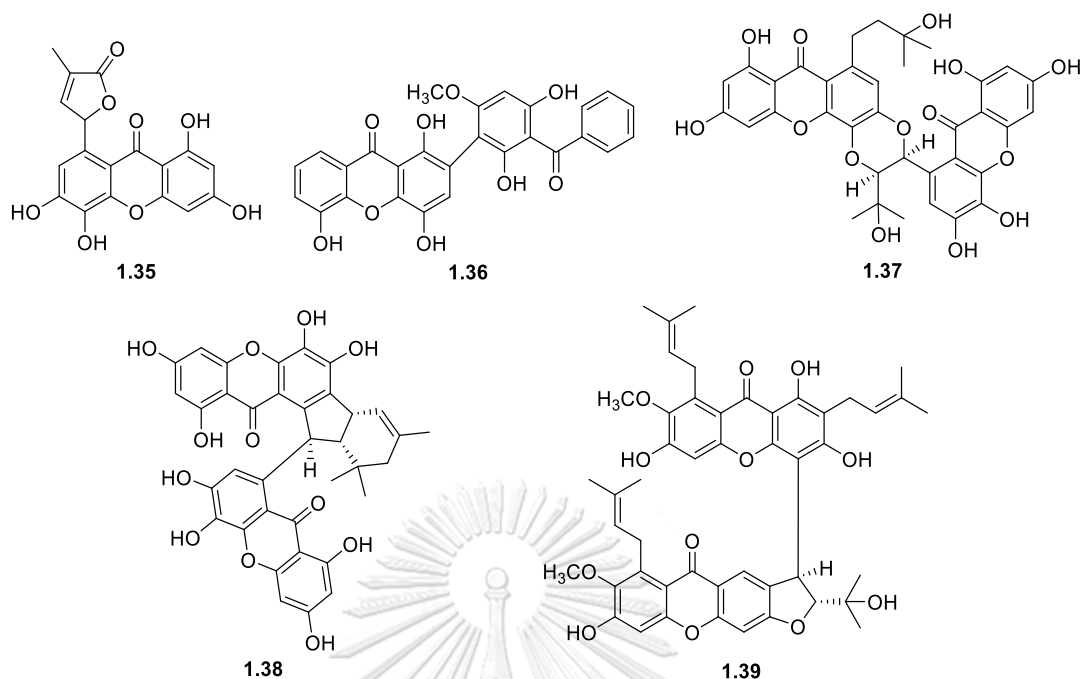


Figure 1.8. Unusual substituted xanthenes (**1.35–1.39**) from *Garcinia* plants.

### 1.3.2. Depsidones

This secondary metabolite class contains two benzene rings connected by ester and ether bridges to generate 11*H*-dibenzo[*b,e*][1,4]-dioxepin-11-one moiety. The compound is found in lichens as the main constituents with common structures containing methyl groups at C-1, C-9, and/or C-6 and oxygenated substituents at C-3 and C-8, based on its biosynthetic occurrence via polyketide pathway. However, a limited number of depsidones are existed in higher plants which are putatively generated from hydroperoxylation reaction of a xanthone carbonyl to form an ester, as described in Figure 1.2 [21, 45]. In *Garcinia* plant, not over than 40 depsidones have been discovered with a typical 1,3,6- or 1,3,8-trioxygenated form, together with other functionalities, such as hydroxy, methoxy, prenyl, and geranyl moieties. Brevipsideone (**1.40**) is the simple depsidone structure obtained from the stem bark of *G. brevipedicellata* with only hydroxy and methoxy groups attached to the skeleton [46]. A depsidone with unusual methyl groups, polyanthadepsidone (**1.41**), was

isolated from *G. polyantha* leaves, as methylated depsidones were commonly found in lichen materials (Figure 1.9) [29].

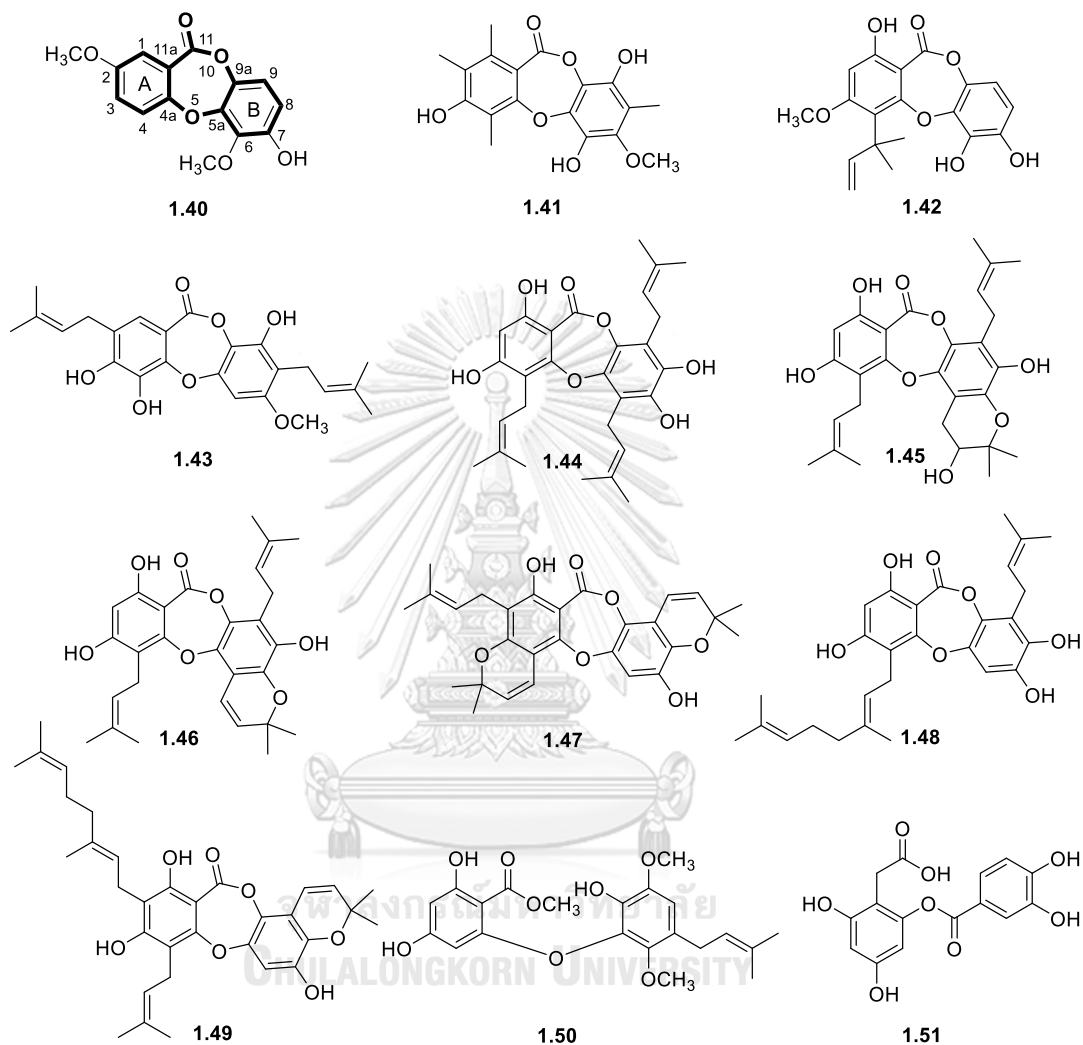


Figure 1.9. Depsidones and its derivatives (1.40–1.51) from *Garcinia* plants.

Six prenylated depsidones including those with modified prenyl units, garcinisidone (1.42), paucinervin Q (1.43), oliveridepsidones A–C (1.44–1.46), and garcinisidone D (1.47), were reported from four *Garcinia* species [47–50]. From the twigs of *G. parvifolia*, geranylated depsidones parvifolidones A and B (1.48 and 1.49) were well characterized (Figure 1.9) [51]. Biological activity studies demonstrated that

**1.43** was cytotoxic against HL-60 and Caco-2 cancer cells with  $IC_{50}$  values of 3.1 and 6.8  $\mu M$ , while **1.47** was found to inhibit Epstein–Barr virus early antigen (EPV-EA) activation induced by TPA with  $IC_{50}$  value of 360 mol ratio/TPA without significant cytotoxicity against Raji cells, which was better than positive control  $\beta$ -carotene.

Pucinerin B (**1.50**), isolated from the stems of *G. paucinervis*, was identified as a pseudodepsidone with two aromatic rings connected by ether linkage [50]. In addition, depside 2-O-(3,4-dihydroxybenzoyl)-2,4,6-trihydroxyphenylacetic acid (**1.51**) was isolated from the pericarps of *G. mangostana* (Figure 1.9) [52]. This type of compound is considered the precursor of depsidones, characterized by two or more phenolic rings linked by an ester bond. Unfortunately, these two substances were reported to have no biological activities.

### 1.3.3. Biphenyls

Among secondary metabolites structurally elucidated from the genus *Garcinia*, biphenyl is one of those having small structures with two aromatic rings linked by C-C bond and substituted by the same functional groups as xanthone and depsidone, including hydroxy, methoxy, and prenylated derivatives. Compared to depsidone, this class of compound is widespread to various *Garcinia* plants with more than 50 structures. Phytochemical investigation on the stems of *G. speciosa* resulted the isolation of two simple biphenyls garcibiphenyl C (**1.52**) and garciosine A (**1.53**), together with garciosine B (**1.54**) bearing methylenedioxy unit formed by an oxidative ring closure of hydroxyl phenol group and adjacent methoxy substituent (Figure 1.10) [53]. A biphenyl with an ester unit, 3-methoxy-5-methoxycarbonyl-4-hydroxy-biphenyl (**1.55**), was identified from *G. oligantha* [54].

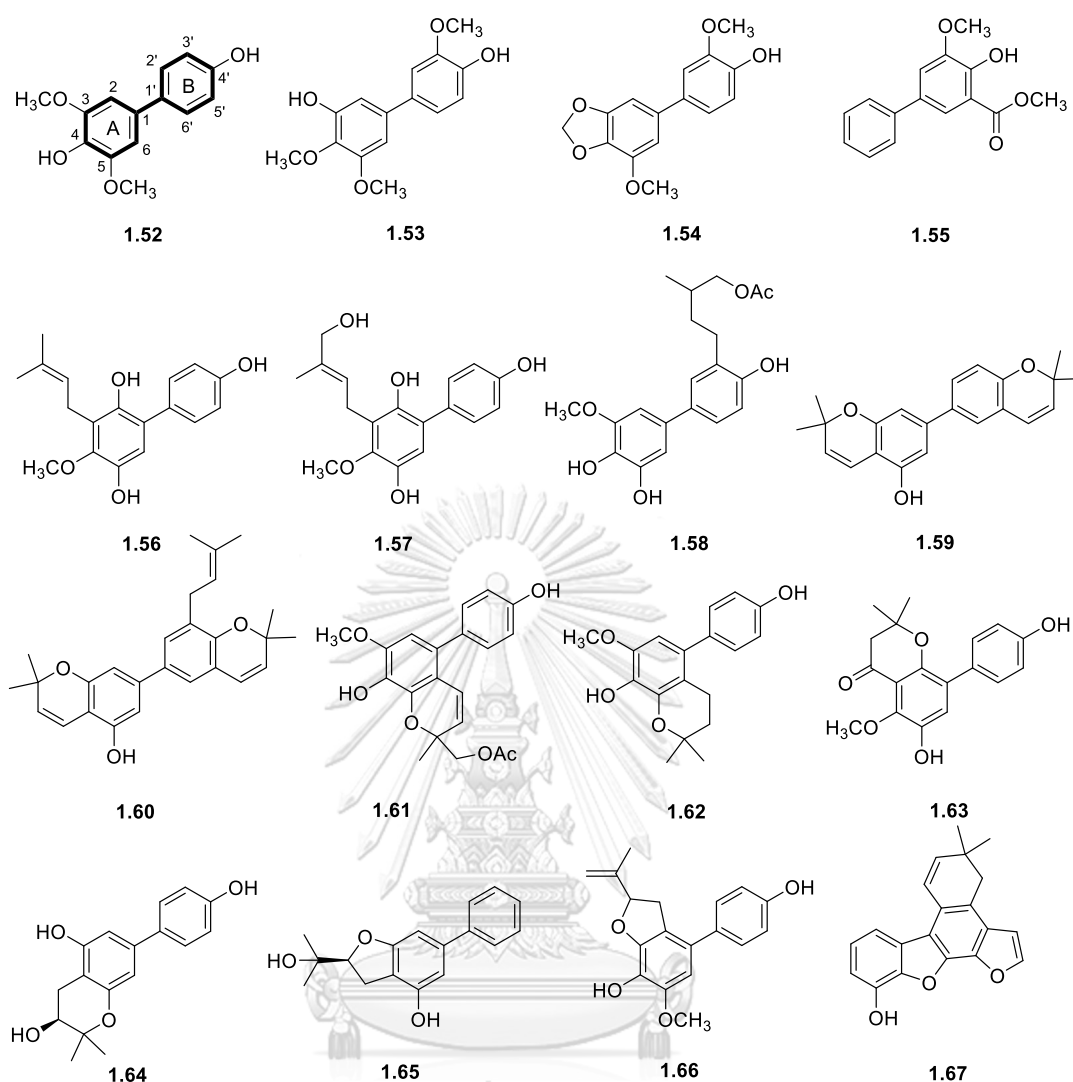


Figure 1.10. Biphenyls (1.52–1.67) from *Garcinia* plants.

A series of prenylated biphenyls were obtained from the twigs of *G. bracteata* and the stems of *G. lancilimba*, including bracteobiphenyls B (1.56) and A (1.57) and garcilancibiphenyls A (1.58) [55, 56]. Biphenyls featuring furan and pyran units, including oblongifoliagarcinines C (1.59) and D (1.60), multibiphenyls B (1.61) and C (1.62), bracteobiphenyl C (1.63), 2,2-dimethyl-3,5-dihydro-7-(4-hydroxyphenyl)chromane (1.64), garciosine C (1.65), and 2-isopropenyl-6-methoxy-7-hydroxy-(4-hydroxyphenyl)-dihydrobenzofuran (1.66), have been reported from five *Garcinia* species [53, 56-59]. Dibenzofuran paucinervin C (1.67) was obtained from the

leaves of *G. paucinervis* [60]. This compound is naturally formed via an intramolecular cyclization of hydroxyl group at either C-2 or C-2' and aromatic carbon at opposite position [61].

Bioactivities study revealed that compounds **1.52–1.54** and **1.65** had anti-HIV-1 effect against  $\Delta^{Tat/Rev}$ MC99 virus in 11A2 cells with  $EC_{50}$  values of 14.2–56.3  $\mu$ M, without significant cytotoxicity on the cells. Compound **1.55** showed potent cytotoxicity against SHSY5Y, A549, and MCF-7 cancer cells at  $IC_{50}$  values of 4.8–7.1  $\mu$ M, while **1.56** and **1.57** had cytotoxic effects against SHSY5Y and MCF-7 cells with  $IC_{50}$  values lower than 10  $\mu$ M. Biphenyls **1.63** was cytotoxic against five cancer cells, including NB4, A549, SHSY5Y, PC3, and MCF-7, whereas **1.64** showed cytotoxic effects on NB4, SHSY5Y, and MCF-7 with  $IC_{50}$  values less than 10  $\mu$ M. Compounds **1.58**, **1.61**, **1.62**, and **1.66** displayed anti-rotavirus activity on rotavirus infected to MA104 cells with  $EC_{50}$  values of 10.9–17.6  $\mu$ M without any cytotoxicity against the cells ( $CC_{50}$ >125  $\mu$ M).

#### 1.3.4. Benzophenones

Biosynthetically, benzophenone is categorized as a xanthone intermediate composed by two aromatic rings connected via carbonyl linkage, so-called diarylketone. Benzophenones appear as one of major *Garcinia* phytochemicals in two forms, which are basic benzophenone with unmodified aromatic rings (Figure 1.11) and polyprenylated benzophenone (PPB)/benzoylphloroglucinol (PPBP) possessing highly rearranged prenyl or geranyl side chains at the ring A of phloroglucinol backbone (Figure 1.12). The latter form commonly features a bicyclo[3.3.1]nonane-2,4,9-trione moiety or more complex cyclized derivatives attached to the 13,14-dihydroxylated benzoyl unit (B-ring), resulting diverse chemical architectures and many of which showed pharmacological potentials, especially as anticancer agent [24].

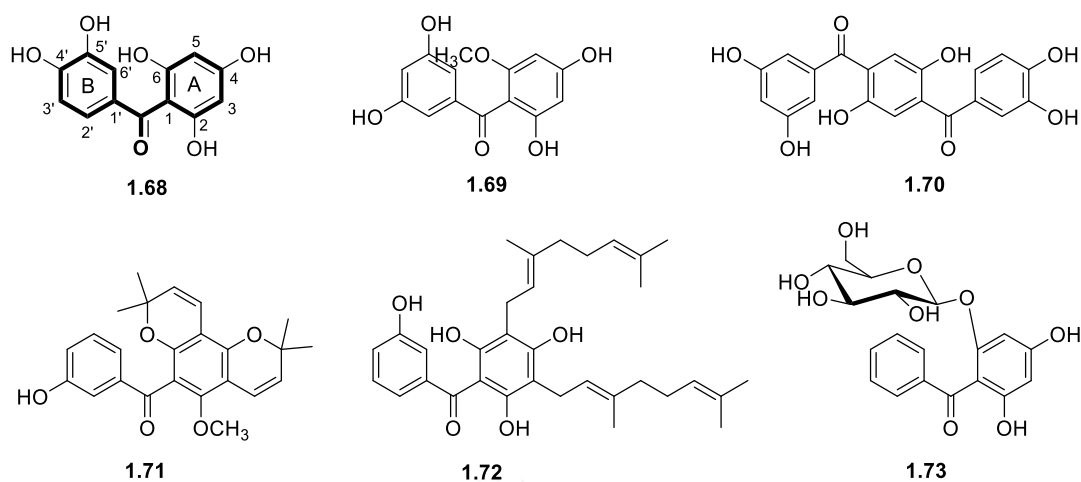


Figure 1.11. Simple benzophenones (**1.68–1.73**) from *Garcinia* plants.

Maclurin (**1.68**) and 2,3',4,5'-tetrahydroxy-6-methoxybenzophenone (**1.69**) are two simple oxygenated benzophenones and garcihombrianone (**1.70**) is a benzophenone bearing benzoyl unit which is the first report of its appearance in the genus *Garcinia*. These compounds were reported from the leaves and twigs of *G. multiflora* and the roots of *G. hombroniana* [27, 62]. Two prenylated and geranylated benzophenones, garciosone B (**1.71**) and gakolanone (**1.72**), were successfully isolated from *G. speciosa* and *G. kola* [53, 63], while garcimangosone D (**1.73**), a benzophenone glycoside, was identified from the fruit hulls of *G. mangostana* (Figure 1.11) [64].

Four PPBs-class compounds were characterized from *G. multiflora* and *G. indica*, including garciniagifolone A (**1.74**), garcinielliptone GC (**1.75**), garcinol (**1.76**), and symphonone H (**1.77**) (Figure 1.12). Compound **1.75** is classified to be a type-A PPB derivative with its benzoyl unit at C-1 of the phloroglucinol skeleton and **1.76** is identified as a type-B PPB with benzoyl ring linked to the C-3. Further cyclization of type-A yields a PPB having an adamantyl skeleton as compound **1.74**, while oxidative coupling between hydroxyl group at C-2 and aromatic carbon at C-16 in type-B constructs a  $\gamma$ -pyrone ring as compound **1.77** [27, 28].

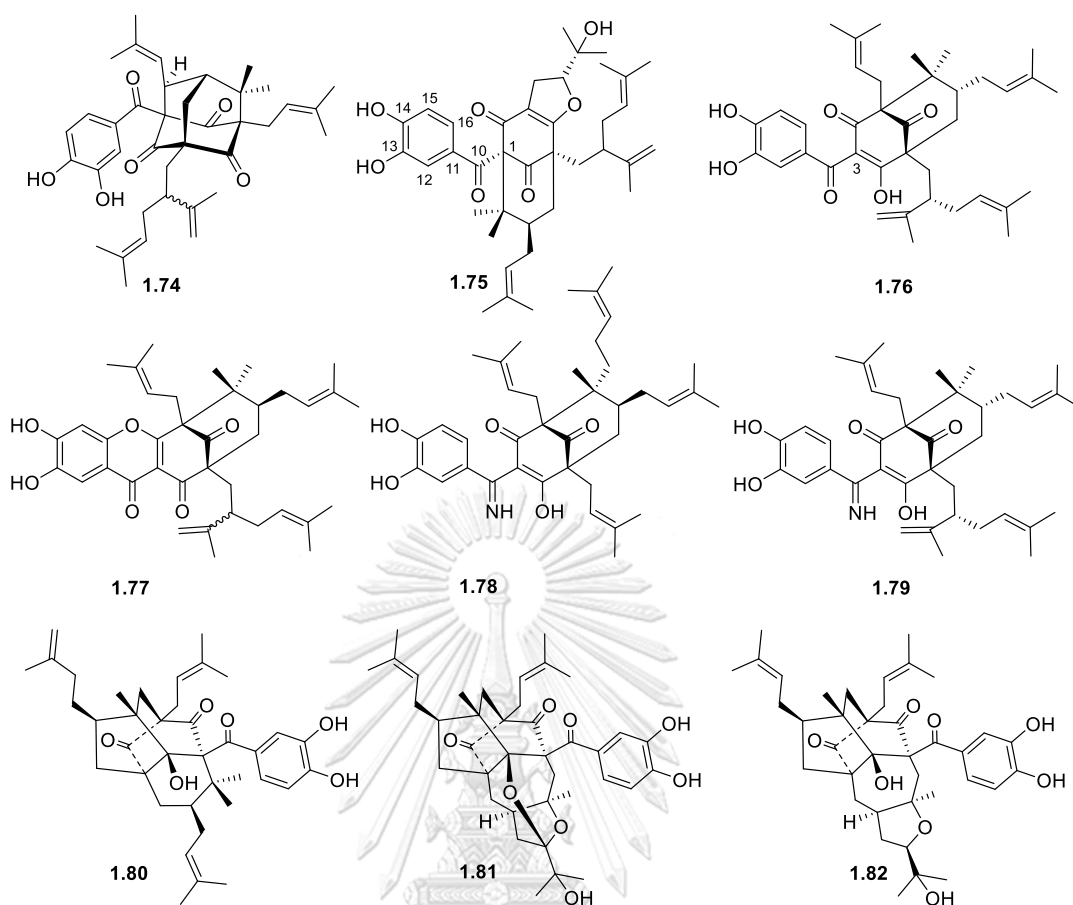


Figure 1.12. Polyprenylated benzophenones (**1.74–1.82**) from *Garcinia* plants.

Two unusual PPBs containing unprecedented imine functionality at C-10, garciyunnanimines A and B (**1.78** and **1.79**), were identified from the chemical investigation of the whole parts of *G. yunnanensis* and were the first occurrence of natural PPBs class with such moiety [65]. PPBs with more complex polycyclic system were observed in garcimulin B (**1.80**) featuring a caged tetracyclo[5.4.1.1<sup>1,5</sup>.0<sup>9,13</sup>]tridecane on the phloroglucinol skeleton [66], as well as (–)-garmultin A (**1.81**) composed by two coupled 2,11-dioxatricyclo[4.4.1.0<sup>3,9</sup>]undecane and tricyclo[4.3.1.0<sup>3,7</sup>]decane cage structures and its precursor, (–)-garmultin C (**1.82**). The isolated compounds were characterized from the leaves and twigs of *G. multiflora* [67].

All PPBs compounds described above showed anticancer activities, including compounds **1.74**, **1.75**, **1.77**, and **1.80–1.82** which displayed cytotoxic properties against five cancer cells (SMMC-7721, A-549, HL-60, MCF-7, and SW480) with  $IC_{50}$  values ranging from 1.8 to 17.4  $\mu$ M, while **1.78** and **1.79** were cytotoxic against Hep G2, A-549, and RPMI-8226 cancer cells with  $IC_{50}$  values of 1.7–10.1  $\mu$ M. Compound **1.82** also demonstrated moderate NO production inhibitory effect in LPS activated RAW 264.7 macrophage cells at  $IC_{50}$  value of 15.1  $\mu$ M and was capable of inducing apoptosis in human erythroleukemia (HEL) cells and inhibiting the expression of Fli-1 protein, an oncogene which plays an important role in carcinogenesis. Moreover, **1.76** was found to induce apoptosis and cell cycle arrest in leukemia, pancreatic, and lung cancer cells, as well as modulate gene expression leading to inhibition of pancreatic cells growth.

### 1.3.5. Flavonoids and biflavonoids

Flavonoid, a group of polyphenolic compounds, is widespread in most of fruits and vegetables and has potent antioxidant and anti-inflammatory capacities. As its natural co-occurrence shares the similar building block and biosynthetic pathway with xanthone, this phytonutrient also appears in *Garcinia* plants with several flavonoid substructures (Figure 1.13) [68]. Pinoцембрin (**1.83**), a flavanone-class compound, along with its glycoside and 3-hydroxy forms, naringenin-7-rhamnoglucoside (**1.84**) and aromadendrin-8-C- $\beta$ -D-glucopyranoside (**1.85**), were identified from three *Garcinia* species [64, 69, 70]. The flavone apigenin (**1.86**) and its prenylated derivative 5,7,4'-trihydroxy-6-[3''-methylbut-3''-enyl]-flavone (**1.87**), isolated from *G. mckeaniana* and *G. xanthochymus*, are the elimination products of a flavanone at C-2 and C-3 [71, 72], while hydroxylation of a flavone at C-3 gives a flavonol class, such as kaempferol (**1.88**) and quercetin (**1.89**) [32].



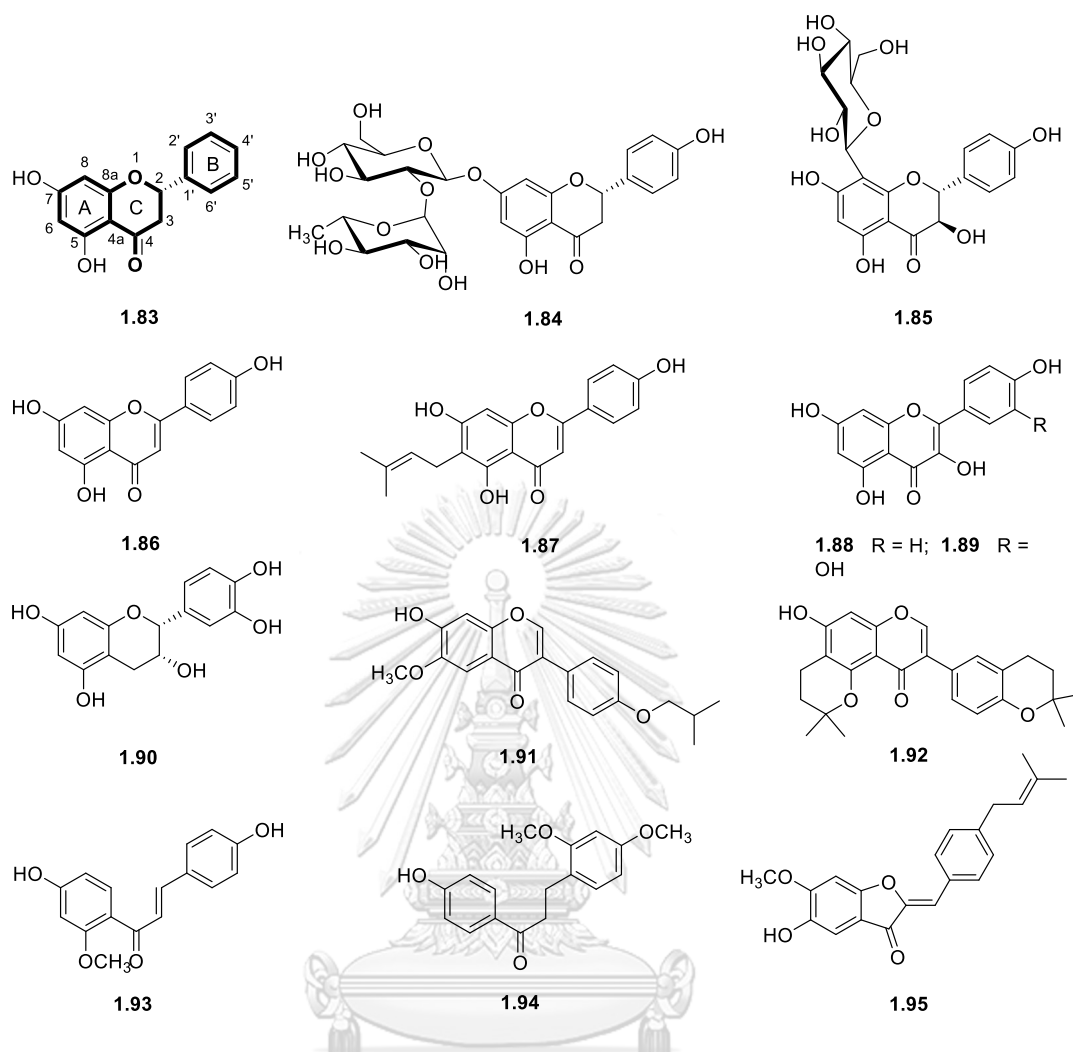


Figure 1.13. Flavonoids (**1.83–1.95**) from *Garcinia* plants.

The flavanol (–)-epicatechin (**1.90**), an addition form of a flavanol, was reported in the pericarps of *G. mangostana* [73]. A 1,2-aryl shift of flavone initiated by radical rearrangement yields an isoflavone, such as paucisoflavone A (**1.91**) and dulcisoflavone (**1.92**) which were originally derived from daidzein and genistein and isolated from the stems of *G. paucinervis* and the green fruits of *G. dulcis* [74, 75]. Compound **1.91** was significantly cytotoxic against NB4, SH-SY5Y, and MCF-7 with IC<sub>50</sub> values lower than 10 μM. A chalcone, 4,4'-dihydroxy-2-methoxychalcone (**1.93**), and a dihydrochalcone, loureirin A (**1.94**), were reported from the seeds of *G. dulcis* [76]. Chalcone is a key intermediate to construct various flavonoid derivatives, including

pauciaurone A (**1.95**), an aurone molecule with five-membered ring in the C-ring of flavonoid skeleton [75].

It is worth noting that pinocembrin, apigenin, kaempferol, quercetin, epicatechin, daidzein, and genistein are common flavonoids that exist in many dietary sources, including propolis, honey, soybean, green and white tea, grape and apple fruits, berries, spinach, and broccoli and they are considered as a basic framework to yield various flavonoid structures in genus *Garcinia*. They were also reported to have broad range of therapeutic potentials for cancer therapy, inflammatory treatment, immune booster, and other degenerative diseases treatment, including diabetes and Alzheimer's disease [77].

Enzymatic coupling reaction of two or more flavonoids lead to the formation of a polymer of flavonoid, such as biflavonoid or flavonoid dimer, trimer, and tetramer, wherein the classification depends on the number of flavonoid molecules connected via C-C and/or C-O-C bonds (Figure 1.14). A previous study showed that a biflavonoid fraction containing morelloflavone (**1.96**), volkensiflavone (**1.97**), and amentoflavone (**1.98**) from *G. madruno* extract exhibited potent atheroprotective activity for cardiovascular diseases treatment by lowering the circulation level of cholesterol and lipid peroxidation product [78]. These three flavonoid dimers are commonly isolated from the polar part of many *Garcinia* species in large amounts. Paucinervin K (**1.99**) is a flavanone-chromone dimer isolated from the leaves of *G. paucinervis* [79]. Dulcisbiflavonoid B (**1.100**), isolated from *G. dulcis* green branches, is a prenylated biflavonoid which is rarely found in nature, while the other two prenylated analogs which are not described in this section, dulcisbiflavonoids A and C, were also isolated from the same species [80].

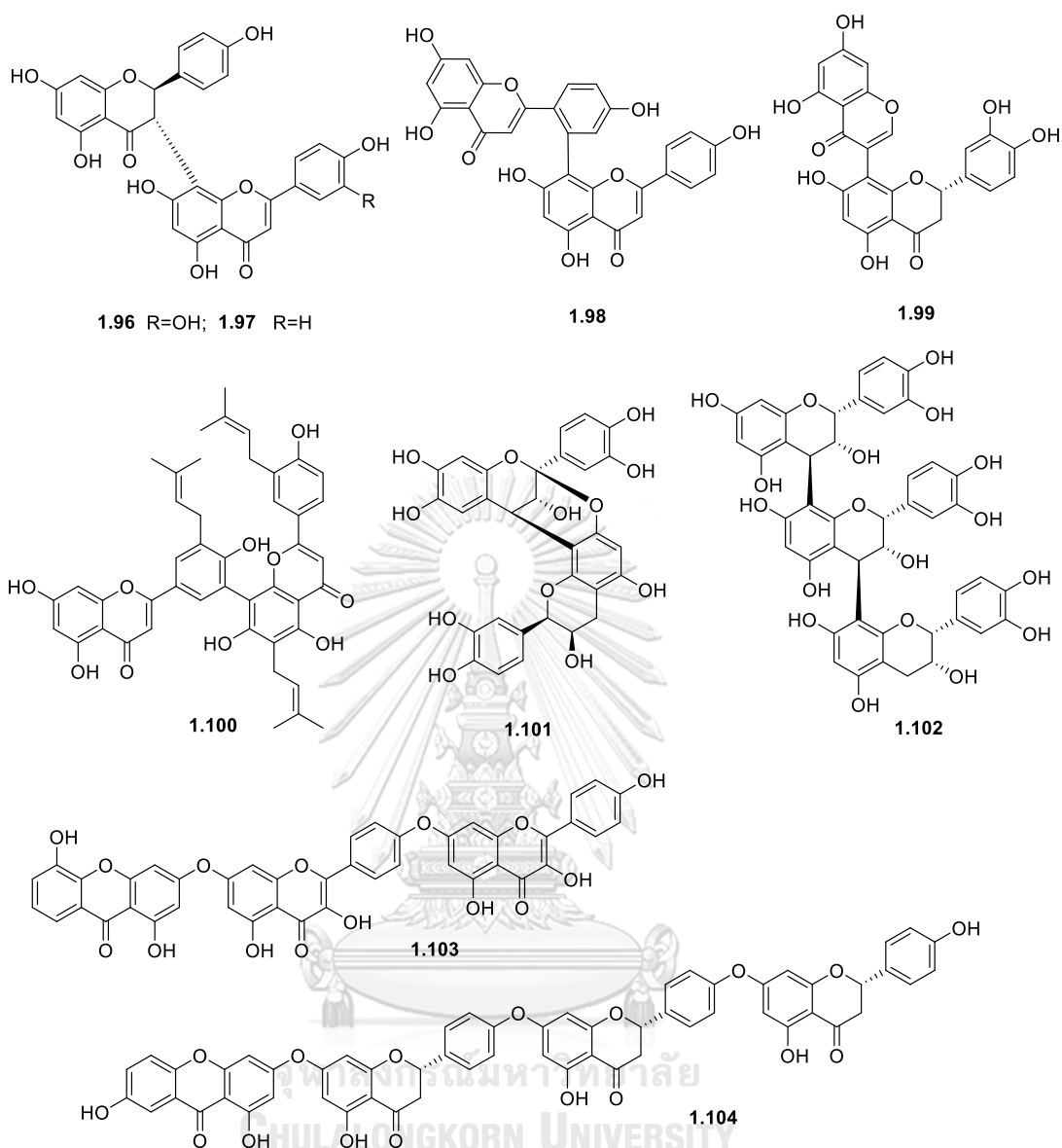


Figure 1.14. Flavonoid dimers and trimers (**1.96–1.104**) from *Garcinia* plants.

A flavanol dimer and trimer, proanthocyanidin A2 (**1.101**) and procyanidin C1 (**1.102**), were reported from the water-soluble fractions of pericarps of *G. mangostana*. The two molecules are obtained from the polymerization of monomer epicatechin and classified to be a group of proanthocyanidin or condensed tannin. Compound **1.101** showed antioxidant and  $\alpha$ -glucosidase inhibitory activities with  $IC_{50}$  values of 11.6 and 3.5  $\mu$ M, respectively [52, 81]. A biflavonol and flavanone trimer

coupling with a trihydroxyxanthone, garcineflavonol A (**1.103**) and garcineflavanone A (**1.104**), were successfully characterized from the stem bark of *G. atroviridis* and both compounds were linked via ether C-O-C bonds. Compound **1.103** displayed AChE and BChE inhibitions with  $IC_{50}$  values of 14.0 and 14.5  $\mu\text{g/mL}$ , while **1.04** selectively inhibited AChE enzyme with  $IC_{50}$  value of 28.5  $\mu\text{g/mL}$  [82].

### 1.3.6. Terpenoid quinones

Most of terpenoid quinones isolated from *Garcinia* plants are categorized as a group of fat-soluble vitamin E molecules, including tocotrienol (with unsaturated isoprene unit) and tocopherol (with saturated isoprene unit) derivatives. These constituents are naturally occurred from the building block homogentisic acid, a derivative of 4-hydroxyphenyl-pyruvic acid, which is subsequently involved in alkylation reaction with phytol diphosphate containing four isoprene unit and followed by decarboxylation and cyclization to form a  $\delta$ -tocotrienol, while reduction isoprene double bonds gives a  $\delta$ -tocopherol. Methylation on both compounds by SAM produces the other derivatives which are defined based on the number and position of methyl units attached to the aromatic part, including  $\alpha$ - (methylated at C-5, C-7, and C-8),  $\beta$ - (methylated at C-5 and C-8), and  $\gamma$ - (methylated at C-7 and C-8) forms [19].

Phytochemical investigation of the stem bark of *G. virgata* led to the purification of  $\delta$ -tocotrienol (**1.105**),  $\beta$ -tocotrienol 2,8-dimethyl-2-[(3*E*,7*E*)-4,8,12-trimethyldeca-3,7,11-trienyl]-5-formylchroman-6-ol (**1.106**), and  $\gamma$ -tocotrienol 2,8-dimethyl-2-[(3*E*,7*E*)-4,8,12-trimethyldeca-3,7,11-trienyl]-7-formylchroman-6-ol (**1.107**) (Figure 1.15) [83]. Meanwhile, 1-dotriacontanol (**1.108**), a metabolite isolated from *G. multiflora*, is formed via dihydropyran ring opening of  $\alpha$ -tocopherol initiated by enzymatic radical reaction [84].

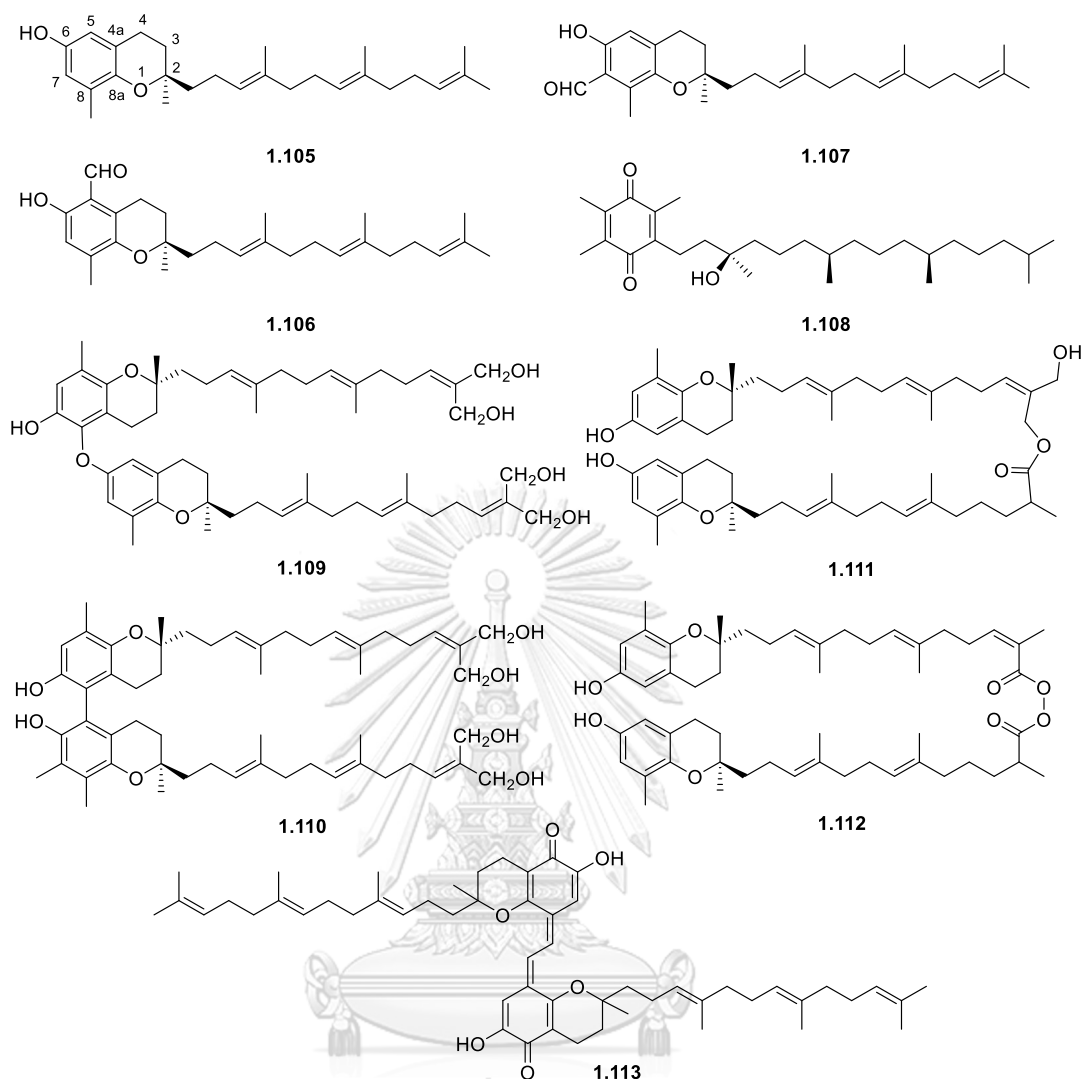


Figure 1.15. Terpenoid quinone derivatives (1.105–1.113) from *Garcinia* plants.

Coupling reaction of two terpenoid quinones resulted the formation of various dimer products, including  $\delta,\delta$ -bi-*O*-amplexichromanol (1.109) and  $\delta,\gamma$ -biamplexichromanol (1.110) with ether and C-C linkages on the chroman moieties, while linkage of two  $\delta$ -tocotrienol derivatives via ester and peroxy ester bonds at the side chains gives  $\delta,\delta$ -biamplexichromanoate A (1.111) and  $\delta,\delta$ -amplexichromanol peroxide (1.112). These four tocotrienol dimers were reported from the stem bark of *G. amplexicaulis*. In addition, a C-C bond formation of two  $\delta$ -tocotrienol derivatives at methyl group of C-8 generates nigrolineaquinone B (1.113) and its putative

biosynthesis pathway has been proposed by A. Raksat *et. al.*, 2019. Compounds **1.109–1.112** were significantly active to inhibit lipid peroxidation enzyme with  $IC_{50}$  values ranging from 1.7 to 9.9  $\mu$ M [85].

### 1.3.7. Phloroglucinols

From acetate biosynthesis pathway, many polyketide-derived natural products are formed, including benzenetriols, well-known as phloroglucinols, which are constituted from a series of coupled acetyl CoA/malonyl CoA units. 5,7-dihydroxy-2,6,8-methylchromone (**1.114**) and 2,3-dihydrochromone derivative (**1.115**), isolated from the pericarps of *G. mangostana*, are two examples of phloroglucinol compounds derived from five and six acetyl CoA/malonyl CoA precursors which are involved in intramolecular cyclization and enolization to form a phloroglucinol skeleton and second cyclization to generate a  $\gamma$ -pyrone moiety. In addition, a chromone glycoside, eucryphin (**1.116**), and a chromone dimer, paucinervin R (**1.117**), were obtained from *G. mangostana* and *G. paucinervis* (Figure 1.16) [52, 76, 86].

Three metabolites 4-geranyl-2-(2'-methylpropionyl)-phloroglucinol (**1.118**), dauphinol F (**1.119**) and dauphinol C (**1.120**) isolated from the roots of *G. dauphinensis* are phloroglucinol derivatives containing geranyl side chains, as well as isobutyryl and 2-methylbutyryl units derived from precursor L-valine and isoleucine amino acids. An intramolecular cyclization of geranyl moiety generates dauphinol A (**1.121**), 3'-methylhyperjovinol B (**1.122**), empetrikarinol B (**1.123**), and empetrifranzinan C (**1.124**) [87].

Garcicowin A (**1.125**) from *G. cowa* and garsubelone B (**1.126**) and garsubelone A (**1.127**) from *G. subelliptica* represent polyprenylated phloroglucinols. Compound **1.127** is the first report of a phloroglucinol constituent possessing an unprecedented 6/6/6/6/6/6/6 heptacyclic ring system derived from its monomer **1.126**. Cytotoxic evaluation showed that compounds **1.118–1.121** and **1.123**

inhibited the growth of A2780 ovarian cancer cells with  $IC_{50}$  values of 4.5–16.4  $\mu M$ , while **1.126** was cytotoxic against HeLa and HepG2 cancer cells with  $IC_{50}$  values of 6.0 and 7.3  $\mu M$ , respectively. In addition, metabolites **1.118–1.122** displayed significant anti-plasmodial activity against *P. falciparum* with  $IC_{50}$  values of 4.7–14.1  $\mu M$  [88, 89].

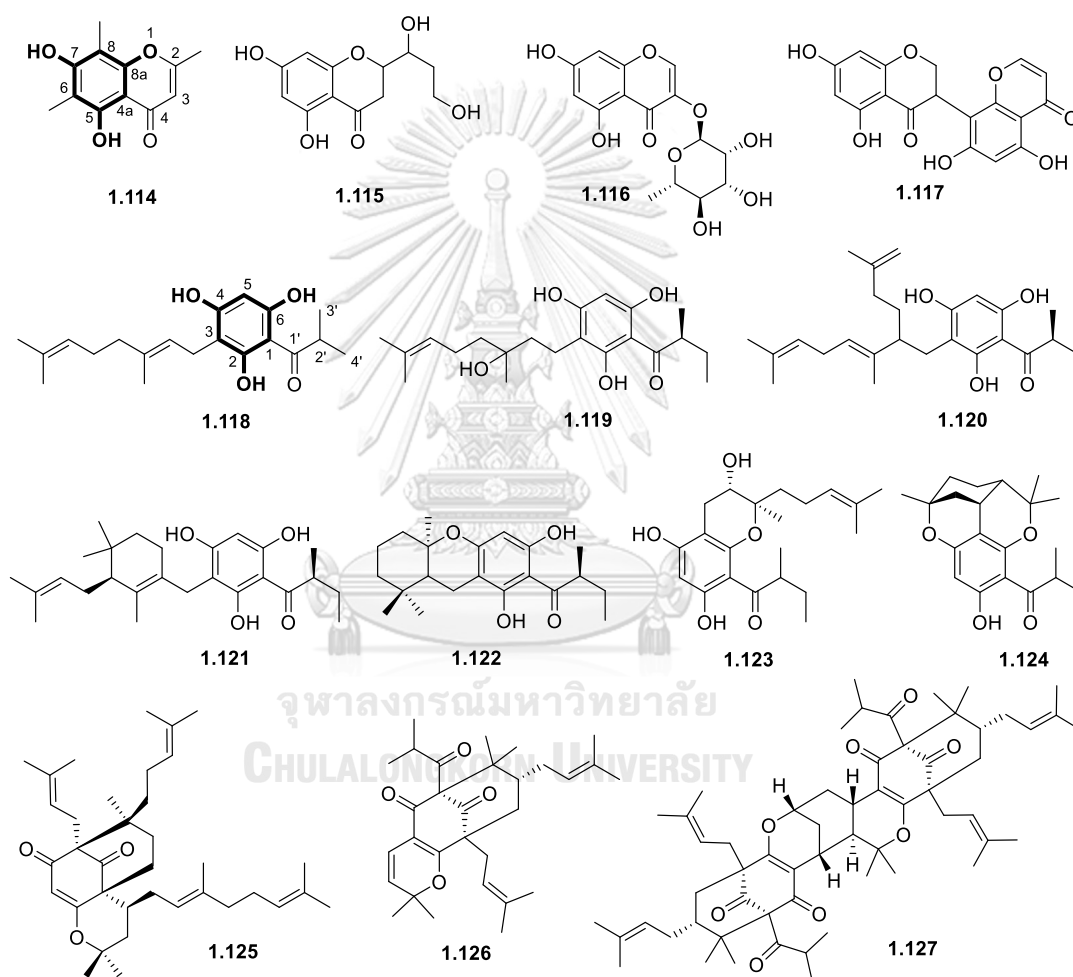


Figure 1.16. Phloroglucinol derivatives (**1.114–1.127**) from *Garcinia* plants.

### 1.3.8. Triterpenoids

Triterpenoid, a mevalonate-derived compound with 30 carbon atoms on the skeleton, is one of major non-phenolic substances that can be found in *Garcinia*

species. Two farnesyl pyrophosphate (FPP) containing  $C_{15}$  building block each incorporate through a series of enzymatic reaction, including electrophilic addition, proton and carbon rearrangements, and hydration to form squalene intermediate. This precursor is subsequently cyclized to generate various triterpenoid structures which mostly feature tetracyclic and pentacyclic ring system [19].

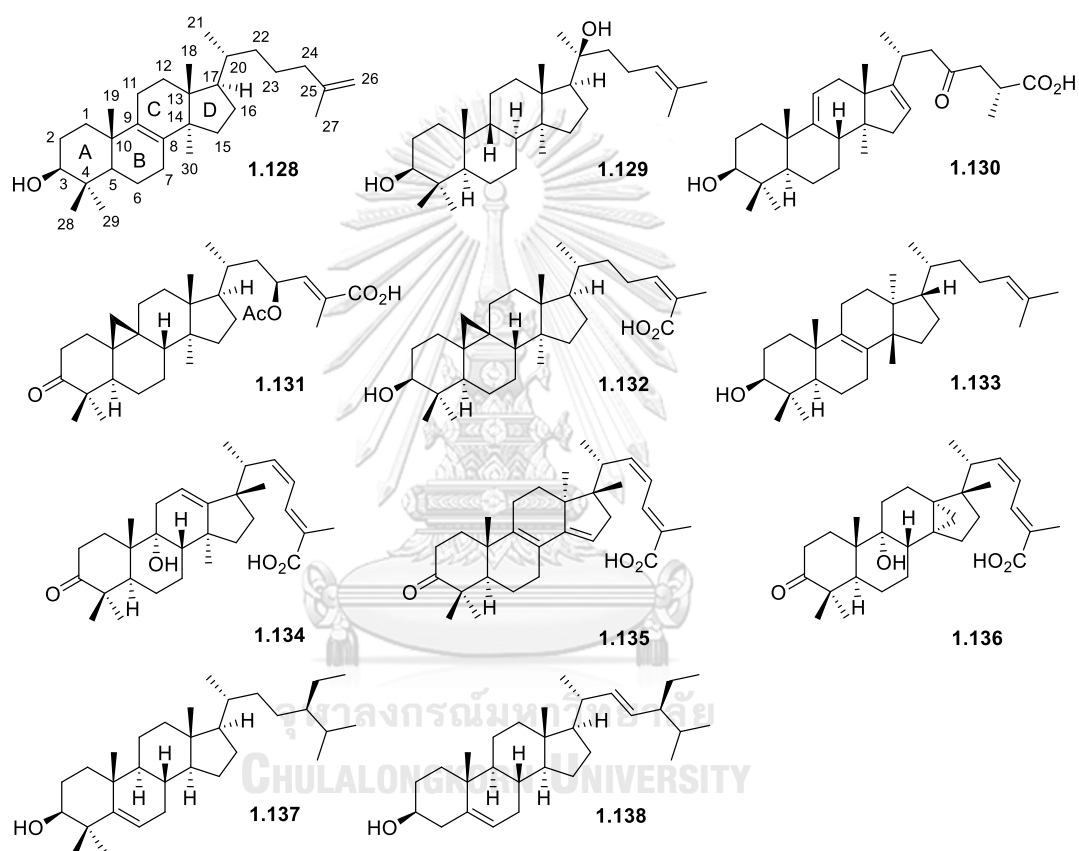


Figure 1.17. Tetracyclic triterpenoids (**1.128**–**1.138**) from *Garcinia* plants.

Lanosta-8,25-en-3 $\beta$ -ol (**1.128**), garcinielliptones Q (**1.129**), and garcihombropane D (**1.130**), isolated from three *Garcinia* species [90-92], are classified to be a lanostane-type structure which is considered to be a basic parent for other triterpenoid derivatives. The formation of a methylene bridge at C-9 and C-10 gives a cycloartane as in 23-acetoxy-mangiferonic acid (**1.131**) and mangiferolic acid (**1.132**)



[93]. An euphane triterpene from *G. eugenifolia* roots, euphadienol (**1.133**), differs from lanostane only in the orientation of methyls C-18 and C-30 [94], while the migration of methyl groups at C-13 and C-14 of lanostane generates a friedolanostane structure, such as (22*Z*,24*E*)-9 $\alpha$ -hydroxy-3-oxo-17,13-friedolanosta-12,22,24-trien-26-oic acid (**1.134**), (22*Z*,24*E*)-3-oxo-17,14-friedolanosta-8,14,22,24-tetraen-26-oic acid (**1.135**), and (22*Z*,24*E*)-9 $\alpha$ -hydroxy-3-oxo-13 $\alpha$ ,30-cyclo-17,13-friedolanosta-22,24-dien-26-oic acid (**1.136**) from the bark of *G. celebica* [47]. Steroids  $\beta$ -sitosterol (**1.137**) and stigmasterol (**1.138**) are the most common phytochemicals found not only in genus *Garcinia*, but also in other higher plants as modified tetracyclic triterpenoids lacking methyl units at C-4 and C-14 (Figure 1.17).

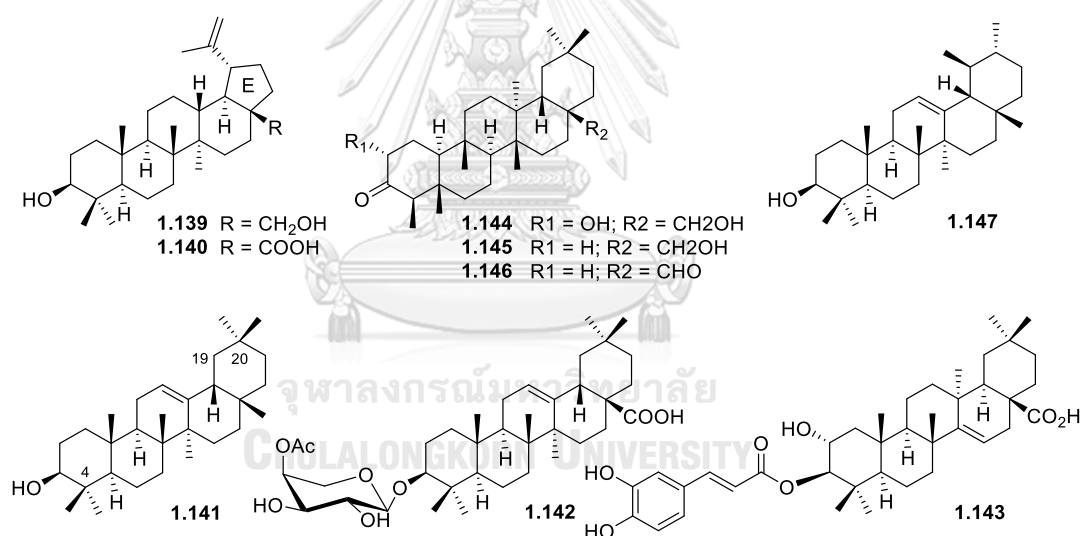


Figure 1.18. Pentacyclic triterpenoids (**1.139–1.143**) from *Garcinia* plants.

Pentacyclic triterpenoid (Figure 1.18) consists five ring system with the new ring E formed via cyclization of the side chain at ring D of tetracyclic triterpenes. Betulin (**1.139**), betulinic acid (**1.140**),  $\beta$ -amyrin (**1.141**), messagenic acid (**1.142**), and 2 $\beta$ -hydroxy-3 $\alpha$ -O-caffeoyltaraxar-14-en-28-oic acid (**1.143**) are the examples of pentacyclic lupane and oleanane triterpenoids. The migration of one of methyl

groups at C-4 to C-5 and C-20 to C-19 allows the formation of friedelane and ursane types, respectively, as in endodesmiadiol (**1.144**), canophyllol (**1.145**), canophyllal (**1.146**) and  $\alpha$ -amyrin (**1.147**) [87, 95-97].

Cycloartane **1.131** displayed melanin deposition inhibition with  $IC_{50}$  values of  $19.4 \mu\text{M}$  by downregulated the expression of tyrosinase gene. The cholinesterase inhibition of compounds **1.140** and **1.143** was reported against AChE and BChE enzymes with  $IC_{50}$  values in the range of  $10.6\text{--}24.2 \mu\text{M}$ , while **1.139** selectively inhibited AChE activity with  $IC_{50}$  value of  $28.5 \mu\text{M}$ . Three friedelanes **1.144**–**1.146** showed anti-plasmodial activity on *P. falciparum* W2 strain with  $IC_{50}$  values of  $13.0\text{--}18.2 \mu\text{M}$ . The combination of **1.141** with cisplatin was capable to induce apoptosis and cell cycle arrest, mediate ROS formation in NTUB1 human bladder carcinoma cells, and reduce the side effect and drug resistance of cisplatin. Oleanane glycoside **1.142** showed apoptosis induction of HL-60 human leukemia cell line at a concentration of  $4.0 \mu\text{M}$  and caused the cell cycle arrest at sub-G1 stage.

### 1.3.9. Miscellaneous compounds

(-)-Hydroxycitric acid (**1.144**), a citric acid from *G. cambogia* fruits, was found to block fat accumulation and this substance have been marketed as a weight loss supplement (Figure 1.19) [18]. Two phenolic glycosides, (2*R*)-1-*O*-4-hydroxy-benzoyl-3-*O*- $\alpha$ -d-glucuronosyl glycerol (**1.145**) and garcinophenylpropanoic acid (**1.146**) and chlorogenic acid (**1.147**) were obtained from three *Garcinia* species [52, 98, 99]. Angelicin B (**1.148**) and 8-hydroxy-6-methoxy-3-pentylisocoumarin (**1.149**) isolated in the twigs of *G. xanthochymus* the stem bark of *G. dulcis* are classified as isocoumarin derivatives which are constructed through acetate pathway [33, 100]. In some cases, isocoumarin metabolites bearing a phenyl ring at C-3, instead of alkyl chains, were recorded and their biosynthesis is proposed to be similar with that of flavonoid. This class of compound is abundant in microbes, such as fungi, bacteria, and lichens,

while it is limited in some higher plant families, including Leguminosae, Asteraceae, Moraceae, and Umbelliferae [101].

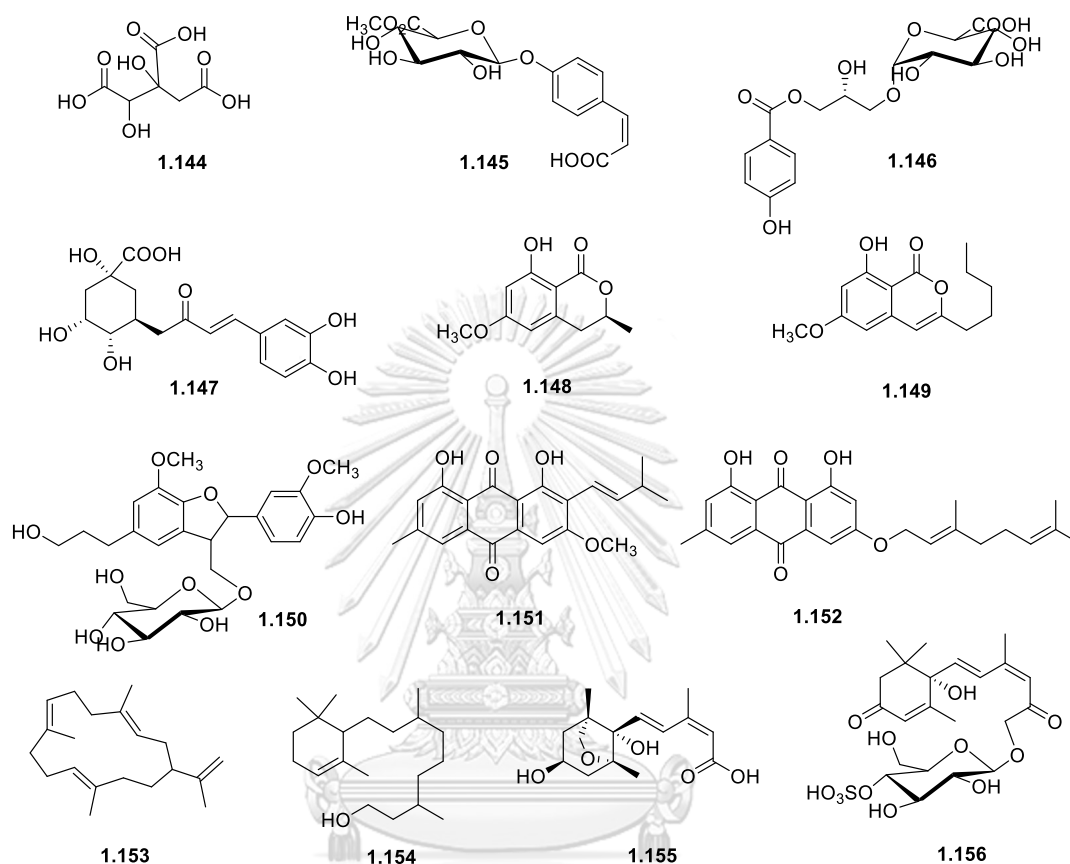


Figure 1.19. Miscellaneous compounds (1.144–1.156) from *Garcinia* plants.

A benzofuran glycoside, 2*R*,3*R*-2,3-dihydro-2-(4'-hydroxy-3'-methoxyphenyl)-3-(glucosyloxymethyl)-7-methoxy-benzofuran-5-propanol (1.150) was reported from the pericarps of *G. mangostana* [81]. Anthraquinones vismiaquinone A (1.151) and 3-geranylemodin (1.152) were isolated from the bark of *G. schomburgkiana* and they shared the same biosynthesis pathway with isocoumarin and phloroglucinol [102]. Two diterpenes, cembrene A (1.153) and 2-cyclohexene- $\gamma,\eta,2,6,6$ -pentamethyl-1-nonanol (1.154), and two megastigmane sesquiterpenes, dihydrophaseic acid (1.155)

and 4-*O*-sulpho- $\beta$ -d-glucopyranosyl abscisate (**1.156**), were identified from the leaves of *G. paucinervis* and the pericarps of *G. mangostana*, respectively [52, 60, 81].

#### 1.4. Cytotoxic evaluation of natural products for preliminary anticancer screening

The MTT assay is one of the most widely used biological tests for preliminary screening of both natural products and synthetic compounds as an anticancer drug candidate. The colorimetric based assay is readily performed on a wide range of cell lines and measure the number of living cells. In this assay, NADH or NADPH produced by mitochondrial dehydrogenase enzymes inside the living cells reduce the tetrazolium salt (3-(4,5-dimethylthiazol-2-yl)-2,5-diphenyltetrazolium bromide) into a colored formazan product at 37°C. The amount of formazan formed is directly proportional to the number of viable cells present in the culture (Figure 1.20). IC<sub>50</sub> value is the concentration of a tested sample that is required to cause the death of 50% of the cells. This value is commonly used to define the degree of cytotoxicity of the substance. The lower the value, the more cytotoxic is the anticancer drug candidate [103, 104].

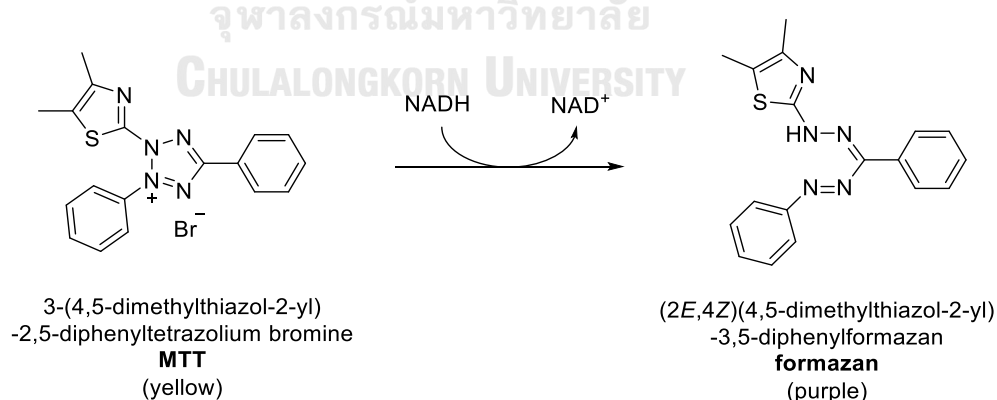


Figure 1.20. Formazan formation through NADH-catalyzed MTT reduction in live cells.

### 1.5. Anti-inflammatory evaluation of natural products on COX enzymes inhibition

Several evidences were reported that severe inflammation can induce apoptosis inhibition as well as increase angiogenesis, genome damage, and cellular proliferation which are typical in carcinogenesis. During the chronic symptom, pro-inflammatory molecules such as cytokines, reactive oxygen species (ROS), and inducible nitric oxide synthase (*i*NOS) are upregulated causing the exponential growth of malignant cells [105]. The use of nonsteroidal anti-inflammatory drugs (NSAIDs) in inflammation and cancer treatment have been reported since significant indications were found that NSAIDs can decrease primary and recurrent cancer incidence. The long term-administration of a NSAID, aspirin, may lower the incidence of esophageal, colorectal, lung, breast, and bladder cancers and the use of other NSAIDs, such as sulindac, ibuprofen, and piroxicam, decreases the risk of existing cancer development [106]. Therefore, eliminating severe inflammation is one of strategies in cancer prevention and the cytokine molecules involved in the process can serve as biomarker for therapy decision.

In this dissertation, we focus on searching anti-inflammatory agent from natural products to inhibit COX enzymes activity. Cyclooxygenase (COX), also known as prostaglandin-endoperoxide synthase (PGHS), is key enzyme comprising two main isoforms, which are COX-1, activated and expressed with constant level by physiological and pathological stimuli, and COX-2, a highly inducible enzyme by pro-inflammatory stimuli [107]. The COX enzymes catalyze the biotransformation of arachidonic acid (AA), a lipid-derived substance released as an intracellular messenger when body tissues get injured or infected, to prostaglandins (PGs) which are responsible as mediators to inflammation reactions in damaged tissues (Figure 1.21) [108]. Nevertheless, uncontrolled biosynthesis of the PG metabolites may also initiate cancer cell development. For example, COX derived prostaglandin E<sub>2</sub> (PGE<sub>2</sub>),

a key mediator in acute inflammation, can induce cancer cells growth by binding its receptor and trigger the signal pathway controlling cell proliferation, migration, apoptosis, and angiogenesis and COX-2 expression was found being elevated in many human cancers. Advanced research in regulation of COX enzymes have been conducted to inhibit the enzyme activities (Figure 1.21) [105, 109].

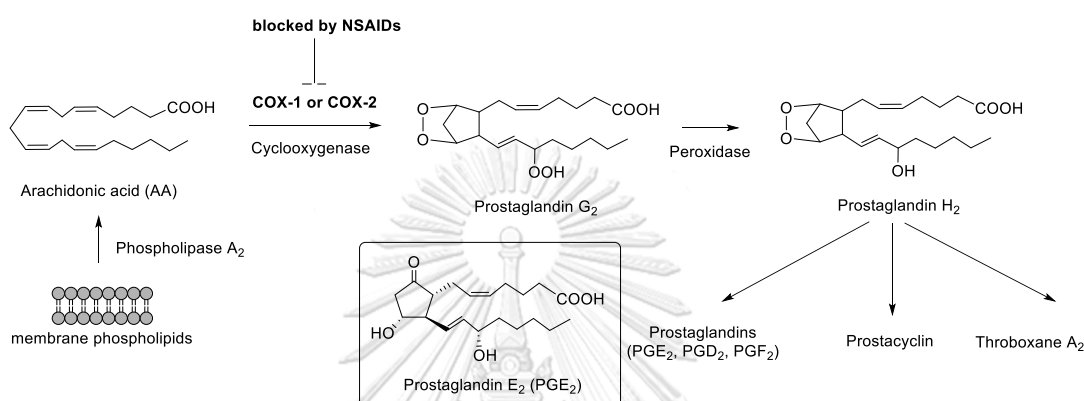


Figure 1.21. Prostaglandins production via arachidonic acid metabolism and a strategy in COX activity inhibition.

The COX inhibition assay is commonly used to screen bioactive compounds from nature or synthetic products as anti-inflammatory agents. The reaction in the assay starts by adding arachidonic acid to the mixtures of COX enzyme, sample, and other reagents. The concentration of PGE<sub>2</sub> generated from the AA transformation by COX enzymes is quantified using prostaglandin E<sub>2</sub> (PGE<sub>2</sub>) EIA kit, a competitive immunoassay for quantitative determination of PGE<sub>2</sub> in biological fluids. PGE<sub>2</sub> in the sample mixture is bound by either PGE<sub>2</sub> monoclonal antibody or alkaline phosphatase enzyme in competitive manner [110]. A chromogenic pNPP substrate is added to react with conjugated enzyme (alkaline phosphatase—PGE<sub>2</sub>) during second incubation. The absorbance of final reaction mixture is measured at 405 nm using UV/Vis spectrophotometer. Sample with high PGE<sub>2</sub> antigen concentration results in lower signal intensity since less substrate react with bound enzyme (blue color) to

produce *p*-nitrophenol (yellow color). This implies that the intensity of the yellow color is inversely proportional to the PGE<sub>2</sub> concentration in the standard or samples (Figure 1.22) [111, 112].

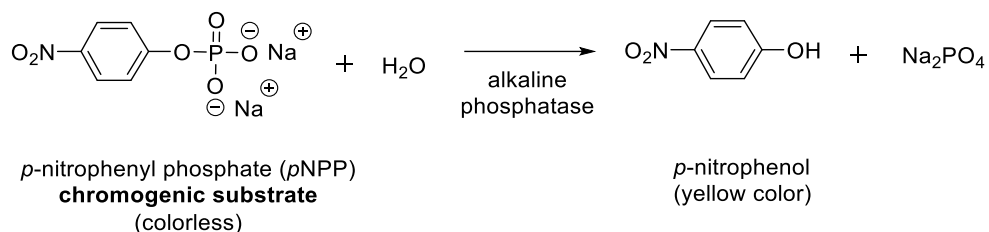


Figure 1.22. Reaction between *p*NPP and alkaline phosphatase enzyme to produce *p*-nitrophenol.

## 1.6. Objectives of the research

In agreement with the above data, exploring phytochemicals from *Garcinia* plants is of high importance to discover and identify novel compounds with promising biological activities, particularly as anticancer candidates. In this work, three *Garcinia* species collected from Indonesia, including *G. cylindrocarpa*, *G. picrorhiza*, and *G. tetrandra*, will be studied since there have been a few reports conducted in terms of their secondary metabolite isolation, with the main objectives of research as follows:

1. To isolate the chemical constituents from the stems of *Garcinia cylindrocarpa* and the stem bark of *Garcinia picrorhiza* and *Garcinia tetrandra*;
2. To elucidate the chemical structure of isolated compounds by spectroscopic analysis, including UV-Vis, FT-IR, 1D (<sup>1</sup>H and <sup>13</sup>C) and 2D (COSY, HSQC, and HMBC) NMR, and HRMS;
3. To evaluate the cytotoxic properties of the isolated compounds against five human cancer cells (KB, HeLa S-3, HT-29, MCF-7, and Hep G2) and anti-inflammatory activity towards COX-1 and COX-2 enzymes inhibition.

## Chapter II

### Phytochemical and biological investigation of the stems of *Garcinia cylindrocarpa*

#### 2.1. Botanical and chemical aspects of *G. cylindrocarpa*



Figure 2.1. The whole plant, leaves, and fruit of *Garcinia cylindrocarpa*.

Family	: Clusiaceae
Genus	: <i>Garcinia</i>
Species	: <i>Garcinia cylindrocarpa</i>
Common name	: Kogbirat
Local name	: Kogbirat (in Maluku Island)

*Garcinia cylindrocarpa* Kosterm is a woody plant and native to Maluku Islands, Indonesia (Figure 2.1). In its place of origin, the species is found in lowland tropical rainforest at altitude of 100 m. It is a medium to large evergreen tree and reaching heights of 15–20 meter with a girth of 20–30 cm. Its leaves are broadly elliptic, and its fruit is turning pink when ripe, which contain 5–6 seeds inside. The ripe fruit is edible but acidic. This species, locally named as Kogbirat, has been used as a traditional medicine for fever remedy [13, 15]. The first report on the chemical constituents of *G. cylindrocarpa* revealed the presence of three pyranoxanthones,



cylindroxanthenes A–C (**2.1–2.3**), from the methanol extract of its stem bark (Figure 2.2). The cytotoxic activity of three compounds was evaluated against five human cancer cell lines (KB, HeLa S-3, HT-29, MCF-7, and Hep G2). The results showed that cylindroxanthone A (**2.1**) exhibited a potent cytotoxicity against KB cells with  $IC_{50}$  value of 2.36  $\mu$ M, while the others showed moderate to inactive against the five cancer cells [13].

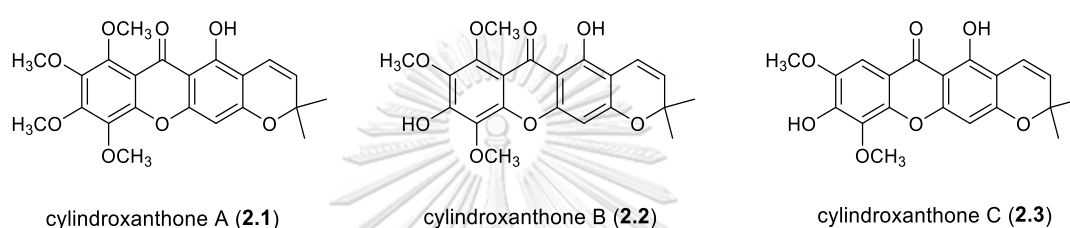


Figure 2.2. Cylindroxanthenes A–C (**2.1–2.3**) from the stem bark of *G. cylindrocarpa*.

As a continuation of our research interest to explore bioactive compounds from *G. cylindrocarpa*, we describe herein the isolation and structure elucidation of four new xanthenes, cylindroxanthenes D–G (**GC1–GC4**), and two new biphenyls, cylindrobiphenyls A and B (**GC5** and **GC6**), along with 28 known compounds from the stems of this plant. The cytotoxic evaluation of the isolated compounds against five human cancer cell lines were also reported.

## 2.2. Experimental

### 2.2.1. General Experiment Procedures

Melting points were determined by Fischer-Johns melting point apparatus. Optical rotations were measured on a Jasco (Oklahoma City, OK, USA) P-1010 polarimeter. IR data were obtained using a Nicolet (Thermo Scientific, Waltham, MA, USA) 6700 FT-IR spectrometer using KBr discs. UV–visible absorption spectra were obtained on a Shimadzu (Kyoto, Japan) UV-2550 UV–vis spectrometer. NMR spectra

were recorded on a Bruker 400 AVANCE spectrometer (400 MHz for  $^1\text{H}$  and 100 MHz for  $^{13}\text{C}$ ) in  $\text{CDCl}_3$  and acetone- $d_6$ . HRESIMS spectra were recorded using a Bruker MICROTOF model mass spectrometer. Silica gel 60G (Merck), silica gel 70–230 mesh (Merck), and Sephadex LH-20 (GE Chemical Corporation) were used for column chromatography. Radial chromatography (Chromatotron model 7924 T, Harrison Research, Palo Alto, California, USA) was carried out on silica gel 60 GF<sub>254</sub> containing gypsum (Merck). For TLC analysis, precoated silica gel 60 GF<sub>254</sub> (0.25 mm; Merck) was used.

### 2.2.2. Plant Material

The stems of *Garcinia cylindrocarpa* were collected from Saumlaki Forest, Southeast West Maluku Islands, Indonesia. The plant was identified by Mrs. Rismita Sari (a botanist at Bogor Botanical Garden, Indonesia). A voucher specimen (No. 630) was deposited at the Herbarium Bogoriense, Bogor Botanical Garden, Indonesia.

### 2.2.3. Extraction and Isolation

The air-dried stems of *G. cylindrocarpa* (3.0 kg) were ground into powder and extracted by maceration at room temperature with MeOH (3 x 15 L) for three days. The solvent was evaporated under reduced pressure to obtain a residue (31.4 g). The crude extract was then suspended in distilled H<sub>2</sub>O and partitioned with CH<sub>2</sub>Cl<sub>2</sub> and EtOAc to afford a CH<sub>2</sub>Cl<sub>2</sub> fraction (6.04 g), an EtOAc fraction (9.23 g), and the remaining aqueous solution. The CH<sub>2</sub>Cl<sub>2</sub>-soluble fraction was subjected to VLC on silica gel (125.0 g) using a gradient of hexanes:EtOAc (90:10–0:100) to obtain nine fractions (D1–D9). Fraction D2 (488.8 mg) was chromatographed on Sephadex LH-20 column (50.0 g) eluted with CH<sub>2</sub>Cl<sub>2</sub>:MeOH (1:1, v/v) to yield subfractions D2.1–D2.3. Subfraction D2.1 (93.2 mg) was separated by repeated Sephadex LH-20 CC (50.0 g) using CH<sub>2</sub>Cl<sub>2</sub>:MeOH (1:1, v/v) to afford compounds **GC4** (4.3 mg) and **GC7** (4.2 mg).

Compound **GC8** (16.7 mg) was yielded from subfraction D2.2 (70.4 mg) by separation using radial chromatography (chromatotron) with hexanes:EtOAc (95:5) as eluent. Subfraction D2.3 (112.0 mg) was separated by repeated chromatotron eluted with hexanes:EtOAc (95:5) to afford compounds **GC9** (3.1 mg), **GC10** (2.0 mg), **GC11** (2.6 mg), **GC12** (9.3 mg), **GC13** (1.5 mg), and **GC14** (4.4 mg).

Fraction D3 (270.3 mg) was loaded to Sephadex LH-20 column (50.0 g) eluted with  $\text{CH}_2\text{Cl}_2$ :MeOH (1:1, v/v) to provide three subfractions (D3.1–D3.3). Compound **GC1** (2.7 mg) was obtained by purification of subfraction D3.1 (54.6 mg) using chromatotron with hexanes: $\text{CH}_2\text{Cl}_2$  (25:75) as eluent. Fraction D4 (229.6 mg) was chromatographed using Sephadex LH-20 column (50.0 g) with  $\text{CH}_2\text{Cl}_2$ :MeOH (1:1, v/v) as eluent to give four subfractions (D4.1–D4.4). Compounds **GC15** (11.6 mg) and **GC16** (1.4 mg) were yielded from subfraction D4.3 (56.5 mg) using chromatotron eluted with hexanes:EtOAc (85:15). Subfraction D4.4 (29.1 mg) was purified by chromatotron using hexanes: $\text{CH}_2\text{Cl}_2$  (25:75) as eluent to obtain compound **GC3** (1.2 mg). Fractionation of fraction D5 (202.1 mg) using Sephadex LH-20 CC (50.0 g) with  $\text{CH}_2\text{Cl}_2$ :MeOH (1:1, v/v) as eluent was performed to obtain subfractions D5.1–D5.4. Compound **GC17** (6.0 mg) was yielded from subfraction D5.1 (67.4 mg) using chromatotron eluted with hexanes:EtOAc (85:15), while compound **GC18** (1.7 mg) was obtained from subfraction D5.2 (42.7 mg) using the same technique with hexanes:acetone (75:25) as eluent.

Fraction D6 (581.0 mg) was subjected to Sephadex LH-20 column (50.0 g) using solvent system of  $\text{CH}_2\text{Cl}_2$ :MeOH (1:1, v/v) to obtain subfractions D6.1–D6.6. Compounds **GC5** (7.2 mg), **GC19** (24.7 mg), and **GC20** (3.6 mg) were successfully afforded from subfraction D6.2 (97.2 mg) using chromatotron with  $\text{CH}_2\text{Cl}_2$ :MeOH (97:3) as eluent. Fractionation of subfraction D6.3 (102.1 mg) was conducted using chromatotron with  $\text{CH}_2\text{Cl}_2$ :MeOH (97:3) as eluent to furnish compounds **GC6** (31.1 mg), **GC21** (1.4 mg), and **GC22** (1.7 mg). A separation technique using chromatotron

was employed to obtain compounds **GC23** (7.2 mg) and **GC24** (11.6 mg) from subfraction D6.4 (45.3 mg) with eluent system of CH<sub>2</sub>Cl<sub>2</sub>:MeOH (97:3). Subfraction D6.5 (85.4 mg) was applied to chromatotron with CH<sub>2</sub>Cl<sub>2</sub>:MeOH (97:3) as eluent to give compounds **GC25** (14.4 mg) and **GC26** (15.5 mg). Compound **GC27** (14.0 mg) was afforded using chromatotron with hexanes:EtOAc (70:30) as eluent from subfraction D6.6 (41.0 mg).

Fraction D7 (204.3 mg) was separated by Sephadex LH-20 CC (50.0 g) with CH<sub>2</sub>Cl<sub>2</sub>:MeOH (1:1, v/v) as eluent to obtain five subfractions (D7.1–D7.5). A chromatotron technique using eluent system of CH<sub>2</sub>Cl<sub>2</sub>:MeOH (97:3) was performed to obtain compounds **GC28** (1.4 mg) and **GC29** (1.7 mg) from subfraction D7.1 (17.2 mg) and compound **GC2** (5.8 mg) from subfraction D7.4 (24.5 mg). The same separation technique was conducted to afford compounds **GC30** (20.4 mg) and **GC31** (7.6 mg) from subfraction D7.2 (80.8 mg) using hexanes:EtOAc (60:40) as eluent. Subfraction D7.3 (56.2 mg) was applied on Sephadex LH-20 CC (25.0 g) with CH<sub>2</sub>Cl<sub>2</sub>:MeOH (1:1, v/v) as eluent to get compound **GC32** (7.7 mg). Finally, fraction D8 (92.1 mg) was separated using Sephadex LH-20 CC (50.0 g) with CH<sub>2</sub>Cl<sub>2</sub>:MeOH (1:1, v/v) to obtain compounds **GC33** (10.5 mg) and **GC34** (18.9 mg).

#### 2.2.4. Cytotoxicity Assay

Compounds **GC1–GC34** were tested to *in vitro* cytotoxic evaluation against KB, HeLa S-3, MCF-7, Hep G2, and HT-29 cancer cell lines using MTT colorimetric method as previously described [113]. Doxorubicin was used as the positive control. The 3-(4,5-dimethylthiazol-2-yl)-2,5-diphenyl-tetrazolium bromide (Sigma Chemical Co., USA) was dissolved in saline to make a 5 mg/mL stock solution. Cancer cells (3 × 10<sup>3</sup> cells) suspended in 100 µg/wells of MEM medium containing 10% fetal calf serum (FCS, Gibco BRL, Life Technologies, NY, USA) were seeded onto a 96-well culture plate (Costar, Corning Incorporated, NY 14831, USA). After 24 h of pre-

incubation at 37 °C in a humidified atmosphere of 5% CO<sub>2</sub>/95% air to allow cellular attachment, various concentrations of test solution (10 μL/well) were added and these were then incubated for 72 h under the above conditions. At the end of the incubation, 10 μL of tetrazolium reagent was added into each well followed by further incubation at 37 °C for 4 h. The supernatant was decanted, and DMSO (100 μL/well) was added to allow formazan solubilization. The optical density (OD) of each well was detected using a Microplate reader at 550 nm and for correction at 595 nm. The 50% inhibition concentration (IC<sub>50</sub> value) was determined by curve fitting.

### 2.3. Results and discussion

The CH<sub>2</sub>Cl<sub>2</sub>-soluble fraction from the stems of *G. cylindrocarpa* was subjected to various chromatographic methods to afford four new xanthenes, cylindroxanthenes D–G (**GC1–GC4**), and two new biphenyls, cylindrobiphenyls A and B (**GC5** and **GC6**), along with 28 previously described xanthenes and biphenyls (**GC7–GC34**). The structures of the new compounds were elucidated using extensive spectroscopic analyses. The known compounds (Figure 2.3) were identified as trapezifolixanthone (**GC7**) [114], cylindroxanthone A (**GC8**) [13], 1,2-dihydro-5-hydroxy-10-methoxy-1,1,2-trimethyl-6*H*-furo[2,3-*c*]xanthen-6-one (**GC9**) [115], 6-hydroxy-11-methoxy-2,2-dimethyl-3*H*,7*H*-pyrano[2,3-*c*]xanthen-7-one (**GC10**) [115], 6-desoxyjacareubin (**GC11**) [116], 6-desoxyisojacareubin (**GC12**) [117], 1,6-dihydroxy-5-methoxy-6,6-dimethylpyrano[2',3':2,3]-xanthone (**GC13**) [118], pancixanthone B (**GC14**) [119], cylindroxanthone B (**GC15**) [13], osajaxanthone (**GC16**) [120], 1,3,5-trihydroxy-2-prenylxanthone (**GC17**) [116],  $\alpha$ -mangostin (**GC18**) [121], garciosine A (**GC19**) [53], garciocine C (**GC20**) [53], 2,3-dihydro-4,7-dihydroxy-2(1-hydroxy-1-methylethyl)-5*H*-furo[3,2-*b*]xanthen-5-one (**GC21**) [122], 1,3,5-trihydroxy-4-prenylxanthone (**GC22**) [117], 2-deprenylrheediaxanthone B (**GC23**) [123], 1,3,5-

trihydroxy-4-(3'-hydroxy-3'-methylbutyl)xanthone (**GC24**) [117], 4',5'-dihydro-1,6,7-trihydroxy-4',4',5'-trimethyl-furano[2',3':3,4]xanthone (**GC25**) [124], neriifolone C (**GC26**) [125], 1,3,5-trihydroxyxanthone (**GC27**) [126], garcimangosxanthone E (**GC28**) [127], 11-hydroxy-1-isomangostin (**GC29**) [128], garcinone D (**GC30**) [129], cratoxylone (**GC31**) [129], 1,3,7-trihydroxy-2-(3-hydroxy-3-methylbutyl)-9*H*-xanthen-9-one (**GC32**) [130], 1,3,5,6-tetrahydroxyxanthone (**GC33**) [128], and 1,3,6,7-tetrahydroxyxanthone (**GC34**) [126] after comparing their  $^1\text{H}$  and  $^{13}\text{C}$  NMR spectroscopic data with previously published data.

### 2.3.1. Structural elucidation of compound **GC1**

*Physical and spectroscopic properties of cylindroxanthone D (GC1):* Yellow needles; mp: 264–266 °C; UV (MeOH)  $\lambda_{\text{max}}$ : 328, 260, and 213 nm; IR  $\nu_{\text{max}}$  (KBr): 3295, 2929, 1657, 1440, and 1255  $\text{cm}^{-1}$ ; for  $^1\text{H}$  (400 MHz, acetone- $d_6$ ) and  $^{13}\text{C}$  (100 MHz, acetone- $d_6$ ) NMR spectroscopic data, see Table 2.1; and HRESIMS  $m/z$  311.0937 [ $\text{M} - \text{H}$ ] $^-$  (calcd. for  $\text{C}_{18}\text{H}_{15}\text{O}_5$ , 311.0919).

Compound **GC1** was isolated as yellow needles. The molecular formula was deduced as  $\text{C}_{18}\text{H}_{16}\text{O}_5$  based on HRESIMS data ( $m/z = 311.0937$  [ $\text{M} - \text{H}$ ] $^-$ , calcd. for  $\text{C}_{18}\text{H}_{15}\text{O}_5$ , 311.0919). The UV spectrum showed absorption bands at  $\lambda_{\text{max}}$  328, 260, and 213 nm, which were characteristic absorbances of a xanthone chromophore. The IR spectrum exhibited strong bands at 3295 and 1657  $\text{cm}^{-1}$ , assigned the presence of hydroxy group and conjugated carbonyl group [117]. The  $^1\text{H}$  NMR spectrum (Table 2.1) exhibited resonances of two *gem*-dimethyl protons at  $\delta_{\text{H}}$  1.39 (each 3H, s, H-4' and H-5'), two sets of methylene protons at  $\delta_{\text{H}}$  1.93 (2H, t,  $J = 6.8$  Hz, H-2') and 2.94 (2H, t,  $J = 6.8$  Hz, H-1'), one aromatic proton at  $\delta_{\text{H}}$  6.15 (1H, s, H-2), and an intramolecular hydrogen-bonded hydroxy group at  $\delta_{\text{H}}$  12.73 (1H, s, 1-OH). Moreover, a characteristic spin system of a 1,2,3-trisubstituted benzene moiety in ring B were observed at  $\delta_{\text{H}}$  7.28 (1H, t,  $J = 8.0$  Hz, H-7), 7.38 (1H, d,  $J = 8.0$  Hz, H-6) and 7.69 (1H,

d,  $J = 8.0$  Hz, H-8), which was further corroborated by COSY correlations of H-6/H-7 and H-7/H-8. The  $^{13}\text{C}$  NMR and HSQC experiments displayed 18 carbon signals, including two methyls at  $\delta_{\text{C}}$  27.0 (C-4') and 27.0 (C-5'), two methylenes at  $\delta_{\text{C}}$  17.0 (C-1') and 32.4 (C-2'), four methines at  $\delta_{\text{C}}$  99.9 (C-2), 116.6 (C-8), 121.8 (C-6), and 125.0 (C-7), nine quaternary carbons at  $\delta_{\text{C}}$  77.3 (C-3'), 101.4 (C-4), 104.2 (C-9a), 122.5 (C-8a), 146.5 (C-10a), 147.2 (C-5), 155.6 (C-4a), 162.0 (C-1), and 162.7 (C-3), and one carbonyl carbon at  $\delta_{\text{C}}$  181.9 (C-9). The  $^1\text{H}$  and  $^{13}\text{C}$  NMR data of **GC1** were closely related to 6-desoxyisojacareubin (**GC12**), except for the double bond of a pyran moiety in **GC12** was reduced to be dihydropyran unit in **GC1**. The COSY correlation of H-1'/H-2' and the HMBC cross-peaks of H-1' with C-3 ( $\delta_{\text{C}}$  162.7), C-4 ( $\delta_{\text{C}}$  101.4), C-4a ( $\delta_{\text{C}}$  155.6), C-2' ( $\delta_{\text{C}}$  32.4), and C-3' ( $\delta_{\text{C}}$  77.3), H-2' with C-4 and C-1' ( $\delta_{\text{C}}$  17.0), and H-4' and H-5' with C-2' and C-3' confirmed the presence of this unit which was fused at C-3 and C-4 with an ether linkage at C-3 (Figure 2.4). Consequently, **GC1** was a dihydro derivative of **GC12**.

### 2.3.2. Structural elucidation of compound GC2

*Physical and spectroscopic properties of cylindroxanthone E (GC2):* Yellow powder;  $[\alpha]_{\text{D}}^{20} + 8.3$  (c 0.50, MeOH); mp: 276–278 °C; UV (MeOH)  $\lambda_{\text{max}}$ : 316, 252, and 206 nm; IR  $\nu_{\text{max}}$  (KBr): 3256, 2900, 1630, 1454, and 1250  $\text{cm}^{-1}$ ; for  $^1\text{H}$  (400 MHz, acetone- $d_6$ ) and  $^{13}\text{C}$  (100 MHz, acetone- $d_6$ ) NMR spectroscopic data, see Table 2.1; and HRESIMS  $m/z$  327.0895  $[\text{M} - \text{H}]^-$  (calcd. for  $\text{C}_{18}\text{H}_{15}\text{O}_6$ , 327.0869).

Compound **GC2** was isolated as a yellow powder with a molecular formula of  $\text{C}_{18}\text{H}_{16}\text{O}_6$ , as suggested by HRESIMS data ( $m/z = 327.0895$   $[\text{M} - \text{H}]^-$ , calcd. for  $\text{C}_{18}\text{H}_{15}\text{O}_6$ , 327.0869). The  $^1\text{H}$  NMR data of **GC2** were closely related to **GC1**, except for the replacement of the  $-\text{CH}_2-\text{CH}_2-$  unit in the dihydropyran ring of **GC1** with a  $-\text{CH}(\text{OH})\text{CH}_2-$  moiety in **GC2** as deduced from the resonances of a set of methylene protons at  $\delta_{\text{H}}$  2.87 (1H, dd,  $J = 20.0, 11.2$  Hz) and 3.18 (1H, dd,  $J = 20.0, 5.2$  Hz), an oxygenated methine proton at  $\delta_{\text{H}}$  3.92 (1H, dd,  $J = 11.2, 5.2$  Hz), and a hydroxy

proton at  $\delta_{\text{H}}$  4.48 (1H, d,  $J = 5.2$  Hz) (Table 2.1). The position of the hydroxyl methine proton at C-2' was assigned by HMBC correlations of H-1' to C-2' ( $\delta_{\text{C}}$  69.0) and C-3' ( $\delta_{\text{C}}$  80.1) and H-4' at  $\delta_{\text{H}}$  1.41 (3H, s) and H-5' at  $\delta_{\text{H}}$  1.35 (3H, s) to C-2' and C-3' (Figure 2.4). The Mosher's method was applied to confirm the absolute configuration at C-2' by treating **2** with (*S*)-MTPACL and (*R*)-MTPACL [131]. Unfortunately, the NMR spectral data of the MTPA esters of **GC2** showed a mixture of the diastereomers. Therefore, **GC2** was a 2'-hydroxy derivative of **GC1**.

### 2.3.3. Structural elucidation of compound **GC3**

*Physical and spectroscopic properties of cylindroxanthone F (GC3)*: Yellow powder; UV (MeOH)  $\lambda_{\text{max}}$ : 333, 280, and 238 nm; IR  $\nu_{\text{max}}$  (KBr): 3280, 2910, 1655, 1438, and 1263  $\text{cm}^{-1}$ ; for  $^1\text{H}$  (400 MHz, acetone- $d_6$ ) and  $^{13}\text{C}$  (100 MHz, acetone- $d_6$ ) NMR spectroscopic data, see Table 2.1; and HRESIMS  $m/z$  267.0305  $[\text{M} - \text{H}]^-$  (calcd. for  $\text{C}_{15}\text{H}_7\text{O}_5$ , 267.0293).

Compound **GC3** was isolated as a yellow powder with a molecular formula  $\text{C}_{15}\text{H}_8\text{O}_5$  determined by HRESIMS ( $m/z = 267.0305$   $[\text{M} - \text{H}]^-$ , calcd. for  $\text{C}_{15}\text{H}_7\text{O}_5$ , 267.0293). The  $^1\text{H}$  and  $^{13}\text{C}$  NMR spectroscopic data were closely related to the structure of **GC1**, except that **GC3** possessed characteristic signals of a furan ring instead of dihydropyran moiety in **GC1**. In this respect, the 1D NMR (Table 2.1) and HSQC experiments showed resonances of two *cis*-olefinic protons at  $\delta_{\text{H}}$  7.38 (d, 1H,  $J = 1.6$  Hz, H-2')/ $\delta_{\text{C}}$  105.3 (C-2') and 7.87 (d, 1H,  $J = 1.6$  Hz, H-1')/ $\delta_{\text{C}}$  145.9 (C-1') [132]. The presence of this furan ring attached at C-3 and C-4 of ring A was further supported by COSY correlation of H-1'/H-2' and HMBC cross-peaks of H-1' with C-3 ( $\delta_{\text{C}}$  161.7), C-4 ( $\delta_{\text{C}}$  109.9), and C-2' and H-2' with C-3 and C-4 (Figure 2.4).



#### 2.3.4. Structural elucidation of compound GC4

*Physical and spectroscopic properties of cylindroxanthone G (GC4):* Yellow needles; mp: 135–136 °C; UV (MeOH)  $\lambda_{\max}$ : 344, 281 and 245 nm; IR  $\nu_{\max}$  (KBr): 3327, 2978, 2929, 1640, 1602, 1455 and 1196  $\text{cm}^{-1}$ ; for  $^1\text{H}$  (400 MHz,  $\text{CDCl}_3$ ) and  $^{13}\text{C}$  NMR (100 MHz,  $\text{CDCl}_3$ ) spectroscopic data, see Table 2.1; and HRESIMS  $m/z$  385.1291  $[\text{M} + \text{H}]^+$  (calcd. for  $\text{C}_{21}\text{H}_{21}\text{O}_7$ , 385.1287).

Compound **GC4** was obtained as yellow needles. A molecular formula of  $\text{C}_{21}\text{H}_{20}\text{O}_7$  was suggested by HRESIMS data ( $m/z = 385.1291$   $[\text{M} + \text{H}]^+$ , calcd. for  $\text{C}_{21}\text{H}_{21}\text{O}_7$ , 385.1287). The UV and IR spectra indicated a similar pattern as those of xanthone core structures [13]. Comparison of the  $^1\text{H}$  and  $^{13}\text{C}$  NMR data of **GC4** with those of **GC8** [13] showed the replacement of the proton signal of a methoxy group in **GC8** with that of an aromatic proton at  $\delta_{\text{H}}$  7.40 (1H, s) in **GC4** which was assigned as H-8 based on its HMBC correlations to C-6 ( $\delta_{\text{C}}$  150.3), C-7 ( $\delta_{\text{C}}$  148.4), C-8a ( $\delta_{\text{C}}$  116.1), C-9 ( $\delta_{\text{C}}$  180.2), and C-10a ( $\delta_{\text{C}}$  147.4) (Figure 2.4). From the above evidences and comparison with literature data, the structure of **GC4** was determined as cylindroxanthone G.

#### 2.3.5. Structural elucidation of compound GC5

*Physical and spectroscopic properties of cylindrobiphenyl A (GC5):* Pale yellow gum;  $[\alpha]_{\text{D}}^{20}$   $-17.2$  (c 0.70,  $\text{CHCl}_3$ ); UV (MeOH)  $\lambda_{\max}$ : 274 and 213 nm; IR  $\nu_{\max}$  (KBr): 3359, 1613, 1510, and 1463  $\text{cm}^{-1}$ ; for  $^1\text{H}$  (400 MHz,  $\text{CDCl}_3$ ) and  $^{13}\text{C}$  (100 MHz,  $\text{CDCl}_3$ ) NMR spectroscopic data, see Table 2.2; and HRESIMS  $m/z$  269.1190  $[\text{M} - \text{H}]^-$  (calcd. for  $\text{C}_{17}\text{H}_{17}\text{O}_3$ , 269.1178).

Compound **GC5** was obtained as pale-yellow gum. Its molecular formula was determined as  $\text{C}_{17}\text{H}_{18}\text{O}_3$  by HRESIMS measurement at  $m/z$  269.1190  $[\text{M} - \text{H}]^-$  (calcd. for  $\text{C}_{17}\text{H}_{17}\text{O}_3$ , 269.1178). The UV absorptions at  $\lambda_{\max}$  274 and 213 nm indicated the presence of benzene chromophore [133]. The IR spectrum showed absorption bands

of hydroxy group ( $3359\text{ cm}^{-1}$ ) and aromatic ring ( $1613\text{ cm}^{-1}$ ). Comparison of the  $^1\text{H}$  and  $^{13}\text{C}$  NMR data with those of **GC20** showed that **GC5** differed from **GC20** in the presence of a 2-hydroxy-3,3-dimethylpyran ring instead of a 2-(1,1-dimethyl-1-hydroxymethyl)dihydrofuran unit, which was characterized by resonances of two methyl protons at  $\delta_{\text{H}}$  1.33 (3H, s, H-5'')/ $\delta_{\text{C}}$  24.7 and 1.39 (3H, s, H-4'')/ $\delta_{\text{C}}$  22.4, a set of methylene protons at  $\delta_{\text{H}}$  2.75 and 2.95 (each 1H, dd,  $J = 17.2, 5.2\text{ Hz}$ , H-1'')/ $\delta_{\text{C}}$  26.3, one oxygenated methine proton at  $\delta_{\text{H}}$  3.86 (1H, t,  $J = 5.2\text{ Hz}$ , H-2'')/ $\delta_{\text{C}}$  69.5 and a quaternary carbon at  $\delta_{\text{C}}$  76.9 (Table 2.2). Attempts to determine the absolute configuration at C-2'' using the same Mosher's analysis as that of **GC2** were also unsuccessfully achieved due to a racemic mixture of **GC5**.

### 2.3.6. Structural elucidation of compound **GC6**

*Physical and spectroscopic properties of cylindrobiphenyl B (GC6):* Pale yellow powder; mp: 101–102 °C; UV (MeOH)  $\lambda_{\text{max}}$ : 270, 231, and 206 nm; IR  $\nu_{\text{max}}$  (KBr): 3364, 1636, 1619, 1500, and  $1467\text{ cm}^{-1}$ ; for  $^1\text{H}$  (400 MHz,  $\text{CDCl}_3$ ) and  $^{13}\text{C}$  (100 MHz,  $\text{CDCl}_3$ ) NMR spectroscopic data, see Table 2.2; and HRESIMS  $m/z$  245.0827 [ $\text{M} - \text{H}$ ] $^-$  (calcd. for  $\text{C}_{14}\text{H}_{13}\text{O}_4$ , 245.0814).

Compound **GC6** was obtained as a pale-yellow powder. Its molecular formula was deduced as  $\text{C}_{14}\text{H}_{14}\text{O}_4$  by HRESIMS data ( $m/z = 245.0827$  [ $\text{M} - \text{H}$ ] $^-$ , calcd. for  $\text{C}_{14}\text{H}_{13}\text{O}_4$ , 245.0814). The  $^1\text{H}$  NMR spectroscopic data of **GC6** were observed to have similar features with those of **GC19**, except the absence of a methoxy proton signal and the replacement of proton signals of 4-substituted 1-hydroxy-2-methoxyphenyl ring with those of a para-disubstituted benzene ring at  $\delta_{\text{H}}$  6.88 (each 1H, d,  $J = 8.4\text{ Hz}$ , H-3'/H-5') and 7.42 (each 1H, d,  $J = 8.4\text{ Hz}$ , H-2'/H-6') in **GC6** (Table 2.2). The COSY spectrum showed correlations of aromatic protons H-2'/H-3' and H-5'/H-6' whereas the HMBC spectrum showed cross-peaks of H-2' and H-6' with C-4' ( $\delta_{\text{C}}$  155.3) and H-3' and H-5' with C-1' ( $\delta_{\text{C}}$  133.9) and C-4' (Figure 2.4). In agreement with the afore-

mentioned data, the structure of **GC6** was unambiguously assigned as cylindrobiphenyl B.

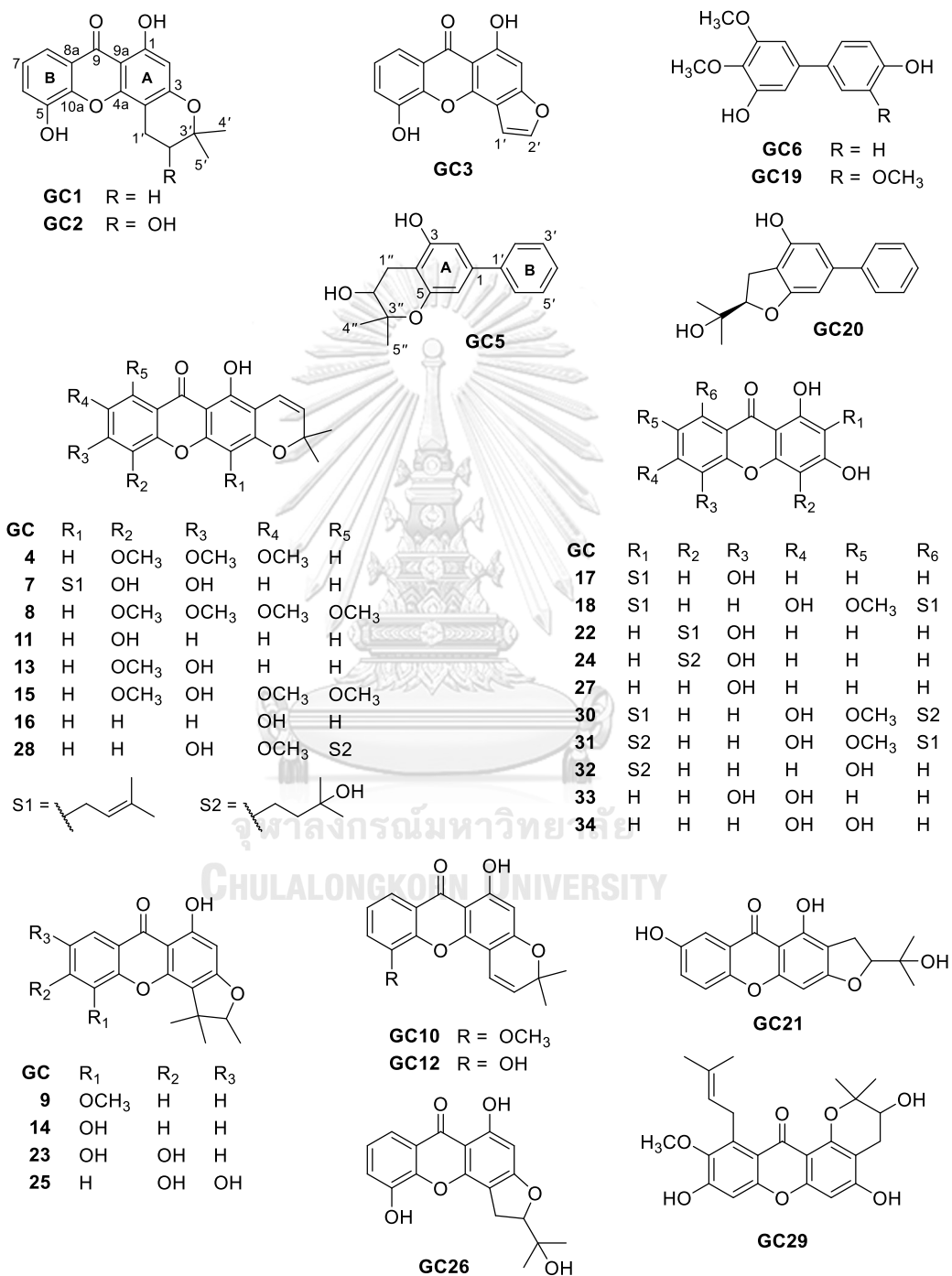


Figure 2.3. Isolated compounds (**GC1–GC34**) from the stems of *Garcinia cylindrocarpa*.

Table 2.1.  $^1\text{H}$  (400 MHz) and  $^{13}\text{C}$  (100 MHz) spectroscopic data of **GC1–GC3** in acetone- $d_6$  (in ppm) and **GC4** in  $\text{CDCl}_3$  ( $\delta$  in ppm)

Position	GC1		GC2		GC3		GC4	
	$\delta_{\text{H}}$ (J in Hz)	$\delta_{\text{C}}$	$\delta_{\text{H}}$ (J in Hz)	$\delta_{\text{C}}$	$\delta_{\text{H}}$ (J in Hz)	$\delta_{\text{C}}$	$\delta_{\text{H}}$ (J in Hz)	$\delta_{\text{C}}$
1		162.0		161.9		161.1		157.6
2	6.15 s	99.9	6.17 s	99.6	6.96 s	95.1		104.9
3		162.7		162.2		161.7		160.7
4		101.4		100.5		109.9	6.43 s	95.4
4a		155.6		155.8		152.4		157.2
10a		146.5		146.4		145.9		147.4
5		147.2		147.2		147.3		141.5
6	7.38 d (8.0)	121.8	7.38 dd (8.0, 1.2)	121.8	7.45 d (8.0)	122.2		150.3
7	7.28 t (8.0)	125.0	7.29 t (8.0)	125.1	7.38 t (8.0)	125.8		148.4
8	7.69 d (8.0)	116.6	7.69 dd (8.0, 1.2)	116.6	7.79 d (8.0)	116.8	7.40 s	100.5
8a		122.5		122.5		121.5		116.1
9		181.9		181.9		183.1		180.2
9a		104.2		104.4		106.3		104.2
1'	2.94 t (6.8)	17.0	2.87 dd (20.0, 11.2)	26.2	7.87 d (1.6)	145.9	6.73 d (10.0)	115.6
			3.18 dd (20.0, 5.2)					

Position	GC1		GC2		GC3		GC4	
	$\delta_H$ (J in Hz)	$\delta_C$	$\delta_H$ (J in Hz)	$\delta_C$	$\delta_H$ (J in Hz)	$\delta_C$	$\delta_H$ (J in Hz)	$\delta_C$
3'		77.3		80.1				78.4
4'	1.39 s	27.0	1.41 s	25.9			1.48 s	28.6
5'	1.39 s	27.0	1.35 s	21.4			1.48 s	28.6
1-OH	12.73 s		12.74 s				13.19 s	
2'-OH			4.48 d (5.2)					
5-OMe							4.04 s	62.1
6-OMe							3.96 s	56.4
7-OMe							4.06 s	61.7

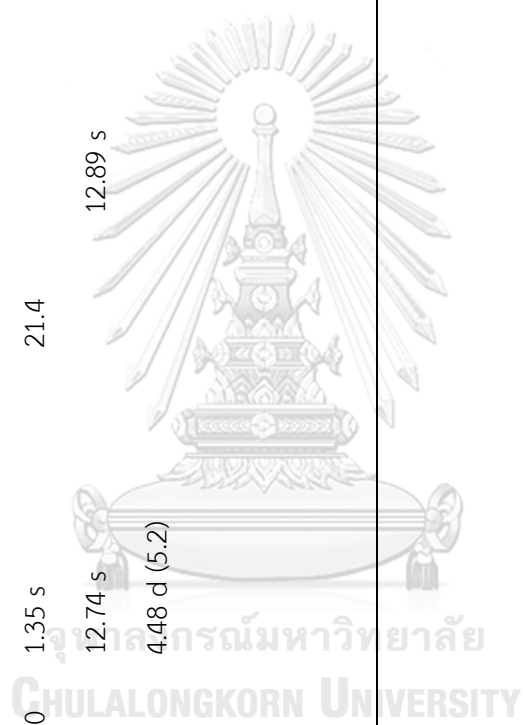


Table 2.2.  $^1\text{H}$  (400 MHz) and  $^{13}\text{C}$  (100 MHz) spectroscopic data of compounds **GC5** and **GC6**

Position	<b>GC5</b> (in $\text{CDCl}_3$ )		<b>GC6</b> (in $\text{CDCl}_3$ )	
	$\delta_{\text{H}}$ ( $J$ in Hz)	$\delta_{\text{C}}$	$\delta_{\text{H}}$ ( $J$ in Hz)	$\delta_{\text{C}}$
1		141.3		137.4
2	6.60 s	106.0	6.63 d (1.6)	103.2
3		154.9		152.6
4		105.8		134.9
5		154.2		149.5
6	6.71 s	108.6	6.78 d (1.6)	106.7
1'		140.7		133.9
2'	7.51 d (8.0)	127.0	7.42 d (8.4)	128.4
3'	7.38 t (8.0)	128.8	6.88 d (8.4)	115.7
4'	7.31 t (8.0)	127.5		155.3
5'	7.38 t (8.0)	128.8	6.88 d (8.4)	115.7
6'	7.51 d (8.0)	127.0	7.42 d (8.4)	128.4
1''	2.75 dd (17.2, 5.2)	26.3		
	2.95 dd (17.2, 5.2)			
2''	3.86 t (5.2)	69.5		
3''		76.9		
4''	1.39 s	22.4		
5''	1.33 s	24.7		
5-OH			5.83 brs	
4'-OH			5.04 brs	
3-OMe			3.92 s	56.1
4-OMe			3.93 s	61.2

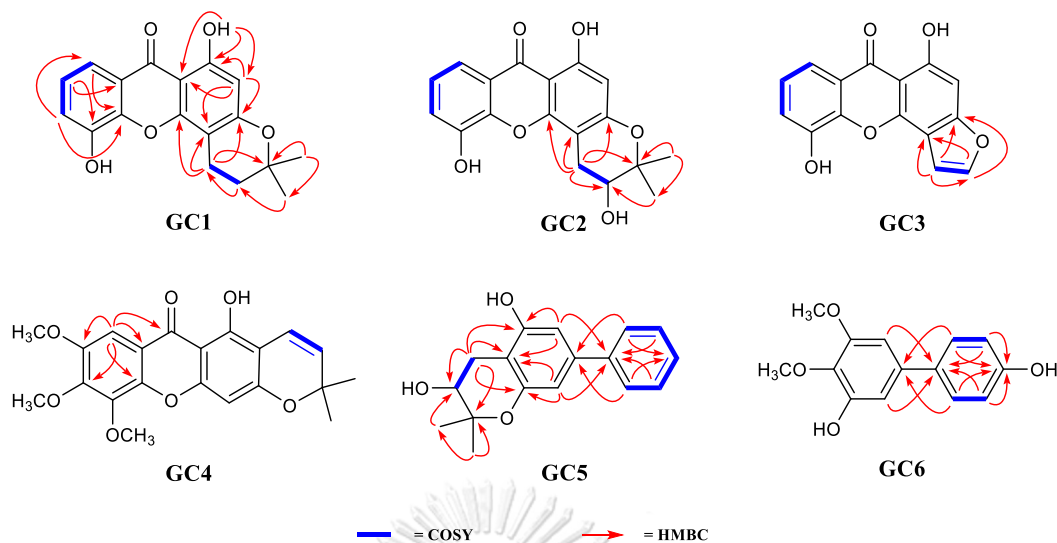


Figure 2.4. Key COSY and HMBC correlations of **GC1–GC6**.

### 2.3.7. Cytotoxic activities of the isolated compounds

Xanthenes and biphenyls isolated from plants were well known to exhibit cytotoxic activities against cancer cells and some of which were reported to have a remarkable cytotoxicity [28, 127, 134]. Moreover, our previous works showed that cylindroxanthone A (**GC8**), 6-desoxyjacareubin (**GC11**), and cylindroxanthone B (**GC15**) isolated from two *Garcinia* species displayed moderate to good cytotoxicity against several human cancer cells [13, 21]. Thus, we evaluated the cytotoxicity of compounds **GC1–GC34** against KB and HeLa S-3 cancer cell lines using modified MTT method [113]. Seven compounds (**GC14**, **GC22**, **GC23**, **GC25**, **GC31**, **GC33**, and **GC34**) with  $IC_{50}$  values lower than  $30 \mu\text{M}$  against these two cancer cells were selected to further investigate their cytotoxicity against MCF-7, Hep G2, and HT-29 cancer cell lines. The results are summarized in Table 2.3. The tested compounds mostly showed moderate to inactive against KB and HeLa S-3 cells. However, a potent cytotoxicity was observed for compound **GC23** against four human cancer cell lines including KB, HeLa S-3, MCF-7, and Hep G2 with  $IC_{50}$  values of 3.41, 5.04, 2.20, and  $6.00 \mu\text{M}$ , respectively. In addition, compound **GC25** selectively showed good

cytotoxicity against MCF-7 cells with  $IC_{50}$  value of  $8.77 \mu M$  and compound **GC31** exhibited good cytotoxicity against HT-29 cells with  $IC_{50}$  value of  $9.18 \mu M$ . Structure-activity relationship studies (Figure 2.3 and Table 2.3) suggested that the presence of hydroxy groups at C-5 and C-6 of furanoxanthenes might be improved the cytotoxicity, as inferred from the comparison of their cytotoxicity with compounds **GC9**, **GC14**, **GC23**, and **GC25**. Among linear pyranoxanthenes (**GC4**, **GC7**, **GC8**, **GC11**, **GC13**, **GC15**, **GC16**, and **GC28**), only compound **GC8** selectively exhibited potent cytotoxicity against KB cell line with  $IC_{50}$  value of  $2.36 \mu M$  due to the methoxy groups which were fully substituted at B-ring.

Table 2.3. *In vitro* cytotoxicity of compounds **GC1–GC34**

Compound	$IC_{50}$ ( $\mu M$ ) $\pm$ SD				
	KB	HeLa S-3	MCF-7	Hep G2	HT-29
<b>GC1</b>	$47.06 \pm 0.29$	inactive	NT	NT	NT
<b>GC2</b>	$32.28 \pm 1.09$	$50.79 \pm 0.71$	NT	NT	NT
<b>GC3</b>	inactive	inactive	NT	NT	NT
<b>GC4</b>	inactive	inactive	NT	NT	NT
<b>GC5</b>	inactive	inactive	NT	NT	NT
<b>GC6</b>	inactive	inactive	NT	NT	NT
<b>GC7</b>	$35.20 \pm 0.88$	$38.08 \pm 0.04$	NT	NT	NT
<b>GC8</b>	$2.36 \pm 0.01$	$75.12 \pm 0.81$	$98.54 \pm 6.16$	$10.41 \pm 0.15$	$25.51 \pm 3.26$
<b>GC9</b>	inactive	inactive	NT	NT	NT
<b>GC10</b>	$73.24 \pm 0.43$	inactive	NT	NT	NT
<b>GC11</b>	$18.56 \pm 0.15$	$19.69 \pm 0.46$	$17.53 \pm 0.06$	$39.35 \pm 1.05$	$69.29 \pm 0.79$
<b>GC12</b>	$78.62 \pm 0.54$	inactive	NT	NT	NT
<b>GC13</b>	inactive	inactive	NT	NT	NT
<b>GC14</b>	$12.13 \pm 0.04$	$20.73 \pm 0.56$	$15.61 \pm 0.32$	$22.84 \pm 0.39$	inactive
<b>GC15</b>	$57.24 \pm 2.56$	$71.38 \pm 0.81$	inactive	$59.53 \pm 0.49$	inactive



Compound	IC <sub>50</sub> (μM) ± SD				
	KB	HeLa S-3	MCF-7	Hep G2	HT-29
<b>GC16</b>	inactive	inactive	NT	NT	NT
<b>GC17</b>	36.50 ± 0.44	59.28 ± 0.40	NT	NT	NT
<b>GC18</b>	36.83 ± 0.46	54.94 ± 0.58	NT	NT	NT
<b>GC19</b>	89.05 ± 3.11	95.25 ± 2.74	NT	NT	NT
<b>GC20</b>	inactive	inactive	NT	NT	NT
<b>GC21</b>	36.06 ± 0.78	32.41 ± 1.11	NT	NT	NT
<b>GC22</b>	22.65 ± 0.08	29.74 ± 1.22	28.59 ± 0.87	50.27 ± 0.47	39.43 ± 1.16
<b>GC23</b>	3.41 ± 0.08	5.04 ± 0.04	2.20 ± 0.05	6.00 ± 0.07	46.50 ± 0.45
<b>GC24</b>	39.93 ± 0.44	40.73 ± 0.48	NT	NT	NT
<b>GC25</b>	13.37 ± 0.17	16.09 ± 0.11	8.77 ± 0.30	11.65 ± 0.06	58.70 ± 1.08
<b>GC27</b>	73.15 ± 0.14	79.02 ± 0.17	NT	NT	NT
<b>GC28</b>	48.95 ± 1.57	43.94 ± 0.82	NT	NT	NT
<b>GC29</b>	inactive	inactive	NT	NT	NT
<b>GC30</b>	30.11 ± 0.54	23.91 ± 0.98	NT	NT	NT
<b>GC31</b>	13.43 ± 0.33	18.90 ± 0.37	32.40 ± 1.32	47.28 ± 1.25	9.18 ± 0.52
<b>GC32</b>	43.63 ± 0.54	44.06 ± 0.32	NT	NT	NT
<b>GC33</b>	21.69 ± 0.47	29.66 ± 0.46	20.93 ± 0.38	20.66 ± 0.26	inactive
<b>GC34</b>	11.31 ± 0.34	26.40 ± 0.28	21.77 ± 0.14	99.69 ± 0.36	77.86 ± 0.57
Doxorubicin	0.02 ± 0.01	0.13 ± 0.01	0.61 ± 0.06	1.07 ± 0.16	0.34 ± 0.07

Note: IC<sub>50</sub> ≤ 10 μM = good cytotoxicity, 10 μM < IC<sub>50</sub> ≤ 30 μM = moderate cytotoxicity, 30 μM < IC<sub>50</sub> ≤ 100 μM = weak cytotoxicity, IC<sub>50</sub> > 100 μM = inactive, NT = not tested.

### Chapter III

## Phytochemical and biological investigation of the stem bark of *Garcinia tetrandra*

### 3.1. Botanical and chemical aspects of *G. tetrandra*

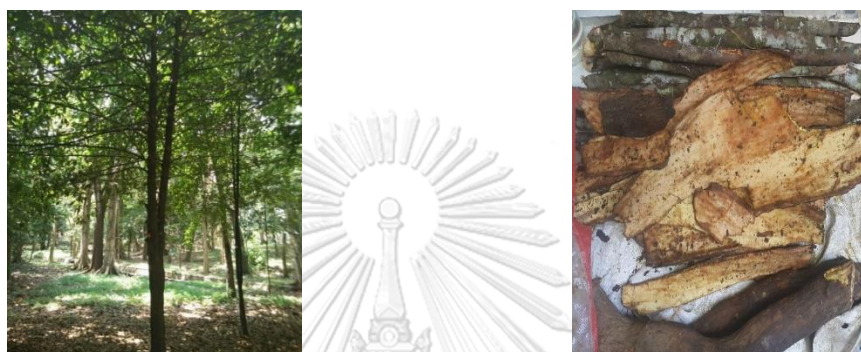


Figure 3.1. The whole plant, stem, and stem bark of *Garcinia tetrandra*.

Family	: Clusiaceae
Genus	: <i>Garcinia</i>
Species	: <i>Garcinia tetrandra</i>
Common name	: Kandis Watu
Local name	: Kandis Watu (Sulawesi Island), Laru (East Nusa Tenggara Province), Mapau (Maluku Island)

*Garcinia tetrandra* Pierre originally exist in Sulawesi, East Nusa Tenggara, and Maluku Islands and commonly named as Kandis Watu (Figure 3.1). In its natural habitat, it is found in tropical rainforest from 30–600 m altitudes and grows on clayey soil. The species is a medium-sized evergreen tree and can reach heights of 18 meter with a girth up to 30 cm. Its fruiting season starts from December to February and the woods are commonly utilized for building construction materials [15, 135].

Phytochemical studies on the stem bark of this species led to the isolation of several types of secondary metabolites such as xanthenes (**3.1–3.3**), polyprenylated benzophenones (**3.4** and **3.5**), and triterpenoids (**3.6–3.8**) (Figure 3.2) and some of them showed antioxidant and antibacterial activities [136].

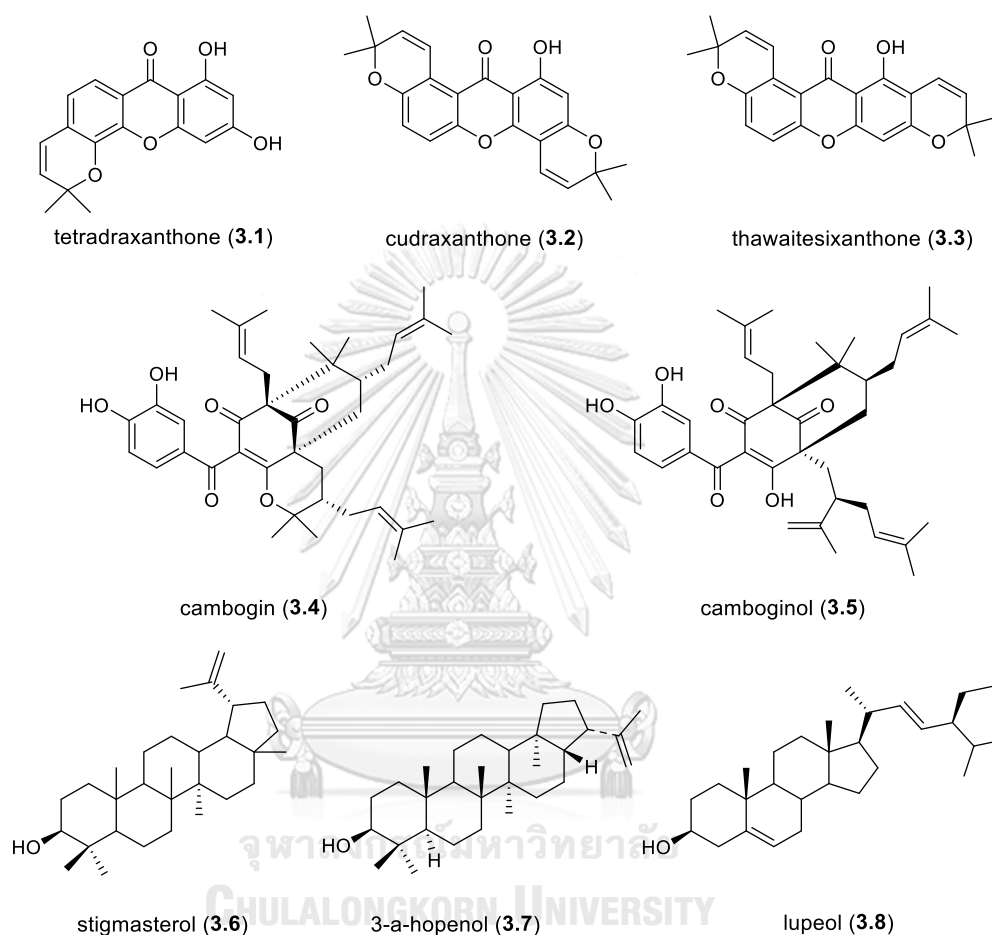


Figure 3.2. Isolated compounds (**3.1–3.8**) from the stem bark of *G. tetrandra*.

As part of our studies to explore novel and bioactive compounds from *Garcinia* species [21, 35, 137], a  $\text{CH}_2\text{Cl}_2$  extract from *G. tetrandra* stem bark was investigated. Herein, the separation, structural characterization, and cytotoxic evaluation of the isolated compounds (**GT1–GT31**) are described.

## 3.2. Experimental

### 3.2.1. General Experimental Procedures

The chromatographic materials and instruments information were the same to those previously reported [137, 138] and as described in Chapter II section 2.2.1. The experimental ECD data were recorded on a JASCO J-815 circular dichroism spectropolarimeter and Semi-preparative HPLC utilized a Waters Delta 600 instrument (Waters Corporation) with a Waters 2996 photodiode array detector using an Apollo C<sub>18</sub> 5  $\mu$ m, 250 x 10.0 mm column.

### 3.2.2. Plant Material

*Garcinia tetrandra* stem bark was collected from Baluran National Park, Banyuwangi, Indonesia (7°55'3" S 114°23'25" E) in November 2016. The plant material was identified by Mr. Deden Mudiana, and a voucher specimen of this plant (no. XVII.J.11.22) was deposited at Purwodadi Botanical Garden, Indonesia.

### 3.2.3. Extraction and Isolation

*G. tetrandra* stem bark (3.0 kg) was macerated with MeOH (each 15 L x 3 days). The filtrate was concentrated by a rotary evaporator to give a residue (71.0 g). The crude extract was suspended in water and partitioned with CH<sub>2</sub>Cl<sub>2</sub> and EtOAc to obtain a CH<sub>2</sub>Cl<sub>2</sub> and an EtOAc fractions. The dried CH<sub>2</sub>Cl<sub>2</sub> fraction (18.6 g) was separated to a quick column chromatography (QCC) separation on silica gel (500.0 g) with a gradient of hexanes-EtOAc (95:5–0:100) to yield seven fractions (A–G). Fraction B (3.5 g) was subjected to a Sephadex LH-20 column (50% CH<sub>2</sub>Cl<sub>2</sub>/MeOH) to afford subfractions B1–B3. Subfraction B2 (1.1 g) was subjected to a Chromatotron using hexanes-acetone (95:5) to give three subfractions (B2.1–B2.3). Subfraction B2.1 (17.2 mg) was separated by a Chromatotron using hexanes-acetone (95:5) to obtain **GT25** (7.4 mg). Subfraction B2.3 (78.4 mg) was separated on a Chromatotron using hexanes-

chloroform (60:40) to yield compound **GT1** (8.1 mg) and a subfraction that was further purified by semi-preparative HPLC using 100% CH<sub>3</sub>CN to give **GT2** (3.6 mg,  $t_R$  = 23.9 min) and **GT3** (4.6 mg,  $t_R$  = 22.7 min). Subfraction B3 (41.0 mg) was separated on a Chromatotron with hexanes-CH<sub>2</sub>Cl<sub>2</sub> (60:40) to obtain **GT26** (8.4 mg) and **GT28** (4.2 mg).

Fraction C (2.2 g) was separated on a Sephadex LH-20 column (50% CH<sub>2</sub>Cl<sub>2</sub>/MeOH) to obtain four subfractions (C1–C4). Subfraction C2 (43.0 mg) was then separated on a Chromatotron with hexanes-CH<sub>2</sub>Cl<sub>2</sub> (10:90) to afford compounds **GT10** (3.2 mg) and **GT11** (3.0 mg). Subfraction C3 (80.9 mg) was separated using a Chromatotron with hexanes-CH<sub>2</sub>Cl<sub>2</sub> (20:80) to yield **GT6** (2.9 mg) and **GT23** (4.1 mg). Subfraction C4 (65.5 mg) was subjected to a Sephadex LH-20 column (50% CH<sub>2</sub>Cl<sub>2</sub>/MeOH) to obtain **GT19** (6.6 mg) and **GT30** (5.0 mg). Fraction D (2.4 g) was passed through a Sephadex LH-20 column (50% CH<sub>2</sub>Cl<sub>2</sub>/MeOH) to give three subfractions (D1–D3). Subfraction D2 (67.1 mg) was purified using a Chromatotron by elution with 100% chloroform to afford **GT24** (8.9 mg). Subfraction D3 (482.4 mg) was then separated on a Chromatotron using hexanes-chloroform (1:1) to give subfractions D3.1–D3.4. Compounds **GT18** (2.8 mg) and **GT27** (2.1 mg) were obtained from subfraction D3.2 (18.9 mg) using a Chromatotron with hexanes-chloroform (1:1). Subfraction D3.3 (227.5 mg) was purified using a Chromatotron with hexanes-CH<sub>2</sub>Cl<sub>2</sub> (20:80) to afford **GT7** (4.1 mg), **GT8** (3.8 mg), **GT12** (8.4 mg), **GT15** (8.5 mg), and **GT31** (1.2 mg).

Fraction E (2.1 g) was separated on silica gel CC using CH<sub>2</sub>Cl<sub>2</sub>-MeOH (98:2) to obtain subfractions E1–E5. Compound **GT29** (13.1 mg) was purified from subfraction E1 (59.4 mg) by Sephadex LH-20 column using 50% CH<sub>2</sub>Cl<sub>2</sub>/MeOH. Compound **GT4** (5.2 mg) was purified from subfraction E2 (15.5 mg) using a Chromatotron with hexanes-acetone (30:70). Subfraction E3 (34.7 mg) was separated on a Chromatotron

with CH<sub>2</sub>Cl<sub>2</sub>-MeOH (30:1) to afford **GT5** (3.7 mg) and **GT9** (4.5 mg). Subfraction E4 (100.6 mg) was purified on a Chromatotron using hexanes-EtOAc (65:35) to obtain **GT13** (8.4 mg), **GT14** (2.9 mg), **GT16** (8.3 mg), and **GT17** (14.5 mg). Fraction F (507.1 mg) was subjected to a Sephadex LH-20 column (50% CH<sub>2</sub>Cl<sub>2</sub>/MeOH) to obtain four subfractions (F1–F4). Subfraction F3 (15.9 mg) was separated on a Chromatotron using CH<sub>2</sub>Cl<sub>2</sub>-MeOH (30:1) to yield **GT21** (6.1 mg). Compounds **GT20** (3.3 mg) and **GT22** (5.7 mg) were afforded from subfraction F4 (31.1 mg) by a Sephadex LH-20 column (50% CH<sub>2</sub>Cl<sub>2</sub>/MeOH).

#### 3.2.4. Cytotoxicity Assay

The isolated compounds (**GT1–GT31**) were tested for their cytotoxicity against Hep G2, HeLa S3, MCF-7, HT-29, and KB cell lines using an MTT colorimetric method with incubation of cells for 72 h [113], as previously described in Chapter II Section 2.2.4.

### 3.3. Results and discussion

Nine new xanthenes (**GT1–GT9**) and 22 known analogues (**GT10–GT31**) were isolated from the CH<sub>2</sub>Cl<sub>2</sub> extract of *G. tetrandra* stem bark through a series of chromatographic techniques (Figure 3.3). Comparison of NMR spectroscopic data with reported data led to the identification of the previously described xanthenes as isocowanin (**GT10**) [139], parvifolixanthone C (**GT11**) [51],  $\alpha$ -mangostin (**GT12**) [140], garcinone D (**GT13**) [129], xanthochymone A (**GT14**) [100], rubraxanthone (**GT15**) [139], parvixanthone G (**GT16**) [36], butyraxanthone D (**GT17**) [141], nigrolineaxanthone E (**GT18**) [142], euxanthone (**GT19**) [143], gentisein (**GT20**) [143], 1,3,6,7-tetrahydroxyxanthone (**GT21**) [126], 1,3,5,6-tetrahydroxyxanthone (**GT22**) [126], nitidaxanthone (**GT23**) [118], cylindroxanthone B (**GT24**) [13], cylindroxanthone A (**GT25**) [13], 9-hydroxycalabaxanthone (**GT26**) [144], macluraxanthone (**GT27**) [145],

3-isomangostin (**GT28**) [146], 3-isomangostin hydrate (**GT29**) [146], dihydroosajaxanthone (**GT30**) [147], and toxyloxanthone B (**GT31**) [148].

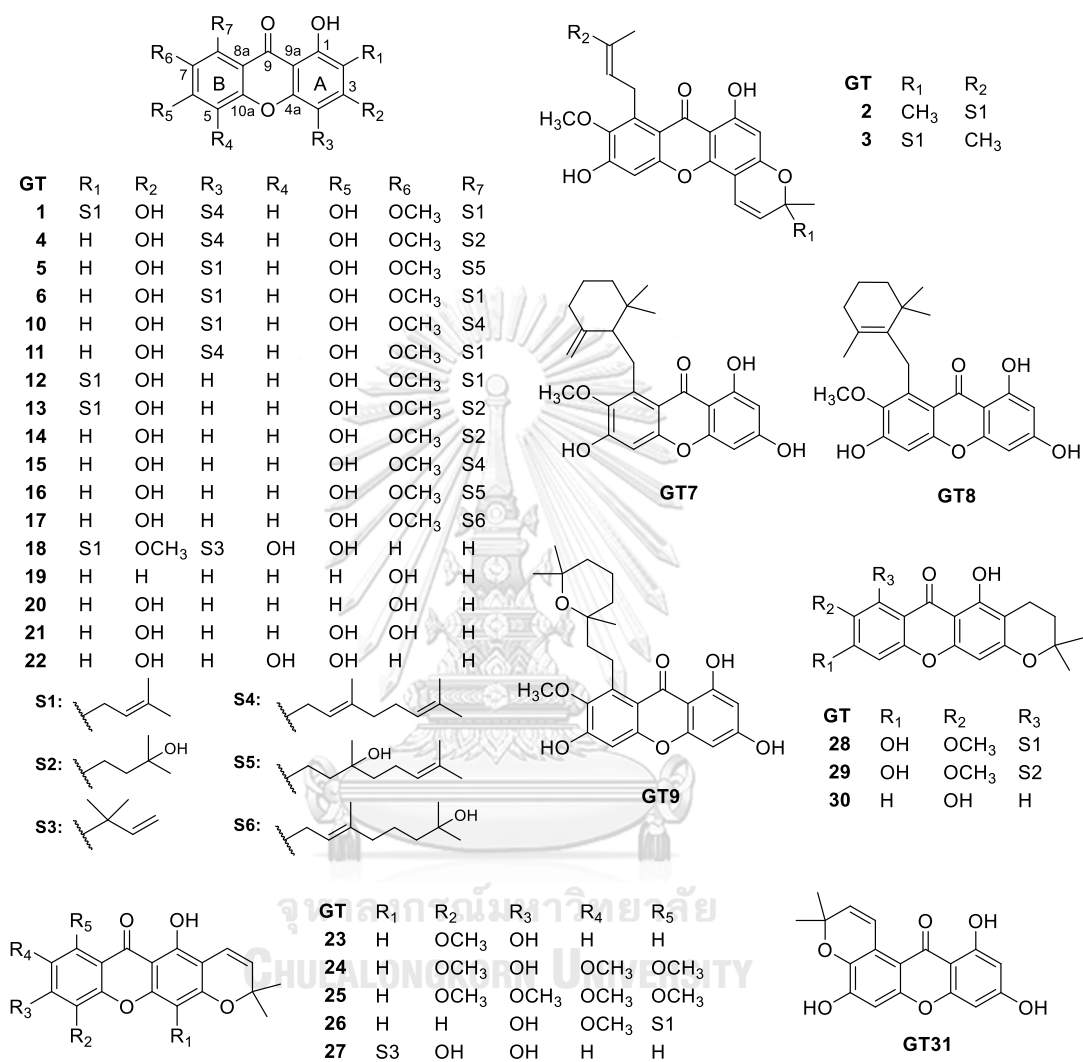


Figure 3.3. Structures of isolated xanthenes (**GT1–GT31**) from the stem bark of *G. tetrandra*.

### 3.3.1. Structural elucidation of compound GT1

*Physical and spectroscopic properties of tetrandraxanthone A (GT1):* Yellow gum; UV (MeOH)  $\lambda_{\text{max}}$  (log  $\epsilon$ ) 316 (4.26), 245 (4.15), 205 (4.19) nm; IR (KBr)  $\nu_{\text{max}}$  3427,

2922, 1635, 1620, 1579, 1462, 1296, 1159  $\text{cm}^{-1}$ ; 1D NMR data (Tables 3.1 and 3.2); and (–)-HRESIMS  $m/z$  545.2922  $[\text{M} - \text{H}]^-$  (calcd for  $\text{C}_{34}\text{H}_{41}\text{O}_6$ , 545.2903).

The (–)-HRESIMS analysis of tetrandraxanthone A (**GT1**) indicated a  $[\text{M} - \text{H}]^-$  peak at  $m/z$  545.2922, assigning to the molecular formula  $\text{C}_{34}\text{H}_{42}\text{O}_6$ . The  $^1\text{H}$  NMR spectrum indicated signals for a hydrogen-bonded hydroxy group at  $\delta_{\text{H}}$  13.68 (1H, s, OH-1), an aromatic methine proton at  $\delta_{\text{H}}$  6.85 (1H, s, H-5), and a methoxy group at  $\delta_{\text{H}}$  3.81 (3H, s, OCH<sub>3</sub>-7) (Table 3.1). A geranyl unit was identified from the resonances of two olefinic protons at  $\delta_{\text{H}}$  5.24 (1H, t,  $J = 6.8$  Hz, H-2'') and 5.05 (1H, t,  $J = 6.4$  Hz, H-6''), three methylene protons at  $\delta_{\text{H}}$  3.51 (2H, d,  $J = 6.8$  Hz, H-1''), 2.09 (2H, m, H-5''), and 2.03 (2H, m, H-4''), and three methyl groups at  $\delta_{\text{H}}$  1.86 (3H, s, H-10''), 1.64 (3H, s, H-8''), and 1.57 (3H, s, H-9''), which was also corroborated by the observed HMBC data (Figure 3.4). The remaining signals of two olefinic protons at  $\delta_{\text{H}}$  5.28 (1H, t,  $J = 6.8$  Hz, H-2') and 5.26 (1H, t,  $J = 6.0$  Hz, H-2'''), two methylene protons at  $\delta_{\text{H}}$  4.10 (2H, d,  $J = 6.0$  Hz, H-1''') and 3.45 (2H, d,  $J = 6.8$  Hz, H-1'), and four methyl groups at  $\delta_{\text{H}}$  1.84 (3H, s, H-5'''), 1.83 (3H, s, H-5'), 1.76 (3H, s, H-4'), and 1.68 (3H, s, H-4''') suggested the presence of two prenyl moieties. The 1D NMR data of **GT1** indicated that it has the same xanthone skeleton as cowagarcinone A [149], with the major differences being in the positions of geranyl and two prenyl units. The HMBC cross-peaks of H-1' with  $\delta_{\text{C}}$  158.7 (C-1), 109.0 (C-2), and 160.1 (C-3) and the deshielded H-1''' with  $\delta_{\text{C}}$  142.7 (C-7), 137.2 (C-8), and 112.2 (C-8a) confirmed unambiguously the positions of the two prenyl moieties at C-2 and C-8 (Figure 3.4). The attachment of the geranyl unit at C-4 in the A-ring was determined from the cross-peaks of H-1'' with  $\delta_{\text{C}}$  160.1 (C-3), 104.5 (C-4), and 152.2 (C-4a). The configuration of the  $\Delta^{2'',3''}$  alkene unit was determined as (2''*E*) according to  $^{13}\text{C}$  NMR data comparison with the geranyl unit of previously reported xanthenes [150], wherein in **GT1**, the resonance of the methylene carbon at C-4'' was more deshielded ( $\Delta\delta_{\text{C}} +8.0$ ), and that of the methyl carbon at C-10'' was more shielded ( $\Delta\delta_{\text{C}} -6.9$ ), than those of garcinianone B (with *Z* configuration).



Compound **GT1** was named tetrandraxanthone A, as shown in Figure 3.3. It is worth noting that the trivial name “tetrandraxanthone” has been used previously for a compound isolated from the title plant [136].

### 3.3.2. Structural elucidation of compound GT2

*Physical and spectroscopic properties of tetrandraxanthone B (GT2):* Brown gum; UV (MeOH)  $\lambda_{\max}$  (log  $\epsilon$ ) 329 (4.31), 244 (4.33), 212 (4.16) nm; IR (KBr)  $\nu_{\max}$  3399, 2926, 1651, 1600, 1575, 1464, 1286, 1176  $\text{cm}^{-1}$ ; 1D NMR data (Tables 3.1 and 3.2); and (–)-HRESIMS  $m/z$  475.2161  $[\text{M} - \text{H}]^-$  (calcd for  $\text{C}_{29}\text{H}_{31}\text{O}_6$ , 475.2121).

The (–)-HRESIMS analysis of tetrandraxanthone B (**GT2**) indicated a  $[\text{M} - \text{H}]^-$  peak at  $m/z$  475.2161, assigning to the molecular formula  $\text{C}_{29}\text{H}_{32}\text{O}_6$ . The  $^1\text{H}$  and  $^{13}\text{C}$  NMR data of **GT2** were nearly identical to those of isocowanin (**GT10**), except that the signals for the prenyl moiety in **GT10** were absent. The 1D NMR data combined with an HSQC experiment indicated signals for *cis*-olefinic protons at  $\delta_{\text{H}}/\delta_{\text{C}}$  6.77 (1H, d,  $J = 10.0$  Hz, H-1')/115.3 and 5.57 (1H, d,  $J = 10.0$  Hz, H-2')/127.0, *gem*-dimethyl groups at  $\delta_{\text{H}}/\delta_{\text{C}}$  1.47 (6H, s, H-4' and H-5')/28.4, and an oxygenated  $\text{sp}^3$  carbon at  $\delta_{\text{C}}$  78.1 (C-3'), revealing the presence of a dimethylpyran unit. The HMBC correlations of H-1' with C-3 ( $\delta_{\text{C}}$  160.1) and H-2' with C-4 ( $\delta_{\text{C}}$  100.5) indicated that this unit is fused at its ether linkage C-3 and C-4 in the A-ring (Figure 3.4).

### 3.3.3. Structural elucidation of compound GT3

*Physical and spectroscopic properties of tetrandraxanthone C (GT3):* Brown gum;  $[\alpha]_{\text{D}}^{20} +5.8$  (c 0.72,  $\text{CHCl}_3$ ); UV (MeOH)  $\lambda_{\max}$  (log  $\epsilon$ ) 321 (4.27), 258 (4.04), 210 (4.11) nm; IR (KBr)  $\nu_{\max}$  3400, 2926, 1649, 1579, 1465, 1278, 1217, 1157  $\text{cm}^{-1}$ ; 1D NMR data (Tables 3.1 and 3.2); and (–)-HRESIMS  $m/z$  475.2134  $[\text{M} - \text{H}]^-$  (calcd for  $\text{C}_{29}\text{H}_{31}\text{O}_6$ , 475.2121).

The (–)-HRESIMS analysis of tetrandraxanthone C (**GT3**) provided a  $[M - H]^-$  peak at  $m/z$  475.2134, indicating to the molecular formula  $C_{29}H_{32}O_6$ . Analysis of the 1D NMR data suggested that **GT3** has a scaffold similar to parvifolixanthone C (**GT11**). The notable differences were in the presence of *cis*-olefinic protons at  $\delta_H/\delta_C$  6.81 (1H, d,  $J = 10.0$  Hz, H-1')/115.7 and 5.52 (1H, d,  $J = 10.0$  Hz, H-2')/125.9 and an oxygenated  $sp^3$  carbon at  $\delta_C$  80.6 (C-3') in **GT3** instead of the C-1' methylene, C-2' olefinic methine, and C-3' quaternary  $sp^2$  carbon signals in **GT11**. The key COSY cross-peaks of H-1'/H-2' and H-4'/H-5' and HMBC cross-peaks from H-1' to C-3 ( $\delta_C$  160.5) and C-3', H-2' to C-4 ( $\delta_C$  100.3) and C-3', H-4' to C-2' and C-5' ( $\delta_C$  22.8), and H-10' to C-3' and C-4' ( $\delta_C$  41.8) indicated the geranyl unit at C-4 to be cyclized (Figure 3.4). The experimental ECD spectrum showed no Cotton effects, indicating that **GT3** was obtained as a racemic mixture.

#### 3.3.4. Structural elucidation of compound GT4

*Physical and spectroscopic properties of tetrandraxanthone D (GT4)*: Brown gum; UV (MeOH)  $\lambda_{max}$  ( $\log \epsilon$ ) 315 (4.26), 243 (4.34), 209 (4.10) nm; IR (KBr)  $\nu_{max}$  3392, 2920, 1645, 1612, 1579, 1462, 1429, 1296, 1153  $cm^{-1}$ ; 1D NMR data (Tables 3.1 and 3.2); and (–)-HRESIMS  $m/z$  495.2425  $[M - H]^-$  (calcd for  $C_{29}H_{35}O_7$ , 495.2383).

The (–)-HRESIMS analysis of tetrandraxanthone D (**GT4**) indicated a  $[M - H]^-$  peak at  $m/z$  495.2425, attributing to the molecular formula  $C_{29}H_{36}O_7$ . Comparison of the 1D NMR data of **GT4** with those of **GT11** suggested the principal difference to be the absence of resonances attributed to a prenyl unit in **GT11**. The signals of two methylene groups at  $\delta_H/\delta_C$  3.46 (2H, m, H-1'')/23.3 and 1.75 (2H, m, H-2'')/45.8, two methyl groups at  $\delta_H/\delta_C$  1.30 (6H, s, H-4'' and H-5'')/29.3, and one oxygenated  $sp^3$  carbon at  $\delta_C$  70.6 (C-3'') were observed instead. The COSY cross-peak of H-1''/H-2'' and key HMBC correlations from H-1'' to C-7 ( $\delta_C$  144.7), C-8 ( $\delta_C$  140.1), C-8a ( $\delta_C$  111.9), and C-2'', H-2'' to C-3'', and H-4''/H-5'' to C-3'' revealed the presence of a 3-hydroxy-3-

methylbut-1-yl fragment at C-8 (Figure 3.4). Thus, **GT4** was assigned as a hydrated derivative of **GT11**.

### 3.3.5. Structural elucidation of compound GT5

*Physical and spectroscopic properties of tetrandraxanthone E (GT5):* Brown gum;  $[\alpha]_D^{20} +1.2$  (c 0.40, MeOH); UV (MeOH)  $\lambda_{\max}$  (log  $\epsilon$ ) 320 (4.37), 241 (4.12), 208 (4.28) nm; IR (KBr)  $\nu_{\max}$  3395, 2922, 1643, 1616, 1580, 1465, 1292, 1150  $\text{cm}^{-1}$ ; 1D NMR data (Tables 3.1 and 3.2); and (–)-HRESIMS  $m/z$  495.2415  $[\text{M} - \text{H}]^-$  (calcd for  $\text{C}_{29}\text{H}_{35}\text{O}_7$ , 495.2383).

The (–)-HRESIMS analysis of tetrandraxanthone E (**GT5**) provided a  $[\text{M} - \text{H}]^-$  peak at  $m/z$  495.2415, indicating to the molecular formula  $\text{C}_{29}\text{H}_{36}\text{O}_7$ . The close NMR data similarities between **GT5** and **GT10** were evident, and these compounds differed only in the chemical shifts corresponding to the geranyl side chain at C-8. A methine group at  $\delta_{\text{H}}$  5.18 (1H, t,  $J = 6.8$  Hz, H-6'') and four methylene groups at  $\delta_{\text{H}}$  3.44 (2H, m, H-1''), 2.19 (2H, m, H-5''), 1.77 (2H, m, H-2''), and 1.58 (2H, m, H-4'') were observed in the  $^1\text{H}$  NMR spectrum, indicating that one of the double bonds in the geranyl unit is hydrated in **GT5**. The COSY correlations of H-1''/H-2'' and key HMBC correlations from H-1'' to C-7 ( $\delta_{\text{C}}$  144.7), C-8 ( $\delta_{\text{C}}$  140.2), and C-2'' ( $\delta_{\text{C}}$  43.7), H-4'' with an oxygenated  $\text{sp}^3$  carbon C-3'' ( $\delta_{\text{C}}$  72.5), and H-10'' with C-2'', C-3'', and C-4'' ( $\delta_{\text{C}}$  42.8) suggested that the double bond at position C-2'' was also hydrated (Figure 3.4). The ECD spectrum showed no Cotton effects, indicating that **GT5** was obtained to be racemic.

### 3.3.6. Structural elucidation of compound GT6

*Physical and spectroscopic properties of tetrandraxanthone F (GT6):* Brown gum; UV (MeOH)  $\lambda_{\max}$  (log  $\epsilon$ ) 316 (4.22), 244 (4.14), 210 (4.13) nm; IR (KBr)  $\nu_{\max}$  3423,

2924, 1641, 1610, 1583, 1458, 1280, 1162  $\text{cm}^{-1}$ ; 1D NMR data (Tables 3.1 and 3.2); and (–)-HRESIMS  $m/z$  409.1682  $[\text{M} - \text{H}]^-$  (calcd for  $\text{C}_{24}\text{H}_{25}\text{O}_6$ , 409.1651).

The (–)-HRESIMS analysis of tetrandraxanthone F (**GT6**) gave a  $[\text{M} - \text{H}]^-$  peak at  $m/z$  409.1682, assigning to the molecular formula  $\text{C}_{24}\text{H}_{26}\text{O}_6$ . The NMR spectroscopic data confirmed that **GT6** is a positional isomer of  $\alpha$ -mangostin (**GT12**), in which the prenyl moiety of **GT6** is attached at C-4. Confirmation for this hypothesis was obtained from the HMBC spectrum, wherein the methylene proton at  $\delta_{\text{H}}$  3.52 (2H, d,  $J = 6.4$  Hz, H-1') correlated with a quaternary carbon at  $\delta_{\text{C}}$  104.4 (C-4) and two oxygenated  $\text{sp}^2$  carbons at  $\delta_{\text{C}}$  161.1 (C-3) and 154.0 (C-4a) (Figure 3.4).

### 3.3.7. Structural elucidation of compound GT7

*Physical and spectroscopic properties of tetrandraxanthone G (GT7):* Brown gum;  $[\alpha]_{\text{D}}^{20} +3.2$  ( $c$  0.35, MeOH); UV (MeOH)  $\lambda_{\text{max}}$  ( $\log \epsilon$ ) 311 (4.05), 243 (4.16), 211 (4.25) nm; IR (KBr)  $\nu_{\text{max}}$  3429, 2922, 1643, 1606, 1579, 1467, 1298, 1161  $\text{cm}^{-1}$ ; 1D NMR data (Tables 3.1 and 3.2); and (–)-HRESIMS  $m/z$  409.1680  $[\text{M} - \text{H}]^-$  (calcd for  $\text{C}_{24}\text{H}_{25}\text{O}_6$ , 409.1651).

The (–)-HRESIMS analysis of tetrandraxanthone G (**GT7**) gave a  $[\text{M} - \text{H}]^-$  peak at  $m/z$  409.1680, attributing to the molecular formula  $\text{C}_{24}\text{H}_{26}\text{O}_6$ . The 1D NMR data of **GT7** resembled those of rubraxanthone (**GT15**), with two *meta*-coupled aromatic protons at  $\delta_{\text{H}}$  6.28 (1H, d,  $J = 2.0$  Hz, H-4) and 6.25 (1H, d,  $J = 2.0$  Hz, H-2), implying the presence of a 1,3-disubstituted A-ring. Key differences between **GT7** and **GT15** occurred for the resonances of the geranyl side chain at C-8. For **GT7**, 1D NMR data combined with HSQC correlations (Table 3.1 and 3.2) indicated characteristic signals for a terminal methylene unit at  $\delta_{\text{H}}/\delta_{\text{C}}$  4.31 and 3.84 (each 1H, s, H-10')/109.9, a benzylic methylene group at  $\delta_{\text{H}}/\delta_{\text{C}}$  3.81 (1H, H-1')/26.1 and 3.32 (1H, t,  $J = 11.6$  Hz, H-1')/26.1, a methine group at  $\delta_{\text{H}}/\delta_{\text{C}}$  2.24 (1H, dd,  $J = 11.6, 3.6$  Hz, H-2')/55.0, and three methylene groups at  $\delta_{\text{H}}/\delta_{\text{C}}$  2.36 (1H, td,  $J = 13.2, 5.2$  Hz, H-4')/31.2, 1.93 (1H, d,  $J =$

13.6 Hz, H-4')/31.2, 1.59 (1H, m, H-5')/23.4, 1.48 (1H, tt,  $J = 12.8, 4.0$  Hz, H-5')/23.4, 1.66 (1H, m, H-6')/35.2, and 1.29 (1H, m, H-6')/35.2, wherein the methylene group signals were mutually coupled according to the COSY cross-peaks of H-4'/H-5' and H-5'/H-6'. The remaining resonances attributed to two methyl groups were observed at  $\delta_{\text{H}}/\delta_{\text{C}}$  1.21 (3H, s, H-9')/28.3 and 0.90 (3H, s, H-8')/28.1. The above data, supported by HMBC cross-peaks of H-1' with C-8 ( $\delta_{\text{C}}$  138.3), H-2' with C-1', C-3' ( $\delta_{\text{C}}$  149.4), and C-7' ( $\delta_{\text{C}}$  34.9), H-8' and H-9' with C-2', C-6', and C-7', and H-10' with C-2', C-3', and C-4', indicated a 6,6-dimethyl-2-methylenecyclohexylmethyl unit (Figure 3.4). The presence of this unit was also corroborated by the similarity of the NMR data to those reported in a flavonoid named ugonin J [151]. The ECD spectrum of **GT7** presented no apparent Cotton effects, suggesting its occurrence as a racemate. Compound **GT7** was thus elucidated as a new xanthone bearing a cyclized geranyl unit, as shown in Figure 3.3.

### 3.3.8. Structural elucidation of compound **GT8**

*Physical and spectroscopic properties of tetrandraxanthone H (GT8):* Brown gum; UV (MeOH)  $\lambda_{\text{max}}$  (log  $\epsilon$ ) 309 (4.12), 243 (4.16), 207 (4.38) nm; IR (KBr)  $\nu_{\text{max}}$  3425, 2921, 1640, 1600, 1573, 1466, 1295, 1168  $\text{cm}^{-1}$ ; 1D NMR data (Tables 3.1 and 3.2); and (–)-HRESIMS  $m/z$  409.1671 [ $\text{M} - \text{H}$ ] $^{-}$  (calcd for  $\text{C}_{24}\text{H}_{25}\text{O}_6$ , 409.1651).

The (–)-HRESIMS data of tetrandraxanthone H (**GT8**) displayed a [ $\text{M} - \text{H}$ ] $^{-}$  peak at  $m/z$  409.1671, assigning to the molecular formula  $\text{C}_{24}\text{H}_{26}\text{O}_6$ . Hence, this compound was found to be isomeric with **GT7**. Detailed analysis of the 1D NMR data for **GT8** revealed the absence of the methine signal at C-2' and the resonances attributed to the  $\Delta^{3',10'}$  alkene unit in **GT7**, which were replaced by resonances of a methyl group at  $\delta_{\text{H}}/\delta_{\text{C}}$  1.27 (3H, s, H-10')/20.9 and two quaternary  $\text{sp}^2$  carbons at  $\delta_{\text{C}}$  135.5 (C-2') and  $\delta_{\text{C}}$  126.7 (C-3'). In addition, the signal of the methylene group at C-1' in **GT7** changed to a singlet at  $\delta_{\text{H}}$  4.32/ $\delta_{\text{C}}$  28.4 in **GT8**. The HMBC cross-peaks (Figure

3.4) of H-1' with C-2' and C-3', H-8'/H-9' with C-2', and H-10' with C-2', C-3', and C-4' ( $\delta_C$  34.8) indicated that the exocyclic double bond of **GT7** was replaced by an endocyclic double bond in **GT8** as depicted in Figure 3.3.

### 3.3.9. Structural elucidation of compound GT9

*Physical and spectroscopic properties of tetrandraxanthone I (GT9):* Pale yellow powder;  $[\alpha]_D^{20} +3.0$  (*c* 0.65, MeOH); UV (MeOH)  $\lambda_{\max}$  ( $\log \epsilon$ ) 313 (4.22), 245 (4.20), 210 (4.16) nm; IR (KBr)  $\nu_{\max}$  3392, 2920, 1645, 1612, 1579, 1462, 1429, 1296, 1153  $\text{cm}^{-1}$ ; 1D NMR data (Tables 3.1 and 3.2); and (–)-HRESIMS  $m/z$  427.1797  $[M - H]^-$  (calcd for  $\text{C}_{24}\text{H}_{27}\text{O}_7$ , 427.1757).

The (–)-HRESIMS analysis of tetrandraxanthone I (**GT9**) provided a  $[M - H]^-$  peak at  $m/z$  437.1210, attributing to the molecular formula  $\text{C}_{24}\text{H}_{26}\text{O}_6$ . The 1D NMR data confirmed the same xanthone moiety as for **GT7**, except for a modification of the side chain at C-8. The 1D NMR data showed signals of five methylene groups at  $\delta_H/\delta_C$  3.43 (2H, m, H-1')/22.9, 1.79 and 1.75 (each 1H, m, H-5')/17.5, 1.72 (2H, m, H-2')/45.9, 1.64 and 1.50 (each 1H, m, H-4')/35.4, and 1.50 and 1.40 (each 1H, m, H-6')/37.7, and three methyl groups at  $\delta_H/\delta_C$  1.34 (3H, s, H-10')/27.5,  $\delta_H/\delta_C$  1.22 (3H, s, H-8')/32.5 and 1.19 (3H, s, H-9')/29.9. The COSY cross-peak of H-1'/H-2' indicated that the two methylene groups at C-1' and C-2' were coupled. The presence of a dihydropyran ring substituted with *gem*-dimethyl groups at C-7' and a methyl group at C-3' was suggested by the COSY cross-peaks of H-4'/H-5' and H-5'/H-6', along with HMBC cross-peaks of H-4' with an oxygenated  $\text{sp}^3$  carbon C-3' ( $\delta_C$  74.0), H-8' and H-9' with C-6' and an oxygenated  $\text{sp}^3$  carbon C-7' ( $\delta_C$  71.6), and H-10' with C-3' and C-4' (Figure 3.4). The ring was connected to C-2', as deduced from the HMBC correlation of H-10' with C-2'. The experimental ECD spectrum showed no Cotton effects, indicating that **GT9** was obtained as a racemic mixture.

Table 3.1. <sup>1</sup>H NMR spectroscopic data (400 MHz) of compounds GT1–GT9 ( $\delta$  in ppm, *J* in Hz)

position	GT1 <sup>a</sup>	GT2 <sup>a</sup>	GT3 <sup>a</sup>	GT4 <sup>b</sup>	GT5 <sup>b</sup>	GT6 <sup>a</sup>	GT7 <sup>a</sup>	GT8 <sup>a</sup>	GT9 <sup>b</sup>
1									
2		6.21, s	6.20, s	6.29, s	6.29, s	6.24, s	6.25, d (2.0)	6.22, d (2.0)	6.19, d (2.4)
3									
4							6.28, d (2.0)	6.28, d (2.0)	6.31, d (2.4)
4a									
10a									
5	6.85, s	6.88, s	6.87, s	6.90, s	6.92, s	6.87, s	6.78, s	6.84, s	6.82, s
6									
7									
8									
8a									
9									
9a									
1'	3.45, d (6.8)	6.77, d (10.0)	6.81, d (10.0)	3.47, d (7.2)	3.47, d (7.2)	3.52, d (6.4)	3.81 <sup>c</sup>	4.32, s	3.43, m
2'	5.28, t (6.8) <sup>c</sup>	5.57, d (10.0)	5.52, d (10.0)	5.29, t (7.2)	5.27, t (7.2)	5.26, t (6.4)	2.24, dd (11.6, 3.6)		1.72, m <sup>c</sup>





position	GT1 <sup>a</sup>	GT2 <sup>a</sup>	GT3 <sup>a</sup>	GT4 <sup>b</sup>	GT5 <sup>b</sup>	GT6 <sup>a</sup>	GT7 <sup>a</sup>	GT8 <sup>c</sup>	GT9 <sup>b</sup>
4"	2.03, m	2.02, m	1.70, s	1.30, s	1.58, m	1.70, s			
5"	2.09, m	2.04, m	1.83, s	1.30, s	2.19, m	1.83, s			
6"	5.05, t (6.4)	5.02, t (6.4)			5.18, t (6.8)				
7"									
8"	1.64, s	1.60, s			1.67, s				
9"	1.57, s	1.54, s			1.87, s				
10"	1.86, s	1.82, s			1.30, s				
1"	4.10, d (6.0)								
2"	5.26, t (6.0) <sup>c</sup>								
3"									
4"	1.68, s								
5"	1.84, s								
OH-1	13.68, s	13.48, s	13.46, s	13.43, s	13.41, s	13.36, s	13.63, s	13.52, s	13.58, s
OH-3	6.32, s								6.07, brs
OH-6	6.40, brs	6.40, brs	6.37, brs						6.37, brs
OCH <sub>3</sub> -7	3.81, s	3.81, s	3.81, s	3.86, s	3.86, s	3.81, s	3.78, s	3.79, s	3.86, s

<sup>a</sup>In CDCl<sub>3</sub>. <sup>b</sup>In acetone-d<sub>6</sub>. <sup>c</sup>Overlapping signals.

Table 3.2.  $^{13}\text{C}$  NMR spectroscopic data (100 MHz) of compounds **GT1–GT9** ( $\delta$  in ppm)

position	GT1 <sup>a</sup>	GT2 <sup>a</sup>	GT3 <sup>a</sup>	GT4 <sup>b</sup>	GT5 <sup>b</sup>	GT6 <sup>a</sup>	GT7 <sup>a</sup>	GT8 <sup>a</sup>	GT9 <sup>b</sup>
1	158.7	163.5	163.5	162.5	162.6	161.8	164.2	164.1	165.1
2	109.0	99.3	99.1	98.4	98.5	98.6	98.3	98.4	98.9
3	160.1	160.1	160.5	162.9	163.0	161.1	162.4	162.4	165.6
4	104.5	100.5	100.3	106.4	106.5	104.4	93.4	93.4	93.9
4a	152.2	151.2	151.1	155.2	155.2	154.0	157.1	157.1	158.1
10a	154.6	154.8	154.8	156.6	156.7	154.8	154.4	154.7	156.5
5	101.7	101.7	101.8	102.8	102.9	101.7	101.4	102.0	102.7
6	155.9	155.8	155.8	157.7	157.7	156.0	156.1	155.9	157.7
7	142.7	143.0	143.0	144.7	144.7	142.9	144.0	143.9	144.8
8	137.2	137.4	137.4	140.1	140.2	137.3	138.3	139.5	140.6
8a	112.2	112.4	112.4	111.9	112.0	112.2	112.6	113.6	112.3
9	182.5	182.2	182.2	183.2	183.3	182.5	182.1	182.4	182.9
9a	103.7	103.9	103.8	104.0	104.1	104.2	104.1	104.2	103.9
1'	21.8	115.3	115.7	22.1	22.3	21.8	26.1	28.4	22.9
2'	122.0	127.0	125.9	123.6	123.6	121.6	55.0	135.5	45.9
3'	134.9	78.1	80.6	135.3	132.6	134.8	149.4	126.7	74.0
4'	26.0	28.4	41.8	40.5	26.0	26.0	31.2	34.8	35.4
5'	18.1	28.4	22.8	27.4	17.9	18.1	23.4	19.6	17.5
6'			124.0	125.1			35.2	41.1	37.7
7'			132.1	131.7			34.9	36.0	71.6
8'			26.0	25.8			28.1	28.8	32.5
9'			17.8	17.7			28.3	28.8	29.9
10'			27.2	16.5			109.9	20.9	27.5
1''	21.9	26.7	26.7	23.3	23.0	26.7			
2''	122.0	123.3	123.3	45.8	43.7	123.3			
3''	137.6	135.8	132.4	70.6	72.5	132.4			

position	GT1 <sup>a</sup>	GT2 <sup>a</sup>	GT3 <sup>a</sup>	GT4 <sup>b</sup>	GT5 <sup>b</sup>	GT6 <sup>a</sup>	GT7 <sup>a</sup>	GT8 <sup>a</sup>	GT9 <sup>b</sup>
4''	39.9	39.8	25.8	29.3	42.8	26.0			
5''	26.6	26.7	18.4	29.3	23.5	18.4			
6''	124.1	124.4			126.4				
7''	131.9	131.4			131.7				
8''	25.8	25.6			26.0				
9''	17.8	17.8			17.9				
10''	16.4	16.7			27.6				
1'''	26.7								
2'''	123.4								
3'''	132.2								
4'''	26.0								
5'''	18.4								
OCH <sub>3</sub> -7	62.2	62.2	62.2	61.7	61.8	62.3	62.0	61.5	61.7

<sup>a</sup>In CDCl<sub>3</sub>. <sup>b</sup>In acetone-*d*<sub>6</sub>.

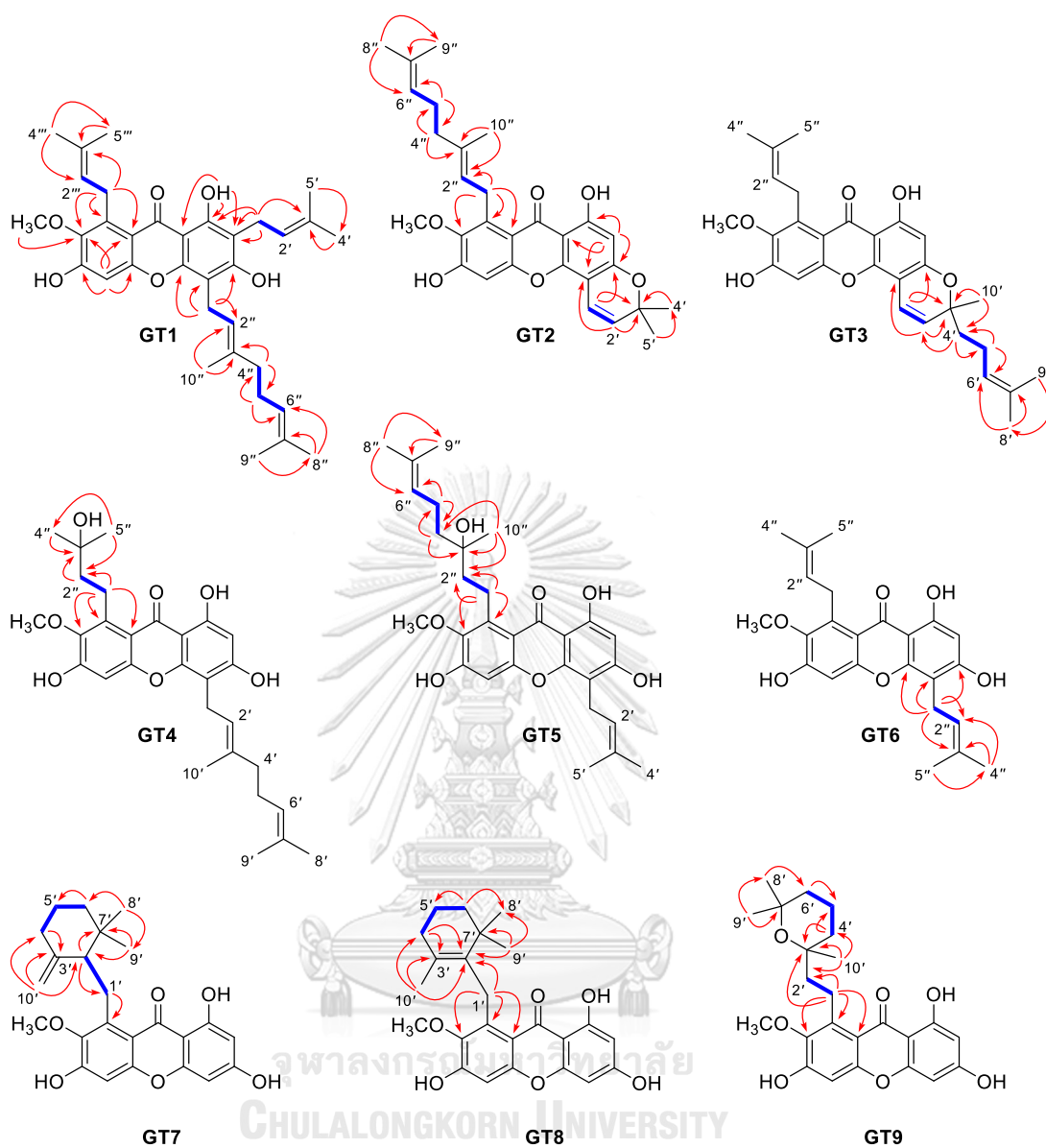


Figure 3.4. Key  $^1\text{H} - ^1\text{H}$  COSY (blue line) and HMBC (red arrow) correlations of tetrandraxanthones A-I (GT1-GT9).

### 3.3.10. Cytotoxic activities of the isolated compounds

Previous reports have revealed that prenylated and geranylated xanthenes isolated from plants, especially in the genus *Garcinia*, possess potent cytotoxic properties against several cancer cell lines [152-155]. Therefore, the isolated compounds, except for **GT12**, **GT13**, **GT18**, and **GT21–GT25**, which have been evaluated in this manner previously [13, 21, 137], were evaluated for their cytotoxic activity against HeLa S3 and KB cells. The active compounds (**GT5**, **GT10**, **GT11**, **GT26**, and **GT27**) with  $IC_{50}$  values lower than  $10 \mu\text{M}$  toward these two cancer cell lines were further evaluated against the other three cell lines, comprising Hep G2, HT-29, and MCF-7 cells. The results are shown in Table 3.3. Compound **GT26** significantly exhibited cytotoxic activities against five cancer cells with  $IC_{50}$  values in the range of  $1.64\text{--}3.39 \mu\text{M}$ . Compound **GT10** and its isomer **GT11** were cytotoxic toward HeLa S3, MCF-7, and KB cells with  $IC_{50}$  values of  $4.33\text{--}4.90 \mu\text{M}$ . Compound **GT5** exhibited selective cytotoxicity toward two cancer cells, MCF-7 and KB, with  $IC_{50}$  values of  $8.80$  and  $7.06 \mu\text{M}$ , whereas **GT27** was cytotoxic toward HeLa S3 and KB, with  $IC_{50}$  values of  $6.74$  and  $7.41 \mu\text{M}$ . Based on a preliminary structure-activity relationship (SAR) analysis, the hydration of pyran and prenyl units in the linear pyranoxanthenes **GT28** and **GT29** decreased their cytotoxic properties compared to **GT26**. Among the 1,3,6,7-tetraoxygenated xanthone derivatives with a geranyl side chain at C-8 (**GT2**, **GT5**, **GT7–GT10**, and **GT15–GT17**), only compound **GT10** was cytotoxic against three cancer cell lines (Table 3.3) due to the presence of unmodified geranyl units at C-8 and unmodified prenyl units at C-4.

Table 3.3. Cytotoxicity data of compounds **GT1–GT31**<sup>a</sup>

compound	IC <sub>50</sub> ± SD (μM)				
	KB	HeLa S3	MCF-7	Hep G2	HT-29
GT1	16.52 ± 0.37	18.35 ± 0.82	NT	NT	NT
GT2	51.91 ± 1.83	60.95 ± 1.87	NT	NT	NT
GT3	>100	>100	NT	NT	NT
GT4	55.36 ± 6.63	>100	NT	NT	NT
GT5	7.06 ± 0.44	15.43 ± 2.75	8.80 ± 0.65	21.91 ± 0.39	47.39 ± 1.40
GT6	14.28 ± 0.93	19.06 ± 1.74	NT	NT	NT
GT7	43.71 ± 0.26	64.03 ± 2.57	NT	NT	NT
GT8	>100	>100	NT	NT	NT
GT9	47.71 ± 2.74	79.40 ± 1.21	NT	NT	NT
GT10	7.26 ± 0.49	9.03 ± 0.13	6.99 ± 0.84	19.38 ± 0.57	46.07 ± 0.76
GT11	4.90 ± 0.33	5.79 ± 0.48	4.33 ± 0.61	13.87 ± 0.14	36.84 ± 0.99
GT12	NT	NT	NT	NT	NT
GT13	NT	NT	NT	NT	NT
GT14	43.16 ± 5.82	>100	NT	NT	NT
GT15	16.01 ± 0.92	34.40 ± 1.12	NT	NT	NT
GT16	25.52 ± 1.44	73.61 ± 5.79	NT	NT	NT
GT17	13.51 ± 0.85	46.33 ± 3.00	NT	NT	NT
GT18	NT	NT	NT	NT	NT
GT19	62.59 ± 9.74	87.27 ± 9.98	NT	NT	NT
GT20	45.03 ± 2.91	>100	NT	NT	NT
GT21	NT	NT	NT	NT	NT
GT22	NT	NT	NT	NT	NT
GT23	NT	NT	NT	NT	NT
GT24	NT	NT	NT	NT	NT
GT25	NT	NT	NT	NT	NT

compound	IC <sub>50</sub> ± SD (μM)				
	KB	HeLa S3	MCF-7	Hep G2	HT-29
<b>GT27</b>	7.41 ± 0.36	6.74 ± 0.28	13.64 ± 1.29	18.58 ± 0.13	47.17 ± 2.39
<b>GT28</b>	14.84 ± 0.27	16.19 ± 0.53	NT	NT	NT
<b>GT29</b>	12.41 ± 1.39	19.41 ± 1.17	NT	NT	NT
<b>GT30</b>	95.05 ± 3.48	>100	NT	NT	NT
<b>GT31</b>	>100	>100	NT	NT	NT
Doxorubicin <sup>b</sup>	0.01 ± 0.002	0.12 ± 0.134	0.49 ± 0.008	1.43 ± 0.182	0.34 ± 0.039

<sup>a</sup>Cytotoxicity was expressed as the mean values of three experiments ± SD; <sup>b</sup>Doxorubicin was used as the positive control.



## Chapter IV

### Phytochemical and biological investigation of the stem bark of *Garcinia picrorhiza*

#### 4.1. Botanical and chemical aspects of *G. picrorhiza*



Figure 4.1. The whole plant, branches, and leaves of *Garcinia picrorhiza*.

Family	: Clusiaceae
Genus	: <i>Garcinia</i>
Species	: <i>Garcinia picrorhiza</i>
Common name	: Sesoot
Local name	: Kayu Ambong, Laloit Ritek (Sulawesi Island), Daun Limon, Kayu Lemon, Sesoot (Maluku Island)

*Garcinia picrorhiza* Miq. is a woody plant that widely grow in Sulawesi, Maluku, and Papua Islands (Figure 4.1), with its origin in Hitu mountain and Laitimor Island, Maluku region. It is an evergreen tree distributed in lower and upper rainforest from 300 up to 2,100 m elevation and thrives on clayey and black soils. The species can reach heights of 18 meter with a girth up to 85 cm. The flowering and fruiting season start from February to August and September to January, respectively, and its



wood is commonly utilized for building construction materials. Local people called this species as “Sesoot” and they usually use a decoction of its roots as energy drinking and supplement [15, 156, 157]. Previous phytochemical investigations on the roots and the stem bark of this plant revealed the existence of several types of secondary metabolites, including 3-hydroxy-isonicotinic acid (4.1), two polyprenylated benzophenones (4.2 and 4.3), and three triterpenoids (4.4–4.6) (Figure 4.2) [156, 158-160].

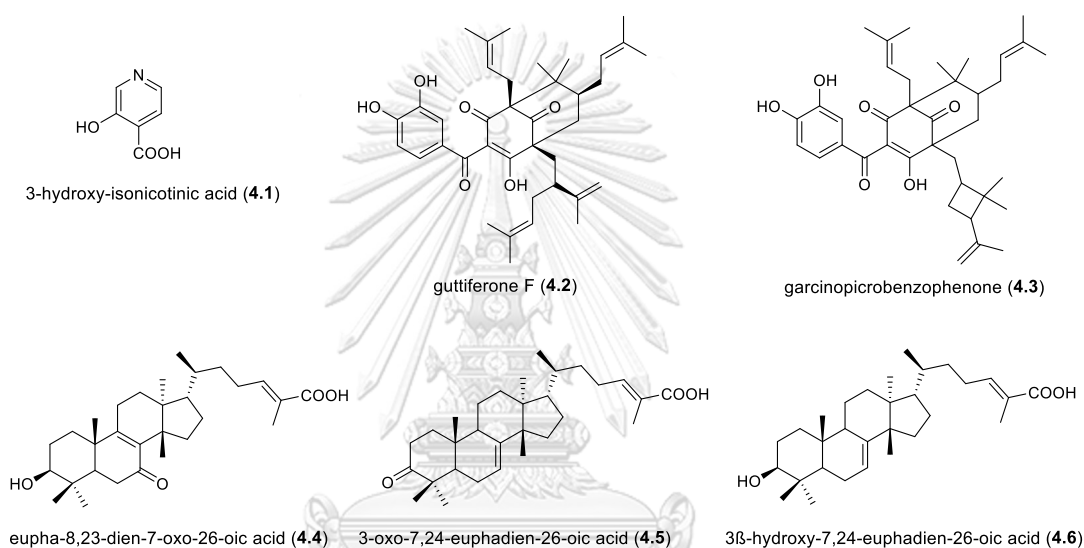


Figure 4.2. Isolated compounds (4.1–4.6) from the roots and the stem bark of *G. picrorhiza*.

จุฬาลงกรณ์มหาวิทยาลัย  
CHULALONGKORN UNIVERSITY

In the continuing search for novel bioactive substances in *Garcinia* plants [13, 35, 135, 137], the stem bark of *G. picrorhiza* was investigated leading to the isolation of known metabolite **GP9** and new picrorhizones A–H (**GP1–GP8**), along with three known benzoylphloroglucinols (**GP10–GP12**). Herein, the isolation and structural elucidation of the isolated compounds, as well as an *in vitro* cytotoxic evaluation of five human cancer cell lines using the MTT viability method and anti-inflammatory activity using COX-1 and COX-2 inhibitory assays are described.

## 4.2. Experimental

### 4.2.1. General Experimental Procedures

The chromatographic materials and instruments information were the same to those previously reported [137, 138] and as described in Chapter III section 3.2.1.

### 4.2.2. Plant Material

*Garcinia picrorhiza* stem bark material was collected from Bogor Botanical Garden, Bogor, Indonesia (6°35'51" S 106°47'55" E) in July 2016. The plant material was identified by Dr. Rismita Sari and a voucher specimen (No. VI.A.26) was deposited at Bogor Botanical Garden, Indonesia.

### 4.2.3. Extraction and Isolation

The air-dried stem bark of *G. picrorhiza* (3.0 kg) was extracted with MeOH (15 L each x 3 days) at room temperature. The solvent was evaporated under reduced pressure to obtain a residue (92.0 g). The crude MeOH extract was suspended in distilled water and partitioned with CH<sub>2</sub>Cl<sub>2</sub> and EtOAc to afford two organic extracts. The dried CH<sub>2</sub>Cl<sub>2</sub> extract (54.1 g) was subjected to silica gel column chromatography and eluted with hexanes/EtOAc (95:5–0:100) to afford fractions A–R. Fraction D (560.0 mg) was chromatographed on a Sephadex LH-20 column with CH<sub>2</sub>Cl<sub>2</sub>/MeOH (1:1) to obtain subfractions D1–D4. Subfraction D2 (51.6 mg) was subjected to a Chromatotron that was eluted with hexanes/CH<sub>2</sub>Cl<sub>2</sub> (90:10) to yield **GP3** (9.2 mg) and **GP12** (1.8 mg). Compound **GP9** (5.6 g) was isolated as a major component from fractions G (4.2 g) and H (5.1 g) after recrystallization using acetone/hexanes (1:2). Fractions I (708.3 mg) and J (556.0 mg) were subjected separately to a Sephadex LH-20 column with a CH<sub>2</sub>Cl<sub>2</sub>/MeOH (1:1) solvent system to give subfractions I1–I4 and J1–J3, respectively. Subfraction I1 (49.2 mg) was purified by a Chromatotron that was eluted with 100% CH<sub>2</sub>Cl<sub>2</sub> to give **GP2** (11.5 mg), while subfraction I2 (55.8 mg) was

chromatographed on an RP-C<sub>18</sub> silica gel column eluted with 70% CH<sub>3</sub>CN/H<sub>2</sub>O to afford **GP6** (5.7 mg). Subfraction J1 (10.3 mg) was purified on semipreparative HPLC using 93% MeOH/H<sub>2</sub>O to yield **GP10** (4.3 mg) and **GP11** (3.2 mg).

Fraction Q (3.3 g) was subjected to silica gel CC eluted with hexanes/EtOAc (75:25–20:80) to give three subfractions (Q1–Q3). Subfraction Q2 (640.2 mg) was separated on silica gel CC using 30% acetone/hexanes to give subfractions Q2.1 and Q2.2. Subfraction Q2.2 (67.5 mg) was separated on a Chromatotron eluted with CH<sub>2</sub>Cl<sub>2</sub>/MeOH (15:1) to afford **GP1** (14.6 mg). Subfraction Q3 (61.2 mg) was separated on a Chromatotron with CH<sub>2</sub>Cl<sub>2</sub>/MeOH (20:1) to afford **GP4** (8.7 mg) and **GP5** (4.2 mg). Fraction R (3.7 g) was subjected to silica gel CC that was eluted with hexanes/EtOAc (70:30–20:80) to give five subfractions (R1–R5). Compound **GP8** (6.0 mg) was purified from subfraction R2 (71.4 mg) using an RP-C<sub>18</sub> silica gel column that was eluted with 70% CH<sub>3</sub>CN/H<sub>2</sub>O, while **GP7** (6.7 mg) was obtained from subfraction R5 (52.6 mg) using Sephadex LH-20 with CH<sub>2</sub>Cl<sub>2</sub>/MeOH (1:1).

#### 4.2.4. X-ray crystallography of GP9

Light yellow single crystals of **GP9** were recrystallized from a mixture of acetone/hexanes (1:2, v/v) in the orthorhombic space group  $P2_12_12_1$  (no. 19) with the following unit cell parameters:  $a = 9.0232(4)$ ,  $b = 18.4443(9)$ ,  $c = 23.7543(11)$  Å,  $V = 3953.3(3)$  Å<sup>3</sup> for Mo-K $\alpha$  radiation;  $a = 9.0225(3)$ ,  $b = 18.3922(6)$ ,  $c = 23.8517(7)$  Å,  $V = 3958.0(2)$  Å<sup>3</sup> for Cu-K $\alpha$  radiation;  $Z = 4$ ;  $D_{\text{calc}} = 1.012$  g cm<sup>-3</sup>. Two diffraction data sets were collected from two crystals at 296(2) K on Bruker APEXII and PROSPECTOR CCD area-detector diffractometers (Mo-K $\alpha$  radiation,  $\lambda = 0.71073$  Å; Cu-K $\alpha$  radiation,  $\lambda = 1.54178$  Å) using the APEX2 Software Suite [161]. The data were processed according to a standard procedure, including integration with SAINT+, multi-scan absorption correction, and scaling by SADABS and then merging by XPREP, implemented in APEX2 Software Suite [161], yielding 7314 and 7201 unique reflections with  $R_{\text{int}} =$

0.0878 and 0.0571, respectively. Two structures were solved by the intrinsic phasing method with SHELXTL XT [162] and refined anisotropically by full matrix least-squares on  $F^2$  with SHELXTL XLMP [163]. The disordered solvents without direct interaction with **GP9** in large intermolecular interstices were removed using PLATON SQUEEZE procedure [164]. The structure refinement converged to final  $R_1 = 0.0612$  for 3657 data and  $R_1 = 0.0571$  for 6034 data with  $F^2 > 2\sigma(F^2)$  for the respective Mo-K $\alpha$  and Cu-K $\alpha$  radiations. The Flack parameter [165] of  $-0.02(12)$  was estimated using copper radiation. Data have been deposited with the Cambridge Crystallographic Data Centre (CCDC nos. 1945943 and 1978321). Copies of these data can be obtained, free of charge, on application to the CCDC via [www.ccdc.cam.ac.uk/conts/retrieving.html](http://www.ccdc.cam.ac.uk/conts/retrieving.html) (or 12 Union Road, Cambridge CB2 1EZ, UK, fax: +44 1223 336033, e-mail: [deposit@ccdc.cam.ac.uk](mailto:deposit@ccdc.cam.ac.uk)).

#### 4.2.5. ECD calculation of **GP6** and **GP9**

To determine the absolute configurations of **GP1–GP9**, ECD calculations using the DFT method were carried out, and the calculated ECD spectra were compared with those derived experimentally. Conformers of **GP6** and **GP9** were optimized by semiempirical PM3 calculation and were fully reoptimized with the DFT method at the B3LYP/6-31G(d) level. Subsequently, the ECD calculations were carried out using the TD-DFT method at the B3LYP/6-31+G(d,p) level with a PCM solvent model (MeOH) and  $n$  states = 50. All the calculations were performed with GAUSSIAN 09 [166] on a DELL PowerEdge T430 server. The ECD spectra were generated using SpecDis 1.71 [167] with  $\sigma = 0.5$ .

#### 4.2.6. Cytotoxicity Assay

The *in vitro* cytotoxic evaluation of compounds **GP1–GP12** against the KB, HeLa S3, HT-29, MCF-7, and Hep G2 cancer cell lines was performed using an MTT

colorimetric method by incubating cells for 72 h, as described previously [137]. The results are expressed as the mean values of three independent experiments. Doxorubicin was used as the positive control.

#### 4.2.7. Cyclooxygenase-1 and -2 Inhibition Assays

COX-1 and COX-2 inhibitory assays were performed in 96-well plate format using purified PGHS-1 from ram seminal vesicles for COX-1 and human recombinant PGHS-2 for COX-2 (Cayman Chemical Co., Ann Arbor, MI, USA), as reported previously [168]. Briefly, the incubation mixture contained 180  $\mu\text{L}$  of 0.1 M TRIS/HCl-buffer (pH 8.0), 50  $\mu\text{M}$   $\text{Na}_2\text{EDTA}$  (only for COX-2), 18mM L-epinephrine bitartrate, 5  $\mu\text{M}$  porcine hematin, and COX-1 or COX-2 enzymes (0.2 U/well). The tested compounds (**GP1–GP11**) dissolved in DMSO with a final concentration of 20  $\mu\text{M}$  were added and the mixture was pre-incubated for 5 mins at room temperature. After incubation, 10  $\mu\text{L}$  of 5  $\mu\text{M}$  arachidonic acid was added to the mixture and incubated for 20 mins at 37°C. The reaction was subsequently stopped by adding 10  $\mu\text{L}$  of 10% (v/v) formic acid. The concentration of  $\text{PGE}_2$  generated in the reaction was quantitatively measured by a competitive  $\text{PGE}_2$  ELISA kit (Enzo Life Sciences Inc., Farmingdale, NY, USA), according to the manufacturer's protocol and previous procedure [168]. The assays were performed in duplicates and repeated over two independent experiments. Indomethacin (1.25  $\mu\text{M}$ ) was dissolved in EtOH and used as the positive control for COX-1. Celecoxib (8.8  $\mu\text{M}$ ), which was used as the positive control for COX-2, was dissolved in DMSO [169].

#### 4.3. Results and discussion

The  $\text{CH}_2\text{Cl}_2$ -soluble fraction from a crude MeOH extract of stem bark from *G. picrorhiza* was separated to yield 12 compounds, including eight new benzoylphloroglucinols (**GP1–GP8**) bearing a cyclobutyl-containing side chain and

four known analogues (**GP9–GP12**). The structures of the known compounds were identified as garcinopicrobenzophenone (**GP9**) [158], 30-*epi*-cambogin (**GP10**) [170], isoxanthochymol (**GP11**) [171], and (+)-30-*epi*-13,14-didehydroxyisogarcinol (**GP12**) [172] through an analysis of their NMR spectroscopic data and comparison with literature data.

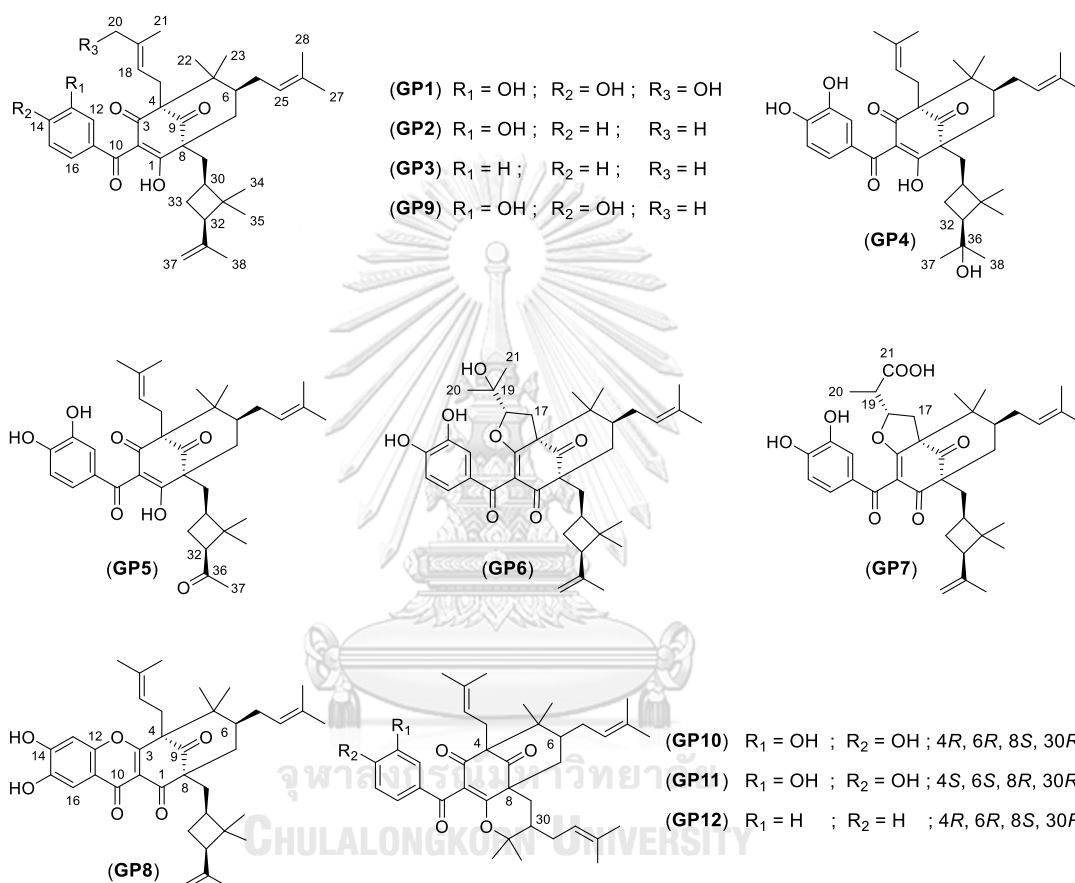


Figure 4.3. Benzoylphloroglucinols (**GP1–GP12**) from the stem bark of *G. picrorhiza*.

#### 4.3.1. Structural elucidation of compound GP1

*Physical and spectroscopic properties of picrorhizone A (GP1)*: Yellow gum;  $[\alpha]_D^{20} +27$  (c 0.10, MeOH); ECD (c 0.001, MeOH)  $\lambda_{\text{max}}$  ( $\Delta\epsilon$ ) 218 (–8.3), 259 (+13.3), 303 (–5.2), 326 (–2.4), 348 (–1.7) nm;  $^1\text{H}$  (400 MHz, methanol- $d_4$ ) and  $^{13}\text{C}$  NMR (100 MHz, methanol- $d_4$ ) spectroscopic data, see Table 4.1; and HRESIMS  $m/z$  641.3455  $[\text{M} + \text{Na}]^+$  (calcd for  $\text{C}_{38}\text{H}_{50}\text{O}_7\text{Na}$ , 641.3454).

The molecular formula of picrorhizone A (**GP1**) was assigned as  $C_{38}H_{50}O_7$  according to the sodium adduct ion at  $m/z$  641.3455  $[M + Na]^+$  in the HRESIMS, which indicated 14 indices of hydrogen deficiency. The  $^1H$  NMR data showed signals for eight methyls at  $\delta_H$  0.84–1.72, an oxygenated methylene at  $\delta_H$  3.96 (2H, s), two terminal olefinic protons at  $\delta_H$  4.52 (1H, s) and 4.74 (1H, s), and two olefinic protons at  $\delta_H$  4.91 (1H, overlap) and 5.35 (1H, br t,  $J = 8.8$  Hz). The proton signals for a 1,3,4-trisubstituted benzene ring [ $\delta_H$  6.76 (1H, d,  $J = 8.4$  Hz), 7.13 (1H, dd,  $J = 8.4, 1.6$  Hz), and 7.14 (1H, d,  $J = 1.6$  Hz)] were also observed (Table 4.1). The characteristic peaks of a methylene at  $\delta_C$  41.8 (C-7), a methine at  $\delta_C$  48.0 (C-6), three  $sp^3$  quaternary carbons at  $\delta_C$  49.0 (C-5), 60.6 (C-8), and 68.9 (C-4), a conjugated carbonyl carbon at  $\delta_C$  196.7 (C-10), an unconjugated carbonyl carbon at  $\delta_C$  210.6 (C-9), and an enolized 1,3-diketo group at  $\delta_C$  195.3 (C-1), 118.4 (C-2), and 193.7 (C-3) were assigned from the combined  $^{13}C$  NMR and HSQC data, suggesting that this metabolite was a benzoylphloroglucinol derivative featuring a bicyclo[3.3.1]nonane skeleton [86, 173–175].

Comprehensive analysis of 1D and 2D NMR data established the 2D structure of **GP1** (Figure 4.4), which closely resembled garcinopicrobenzophenone (**GP9**) [158], a major compound of this plant. The only difference between compounds **GP1** and **GP9** was that the resonance for one of the methyl groups on the prenyl unit in **GP9** was replaced by an oxygenated methylene group at  $\delta_H$  3.96 (2H, s, H-20)/ $\delta_C$  68.9 in **GP1**, indicating the oxidation of that methyl group to a hydroxymethyl moiety. The COSY correlation of H<sub>2</sub>-17/H-18 and multiple HMBC correlations from H<sub>2</sub>-17 to C-3, C-4, C-9, and C-19, H<sub>2</sub>-20 to C-18, C-19, and C-21, and H<sub>3</sub>-21 to C-18, C-19, and C-20 confirmed a 4-hydroxy-3-methyl-2-butenyl side chain at C-4 in **GP1** (Figure 4.4). The NOESY experiment (Figure 4.5) showed  $^1H$ – $^1H$  interactions of H-18/H<sub>2</sub>-20 and H-17a/H<sub>3</sub>-21, indicating an *E*-configuration of the  $\Delta^{18(19)}$  double bond.

Table 4.1.  $^1\text{H}$  (400 MHz) and  $^{13}\text{C}$  (100 MHz) NMR spectroscopic data of compounds GP1– GP3 ( $\delta$  in ppm)

position	GP1 <sup>a</sup>		GP2 <sup>a</sup>		GP3 <sup>b</sup>	
	$\delta_{\text{C}}$	$\delta_{\text{H}}$ ( $\nu$ in Hz)	$\delta_{\text{C}}$	$\delta_{\text{H}}$ ( $\nu$ in Hz)	$\delta_{\text{C}}$	$\delta_{\text{H}}$ ( $\nu$ in Hz)
1	195.3		195.3		193.5	
2	118.4		118.5		116.2	
3	193.7		194.6		197.6	
4	68.9		68.9		69.1	
5	49.0		49.5		49.0	
6	48.0	1.49, m	47.7	1.50, m	46.7	1.41, m
7 <sub>eq</sub>	41.8	2.22, d (13.6)	41.8	2.21, d (14.0)	40.8	2.33, d (14.0)
7 <sub>ax</sub>		2.03, dd (13.6, 6.8)		2.03, dd (14.0, 6.0)		2.08 <sup>c</sup>
8	60.6		59.6 <sup>d</sup>		58.2	
9	210.6		209.5		208.7	
10	196.7		198.3		196.9	
11	130.5		140.2		136.9	
12	117.6	7.14, d (1.6)	116.1	7.00, d (1.6)	129.3	7.57, d (7.2)
13	145.8		158.6		128.0	7.38, t (7.2)
14	152.2		120.7	6.98, dd (7.6, 1.6)	132.9	7.52, t (7.2)
15	115.5	6.76, d (8.4)	130.0	7.19, t (7.6)	128.0	7.38, t (7.2)
16	124.4	7.13, dd (8.4, 1.6)	121.1	6.96, dd (7.6, 1.6)	129.3	7.57, d (7.2)
17a	26.8	2.76, dd (13.2, 8.8)	27.0	2.69, dd (12.8, 8.8)	26.7	2.71, dd (12.4, 9.6)
17b		2.59, br d (13.2)		2.57, br d (12.8)		2.50, br d (12.4)
18	122.6	5.35, br t (8.8)	120.7	4.99, br d (8.8)	120.3	5.09, br t (9.6)
19	138.4		136.0		135.0	
20	68.9	3.96, s	26.4	1.71, s	26.3	1.82, s
21	14.2	1.72, s	18.3	1.67, s	18.3	1.67, s
22	23.2	1.19, s	23.0	1.19, s	22.7	1.16, s
23	27.4	1.00, s	27.3	1.00, s	27.1	0.97, s



position	GP1 <sup>a</sup>		GP2 <sup>b</sup>		GP3 <sup>b</sup>	
	$\delta_C$	$\delta_H$ (J in Hz)	$\delta_C$	$\delta_H$ (J in Hz)	$\delta_C$	$\delta_H$ (J in Hz)
24a	30.3	2.16 <sup>c</sup>	30.3	2.13 <sup>c</sup>	29.0	2.14 <sup>c</sup>
24b		2.11 <sup>c</sup>		2.07 <sup>c</sup>		2.05 <sup>c</sup>
25	125.8	4.91 <sup>c</sup>	125.4	4.88 <sup>c</sup>	124.2	4.87, m
26	133.6		133.8		133.0	
27	26.0	1.67, s	26.0	1.67, s	26.0	1.67, s
28	18.2	1.52, s	18.2	1.51, s	18.0	1.50, s
29a	33.4	1.94, d (13.2)	33.4	1.96, d (13.6)	32.3	2.03 <sup>c</sup>
29b		1.64 <sup>c</sup>		1.62 <sup>c</sup>		1.79 <sup>c</sup>
30	39.8	1.82 <sup>c</sup>	40.0	1.77 <sup>c</sup>	38.4	1.82 <sup>c</sup>
31	43.7		43.8		43.0	
32	51.1	2.25 <sup>c</sup>	51.1	2.27, dd (11.6, 4.8)	50.2	2.24 <sup>c</sup>
33a	30.4	1.75 <sup>c</sup>	30.4	1.75 <sup>c</sup>	29.7	1.76 <sup>c</sup>
33b		1.67 <sup>c</sup>		1.65 <sup>c</sup>		1.72 <sup>c</sup>
34	30.6	1.21, s	30.7	1.22, s	30.3	1.23, s
35	16.5	0.84, s	16.5	0.85, s	16.2	0.85, s
36	146.6		146.6		146.0	
37a	109.6	4.74, s	109.7	4.74, s	109.2	4.75, s
37b		4.52, s		4.53, s		4.53, s
38	23.4	1.63, s	23.4	1.63, s	23.2	1.64, s

<sup>a</sup>Recorded in CD<sub>3</sub>OD. <sup>b</sup>Recorded in CDCl<sub>3</sub>. <sup>c</sup>Overlapping signals. <sup>d</sup>Data were extracted from the HMBC spectrum.

#### 4.3.2. Structural elucidation of compound GP2 and GP3

*Physical and spectroscopic properties of picrorhizone B (GP2):* Pale brown gum;  $[\alpha]_D^{20} +12$  (c 0.10, MeOH); ECD (c 0.001, MeOH)  $\lambda_{\max} (\Delta\epsilon)$  218 (−4.2), 261 (+8.2), 305 (−4.4), 326 (−3.1), 348 (−2.3) nm; <sup>1</sup>H (400 MHz, methanol-*d*<sub>4</sub>) and <sup>13</sup>C NMR (100 MHz, methanol-*d*<sub>4</sub>) spectroscopic data, see Table 4.1; and HRESIMS *m/z* 585.3532 [M − H]<sup>−</sup> (calcd for C<sub>38</sub>H<sub>49</sub>O<sub>5</sub>, 585.3580).

*Physical and spectroscopic properties of picrorhizone C (GP3):* White gum;  $[\alpha]_D^{20} +15$  (c 0.10, CHCl<sub>3</sub>); ECD (c 0.001, MeOH)  $\lambda_{\max}$  ( $\Delta\epsilon$ ) 212 (+20.0), 241 (−3.1), 272 (+8.5), 301 (−15.0) nm; <sup>1</sup>H (400 MHz, CDCl<sub>3</sub>) and <sup>13</sup>C NMR (100 MHz, CDCl<sub>3</sub>) spectroscopic data, see Table 4.1; and HRESIMS  $m/z$  593.3587 [M + Na]<sup>+</sup> (calcd for C<sub>38</sub>H<sub>50</sub>O<sub>4</sub>Na, 593.3607).

The molecular formulas of picrorhizones B (GP2) and C (GP3) were determined to be C<sub>38</sub>H<sub>50</sub>O<sub>5</sub> and C<sub>38</sub>H<sub>50</sub>O<sub>4</sub> based on an [M − H]<sup>−</sup> ion at  $m/z$  585.3532 and an [M + Na]<sup>+</sup> ion at  $m/z$  593.3587 in the HRESIMS data, respectively. A comparison of the <sup>1</sup>H and <sup>13</sup>C NMR data of GP2 and GP3 with those of GP9 showed that the structural differences were restricted to the benzoyl unit. The 1D NMR and HSQC data displayed resonances corresponding to a 1,3-disubstituted benzoyl ring in GP2 at  $\delta_H/\delta_C$  6.96 (1H, dd,  $J = 7.6, 1.6$  Hz)/121.1, 6.98 (1H, dd,  $J = 7.6, 1.6$  Hz)/120.7, 7.00 (1H, d,  $J = 1.6$  Hz)/116.1, and 7.19 (1H, t,  $J = 7.6$  Hz)/130.0 (Table 4.1) [176]. The COSY correlations of H-14/H-15 and H-15/H-16 and HMBC cross-peaks from H-12 to C-10 ( $\delta_C$  198.3), C-13 ( $\delta_C$  158.6), C-14, and C-16, H-14 to C-12, C-13, and C-16, H-15 to C-11 ( $\delta_C$  140.2), C-13, and C-16, and H-16 to C-10, C-12, and C-14 confirmed the presence of the ring in GP2 (Figure 4.4). In the <sup>1</sup>H NMR spectrum of GP3 (Table 4.1), the resonances of five aromatic methine protons appeared in the region of  $\delta_H$  7.33–7.56, representing an unsubstituted benzoyl unit [177]. The <sup>1</sup>H–<sup>1</sup>H correlations of the contiguous spin system from H-12 to H-16 in the COSY spectrum and the cross-peaks of H-12/H-16 with C-10, C-12, C-14, and C-16, H-13/H-15 with C-11, C-13, and C-15, and H-14 with C-12 and C-16 in the HMBC spectrum completed the assignment of the unit (Figure 4.4).

#### 4.3.3. Structural elucidation of compound GP4

*Physical and spectroscopic properties of picrorhizone D (GP4):* Yellow gum;  $[\alpha]_D^{20} +34$  (c 0.10, MeOH); ECD (c 0.001, MeOH)  $\lambda_{\max}$  ( $\Delta\epsilon$ ) 234 (−0.9), 265 (+6.0), 303 (−

5.2), 326 (−1.5), 348 (−1.2) nm;  $^1\text{H}$  (400 MHz, methanol- $d_4$ ) and  $^{13}\text{C}$  NMR (100 MHz, methanol- $d_4$ ) spectroscopic data, see Table 4.2; and HRESIMS  $m/z$  643.3610  $[\text{M} + \text{Na}]^+$  (calcd for  $\text{C}_{38}\text{H}_{52}\text{O}_7\text{Na}$ , 643.3611).

Based on the observed  $[\text{M} + \text{Na}]^+$  peak at  $m/z$  643.3610 in the HRESIMS data, the molecular formula of picrorhizone D (**GP4**) was established as  $\text{C}_{38}\text{H}_{52}\text{O}_7$ . The  $^1\text{H}$  NMR data of **GP4** closely resembled those of **GP9**, except for the lack of terminal olefinic proton signals in **GP4**. Two methyl resonances observed at  $\delta_{\text{H}}/\delta_{\text{C}}$  1.03 (s, H<sub>3</sub>-37)/29.7 and 1.16 (s, H<sub>3</sub>-38)/27.9 in the NMR data of **GP4** (Table 4.2) indicated the hydration of the propylene moiety, which was supported by its HRESIMS data analysis indicating one less index of hydrogen deficiency and one more oxygen atom than **GP9**. This interpretation was confirmed by the HMBC correlation of H<sub>3</sub>-37/H<sub>3</sub>-38 with C-32 ( $\delta_{\text{C}}$  54.9) and C-36 ( $\delta_{\text{C}}$  72.6), suggesting that the two methyl groups were located at the oxygenated C-36 (Figure 4.4).

#### 4.3.4. Structural elucidation of compound GP5

*Physical and spectroscopic properties of picrorhizone E (GP5):* Yellow gum;  $[\alpha]_{\text{D}}^{20}$  +5 (c 0.10, MeOH); ECD (c 0.001, MeOH)  $\lambda_{\text{max}}$  ( $\Delta\epsilon$ ) 224 (+7.0), 238 (+1.5), 263 (+8.5), 305 (−14.0), 327 (−1.2), 348 (−1.2) nm;  $^1\text{H}$  (400 MHz, methanol- $d_4$ ) and  $^{13}\text{C}$  NMR (100 MHz, methanol- $d_4$ ) spectroscopic data, see Table 4.2; and HRESIMS  $m/z$  627.3300  $[\text{M} + \text{Na}]^+$  (calcd for  $\text{C}_{37}\text{H}_{48}\text{O}_7\text{Na}$ , 627.3298).

Picrorhizone E (**GP5**) was determined to have the molecular formula  $\text{C}_{37}\text{H}_{48}\text{O}_7$  based on an  $[\text{M} + \text{Na}]^+$  ion at  $m/z$  627.3300 in the HRESIMS data. A comparison of the  $^1\text{H}$  and  $^{13}\text{C}$  NMR data of **GP4** and **GP5** indicated that the two compounds differed only at the C-32 substituent of the cyclobutyl unit. The resonances for a methyl group and an oxygenated carbon ( $\delta_{\text{C}}$  72.6) in **GP4** were replaced by a carbonyl carbon resonating at  $\delta_{\text{C}}$  211.3 in **GP5** (Table 4.2), which was also supported by its HRESIMS data analysis indicating 16 amu units less than **GP4**. The above data, which

was corroborated by HMBC correlations (Figure 4.4) of methine H-32 [ $\delta_{\text{H}}$  2.84 (1H, dd,  $J = 9.4, 7.2$  Hz)] to C-36 ( $\delta_{\text{C}}$  211.3) and H<sub>3</sub>-37 ( $\delta_{\text{H}}$  2.02) with C-32 ( $\delta_{\text{C}}$  55.8) and C-36, suggested that C-36 was oxidized to a carbonyl carbon.

Table 4.2.  $^1\text{H}$  (400 MHz) and  $^{13}\text{C}$  (100 MHz) NMR spectroscopic data of compounds **GP4** and **GP5** ( $\delta$  in ppm)

position	GP4 <sup>a</sup>		GP5 <sup>a</sup>	
	$\delta_{\text{C}}$	$\delta_{\text{H}}$ (J in Hz)	$\delta_{\text{C}}$	$\delta_{\text{H}}$ (J in Hz)
1	194.8		194.5	
2	118.4		119.1	
3	193.5		193.7	
4	68.8		68.7	
5	49.3		49.1	
6	47.9	1.49, m	48.1	1.46, m
7 <sub>eq</sub>	41.7	2.21, d (14.4)	41.7	2.18 <sup>c</sup>
7 <sub>ax</sub>		2.02, dd (14.4, 6.4)		1.98, dd (14.0, 6.4)
8	60.4 <sup>d</sup>		60.9 <sup>d</sup>	
9	210.0		211.3	
10	196.4		197.0	
11	130.0		131.4	
12	117.3	7.20, d (1.6)	117.4	7.19, d (1.6)
13	146.2		146.1	
14	152.5		151.9	
15	115.2	6.72, d (8.4)	115.2	6.71, d (8.4)
16	125.0	7.03, dd (8.4, 1.6)	124.6	7.04, dd (8.4, 1.6)
17a	27.1	2.70, dd (12.8, 9.2)	27.2	2.67, dd (12.8, 8.0)
17b		2.54, br d (12.8)		2.54, br d (12.8)
18	121.1	5.01, br t (9.2)	121.6	5.00, br t (8.0)

position	GP4 <sup>a</sup>		GP5 <sup>a</sup>	
	$\delta_C$	$\delta_H$ (J in Hz)	$\delta_C$	$\delta_H$ (J in Hz)
19	135.8		135.1	
20	26.4	1.72, s	26.4	1.70, s
21	18.3	1.69, s	18.3	1.68, s
22	23.1	1.19, s	23.3	1.19, s
23	27.3	0.99, s	27.4	0.97, s
24a	30.2	2.13 <sup>c</sup>	30.3	2.18 <sup>c</sup>
24b		2.09 <sup>c</sup>		2.13 <sup>c</sup>
25	125.6	4.89 <sup>c</sup>	125.9	4.91, t (8.0)
26	133.7		133.4	
27	26.0	1.67, s	26.0	1.65, s
28	18.2	1.52, s	18.2	1.51, s
29a	33.2	1.96, d (12.8)	33.5	1.92, d (12.0)
29b		1.64 <sup>c</sup>		1.60 <sup>c</sup>
30	40.7	1.64 <sup>c</sup>	40.3	1.88 <sup>c</sup>
31	44.1		45.8	
32	54.9	1.70 <sup>c</sup>	55.8	2.84, dd (9.4, 7.2)
33a	29.0	1.70 <sup>c</sup>	27.5	1.95 <sup>c</sup>
33b		1.65 <sup>c</sup>		1.71 <sup>c</sup>
34	31.8	1.16, s	30.2	1.34, s
35	17.8	1.13, s	17.2	0.94, s
36	72.6		211.3	
37a	29.7	1.03, s	30.2	2.02, s
37b				
38	27.9	1.16, s		

<sup>a</sup>Recorded in CD<sub>3</sub>OD. <sup>b</sup>Recorded in CDCl<sub>3</sub>. <sup>c</sup>Overlapping signals. <sup>d</sup>Data were extracted from HMBC spectrum.

#### 4.3.5. Structural elucidation of compound GP6

*Physical and spectroscopic properties of picrorhizone F (GP6):* Pale yellow gum;  $[\alpha]_D^{20} +11$  (c 0.10, MeOH); ECD (c 0.001, MeOH)  $\lambda_{\max} (\Delta\epsilon)$  219 (+33.1), 265 (−28.7), 306 (+6.0), 332 (+2.8), 344 (+2.6) nm;  $^1\text{H}$  (400 MHz, methanol- $d_4$ ) and  $^{13}\text{C}$  NMR (100 MHz, methanol- $d_4$ ) spectroscopic data, see Table 4.3; and HRESIMS  $m/z$  619.3637  $[\text{M} + \text{H}]^+$  (calcd for  $\text{C}_{38}\text{H}_{51}\text{O}_7$ , 619.3635) and 641.3468  $[\text{M} + \text{Na}]^+$  (calcd for  $\text{C}_{38}\text{H}_{50}\text{O}_7\text{Na}$ , 641.3454).

The molecular formula of picrorhizone F (**GP6**) was determined to be  $\text{C}_{38}\text{H}_{50}\text{O}_7$  according to the HRESIMS data at  $m/z$  619.3637  $[\text{M} + \text{H}]^+$  and 641.3468  $[\text{M} + \text{Na}]^+$ . The NMR data analysis showed that **GP6** and **GP9** were structurally related. The major difference was that the resonances associated with the prenyl unit in **GP9** were absent in **GP6** and replaced by signals for two methyls at  $\delta_{\text{H}}/\delta_{\text{C}}$  1.04 (s,  $\text{H}_3$ -20)/25.4 and 1.08 (s,  $\text{H}_3$ -21)/25.5, a methylene at  $\delta_{\text{H}}/\delta_{\text{C}}$  2.25 (dd,  $J = 13.6, 6.8$  Hz, H-17b) and 2.65 (dd,  $J = 13.6, 10.0$  Hz, H-17a)/27.4, an oxygenated methine at  $\delta_{\text{H}}/\delta_{\text{C}}$  4.61 (dd,  $J = 10.0, 6.8$  Hz, H-18)/94.1, and an oxygenated tertiary carbon at  $\delta_{\text{C}}$  71.9 (C-19) (Table 4.3). The shielding of one of carbonyl carbons at  $\delta_{\text{C}}$  177.9 (C-3) in **GP6** compared to that of **GP9** ( $\delta_{\text{C}}$  193.8) indicated that one oxygen of the enolic system was enolized. The COSY correlation of  $\text{H}_2$ -17/H-18 and HMBC cross-peaks of  $\text{H}_2$ -17 with C-3, C-4, C-5, C-9, C-18, and C-19, H-18 with C-3, C-20 and C-21,  $\text{H}_3$ -20 with C-18 and C-21, and  $\text{H}_3$ -21 with C-19 and C-20 showed cyclization of the C-4 prenyl unit to C-3 via an ether bridge to form the 2-(2''-hydroxyprop-2''-yl)tetrahydrofuran ring (Figure 4.4) [178].

#### 4.3.6. Structural elucidation of compound GP7

*Physical and spectroscopic properties of picrorhizone G (GP7):* Pale yellow gum;  $[\alpha]_D^{20} +8$  (c 0.10, MeOH); ECD (c 0.001, MeOH)  $\lambda_{\max} (\Delta\epsilon)$  220 (+27.6), 266 (−24.8), 303 (+6.3), 326 (+2.8), 343 (+1.4) nm;  $^1\text{H}$  (400 MHz, methanol- $d_4$ ) and  $^{13}\text{C}$  NMR

(100 MHz, methanol- $d_4$ ) spectroscopic data, see Table 4.3; and HRESIMS  $m/z$  655.3245  $[M + Na]^+$  (calcd for  $C_{38}H_{48}O_8Na$ , 655.3247).

The HRESIMS data analysis of picrorhizone G (**GP7**) at  $m/z$  655.3245  $[M + Na]^+$  indicated a molecular formula of  $C_{38}H_{48}O_8$  with a hydrogen deficiency index of 15. Its  $^1H$  and  $^{13}C$  NMR data were similar to those of **GP6**. The differences involved the tetrahydrofuran ring in which signals for a methine at  $\delta_H/\delta_C$  2.56 (m, H-19)/46.1 and a carbonyl carbon at  $\delta_C$  176.3 (C-21) in **GP7** were observed instead of the resonances for the *gem*-dimethyl group and oxygenated tertiary carbon in **GP6** (Table 4.3). The carbonyl carbon was part of a hydroxycarbonyl group according to its carbon chemical shift and HRESIMS analysis. The above argument, which was supported by the COSY correlations of H<sub>2</sub>-17/H-18 and H-18/H-19, and the HMBC correlations of H<sub>2</sub>-17 with C-3, C-4, C-9, C-18, and C-19, H-18 with C-20 and C-21, H-19 with C-18, C-20, and C-21, and H<sub>3</sub>-20 with C-18, C-19, and C-21, suggested a modified C-18 substituent as shown in Figure 4.4.

#### 4.3.7. Structural elucidation of compound GP8

*Physical and spectroscopic properties of picrorhizone H (GP8):* Pale yellow gum;  $[\alpha]_D^{20}$   $-7$  ( $c$  0.10, MeOH); ECD ( $c$  0.001, MeOH)  $\lambda_{max}$  ( $\Delta\epsilon$ ) 226 (+25.2), 259 (−32.8), 303 (−2.5), 320 (+3.7), 350 (+2.9) nm;  $^1H$  (400 MHz, methanol- $d_4$ ) and  $^{13}C$  NMR (100 MHz, methanol- $d_4$ ) spectroscopic data, see Table 4.3; and HRESIMS  $m/z$  601.3526  $[M + H]^+$  (calcd for  $C_{38}H_{49}O_6$ , 601.3529) and 623.3343  $[M + Na]^+$  (calcd for  $C_{38}H_{48}O_6Na$ , 623.3349).

The molecular formula of picrorhizone H (**GP8**) was deduced to be  $C_{38}H_{48}O_6$  according to its  $[M + H]^+$  ion at  $m/z$  601.3526 and  $[M + Na]^+$  ion at  $m/z$  623.3343 in the HRESIMS, which was indicative of one more index of hydrogen deficiency than in the known metabolite **GP9**. The  $^1H$  and  $^{13}C$  NMR spectra were identical to the portions of **GP9** possessing a phloroglucinol skeleton with two prenyl and one 3-

isopropenyl-2,2-dimethylcyclobutylmethyl units. Unlike compound **GP9**, two aromatic singlets at  $\delta_{\text{H}}$  6.95 (H-13) and 7.44 (H-16) were identified in the  $^1\text{H}$  NMR data of **GP8**. The HMBC spectrum exhibited cross-peaks of H-13 with C-11 ( $\delta_{\text{C}}$  118.1) and three oxygenated carbons C-12 ( $\delta_{\text{C}}$  147.1), C-14 ( $\delta_{\text{C}}$  154.9), and C-15 ( $\delta_{\text{C}}$  151.3), as well as H-16 with C-12, C-14, C-15, and carbonyl carbon C-10 ( $\delta_{\text{H}}$  174.4), making it assignable to the 1,2,4,5-tetrasubstituted benzoyl ring in **GP8**. The  $^{13}\text{C}$  NMR data of **GP8** displayed the characteristic signals of an enolized 1,3-diketo group at  $\delta_{\text{C}}$  194.9, 119.2, and 178.8. The HMBC correlations from H<sub>2</sub>-17 to C-3 ( $\delta_{\text{C}}$  178.8), C-4 ( $\delta_{\text{C}}$  64.6), and C-9 ( $\delta_{\text{C}}$  207.8) and H<sub>2</sub>-29 to C-1 ( $\delta_{\text{C}}$  194.9), C-7 ( $\delta_{\text{C}}$  41.5), C-8 ( $\delta_{\text{C}}$  66.2), and C-9 permitted construction of the other linkage between C-3 and C-12 (Figure 4.4) [179, 180].

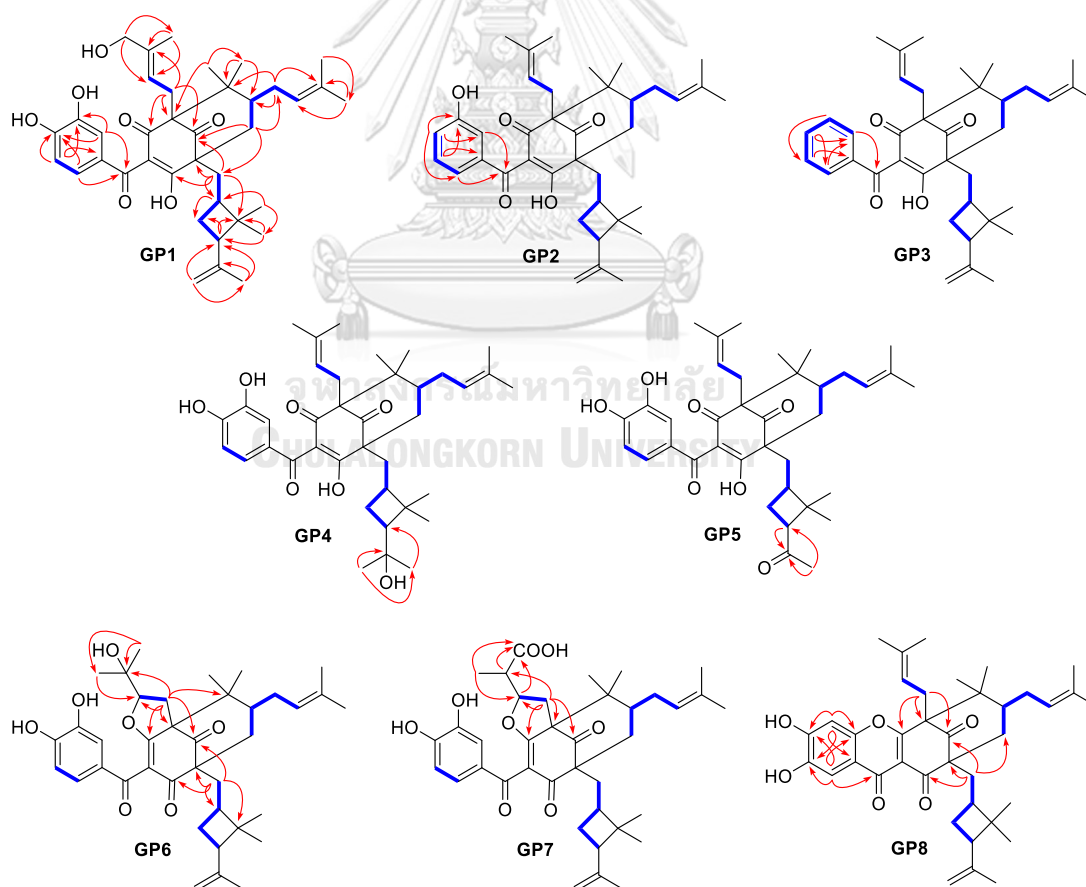


Figure 4.4. Key COSY (blue line) and HMBC (red arrow) correlations of picrorhizones A–H (**GP1**–**GP8**).



Table 4.3.  $^1\text{H}$  (400 MHz) and  $^{13}\text{C}$  (100 MHz) NMR spectroscopic data of compounds GP6– GP8 ( $\delta$  in ppm)

position	GP6 <sup>a</sup>		GP7 <sup>a</sup>		GP8 <sup>a</sup>	
	$\delta_{\text{C}}$	$\delta_{\text{H}}$ ( $\nu$ in Hz)	$\delta_{\text{C}}$	$\delta_{\text{H}}$ ( $\nu$ in Hz)	$\delta_{\text{C}}$	$\delta_{\text{H}}$ ( $\nu$ in Hz)
1	197.8		197.5		194.9	
2	119.3		119.3		119.2	
3	177.9		177.4		178.8	
4	69.0		68.9		64.6	
5	47.9		47.8		49.5	
6	46.9	1.66, m	46.9	1.66, m	47.8	1.51, m
7 <sub>eq</sub>	41.1	2.09, d (14.0)	41.1	2.08, d (13.6)	41.5	2.25, d (14.0)
7 <sub>ax</sub>		2.02, dd (14.0, 6.4)		2.03, dd (13.6, 6.8)		2.03, dd (14.0, 5.6)
8	61.9		62.0		66.2	
9	207.8		207.7		207.8	
10	193.2		192.8		174.4	
11	130.6		130.5		118.1	
12	116.7	7.29, d (1.6)	116.5	7.25, d, (1.6)	147.1	
13	146.7		146.6		104.0	6.95, s
14	152.9		152.9		154.9	
15	115.6	6.75, dd (8.0)	115.8	6.78, d (8.0)	151.3	
16	124.9	7.16, dd (8.0, 1.6)	124.6	7.14, dd (8.0, 1.6)	109.6	7.44, s
17a	27.4	2.65, dd (13.6, 10.0)	31.0	2.48 <sup>c</sup>	27.6	2.91, dd (13.6, 9.2)
17b		2.25, dd (13.6, 6.8)				2.86, d (13.6)
18	94.1	4.61, dd (10.0, 6.8)	88.9	4.89 <sup>c</sup>	119.7	4.62 <sup>c</sup>
19	71.9		46.1	2.56, m	136.1	
20	25.4	1.04, s	13.6	1.03, d (6.8)	26.0	1.42, s

position	GP6 <sup>a</sup>		GP7 <sup>a</sup>		GP8 <sup>a</sup>	
	$\delta_C$	$\delta_H$ (J in Hz)	$\delta_C$	$\delta_H$ (J in Hz)	$\delta_C$	$\delta_H$ (J in Hz)
21	25.5	1.08, s	176.3		18.5	1.73, s
22	24.2	1.25, s	24.2	1.24, s	22.5	1.27, s
23	27.5	1.11, s	27.5	1.10, s	26.9	1.12, s
24a	30.8	2.51, dd (14.0, 9.2)	30.8	2.53 <sup>c</sup>	30.4	2.03, d (14.0)
24b		2.42, d (14.0)		2.41, d (14.8)		1.78 <sup>c</sup>
25	126.0	4.88 <sup>c</sup>	125.9	4.88 <sup>c</sup>	124.7	4.90 <sup>c</sup>
26	134.0		134.1		134.3	
27	26.0	1.67, s	26.0	1.67, s	26.0	1.64, s
28	18.4	1.58, s	18.4	1.59, s	18.0	1.41, s
29a	33.6	1.82, d (13.6)	33.5	1.81, d (14.0)	31.8	1.84 <sup>c</sup>
29b		1.57 <sup>c</sup>		1.58 <sup>c</sup>		1.71 <sup>c</sup>
30	39.7	1.72 <sup>c</sup>	39.6	1.75, dd (10.0, 8.8)	39.3	1.84 <sup>c</sup>
31	43.6		43.5		43.5	
32	51.2	2.19 <sup>c</sup>	51.2	2.19, dd (10.0, 8.0)	51.4	2.25 <sup>c</sup>
33a	30.3	1.59 <sup>c</sup>	30.2	1.58 <sup>c</sup>	30.5	1.78 <sup>c</sup>
33b		1.51 <sup>c</sup>		1.53 <sup>c</sup>		1.76 <sup>c</sup>
34	30.5	1.19, s	30.4	1.19, s	30.6	1.18, s
35	16.4	0.79, s	16.4	0.78, s	16.4	0.84, s
36	146.6		146.6		146.6	
37a	109.7	4.70, s	109.7	4.69, s	109.7	4.77, s
37b		4.46, s		4.45, s		4.61, s
38	23.3	1.60, s	23.3	1.60, s	23.4	1.64, s

<sup>a</sup>Recorded in CD<sub>3</sub>OD. <sup>b</sup>Recorded in CDCl<sub>3</sub>. <sup>c</sup>Overlapping signals.

#### 4.3.8. Determining relative and absolute configurations of GP1–GP9

The relative configuration of **GP1** was deduced on the basis of the <sup>1</sup>H–<sup>1</sup>H coupling constants, carbon chemical shifts, and NOESY experiments. The coupling

constant between H-6 and H-7<sub>ax</sub> ( $^3J_{6,7ax} = 6.8$  Hz) and chemical shifts at  $\delta_C$  48.0 (C-6) and 27.4 (C-23) in the  $^{13}\text{C}$  NMR spectrum of **GP1** favored an axial orientation for the prenyl unit at C-6 (Table 4.1), since the equatorial position of a C-6 substituent showed  $^3J_{6,7ax} \approx 13.0$  Hz and chemical shifts at  $\delta_C$  40–42 (C-6) and 16–18 (C-23) [174, 178, 181]. The NOESY correlations of H-17b/H<sub>3</sub>-23, H<sub>3</sub>-23/H-6, H-7<sub>ax</sub>/H<sub>3</sub>-23, and H<sub>3</sub>-22/H-24a in **GP1** suggested equatorial orientations for CH<sub>2</sub>-17 and CH<sub>3</sub>-22 and axial orientations for CH<sub>3</sub>-23 and CH<sub>2</sub>-24. Although the correlation of H<sub>2</sub>-29 with its neighboring protons was not observed, CH<sub>2</sub>-29 had to be equatorially oriented since the bridged bicyclic ring system of **GP1** required that the side chains at C-4 and C-8 be equatorially oriented (Figure 4.5). In addition, the  $^1\text{H}$ – $^1\text{H}$  NOESY interactions of H-30/H-32, H-30/H<sub>3</sub>-34, and H-32/H<sub>3</sub>-34 indicated that methines H-30 and H-32 in the cyclobutyl ring were cofacial (Figure 4.5). The chemical shifts of the *gem*-dimethyl groups at  $\delta_C$  30.6 (C-34) and 16.5 (C-35) supported the same orientation of H-30 and H-32, since the opposite orientation of two methine protons in the cyclobutyl unit was indicated by the presence of the *gem*-dimethyl group resonances at  $\delta_C$  23.6–25.1, as reported in caloinophyllin A and brasiliensophyllic acids A and B [182, 183].

The relative configurations of **GP2–GP9** in the bicyclo[3.3.1]nonane core resembled **GP1** based on the  $^3J_{6,7ax}$  value, the C-6 and C-23 chemical shifts, and the NOESY data. The  $\beta$ -orientation of H-18 in **GP6** was confirmed by the NOE correlations of H-17b/H-18 and H-18/H<sub>3</sub>-22 (Figure 4.5) and by comparing its NMR data with those of nujiangefolin C and thorelione B regarding the dihydrofuran moiety [178, 184]. The orientation of H-18 in **GP7** was also assigned to be the same as **GP6** based on its NOE interactions, except for the relative configuration at C-19 of **GP7**, which remained undetermined.

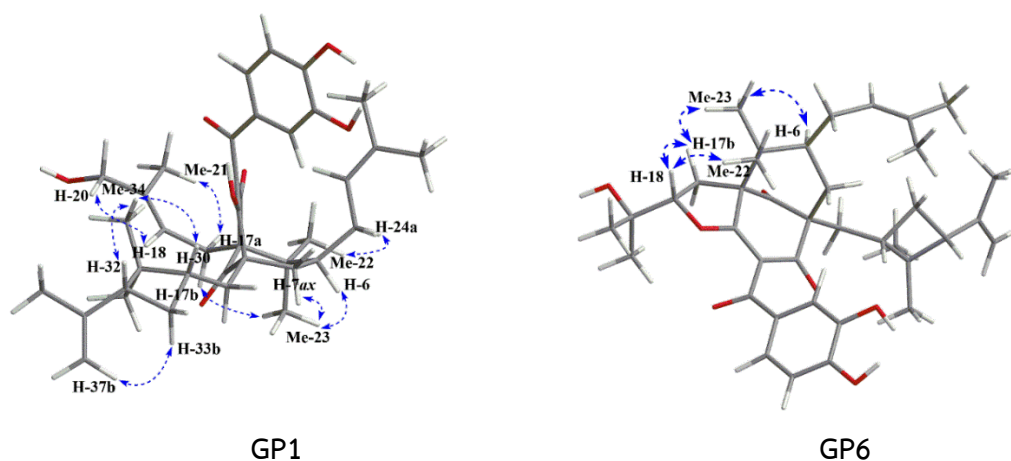


Figure 4.5. Key NOE correlations (blue dashed line) of compounds **GP1** and **GP6**.

The absolute configurations of **GP1** and **GP9** were determined by two methods. The absolute configurations were established by X-ray diffraction using Cu- $K\alpha$  radiation combined with ECD data. The calculated ECD spectrum of **GP9a** was in good agreement with the experimental ECD spectrum of **GP9**, indicating a (4*S*,6*S*,8*S*,30*S*,32*R*) absolute configuration of **GP9** (Figure 4.6). The effect of opposite configurations of the cyclobutyl ring on the ECD spectra was also assessed. The calculated spectra of **GP9a** and its diastereomer (4*S*,6*S*,8*S*,30*R*,32*S*)-**GP9b** were highly similar, suggesting that the ECD spectra were marginally influenced by different configurations at C-30 and C-32 (Figure C63, Supporting Information), although the optimized structure model **GP9a** was more energetically favorable than **GP9b**. The X-ray diffraction data analysis of **GP9** using Cu- $K\alpha$  radiation unequivocally confirmed the absolute configuration (Figure 4.6). The (4*S*,6*S*,8*S*,30*S*,32*R*) absolute configuration of **1** was defined based on the fact that the experimental ECD spectra of **GP1** and **GP9** were similar. The absolute configurations of **GP2–GP5** were determined as (4*S*,6*S*,8*S*,30*S*,32*R*), (4*S*,6*S*,8*S*,30*S*,32*R*), (4*S*,6*S*,8*S*,30*S*,32*S*), (4*S*,6*S*,8*S*,30*S*,32*S*), respectively, based on the similarity of their experimental ECD spectra with those of **GP1** and **GP9** (Figure C63, Supporting Information).

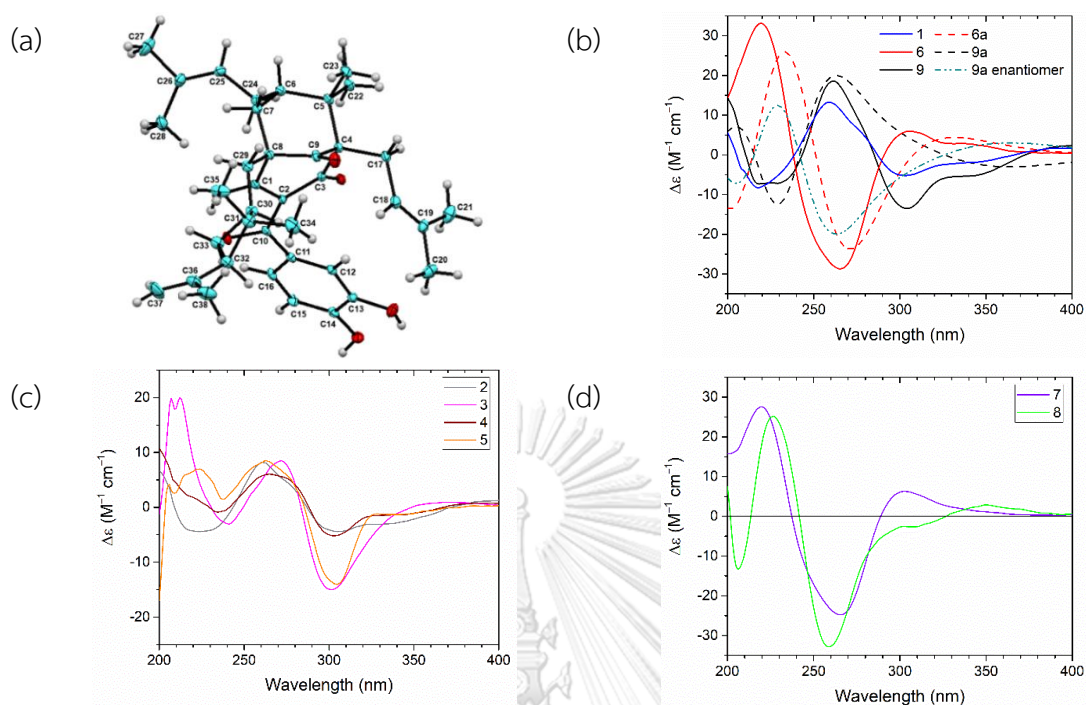


Figure 4.6. (a) ORTEP diagram for compound **GP9**; (b) Comparison of calculated ((4*S*,6*S*,8*S*,30*S*,32*R*)-**GP9a**, (4*R*,6*R*,8*R*,30*R*,32*S*)-**GP9a** enantiomer, (4*R*,6*S*,8*R*,19*S*,30*S*,32*R*)-**GP6a**) and experimental (**GP1**, **GP6**, **GP9**) ECD spectra; (c,d) experimental ECD spectra for **GP2–GP8**.

The calculated ECD curve of **GP6a** was in a good agreement with the experimental ECD spectrum of **GP6** (Figure 4.6), indicating a (4*R*,6*S*,8*R*,19*S*,30*S*,32*R*) absolute configuration. The (4*R*,6*S*,8*R*,19*S*,30*S*,32*R*) and (4*R*,6*S*,8*R*,30*S*,32*R*) absolute configurations of **GP7** and **GP8**, respectively, were defined by comparison of their experimental ECD data with those of **GP6**. It is worth noting that compounds **GP6–GP8** displayed antipodal experimental ECD spectra relative to those of **GP1–GP5** and **GP9**, although the corresponding compounds shared the same side chain orientations of the bicyclo[3.3.1]nonane moiety. This finding could imply that the keto-enol tautomerism in the core structure might affect the molecular conformation

and hence the ECD curves (Figure 4.6), as explained by a previous study reporting the opposite ECD spectra of two methylated (+)-guttiferone K derivatives with a different enolized position [174]. The above-mentioned data suggested that **GP1–GP5** and **GP9** mainly exist in C-1 enol and C-3 keto forms, while compounds **GP6–GP8** are present in C-1 keto form and enolized C-3 via ether ring closure.

#### 4.3.9. Cytotoxic and anti-inflammatory activities of the isolated compounds

Several polyprenylated benzoylphloroglucinols from the genus *Garcinia* have been previously reported to have anticancer and anti-inflammatory activities [18, 67, 86, 173, 185, 186]. For example, (–)-garcimultin D, a benzoylphloroglucinol featuring a tricyclo[4.3.1.0<sup>3,7</sup>]decane core, induces apoptosis in human erythroleukemia cells and G1-phase cell-cycle arrest and inhibits leukemia oncogene expression [67]. Another benzoylphloroglucinol-type compound, garcinol, shows anti-inflammatory effects by inhibiting iNOS and COX-2 expressions and NF-κB and JAK/STAT-1 activation in LPS-activated macrophages [18]. The above evidence prompted us to evaluate the isolated compounds (**GP1–GP12**) for their cytotoxic properties against KB, HeLa S3, HT-29, MCF-7, and Hep G2 cancer cell lines using an MTT viability assay and for anti-inflammatory activity on COX-1 and COX-2 enzymes. Compound **GP12** was not tested for cyclooxygenase assays due to its small sample size.

Based on the cytotoxicity results (Table 4.4), most of the compounds (**GP3**, **GP5**, **GP6**, **GP8–GP11**) were cytotoxic against KB cancer cells, with IC<sub>50</sub> values ranging from 5.2 to 9.9 μM. Surprisingly, only compound **GP6** showed cytotoxicity against MCF-7 and Hep G2 cancer cells with IC<sub>50</sub> values of 9.3 and 9.4 μM, respectively, when compared with the other compounds (**GP1–GP5**, **GP7–GP9**) bearing a similar cyclobutyl moiety. Among compounds **GP1–GP5** and **GP9** tested against HeLa S3 cancer cells, compounds **GP1** and **GP9** possessed cytotoxicity with IC<sub>50</sub> values of 8.0

and 7.2  $\mu\text{M}$ , respectively, indicating that the presence of both 3,4-dihydroxybenzoyl moiety and terminal double bond at the cyclobutyl unit may be required to enhance cytotoxicity. Compounds **GP10** and **GP11** were cytotoxic against MCF-7 cancer cells with  $\text{IC}_{50}$  values of 5.9 and 7.2  $\mu\text{M}$ , respectively, while no cytotoxicity was found for **GP12**. These results suggest that the absence of the 3,4-dihydroxybenzoyl moiety may reduce the cytotoxic properties against those cancer cells.

Table 4.4. Cytotoxic activity<sup>a</sup> of compounds **GP1**, **GP3**, **GP5**, **GP6**, and **GP8–GP11** after 72 h of treatment

Compound	$\text{IC}_{50} \pm \text{SD} (\mu\text{M})$				
	KB	HeLa S3	MCF-7	Hep G2	HT-29
<b>GP1</b>	>10	8.0 $\pm$ 0.9	NT	NT	NT
<b>GP2</b>	9.9 $\pm$ 0.1	>10	>10	>10	>10
<b>GP5</b>	7.4 $\pm$ 0.7	>10	>10	>10	>10
<b>GP6</b>	5.9 $\pm$ 0.4	6.0 $\pm$ 0.4	9.3 $\pm$ 1.7	9.4 $\pm$ 0.8	>10
<b>GP8</b>	5.2 $\pm$ 0.7	6.2 $\pm$ 0.1	>10	>10	>10
<b>GP9</b>	7.0 $\pm$ 0.2	7.2 $\pm$ 0.4	>10	>10	>10
<b>GP10</b>	6.4 $\pm$ 0.7	>10	5.9 $\pm$ 0.1	>10	>10
<b>GP11</b>	5.3 $\pm$ 0.1	>10	7.2 $\pm$ 0.1	>10	>10
Doxorubicin <sup>b</sup>	0.02 $\pm$ 0.01	0.15 $\pm$ 0.02	1.29 $\pm$ 0.02	1.00 $\pm$ 0.17	0.59 $\pm$ 0.03

<sup>a</sup>Results are expressed as the mean values of three experiments  $\pm$  SD; the other isolated compounds were inactive ( $\text{IC}_{50} > 10 \mu\text{M}$ ); NT: not tested. <sup>b</sup>Doxorubicin was used as the positive control.

The COX-1 and COX-2 assays (Table 4.5) revealed that only compounds **GP6–GP8** displayed selective inhibitory activity (>10% inhibition) towards COX-1 at a concentration of 20  $\mu\text{M}$ . The highest activity was found for **GP8** (35.2  $\pm$  9.6%

inhibition). None of compounds led greater than 10% COX-2 inhibition at 20  $\mu\text{M}$ . Preliminary structure-activity relationship studies suggest that the presence of the keto group at C-1 and enolized C-3 in compounds **GP6–GP8** seems to be important for increasing the COX-1 inhibitory activity.

Table 4.5. COX-1 and COX-2 inhibitory activity<sup>a</sup> of compounds **GP1–GP11**.

Compound	% inhibition $\pm$ SD	
	COX-1	COX-2
GP1	<10	<10
GP2	<10	<10
GP3	<10	<10
GP4	<10	<10
GP5	<10	<10
GP6	10.7 $\pm$ 8.8	<10
GP7	11.9 $\pm$ 1.8	<10
GP8	35.2 $\pm$ 9.6	<10
GP9	<10	<10
GP10	<10	<10
GP11	<10	<10

<sup>a</sup>The experiment was performed in duplicates and repeated twice. The final concentration of compounds used in the assay was 20  $\mu\text{M}$ . Indomethacin (1.25  $\mu\text{M}$ ) and celecoxib (8.8  $\mu\text{M}$ ) were used as positive control with % inhibition of 78.4  $\pm$  4.1 and 83.5  $\pm$  4.8, respectively. NT: not tested.

#### 4.4. Chemotaxonomic study

Polyprenylated benzoylphloroglucinols (PPBPs) are commonly found in specific genera belonging to the Clusiaceae family, including *Garcinia*, *Clusia*, and *Rheedia*. The PPBPs that have been hitherto isolated mostly possess a



bicyclo[3.3.1]nonane backbone connected to the benzoyl unit and some structural modifications occur at the prenyl or geranyl side chains, which attach to the bicyclic ring system [24]. The new compounds, picrorhizones A–H (**GP1–GP8**), are unique PPBPs that share a cyclobutyl moiety derived from a geranyl unit which are rarely found in plants. Garcinopicrobenzophenone and eugeniaphenone were the only PPBPs bearing this moiety reported previously from *G. picrorhiza* and *G. eugeniaefolia* [158, 187], while the PPBPs with ring expansion on the modified geranyl unit (cyclopentyl and cyclohexyl moieties), such as thorelione A and coccinone F, were isolated from *Calophyllum thorelii* and *Moronobea coccinea* [179, 184]. The cytotoxicity results suggest that the PPBP compound class could be used as a lead compounds in cancer research. Previous reports also support the ability of PPBPs to inhibit the growth of various cancer cells through different mechanism of actions, such as cell cycle arrest and ROS generation induction leading to autophagy and apoptosis [24, 67, 185].

## Chapter V

### Conclusion

A total of 70 secondary metabolites, including 23 previously unreported structures and 47 known analogues, were successfully isolated and characterized from three Indonesian *Garcinia* species, *G. cylindrocarpa*, *G. tetrandra*, and *G. picrorhiza*. These *Garcinia* phytochemicals are identified as xanthone and biphenyl derivatives bearing simple oxygenated functional groups and prenyl and geranyl side chains and polyprenylated benzoylphloroglucinols. Interestingly, the new metabolites tetrandraxanthonones G–H contain uncommon cyclized geranyl units at C-8 of the xanthone skeleton and the new picrorhizone derivatives possess an unusual cyclobutyl-containing side chain attached to the core structure. Cytotoxic activity study showed that 9-hydroxycalabaxanthone, a pyranoxanthone isolated from *G. tetrandra*, was significantly active against all five human cancer cell lines (HeLa S3, Hep G2, HT-29, MCF-7, and KB) with  $IC_{50}$  values lower than  $3.5 \mu\text{M}$ , while 2-deprenylrheediaxanthone B from *G. cylindrocarpa* and picrorhizone F from *G. picrorhiza* displayed cytotoxic effects against four cancer cells, except HT-29, with  $IC_{50}$  values lower than  $10 \mu\text{M}$ . In addition, picrorhizone H possessed the highest inhibitory effect towards COX-1 ( $35.2 \pm 9.6\%$  inhibition at  $20 \mu\text{M}$ ).

The outcome of this work is expected to enrich information about chemical diversity of the genus *Garcinia*. It also provides an insight about lead compounds which have promising cytotoxic properties for further chemical modification and pharmacological study to develop anticancer drug candidates in future, not only showing remarkable activity against cancer cells, but also having minor adverse effects in human body.

## REFERENCES



จุฬาลงกรณ์มหาวิทยาลัย  
**CHULALONGKORN UNIVERSITY**

1. IARC, 2018, *Cancer fact sheets*. Available from: <http://gco.iarc.fr/today/fact-sheets-cancers>.
2. NCI, 2015, *Understanding Cancer*. Available from: <https://www.cancer.gov/about-cancer/understanding>.
3. Rayan, A., J. Raiyn, and M. Falah, *Nature is the best source of anticancer drugs: Indexing natural products for their anticancer bioactivity*. PLOS ONE, 2017. **12**(11): p. 1-12.
4. Urruticoechea, A., et al., *Recent advances in cancer therapy: an overview*. Current Pharmaceutical Design, 2010. **16**(1): p. 3-10.
5. Baudino, T.A., *Targeted cancer therapy: The next generation of cancer treatment*. Current Drug Discovery and Technology, 2015. **12**(1): p. 3-20.
6. Ziad, A., et al., *Natural products as cytotoxic agents in chemotherapy against cancer*. IntechOpen, 2018: p. 1-10
7. Demain, A.L. and P. Vaishnav, *Natural products for cancer chemotherapy*. Microbial biotechnology, 2011. **4**(6): p. 687-699.
8. Amaral, R.G., et al., *Natural products as treatment against cancer: A historical and current vision*. Clinics in Oncology, 2019. **4**: p. 1-5.
9. Cragg, G.M. and J.M. Pezzuto, *Natural products as a vital source for the discovery of cancer chemotherapeutic and chemopreventive agents*. Medical principles and practice : international journal of the Kuwait University, Health Science Centre, 2016: p. 41-59.
10. Mann, J., *Natural products in cancer chemotherapy: past, present and future*. Nature Reviews Cancer, 2002. **2**(2): p. 143-8.
11. Lim, T.K., *Edible medicinal and non-medicinal plants: Volume 2, fruits*. 2012: p. 1-1088.
12. Sweeney, P.W., *Systematics and floral evolution in the plant genus *Garcinia* (Clusiaceae)*. University Of Missouri- St. Louis, USA, 2007: p. 132.
13. Sukandar, E.R., et al., *Cylindroxanthonones A–C, three new xanthonones and their cytotoxicity from the stem bark of *Garcinia cylindrocarpa**. Fitoterapia, 2016. **108**: p. 62-65.
14. Sulassih, Sobir, and E. Santosa, *Phylogenetic analysis of mangosteen (*Garcinia mangostana* L.) and its relatives based on morphological and inter simple sequence repeat (ISSR) markers*. Sabrao Journal of Breeding and Genetics, 2013. **45**(3): p. 478-490.

15. Uji, T., *Keanekaragaman persebaran dan potensi jenis-jenis Garcinia di Indonesia*. Berkala Penelitian Hayati, 2007. 12: p. 129-135.
16. Grosvenor, P.W., et al., *Medicinal plants from Riau province, Sumatra, Indonesia. Part 1: Uses*. Journal of Ethnopharmacology, 1995. **45**(2): p. 75-95.
17. Damiyanti, M., et al., *Effect of mangosteen (Garcinia mangostana) peel solution on human enamel surface color*. Journal of Medical Sciences, 2014. **14**: p. 297-302.
18. Semwal, R.B., et al., *A comprehensive scientific overview of Garcinia cambogia*. Fitoterapia, 2015. **102**: p. 134-148.
19. Dewick, P.M., *Medicinal natural products: A biosynthetic approach: Third Edition*. Medicinal Natural Products: A Biosynthetic Approach: Third Edition, 2009: p. 1-539.
20. El-Awaad, I.A.M., *Cytochrome P450 enzymes involved in xanthone biosynthesis in Hypericum species*, in *Fakultät für Lebenswissenschaften*. Technischen Universität Carolo-Wilhelmina: Germany, 2016: p. 141.
21. Sukandar, E.R., et al., *New depsidones and xanthone from the roots of Garcinia schomburgkiana*. Fitoterapia, 2016. **111**: p. 73-77.
22. Chizzali, C., et al., *Differential expression of biphenyl synthase gene family members in fire-blight-infected apple 'Holsteiner Cox'*. Plant Physiology, 2012. **158**(2): p. 864-875.
23. Ciochina, R. and R.B. Grossman, *Polycyclic polyprenylated acylphloroglucinols*. Chemical Reviews, 2006. **106**(9): p. 3963-3986.
24. Wu, S.-B., C. Long, and E.J. Kennelly, *Structural diversity and bioactivities of natural benzophenones*. Natural Product Reports, 2014. **31**(9): p. 1158-1174.
25. Pal, S. and M. Pal, *Chapter 2 - Natural sources, biosynthesis, and biological activities*, in *Isocoumarin, thiaisocoumarin and phosphaisocoumarin*, S. Pal and M. Pal, Editors. 2019, Elsevier. p. 17-37.
26. Negi, J.S., et al., *Naturally occurring xanthenes: chemistry and biology*. Journal of Applied Chemistry, 2013. **2013**: p. 1-9.
27. Yang, H., et al., *Phenolic derivatives from Garcinia multiflora Champion ex Bentham and their chemotaxonomic significance*. Biochemical Systematics and Ecology, 2020. **88**: p. 103981.
28. Brito, L.d.C., A.L.R. Berenger, and M.R. Figueiredo, *An overview of anticancer activity of Garcinia and Hypericum*. Food and Chemical Toxicology, 2017. **109**: p. 847-862.

29. Lannang, A.M., et al., *A new depsidone derivative from the leaves of Garcinia polyantha*. Natural Product Research, 2018. **32**(9): p. 1033-1038.
30. Zhang, B.-J., et al., *Cytotoxic prenylated xanthenes from the leaves of Garcinia bracteata*. Planta Medica, 2019. **85**(06): p. 444-452.
31. Nguyen, N.K., et al.,  *$\alpha$ -glucosidase inhibitory xanthenes from the roots of Garcinia fusca*. Chemistry & Biodiversity, 2017. **14**(10): p. 1-8.
32. Raksat, A., et al., *A tocotrienol quinone dimer and xanthenes from the leaf extract of Garcinia nigrolineata*. Fitoterapia, 2019. **136**: p. 1-6.
33. Thepthong, P., et al., *Prenylated xanthenes from the stem bark of Garcinia dulcis*. Phytochemistry Letters, 2017. **21**: p. 32-37.
34. Raksat, A., et al., *Phloroglucinol benzophenones and xanthenes from the leaves of Garcinia cowa and their nitric oxide production and  $\alpha$ -glucosidase inhibitory activities*. Journal of Natural Products, 2020. **83**(1): p. 164-168.
35. Kaennakam, S., P. Siripong, and S. Tip-Pyang, *Kaennacowanols A-C, three new xanthenes and their cytotoxicity from the roots of Garcinia cowa*. Fitoterapia, 2015. **102**: p. 171-176.
36. Xu, Y.J., et al., *Xanthenes from Garcinia parvifolia*. Journal of Natural Products, 2001. **64**(9): p. 1191-1195.
37. Tang, Y.-X., et al., *Xanthone derivatives from the leaves of Garcinia oligantha*. European Journal of Medicinal Chemistry, 2019. **181**: p. 1-13.
38. Yang, J., et al., *Cytotoxic xanthone derivatives from the twigs of Garcinia oligantha*. Phytochemistry, 2020. **174**: p. 1-10.
39. Chen, Y., et al., *Caged polyprenylated xanthenes from the resin of Garcinia hanburyi*. Fitoterapia, 2016. **109**: p. 106-112.
40. Xu, Y.J., et al., *Novel cytotoxic, polyprenylated heptacyclic xanthonoids from Indonesian Garcinia gaudichaudii (Guttiferae)*. Organic Letters, 2000. **2**(24): p. 3945-3948.
41. Chen, Y., et al., *Two unusual xanthenes from the bark of Garcinia xanthochymus*. Helvetica Chimica Acta, 2011. **94**(4): p. 662-668.
42. Lien Do, T.M., et al., *Schomburgkixanthone, a novel bixanthone from the twigs of Garcinia schomburgkiana*. Natural Product Research, 2020: p. 1-6.
43. Liu, Q., et al., *Nitric oxide inhibitory xanthenes from the pericarps of Garcinia mangostana*. Phytochemistry, 2016. **131**: p. 115-123.

44. Wang, W., et al., *A novel xanthone dimer derivative with antibacterial activity isolated from the bark of Garcinia mangostana*. *Natural Product Research*, 2018. **32**(15): p. 1769-1774.
45. Ibrahim, S.R.M., et al., *Biologically active fungal depsidones: Chemistry, biosynthesis, structural characterization, and bioactivities*. *Fitoterapia*, 2018. **129**: p. 317-365.
46. Ngoupayo, J., et al., *Brevipsidone, a new depsidone and other  $\alpha$ -glucosidase inhibitors from Garcinia Brevipedicellata (Clusiaceae)*. *Natural Product Communications*, 2007. **2**(11): p. 1141-1144.
47. Bui, T.Q., et al., *A depsidone and six triterpenoids from the bark of Garcinia celebica*. *Tetrahedron Letters*, 2016. **57**(23): p. 2524-2529.
48. Ha, L.D., et al., *Oliveridepsidones A–D, antioxidant depsidones from Garcinia oliveri*. *Magnetic Resonance in Chemistry*, 2012. **50**(3): p. 242-245.
49. Ito, C., et al., *Cancer chemopreventive agents. new depsidones from Garcinia plants*. *Journal of Natural Products*, 2001. **64**(2): p. 147-150.
50. Jia, C., et al., *New depsidone and dichromone from the stems of Garcinia paucinervis with antiproliferative activity*. *Journal of Natural Medicines*, 2019. **73**(1): p. 278-282.
51. Rukachaisirikul, V., et al., *Phloroglucinols, depsidones and xanthenes from the twigs of Garcinia parvifolia*. *Tetrahedron*, 2006. **62**(36): p. 8578-8585.
52. Yoshimura, M., et al., *Polyphenolic constituents of the pericarp of mangosteen (Garcinia mangostana L.)*. *Journal of Agricultural and Food Chemistry*, 2015. **63**(35): p. 7670-7674.
53. Pailee, P., et al., *Anti-HIV and cytotoxic biphenyls, benzophenones and xanthenes from stems, leaves and twigs of Garcinia speciosa*. *Phytochemistry*, 2018. **147**: p. 68-79.
54. Liu, G., et al., *A new biphenyl from Garcinia oligantha and its cytotoxicity*. *Asian Journal of Chemistry*, 2015. **27**(7): p. 2731-2732.
55. Gao, X.-M., et al., *New biphenyls from Garcinia lancilimba*. *Phytochemistry Letters*, 2018. **27**: p. 219-222.
56. Li, Y., et al., *Biphenyl derivatives from the twigs of Garcinia bracteata and their biological activities*. *Phytochemistry Letters*, 2015. **11**: p. 24-27.
57. Gao, X.-M., et al., *New Biphenyls from Garcinia multiflora*. *Journal of the Brazilian Chemical Society*, 2016. **27**: p. 10-14.

58. Ji, B.-K., et al., *Two new biphenyls from the stems of Garcinia tetralata*. *Natural Product Research*, 2017. **31**(13): p. 1544-1550.
59. Wu, X., et al., *New Biphenyl Constituents from Garcinia oblongifolia*. *Helvetica Chimica Acta*, 2008. **91**(5): p. 938-943.
60. Gao, X.-M., et al., *Identification and evaluation of apoptotic compounds from Garcinia paucinervis*. *Bioorganic & Medicinal Chemistry*, 2010. **18**(14): p. 4957-4964.
61. Beerhues, L. and B. Liu, *Biosynthesis of biphenyls and benzophenones – Evolution of benzoic acid-specific type III polyketide synthases in plants*. *Phytochemistry*, 2009. **70**(15): p. 1719-1727.
62. Salleh, W.M.N.H.W., et al., *A new xanthone and a new benzophenone from the roots of Garcinia hombroniana*. *Phytochemistry Letters*, 2020. **35**: p. 216-219.
63. Akoro, S.M., et al., *Gakolanone: a new benzophenone derivative from Garcinia kola Heckel stem-bark*. *Natural Product Research*, 2020. **34**(2): p. 241-250.
64. Mohamed, G.A., et al., *New xanthenes and cytotoxic constituents from Garcinia mangostana fruit hulls against human hepatocellular, breast, and colorectal cancer cell lines*. *Journal of Ethnopharmacology*, 2017. **198**: p. 302-312.
65. Zheng, D., et al., *Garcinyunnanimes A–C, novel cytotoxic polycyclic polyprenylated acylphloroglucinol imines from Garcinia yunnanensis*. *Organic Chemistry Frontiers*, 2017. **4**(11): p. 2102-2108.
66. Fan, Y.-M., et al., *Two unusual polycyclic polyprenylated acylphloroglucinols, including a pair of enantiomers from Garcinia multiflora*. *Organic Letters*, 2015. **17**(9): p. 2066-2069.
67. Tian, D.S., et al., *Garmultins A–G, biogenetically related polycyclic acylphloroglucinols from Garcinia multiflora*. *Organic Letters*, 2016. **18**(22): p. 5904-5907.
68. Aoki, T., T. Akashi, and S.-i. Ayabe, *Flavonoids of leguminous plants: structure, biological activity, and biosynthesis*. *Journal of Plant Research*, 2000. **113**(4): p. 475-488.
69. Agunbiade, R.Y., et al., *Isolation, characterization, crystal structure, free radical scavenging- and computational studies of 9-[4-(propan-2-yl)phenyl]-3,4,5,6,7,9-hexahydro-1H-xanthene-1,8(2H)-dione from Garcinia kola seeds*. *Journal of Molecular Structure*, 2017. **1144**: p. 396-405.



70. Chaturonrutsamee, S., et al., *Polycyclic polyprenylated acylphloroglucinols and biphenyl derivatives from the roots of *Garcinia nuntasaenii* Ngerns. & Suddee*. *Phytochemistry*, 2018. **146**: p. 63-74.
71. Auranwiwat, C., et al., *A new xanthone and a biphenyl from the flower and twig extracts of *Garcinia mckeaniana**. *Natural Product Research*, 2019: p. 1-6.
72. Chen, Y., et al., *Adamantyl derivatives and rearranged benzophenones from *Garcinia xanthochymus* fruits*. *RSC Advances*, 2017. **7**(28): p. 17289-17296.
73. Ibrahim, S.R.M., et al., *Garcixanthone A, a new cytotoxic xanthone from the pericarps of *Garcinia mangostana**. *Journal of Asian Natural Products Research*, 2019. **21**(3): p. 291-297.
74. Deachathai, S., et al., *Phenolic compounds from the fruit of *Garcinia dulcis**. *Phytochemistry*, 2005. **66**(19): p. 2368-2375.
75. Hu, Q., et al., *Flavonoids from *Garcinia paucinervis* and their biological activities*. *Chemistry of Natural Compounds*, 2014. **50**(6): p. 994-997.
76. Deachathai, S., S. Phongpaichit, and W. Mahabusarakam, *Phenolic compounds from the seeds of *Garcinia dulcis**. *Natural Product Research*, 2008. **22**(15): p. 1327-1332.
77. Panche, A.N., A.D. Diwan, and S.R. Chandra, *Flavonoids: an overview*. *Journal of Nutritional Science*, 2016. **5**: p. 1-15.
78. Osorio, E., J. Londoño, and J. Bastida, *Low-density lipoprotein (LDL)-antioxidant biflavonoids from *Garcinia madruno**. *Molecules*, 2013. **18**(5): p. 6092-100.
79. Jia, C., et al., *A new biflavonoid and a new triterpene from the leaves of *Garcinia paucinervis* and their biological activities*. *Journal of Natural Medicines*, 2017. **71**(4): p. 642-649.
80. Abdullah, I., et al., *Prenylated biflavonoids from the green branches of *Garcinia dulcis**. *Phytochemistry Letters*, 2018. **23**: p. 176-179.
81. Tran, T.H., et al., *A new megastigmane sulphoglycoside and polyphenolic constituents from pericarps of *Garcinia mangostana**. *Natural Product Research*, 2016. **30**(14): p. 1598-1604.
82. Tan, W.-N., et al., *New cholinesterase inhibitors from *Garcinia atroviridis**. *Fitoterapia*, 2014. **97**: p. 261-267.

83. Merza, J., et al., *Prenylated xanthenes and tocotrienols from Garcinia virgata*. *Phytochemistry*, 2004. **65**(21): p. 2915-2920.
84. Ting, C.-W., et al., *A new benzoylphloroglucinol derivative with an adamantyl skeleton and other constituents from Garcinia multiflora: effects on neutrophil pro-inflammatory responses*. *Chemistry & Biodiversity*, 2012. **9**(1): p. 99-105.
85. Lavaud, A., et al., *A tocotrienol series with an oxidative terminal prenyl unit from Garcinia amplexicaulis*. *Phytochemistry*, 2015. **109**: p. 103-110.
86. Cheng, L.Y., et al., *Acylphloroglucinol derivatives from Garcinia multiflora with anti-inflammatory effect in LPS-Induced RAW264.7 macrophages*. *Molecules*, 2018. **23**(10).
87. Fuentes, R.G., et al., *Phloroglucinols from the roots of Garcinia dauphinensis and their antiproliferative and antiplasmodial activities*. *Journal of Natural Products*, 2019. **82**(3): p. 431-439.
88. Wang, Y.-L., et al., *Garsubelone A, the first dimeric polycyclic polyprenylated acylphloroglucinols with complicated heptacyclic architecture from Garcinia subelliptica*. *Organic Letters*, 2019. **21**(5): p. 1534-1537.
89. Xu, G., et al., *Cytotoxic acylphloroglucinol derivatives from the twigs of Garcinia cowa*. *Journal of Natural Products*, 2010. **73**(2): p. 104-108.
90. Elya, B., et al., *Triterpenoids from Garcinia rigida*. *Records of Natural Products*, 2011. **5**: p. 56-59.
91. Lin, K.-W., et al., *Cytotoxic and antioxidant constituents from Garcinia subelliptica*. *Food Chemistry*, 2012. **135**(2): p. 851-859.
92. Saputri, F.C. and I. Jantan, *Inhibitory activities of compounds from the twigs of Garcinia hombroniana Pierre on human low-density lipoprotein (LDL) oxidation and platelet aggregation*. *Phytotherapy Research*, 2012. **26**(12): p. 1845-1850.
93. Nugroho, A.E., et al., *Cycloartane triterpenoids with anti-melanin deposition activity*. *Natural Product Communications*, 2018. **13**(7): p. 809-812.
94. Jong, V.Y.M., et al., *Cycloartane triterpenoids acid from Garcinia eugenifolia*. *Asian Journal of Chemistry*, 2013. **25**(3): p. 1199-1202.
95. Jamila, N., et al., *Cholinesterase inhibitory triterpenoids from the bark of Garcinia hombroniana*. *Journal of Enzyme Inhibition and Medicinal Chemistry*, 2015. **30**(1): p. 133-139.

96. Lannang, A.M., B.S. Noudou, and N. Sewald, *Ovalifolone A and B: New friedelane derivatives from Garcinia ovalifolia*. *Phytochemistry Letters*, 2013. **6**(2): p. 157-161.
97. Wang, L.-l., et al., *Two novel triterpenoids with antiproliferative and apoptotic activities in human leukemia cells isolated from the resin of Garcinia hanburyi*. *Planta Medica*, 2008. **74**(14): p. 1735-1740.
98. Stark, T.D., et al., *Two new benzoyl glucuronosyl glycerols from the leaves of Garcinia buchananii Baker*. *Phytochemistry Letters*, 2017. **19**: p. 187-190.
99. Youn, U.J., et al., *Bioactive polyprenylated benzophenone derivatives from the fruits extracts of Garcinia xanthochymus*. *Bioorganic & Medicinal Chemistry Letters*, 2017. **27**(16): p. 3760-3765.
100. Trisuwan, K., et al., *Oxygenated xanthenes and biflavanoids from the twigs of Garcinia xanthochymus*. *Tetrahedron Letters*, 2014. **55**(26): p. 3600-3602.
101. Saikia, P. and S. Gogoi, *Isocoumarins: General Aspects and recent advances in their synthesis*. *Advanced Synthesis & Catalysis*, 2018. **360**(11): p. 2063-2075.
102. Kaennakam, S., et al., *Two new xanthenes and cytotoxicity from the bark of Garcinia schomburgkiana*. *Journal of Natural Medicines*, 2019. **73**(1): p. 257-261.
103. Florento, L., et al., *Comparison of cytotoxic activity of anticancer drugs against various human tumor cell lines using in vitro cell-based approach*. *International Journal of Biomedical Science : IJBS*, 2012. **8**(1): p. 76-80.
104. McCauley, J., A. Zivanovic, and D. Skropeta, *Bioassays for anticancer activities, in Metabolomics tools for natural product discovery: methods and protocols*, U. Roessner and D.A. Dias, Editors. 2013, Humana Press: Totowa, NJ. p. 191-205.
105. Rayburn, E.R., S.J. Ezell, and R. Zhang, *Anti-inflammatory agents for cancer therapy*. *Molecular and Cellular Pharmacology*, 2009. **1**(1): p. 29-43.
106. Zhang, Z., F. Chen, and L. Shang, *Advances in antitumor effects of NSAIDs*. *Cancer Management and Research*, 2018. **10**: p. 4631-4640.
107. Hilovska, L., R. Jendzelovsky, and P. Fedorocko, *Potency of non-steroidal anti-inflammatory drugs in chemotherapy*. *Molecular and Clinical Oncology*, 2015. **3**(1): p. 3-12.
108. Wong, R.S.Y., *Role of Nonsteroidal Anti-Inflammatory Drugs (NSAIDs) in cancer prevention and cancer promotion*. *Advances in Pharmacological Sciences*, 2019. **2019**: p. 1-10.

109. Wang, D. and R.N. Dubois, *Prostaglandins and cancer*. *Gut*, 2006. **55**(1): p. 115-122.
110. Enzo Life Science, *PGE2 ELISA kit*. Farmingdale, NY, 2017: Global Headquarters Enzo Life Sciences Inc.
111. Enzo Life Science, 2017, *What are the differences between ELISA assay types?*. Available from: <http://www.enzolifesciences.com/science-center/technotes/2017/april/what-are-the-differences-between-elisa-assay-types?/>.
112. Sigma Aldrich, *Prostaglandin E2 EIA*. Saint Louis, MO, 2019: Sigma-Aldrich Inc.
113. Kongkathip, N., et al., *Potent antitumor activity of synthetic 1,2-naphthoquinones and 1,4-naphthoquinones*. *Bioorganic & Medicinal Chemistry*, 2003. **11**(14): p. 3179-3191.
114. Somanathan, R. and M.U.S. Sultanbawa, *Chemical investigation of ceylonese plants. Part VIII. Trapezifolixanthone, a new di-isoprenylated xanthone from the bark of Calophyllum trapezifolium Thw. (Guttiferae)*. *Journal of the Chemical Society, Perkin Transactions 1*, 1974(0): p. 2515-2517.
115. Locksley, H.D., A.J. Quillinan, and F. Scheinmann, *Extractives from Guttiferae. Part XXIII. An unambiguous synthesis of 6-deoxyjacareubin and related 3,3- and 1,1-dimethylallyl and annulated xanthenes*. *Journal of the Chemical Society C: Organic*, 1971(0): p. 3804-3814.
116. Kawamura, F., et al., *Two antifungal xanthenes from the heartwood of Calophyllum Symingtonianum*. *Japan Agricultural Research Quarterly: JARQ*, 2012. **46**(2): p. 181-185.
117. Sabphon, C., T. Sermboonpaisarn, and P. Sawasdee, *Cholinesterase inhibitory activities of xanthenes from Anaxagorea luzonensis A. Gray*. *Journal of Medicinal Plants Research*, 2012. **6**(21): p. 3781-3785.
118. Ee, G.C.L., et al., *A new xanthone from Garcinia nitida*. *Natural Product Research*, 2012. **26**(9): p. 830-835.
119. Ito, C., et al., *A novel dibenzofuran and two new xanthenes from Calophyllum panicflorum*. *Chemical & Pharmaceutical Bulletin*, 1996. **44**(2): p. 441-443.
120. Daud, S.B., et al., *A new coumarin from Calophyllum hosei*. *Natural Product Research*, 2014. **28**(19): p. 1534-1538.
121. Anggia, V., A. Bakhtiar, and D. Arbain, *The Isolation of xanthenes from trunk latex of Garcinia mangostana Linn. and their antimicrobial activities*. *Indonesian Journal of Chemistry*, 2015. **15**(2): p. 187-193.

122. Rui, D.-Y., et al., *Chemical constituents of Hypericum petiolulatum*. Chemistry of Natural Compounds, 2017. **53**(3): p. 457-462.
123. Kainz, K.P., et al., *2-Deprenyl-rheediaxanthone b isolated from Metaxya rostrata induces active cell death in colorectal tumor cells*. PLOS ONE, 2013. **8**(6): p. e65745.
124. Locksley, H.D. and I.G. Murray, *Extractives from Guttiferae. Part XIX. The isolation and structure of two benzophenones, six xanthenes and two biflavonoids from the heartwood of Allanblackia floribunda Oliver*. Journal of the Chemical Society C: Organic, 1971(0): p. 1332-1340.
125. Nuangnaowarat, W., W. Phupong, and M. Isaka, *New xanthenes from the barks of Cratoxylum sumatranum ssp. neriifolium*. Heterocycles, 2010. **81**(10): p. 2235-2341.
126. Frahm, A.W. and R.K. Chaudhuri, *13 C NMR spectroscopy of substituted xanthenes—II: 13C NMR spectral study of polyhydroxy xanthenes*. Tetrahedron, 1979. **35**(17): p. 2035-2038.
127. Zhou, M., et al., *New biphenyl derivatives from the leaves of Nicotiana tabacum and their cytotoxic activity*. Phytochemistry Letters, 2015. **14**: p. 226-229.
128. Sia, G.-L., et al., *Minor xanthenes from the bark of Cratoxylum cochinchinense*. Phytochemistry, 1995. **38**(6): p. 1521-1528.
129. Bennett, G.J., et al., *Triterpenoids, tocotrienols and xanthenes from the bark of Cratoxylum cochinchinense*. Phytochemistry, 1993. **32**(5): p. 1245-1251.
130. Garcia Cortez, D.A., et al., *Xanthenes, triterpenes and a biphenyl from Kielmeyera coriacea*. Phytochemistry, 1998. **47**(7): p. 1367-1374.
131. Deng, L., et al., *Coniochaetones E-I, new 4H-chromen-4-one derivatives from the Cordyceps-colonizing fungus Fimetariella sp.* Fitoterapia, 2013. **89**: p. 8-14.
132. Klaiklay, S., et al., *Friedolanostanes and xanthenes from the twigs of Garcinia hombroniana*. Phytochemistry, 2013. **85**: p. 161-166.
133. Chen, J.-J., et al., *Benzopyrans, biphenyls and xanthenes from the root of Garcinia linii and their activity against Mycobacterium tuberculosis*. Planta Medica, 2006. **72**(05): p. 473-477.
134. Kim, C.S., et al., *Isolation of bioactive biphenyl compounds from the twigs of Chaenomeles sinensis*. Bioorganic & Medicinal Chemistry Letters, 2016. **26**(2): p. 351-354.

135. Sukandar, E.R., et al., *Tetrandraxanthonones A–I, prenylated and geranylated xanthonones from the stem bark of Garcinia tetrandra*. *Journal of Natural Products*, 2019. **82**(5): p. 1312-1318.
136. Sri, H., et al., *A new pyrano xanthone from the stem barks of Garcinia tetrandra Pierre*. *Journal of Biological Sciences*, 2008. **8**: p. 137-142.
137. Sukandar, E.R., et al., *Xanthonones and biphenyls from the stems of Garcinia cylindrocarpa and their cytotoxicity*. *Fitoterapia*, 2018. **130**: p. 112-117.
138. Kaennakam, S., et al., *Veluflavanones A–P, cytotoxic geranylated flavanones from Dalbergia velutina Stems*. *Journal of Natural Products*, 2019. **82**(2): p. 276-282.
139. Ampofo, S.A. and P.G. Waterman, *Xanthonones from three Garcinia species*. *Phytochemistry*, 1986. **25**(10): p. 2351-2355.
140. Al-Massarani, S., et al., *Phytochemical, antimicrobial and antiprotozoal evaluation of Garcinia Mangostana pericarp and  $\alpha$ -Mangostin, Its major xanthone derivative*. *Molecules*, 2013. **18**(9): p. 10599.
141. Zelefack, F., et al., *Cytotoxic and antiplasmodial xanthonones from Pentadesma butyracea*. *Journal of Natural Products*, 2009. **72**(5): p. 954-7.
142. Rukachaisirikul, V., et al., *Xanthonones from the stem bark of Garcinia nigrolineata*. *Phytochemistry*, 2003. **64**(6): p. 1149-1156.
143. Li, W., et al., *Xanthonones and flavonoids of Polygala caudata*. *Pharmacy and Pharmacology Communications*, 1998. **4**(8): p. 415-417.
144. K. Sen, A., et al., *A xanthone from Garcinia mangostana*. *Phytochemistry*, 1980. **19**(10): p. 2223-2225.
145. Delle Monache, F., et al., *Three new xanthonones and macluraxanthone from Rheedea benthamiana Pl. Triana (Guttiferae)*. *Journal of the Chemical Society, Perkin Transactions*, 1981, **1**: p. 484-488.
146. Mahabusarakam, W., P. Wiriyaichitra, and W.C. Taylor, *Chemical constituents of Garcinia mangostana*. *Journal of Natural Products*, 1987. **50**(3): p. 474-478.
147. Meechai, I., et al., *Dihydroosajaxanthone: a new natural xanthone from the branches of Garcinia schomburgkiana Pierre (Autumn 2018)*. *Iranian Journal of Pharmaceutical Research*, 2018: p. 1347-1352.

148. Cotterill, P.J. and F. Scheinmann, *A revised structure for toxylloxanthone B*. Journal of the Chemical Society, Chemical Communications, 1975(16): p. 664-665.
149. Mahabusarakam, W., P. Chairerk, and W.C. Taylor, *Xanthones from Garcinia cowa Roxb. latex*. Phytochemistry, 2005. **66**(10): p. 1148-1153.
150. Chiang, Y.-M., et al., *Xanthones and benzophenones from the stems of Garcinia multiflora*. Journal of Natural Products, 2003. **66**(8): p. 1070-1073.
151. Huang, Y.-L., et al., *Antioxidant flavonoids from the rhizomes of Helminthostachys zeylanica*. Phytochemistry, 2003. **64**(7): p. 1277-1283.
152. Chantarasriwong, O., et al., *Chemistry and biology of the caged Garcinia xanthones*. Chemistry (Weinheim an der Bergstrasse, Germany), 2010. **16**(33): p. 9944-9962.
153. Genovese, S., et al., *Recent developments in the pharmacology of prenylated xanthones*. Drug Discovery Today, 2016. **21**(11): p. 1814-1819.
154. Ren, Y., et al., *Cytotoxic and NF- $\kappa$ B inhibitory constituents of the stems of Cratoxylum cochinchinense and their semisynthetic analogues*. Journal of Natural Products, 2011. **74**(5): p. 1117-1125.
155. Ren, Y., et al., *Absolute configuration of (-)-gambogic acid, an antitumor agent*. Journal of Natural Products, 2011. **74**(3): p. 460-463.
156. Muharni, M., E. Elfita, and E. Pertiwi, *Antibacterial activity of xanthone from ethyl acetate extract of the steam bark of Garcinia picrorrhiza Miq.* ALCHEMY Jurnal Penelitian Kimia, 2017. **13**(2): p. 12.
157. Radji, M., A. Sumiati, and N. Indani, *Uji mutagenisitas dan anti kanker ekstrak aseton dan n-heksana dari kulit batang Sesoot (Garcinia picrorrhiza Miq.)*. Pharmaceutical Sciences and Research (PSR), 2004. **1**: p. 69-78.
158. Soemiati, A., et al., *A novel cytotoxic polyisoprenylbenzophenone derivative compound from Garcinia picrorrhiza Miq.* ITE Letters on Batteries, New Technologies & Medicine, 2006. **7**: p. 1-5.
159. Soemiati, A., et al., *Isolasi dan identifikasi senyawa triterpenoid dan asam 3-hidroksinikotinat dari ekstrak diklorometana akar Garcinia picrorrhiza Miq.* Indonesian Journal of Applied Chemistry, 2010. **12**: p. 15-19.

160. Swasono, R.T., *Bioactive secondary metabolites from Australian invertebrates, Indonesian marine sponges, and an Indonesian terrestrial plant*. M.Phil. Thesis, The University of Queensland, Australia, 2006: p. 125.
161. Bruker, *APEX2 v. 2014.9-0*. 2014, Madison, WI: Bruker AXS Inc.
162. XT, B.S., *Program for crystal structure solution, v. (2014)/4*. 2014, Madison, WI: Bruker AXS Inc.
163. Bruker, *SHELXTL XLMP Program for crystal structure refinement - Multi-CPU, v. 2018/3*. 2018, Madison, WI: Bruker AXS Inc.
164. Spek, A.L., *PLATON SQUEEZE: a tool for the calculation of the disordered solvent contribution to the calculated structure factors*. Acta Crystallographica Section C: Structural Chemistry, 2015. **71**(Pt 1): p. 9-18.
165. Parsons, S., H.D. Flack, and T. Wagner, *Use of intensity quotients and differences in absolute structure refinement*. Acta Crystallographica Section B: Structural Science, Crystal Engineering and Materials, 2013. **69**(Pt 3): p. 249-259.
166. Frisch, M.J., et al., *Gaussian 09, revision A.01*. 2009, Wallingford, CT: Gaussian Inc.
167. Bruhn, T., et al., *SpecDis: quantifying the comparison of calculated and experimental electronic circular dichroism spectra*. Chirality, 2013. **25**(4): p. 243-249.
168. Tran, H.T., et al., *Anti-inflammatory and antiproliferative compounds from Sphaeranthus africanus*. Phytomedicine, 2019. **62**: p. 152951.
169. Lajter, I., et al., *Inhibition of COX-2 and NF-kappaB1 gene expression, NO production, 5-LOX, and COX-1 and COX-2 enzymes by extracts and constituents of Onopordum acanthium*. Planta Medica, 2015. **81**(14): p. 1270-6.
170. Fuller, R.W., et al., *Guttiferone F, the first prenylated benzophenone from Allanblackia stuhlmannii*. Journal of Natural Products, 1999. **62**(1): p. 130-132.
171. Gustafson, K.R., et al., *The guttiferones, HIV-inhibitory benzophenones from Symphonia globulifera, Garcinia livingstonei, Garcinia ovalifolia and Clusia rosea*. Tetrahedron, 1992. **48**(46): p. 10093-10102.
172. Boyce, J.H., V. Eschenbrenner-Lux, and J.A. Porco, *Syntheses of (+)-30-epi-, (-)-6-epi-, (±)-6,30-epi-13,14-didehydroxyisogarcinol and (±)-6,30-epi-garcimultiflorone A utilizing highly diastereoselective, lewis acid-controlled cyclizations*. Journal of the American Chemical Society, 2016. **138**(44): p. 14789-14797.



173. Cheng, L.-Y., et al., *Polyprenylated polycyclic acylphloroglucinol: Angiogenesis inhibitor from *Garcinia multiflora**. *Bioorganic & Medicinal Chemistry Letters*, 2018. **28**(10): p. 1860-1863.
174. Le, D.H., et al., *Polyprenylated benzoylphloroglucinols with DNA polymerase inhibitory activity from the fruits of *Garcinia schomburgkiana**. *Journal of Natural Products*, 2016. **79**(7): p. 1798-1807.
175. Zhang, H., et al., *Cytotoxic and anti-inflammatory prenylated benzoylphloroglucinols and xanthenes from the twigs of *Garcinia esculenta**. *Journal of Natural Products*, 2014. **77**(7): p. 1700-1707.
176. Chen, J.J., et al., *Benzophenone derivatives from the fruits of *Garcinia multiflora* and their anti-inflammatory activity*. *Journal of Natural Products*, 2009. **72**(2): p. 253-258.
177. Zhang, H., et al., *Prenylated benzoylphloroglucinols and xanthenes from the leaves of *Garcinia oblongifolia* with anti-enteroviral activity*. *Journal of Natural Products*, 2014. **77**(4): p. 1037-1046.
178. Xia, Z.-X., et al., *Bioassay-guided isolation of prenylated xanthenes and polycyclic acylphloroglucinols from the leaves of *Garcinia nuijiangensis**. *Journal of Natural Products*, 2012. **75**(8): p. 1459-1464.
179. Marti, G., et al., *Antiplasmodial benzophenone derivatives from the root barks of *Symphonia globulifera* (Clusiaceae)*. *Phytochemistry*, 2010. **71**(8): p. 964-974.
180. Masullo, M., et al., *Polyisoprenylated benzophenone derivatives from the fruits of *Garcinia cambogia* and their absolute configuration by quantum chemical circular dichroism calculations*. *Tetrahedron*, 2010. **66**(1): p. 139-145.
181. Fu, W., et al., *Prenylated benzoylphloroglucinols and biphenyl derivatives from the leaves of *Garcinia multiflora* Champ.* *RSC Advances*, 2015. **5**(95): p. 78259-78267.
182. Cottiglia, F., et al., *New chromanone acids with antibacterial activity from *Calophyllum brasiliense**. *Journal of Natural Products*, 2004. **67**(4): p. 537-541.
183. Ponguschariyagul, S., et al., *Caloinophyllin A, a new chromanone derivative from *Calophyllum inophyllum* roots*. *Natural Product Research*, 2018. **32**(21): p. 2535-2541.
184. Nguyen, L.-T.T., et al., *Polyisoprenylated acylphloroglucinols and a polyisoprenylated tetracyclic xanthone from the bark of *Calophyllum thorelii**. *Tetrahedron Letters*, 2012. **53**(34): p. 4487-4493.

185. Boonyong, C., et al., *Benzophenones and xanthone derivatives from *Garcinia schomburgkiana*-induced P-glycoprotein overexpression in human colorectal Caco-2 cells via oxidative stress-mediated mechanisms*. *Phytomedicine*, 2017. **27**: p. 8-14.
186. Santa-Cecilia, F.V., et al., *Antinociceptive and anti-inflammatory properties of 7-epiclusianone, a prenylated benzophenone from *Garcinia brasiliensis**. *European Journal of Pharmacology*, 2011. **670**(1): p. 280-285.
187. Hartati, S., et al., *A novel polyisoprenyl benzophenone derivative from *Garcinia eugeniaefolia**. *Journal of Asian Natural Products Research*, 2008. **10**(6): p. 509-513.





APPENDIX

จุฬาลงกรณ์มหาวิทยาลัย  
**CHULALONGKORN UNIVERSITY**

## LIST OF FIGURES AND TABLES (APPENDIX)

	Page
<b>PART I: Chemical constituents from the stems of <i>G. cylindrocarpa</i></b>	
Figure A1. $^1\text{H}$ NMR spectrum of cylindroxanthone D ( <b>GC1</b> ) in acetone- $d_6$ .....	128
Figure A2. $^{13}\text{C}$ NMR spectrum of cylindroxanthone D ( <b>GC1</b> ) in acetone- $d_6$ .....	128
Figure A3. COSY spectrum of cylindroxanthone D ( <b>GC1</b> ) in acetone- $d_6$ .....	129
Figure A4. HSQC spectrum of cylindroxanthone D ( <b>GC1</b> ) in acetone- $d_6$ .....	129
Figure A5. HMBC spectrum of cylindroxanthone D ( <b>GC1</b> ) in acetone- $d_6$ .....	130
Figure A6. HRESIMS spectrum of cylindroxanthone D ( <b>GC1</b> ) in MeCN.....	130
Figure A7. $^1\text{H}$ NMR spectrum of cylindroxanthone E ( <b>GC2</b> ) in acetone- $d_6$ .....	131
Figure A8. $^{13}\text{C}$ NMR spectrum of cylindroxanthone E ( <b>GC2</b> ) in acetone- $d_6$ .....	131
Figure A9. COSY spectrum of cylindroxanthone E ( <b>GC2</b> ) in acetone- $d_6$ .....	132
Figure A10. HSQC spectrum of cylindroxanthone E ( <b>GC2</b> ) in acetone- $d_6$ .....	132
Figure A11. HMBC spectrum of cylindroxanthone E ( <b>GC2</b> ) in acetone- $d_6$ .....	133
Figure A12. HRESIMS spectrum of cylindroxanthone E ( <b>GC2</b> ) in MeCN.....	133
Figure A13. $^1\text{H}$ NMR spectrum of cylindroxanthone F ( <b>GC3</b> ) in acetone- $d_6$ .....	134
Figure A14. $^{13}\text{C}$ NMR spectrum of cylindroxanthone F ( <b>GC3</b> ) in acetone- $d_6$ .....	134
Figure A15. COSY spectrum of cylindroxanthone F ( <b>GC3</b> ) in acetone- $d_6$ .....	135
Figure A16. HSQC spectrum of cylindroxanthone F ( <b>GC3</b> ) in acetone- $d_6$ .....	135
Figure A17. HMBC spectrum of cylindroxanthone F ( <b>GC3</b> ) in acetone- $d_6$ .....	136
Figure A18. HRESIMS spectrum of cylindroxanthone F ( <b>GC3</b> ) in MeCN.....	136
Figure A19. $^1\text{H}$ NMR spectrum of cylindroxanthone G ( <b>GC4</b> ) in $\text{CDCl}_3$ .....	137
Figure A20. $^{13}\text{C}$ NMR spectrum of cylindroxanthone G ( <b>GC4</b> ) in $\text{CDCl}_3$ .....	137
Figure A21. COSY spectrum of cylindroxanthone G ( <b>GC4</b> ) in $\text{CDCl}_3$ .....	138

Figure A22. HSQC spectrum of cylindroxanthone G ( <b>GC4</b> ) in CDCl <sub>3</sub> .....	138
Figure A23. HMBC spectrum of cylindroxanthone G ( <b>GC4</b> ) in CDCl <sub>3</sub> .....	139
Figure A24. HRESIMS spectrum of cylindroxanthone G ( <b>GC4</b> ) in CH <sub>2</sub> Cl <sub>2</sub> .....	139
Figure A25. <sup>1</sup> H NMR spectrum of cylindrobiphenyl A ( <b>GC5</b> ) in CDCl <sub>3</sub> .....	140
Figure A26. <sup>13</sup> C NMR spectrum of cylindrobiphenyl A ( <b>GC5</b> ) in CDCl <sub>3</sub> .....	140
Figure A27. COSY spectrum of cylindrobiphenyl A ( <b>GC5</b> ) in CDCl <sub>3</sub> .....	141
Figure A28. HSQC spectrum of cylindrobiphenyl A ( <b>GC5</b> ) in CDCl <sub>3</sub> .....	141
Figure A29. HMBC spectrum of cylindrobiphenyl A ( <b>GC5</b> ) in CDCl <sub>3</sub> .....	142
Figure A30. HRESIMS spectrum of cylindrobiphenyl A ( <b>GC5</b> ) in MeCN.....	142
Figure A31. <sup>1</sup> H NMR spectrum of cylindrobiphenyl B ( <b>GC6</b> ) in CDCl <sub>3</sub> .....	143
Figure A32. <sup>13</sup> C NMR spectrum of cylindrobiphenyl B ( <b>GC6</b> ) in CDCl <sub>3</sub> .....	143
Figure A33. COSY spectrum of cylindrobiphenyl B ( <b>GC6</b> ) in CDCl <sub>3</sub> .....	144
Figure A34. HSQC spectrum of cylindrobiphenyl B ( <b>GC6</b> ) in CDCl <sub>3</sub> .....	144
Figure A35. HMBC spectrum of cylindrobiphenyl B ( <b>GC6</b> ) in CDCl <sub>3</sub> .....	145
Figure A36. HRESIMS spectrum of cylindrobiphenyl B ( <b>GC6</b> ) in MeCN.....	145
Figure B1. <sup>1</sup> H NMR spectrum of tetrandraxanthone A ( <b>GT1</b> ) in CDCl <sub>3</sub> .....	146
Figure B2. <sup>13</sup> C NMR spectrum of tetrandraxanthone A ( <b>GT1</b> ) in CDCl <sub>3</sub> .....	146
Figure B3. COSY spectrum of tetrandraxanthone A ( <b>GT1</b> ) in CDCl <sub>3</sub> .....	147
Figure B4. HSQC spectrum of tetrandraxanthone A ( <b>GT1</b> ) in CDCl <sub>3</sub> .....	147
Figure B5. HMBC spectrum of tetrandraxanthone A ( <b>GT1</b> ) in CDCl <sub>3</sub> .....	148
Figure B6. HRESIMS spectrum of tetrandraxanthone A ( <b>GT1</b> ) in MeCN.....	148
Figure B7. <sup>1</sup> H NMR spectrum of tetrandraxanthone B ( <b>GT2</b> ) in CDCl <sub>3</sub> .....	149
Figure B8. <sup>13</sup> C NMR spectrum of tetrandraxanthone B ( <b>GT2</b> ) in CDCl <sub>3</sub> .....	149
Figure B9. COSY spectrum of tetrandraxanthone B ( <b>GT2</b> ) in CDCl <sub>3</sub> .....	150

Figure B10. HSQC spectrum of tetrandraxanthone B ( <b>GT2</b> ) in CDCl <sub>3</sub> .....	150
Figure B11. HMBC spectrum of tetrandraxanthone B ( <b>GT2</b> ) in CDCl <sub>3</sub> .....	151
Figure B12. HRESIMS spectrum of tetrandraxanthone B ( <b>GT2</b> ) in MeCN.....	151
Figure B13. <sup>1</sup> H NMR spectrum of tetrandraxanthone C ( <b>GT3</b> ) in CDCl <sub>3</sub> .....	152
Figure B14. <sup>13</sup> C NMR spectrum of tetrandraxanthone C ( <b>GT3</b> ) in CDCl <sub>3</sub> .....	152
Figure B15. COSY spectrum of tetrandraxanthone C ( <b>GT3</b> ) in CDCl <sub>3</sub> .....	153
Figure B16. HSQC spectrum of tetrandraxanthone C ( <b>GT3</b> ) in CDCl <sub>3</sub> .....	153
Figure B17. HMBC spectrum of tetrandraxanthone C ( <b>GT3</b> ) in CDCl <sub>3</sub> .....	154
Figure B18. HRESIMS spectrum of tetrandraxanthone C ( <b>GT3</b> ) in MeCN.....	154
Figure B19. <sup>1</sup> H NMR spectrum of tetrandraxanthone D ( <b>GT4</b> ) in acetone- <i>d</i> <sub>6</sub> .....	155
Figure B20. <sup>13</sup> C NMR spectrum of tetrandraxanthone D ( <b>GT4</b> ) in acetone- <i>d</i> <sub>6</sub> .....	155
Figure B21. COSY spectrum of tetrandraxanthone D ( <b>GT4</b> ) in acetone- <i>d</i> <sub>6</sub> .....	156
Figure B22. HSQC spectrum of tetrandraxanthone D ( <b>GT4</b> ) in acetone- <i>d</i> <sub>6</sub> .....	156
Figure B23. HMBC spectrum of tetrandraxanthone D ( <b>GT4</b> ) in acetone- <i>d</i> <sub>6</sub> .....	157
Figure B24. HRESIMS spectrum of tetrandraxanthone D ( <b>GT4</b> ) in MeCN.....	157
Figure B25. <sup>1</sup> H NMR spectrum of tetrandraxanthone E ( <b>GT5</b> ) in acetone- <i>d</i> <sub>6</sub> .....	158
Figure B26. <sup>13</sup> C NMR spectrum of tetrandraxanthone E ( <b>GT5</b> ) in acetone- <i>d</i> <sub>6</sub> .....	158
Figure B27. COSY spectrum of tetrandraxanthone E ( <b>GT5</b> ) in acetone- <i>d</i> <sub>6</sub> .....	159
Figure B28. HSQC spectrum of tetrandraxanthone E ( <b>GT5</b> ) in acetone- <i>d</i> <sub>6</sub> .....	159
Figure B29. HMBC spectrum of tetrandraxanthone E ( <b>GT5</b> ) in acetone- <i>d</i> <sub>6</sub> .....	160
Figure B30. HRESIMS spectrum of tetrandraxanthone E ( <b>GT5</b> ) in MeCN.....	160
Figure B31. <sup>1</sup> H NMR spectrum of tetrandraxanthone F ( <b>GT6</b> ) in CDCl <sub>3</sub> .....	161
Figure B32. <sup>13</sup> C NMR spectrum of tetrandraxanthone F ( <b>GT6</b> ) in CDCl <sub>3</sub> .....	161
Figure B33. COSY spectrum of tetrandraxanthone F ( <b>GT6</b> ) in CDCl <sub>3</sub> .....	162

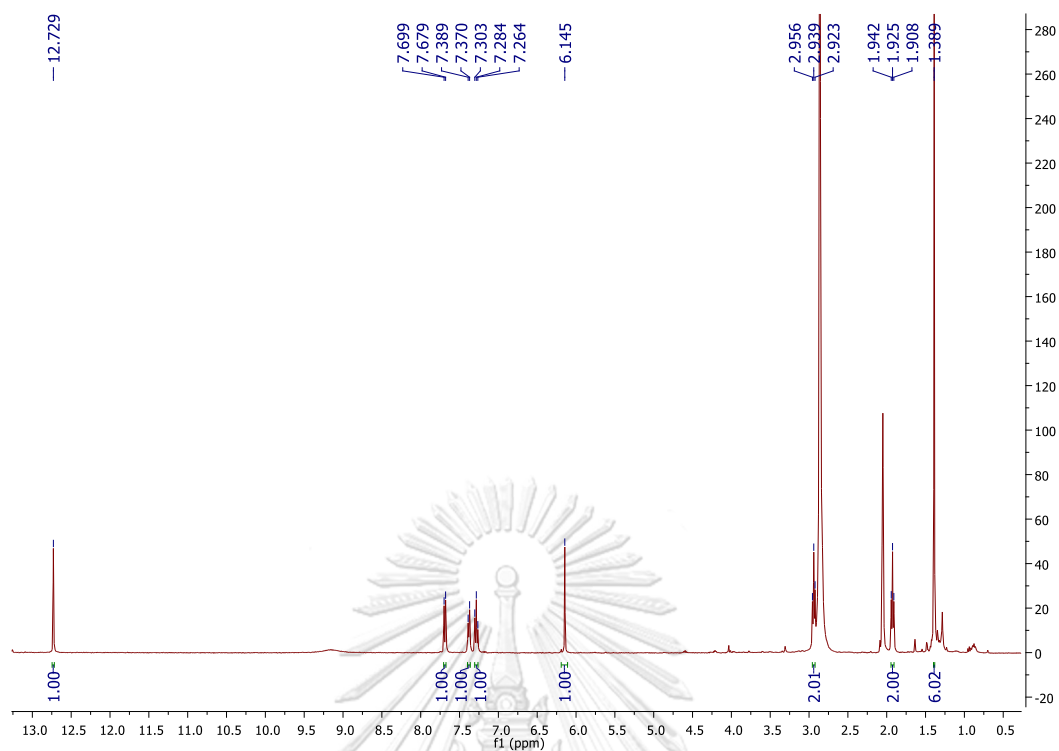
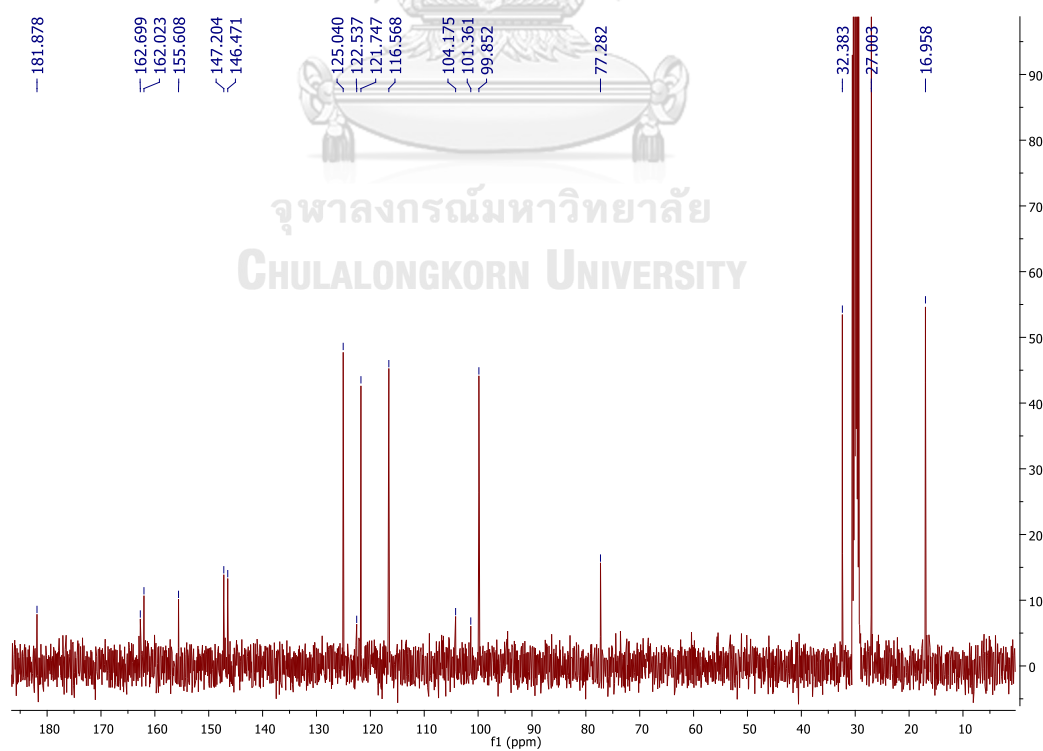
Figure B34. HSQC spectrum of tetrandraxanthone F ( <b>GT6</b> ) in CDCl <sub>3</sub> .....	162
Figure B35. HMBC spectrum of tetrandraxanthone F ( <b>GT6</b> ) in CDCl <sub>3</sub> .....	163
Figure B36. HRESIMS spectrum of tetrandraxanthone F ( <b>GT6</b> ) in MeCN.....	163
Figure B37. <sup>1</sup> H NMR spectrum of tetrandraxanthone G ( <b>GT7</b> ) in CDCl <sub>3</sub> .....	164
Figure B38. <sup>13</sup> C NMR spectrum of tetrandraxanthone G ( <b>GT7</b> ) in CDCl <sub>3</sub> .....	164
Figure B39. COSY spectrum of tetrandraxanthone G ( <b>GT7</b> ) in CDCl <sub>3</sub> .....	165
Figure B40. HSQC spectrum of tetrandraxanthone G ( <b>GT7</b> ) in CDCl <sub>3</sub> .....	165
Figure B41. HMBC spectrum of tetrandraxanthone G ( <b>GT7</b> ) in CDCl <sub>3</sub> .....	166
Figure B42. HRESIMS spectrum of tetrandraxanthone G ( <b>GT7</b> ) in MeCN.....	166
Figure B43. <sup>1</sup> H NMR spectrum of tetrandraxanthone H ( <b>GT8</b> ) in CDCl <sub>3</sub> .....	167
Figure B44. <sup>13</sup> C NMR spectrum of tetrandraxanthone H ( <b>GT8</b> ) in CDCl <sub>3</sub> .....	167
Figure B45. COSY spectrum of tetrandraxanthone H ( <b>GT8</b> ) in CDCl <sub>3</sub> .....	168
Figure B46. HSQC spectrum of tetrandraxanthone H ( <b>GT8</b> ) in CDCl <sub>3</sub> .....	168
Figure B47. HMBC spectrum of tetrandraxanthone H ( <b>GT8</b> ) in CDCl <sub>3</sub> .....	169
Figure B48. HRESIMS spectrum of tetrandraxanthone H ( <b>GT8</b> ) in MeCN.....	169
Figure B49. <sup>1</sup> H NMR spectrum of tetrandraxanthone I ( <b>GT9</b> ) in acetone- <i>d</i> <sub>6</sub> .....	170
Figure B50. <sup>13</sup> C NMR spectrum of tetrandraxanthone I ( <b>GT9</b> ) in acetone- <i>d</i> <sub>6</sub> .....	170
Figure B51. COSY spectrum of tetrandraxanthone I ( <b>GT9</b> ) in acetone- <i>d</i> <sub>6</sub> .....	171
Figure B52. HSQC spectrum of tetrandraxanthone I ( <b>GT9</b> ) in acetone- <i>d</i> <sub>6</sub> .....	171
Figure B53. HMBC spectrum of tetrandraxanthone I ( <b>GT9</b> ) in acetone- <i>d</i> <sub>6</sub> .....	172
Figure B54. HRESIMS spectrum of tetrandraxanthone I ( <b>GT9</b> ) in MeCN.....	172
Figure C1. <sup>1</sup> H NMR spectrum of picrorhizone A ( <b>GP1</b> ) in methanol- <i>d</i> <sub>4</sub> .....	173
Figure C2. <sup>13</sup> C NMR spectrum of picrorhizone A ( <b>GP1</b> ) in methanol- <i>d</i> <sub>4</sub> .....	173
Figure C3. COSY spectrum of picrorhizone A ( <b>GP1</b> ) in methanol- <i>d</i> <sub>4</sub> .....	174

Figure C4. HSQC spectrum of picrorhizone A ( <b>GP1</b> ) in methanol- $d_4$ .....	174
Figure C5. HMBC spectrum of picrorhizone A ( <b>GP1</b> ) in methanol- $d_4$ .....	175
Figure C6a. NOESY spectrum of picrorhizone A ( <b>GP1</b> ) in methanol- $d_4$ .....	175
Figure C6b. Expanded NOESY spectrum of picrorhizone A ( <b>GP1</b> ) in methanol- $d_4$ .....	176
Figure C7. HRESIMS spectrum of picrorhizone A ( <b>GP1</b> ) in methanol .....	176
Figure C8. $^1\text{H}$ NMR spectrum of picrorhizone B ( <b>GP2</b> ) in methanol- $d_4$ .....	177
Figure C9. $^{13}\text{C}$ NMR spectrum of picrorhizone B ( <b>GP2</b> ) in methanol- $d_4$ .....	177
Figure C10. COSY spectrum of picrorhizone B ( <b>GP2</b> ) in methanol- $d_4$ .....	178
Figure C11. HSQC spectrum of picrorhizone B ( <b>GP2</b> ) in methanol- $d_4$ .....	178
Figure C12. HMBC spectrum of picrorhizone B ( <b>GP2</b> ) in methanol- $d_4$ .....	179
Figure C13. NOESY spectrum of picrorhizone B ( <b>GP2</b> ) in methanol- $d_4$ .....	179
Figure C14. HRESIMS spectrum of picrorhizone B ( <b>GP2</b> ) in methanol- $d_4$ .....	180
Figure C15. $^1\text{H}$ NMR spectrum of picrorhizone C ( <b>GP3</b> ) in $\text{CDCl}_3$ .....	181
Figure C16. $^{13}\text{C}$ NMR spectrum of picrorhizone C ( <b>GP3</b> ) in $\text{CDCl}_3$ .....	181
Figure C17. COSY spectrum of picrorhizone C ( <b>GP3</b> ) in $\text{CDCl}_3$ .....	182
Figure C18. HSQC spectrum of picrorhizone C ( <b>GP3</b> ) in $\text{CDCl}_3$ .....	182
Figure C19. HMBC spectrum of picrorhizone C ( <b>GP3</b> ) in $\text{CDCl}_3$ .....	183
Figure C20. NOESY spectrum of picrorhizone C ( <b>GP3</b> ) in $\text{CDCl}_3$ .....	183
Figure C21. HRESIMS spectrum of picrorhizone C ( <b>GP3</b> ) in MeCN .....	184
Figure C22. $^1\text{H}$ NMR spectrum of picrorhizone D ( <b>GP4</b> ) in methanol- $d_4$ .....	185
Figure C23. $^{13}\text{C}$ NMR spectrum of picrorhizone D ( <b>GP4</b> ) in methanol- $d_4$ .....	185
Figure C24. COSY spectrum of picrorhizone D ( <b>GP4</b> ) in methanol- $d_4$ .....	186
Figure C25. HSQC spectrum of picrorhizone D ( <b>GP4</b> ) in methanol- $d_4$ .....	186
Figure C26. HMBC spectrum of picrorhizone D ( <b>GP4</b> ) in methanol- $d_4$ .....	187



Figure C27. NOESY spectrum of picrorhizone D ( <b>GP4</b> ) in methanol- $d_4$ .....	187
Figure C28. HRESIMS spectrum of picrorhizone D ( <b>GP4</b> ) in methanol.....	188
Figure C29. $^1\text{H}$ NMR spectrum of picrorhizone E ( <b>GP5</b> ) in methanol- $d_4$ .....	189
Figure C30. $^{13}\text{C}$ NMR spectrum of picrorhizone E ( <b>GP5</b> ) in methanol- $d_4$ .....	189
Figure C31. COSY spectrum of picrorhizone E ( <b>GP5</b> ) in methanol- $d_4$ .....	190
Figure C32. HSQC spectrum of picrorhizone E ( <b>GP5</b> ) in methanol- $d_4$ .....	190
Figure C33. HMBC spectrum of picrorhizone E ( <b>GP5</b> ) in methanol- $d_4$ .....	191
Figure C34. NOESY spectrum of picrorhizone E ( <b>GP5</b> ) in methanol- $d_4$ .....	191
Figure C35. HRESIMS spectrum of picrorhizone E ( <b>GP5</b> ) in methanol.....	192
Figure C36. $^1\text{H}$ NMR spectrum of picrorhizone F ( <b>GP6</b> ) in methanol- $d_4$ .....	193
Figure C37. $^{13}\text{C}$ NMR spectrum of picrorhizone F ( <b>GP6</b> ) in methanol- $d_4$ .....	193
Figure C38. COSY spectrum of picrorhizone F ( <b>GP6</b> ) in methanol- $d_4$ .....	194
Figure C39. HSQC spectrum of picrorhizone F ( <b>GP6</b> ) in methanol- $d_4$ .....	194
Figure C40. HMBC spectrum of picrorhizone F ( <b>GP6</b> ) in methanol- $d_4$ .....	195
Figure C41. NOESY spectrum of picrorhizone F ( <b>GP6</b> ) in methanol- $d_4$ .....	195
Figure C42. HRESIMS spectrum of picrorhizone F ( <b>GP6</b> ) in methanol.....	196
Figure C43. $^1\text{H}$ NMR spectrum of picrorhizone G ( <b>GP7</b> ) in methanol- $d_4$ .....	197
Figure C44. $^{13}\text{C}$ NMR spectrum of picrorhizone G ( <b>GP7</b> ) in methanol- $d_4$ .....	197
Figure C45. COSY spectrum of picrorhizone G ( <b>GP7</b> ) in methanol- $d_4$ .....	198
Figure C46. HSQC spectrum of picrorhizone G ( <b>GP7</b> ) in methanol- $d_4$ .....	198
Figure C47. HMBC spectrum of picrorhizone G ( <b>GP7</b> ) in methanol- $d_4$ .....	199
Figure C48. NOESY spectrum of picrorhizone G ( <b>GP7</b> ) in methanol- $d_4$ .....	199
Figure C49. HRESIMS spectrum of picrorhizone G ( <b>GP7</b> ) in methanol.....	200
Figure C50. $^1\text{H}$ NMR spectrum of picrorhizone H ( <b>GP8</b> ) in methanol- $d_4$ .....	201

Figure C51. $^{13}\text{C}$ NMR spectrum of picrorhizone H ( <b>GP8</b> ) in methanol- $d_4$ .....	201
Figure C52. COSY spectrum of picrorhizone H ( <b>GP8</b> ) in methanol- $d_4$ .....	202
Figure C53. HSQC spectrum of picrorhizone H ( <b>GP8</b> ) in methanol- $d_4$ .....	202
Figure C54. HMBC spectrum of picrorhizone H ( <b>GP8</b> ) in methanol- $d_4$ .....	203
Figure C55. NOESY spectrum of picrorhizone H ( <b>GP8</b> ) in methanol- $d_4$ .....	203
Figure C56. HRESIMS spectrum of picrorhizone H ( <b>GP8</b> ) in methanol.....	204
Figure C57. $^1\text{H}$ NMR spectrum of garcinopicrobenzophenone ( <b>GP9</b> ) in methanol- $d_4$ .....	205
Figure C58. $^{13}\text{C}$ NMR spectrum of garcinopicrobenzophenone ( <b>GP9</b> ) in methanol- $d_4$ .....	205
Figure C59. COSY spectrum of garcinopicrobenzophenone ( <b>GP9</b> ) in methanol- $d_4$ .....	206
Figure C60. HSQC spectrum of garcinopicrobenzophenone ( <b>GP9</b> ) in methanol- $d_4$ .....	206
Figure C61. HMBC spectrum of garcinopicrobenzophenone ( <b>GP9</b> ) in methanol- $d_4$ .....	207
Figure C62. NOESY spectrum of garcinopicrobenzophenone ( <b>GP9</b> ) in methanol- $d_4$ .....	207
Figure C63. (a) Calculated ( <b>6a</b> , <b>6b</b> , <b>9a</b> , <b>9a</b> enantiomer, <b>9b</b> ) and experimental ECD spectra ( <b>1–9</b> ) of <b>GP1–GP9</b> and (b) Optimized structures and molecular energies ( $E$ ) from ECD calculation using TD-DFT method for diastereomeric models <b>9a</b> and <b>9b</b> , as well as <b>6a</b> and <b>6b</b> .....	208
Table C1. $^1\text{H}$ (400 MHz) and $^{13}\text{C}$ (100 MHz) NMR spectroscopic data of <b>GP9</b> in methanol- $d_4$ .....	209

Figure A1.  $^1\text{H}$  NMR spectrum of cylindroxanthone D (**GC1**) in acetone- $d_6$ Figure A2.  $^{13}\text{C}$  NMR spectrum of cylindroxanthone D (**GC1**) in acetone- $d_6$

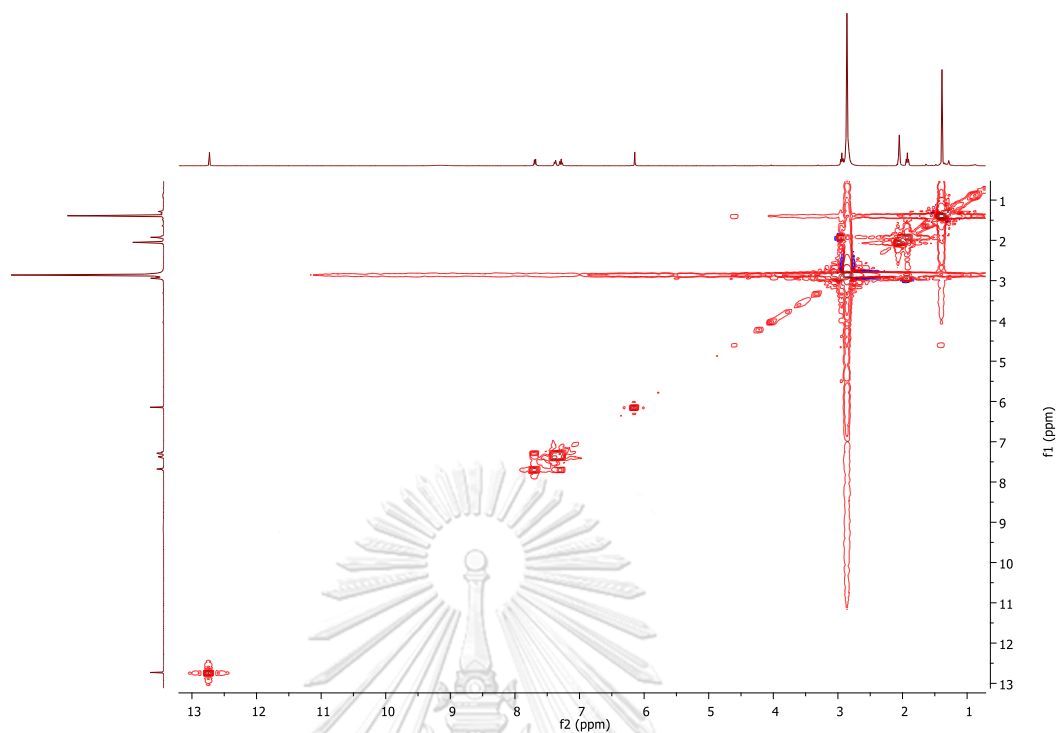


Figure A3. COSY spectrum of cylindroxanthone D (**GC1**) in acetone- $d_6$

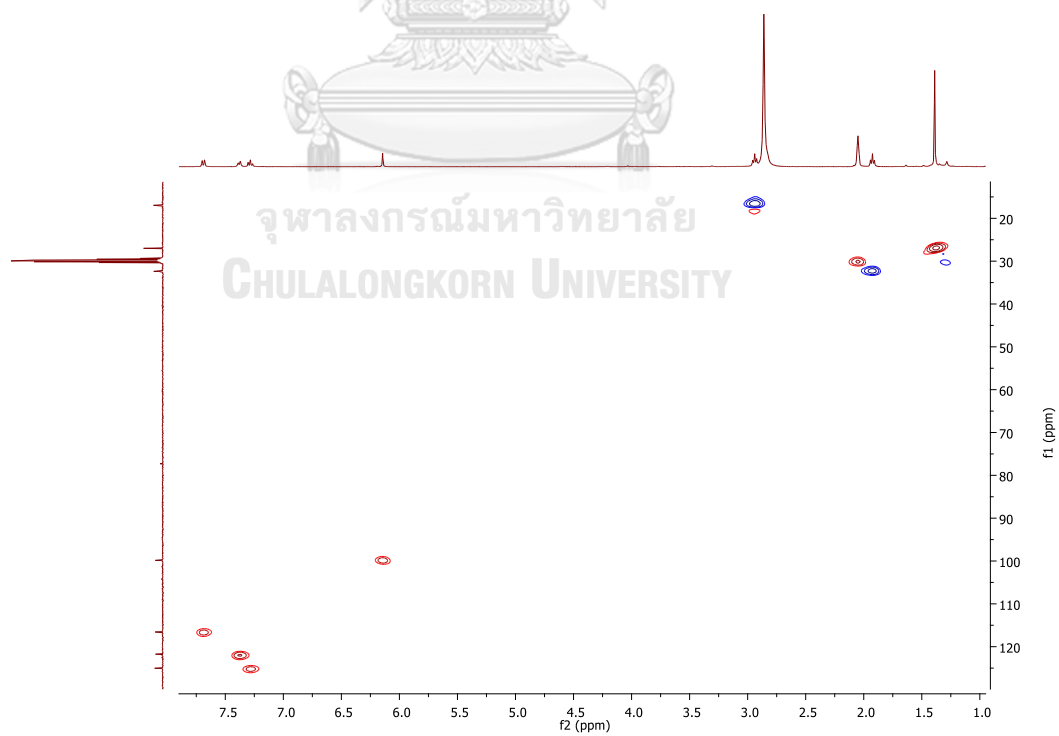
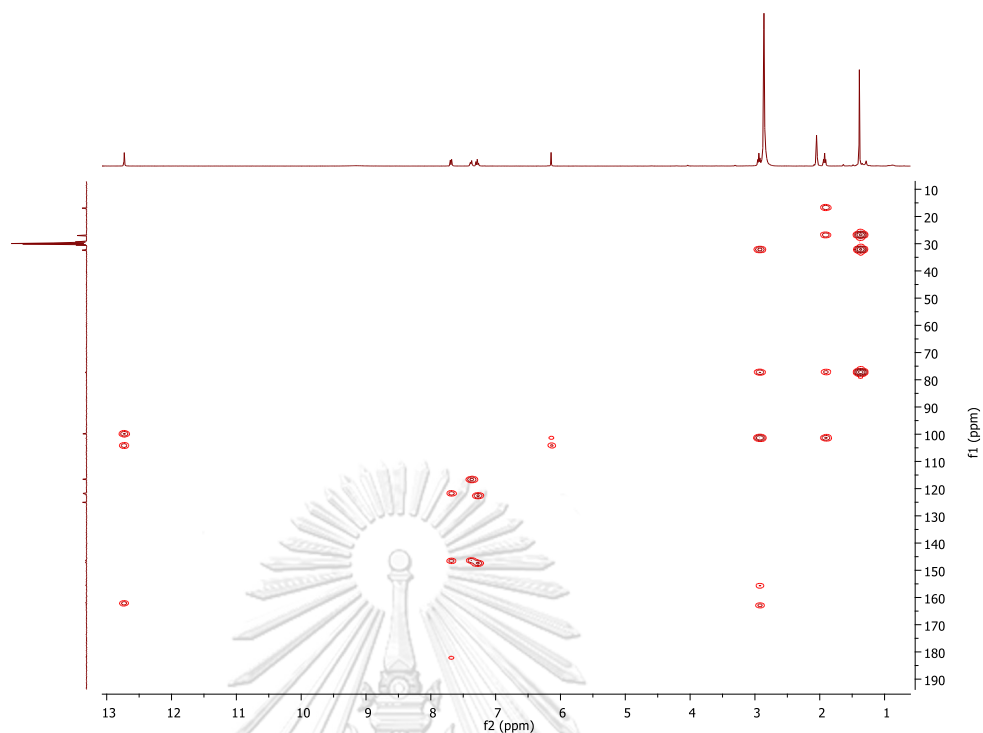


Figure A4. HSQC spectrum of cylindroxanthone D (**GC1**) in acetone- $d_6$

Figure A5. HMBC spectrum of cylindroxanthone D (GC1) in acetone- $d_6$ 

### Mass Spectrum List Report

<b>Analysis Info</b>		Acquisition Date	3/16/2018 12:25:31 PM
Analysis Name	D:\Data\Data Service\180316_neg_GCD-18.d	Operator	CU.
Method	NV_neg_0.3min_profile_1segment_lowNubulizerDrygas(2).m	Instrument / Ser#	micrOTOF-Q II 10335
Sample Name	180316_neg_GCD-18	Comment	

#### Acquisition Parameter

Source Type	ESI	Ion Polarity	Negative	Set Nebulizer	0.4 Bar
Focus	Not active	Set Capillary	4000 V	Set Dry Heater	200 °C
Scan Begin	50 m/z	Set End Plate Offset	-500 V	Set Dry Gas	4.0 l/min
Scan End	1500 m/z	Set Collision Cell RF	150.0 Vpp	Set Divert Valve	Waste

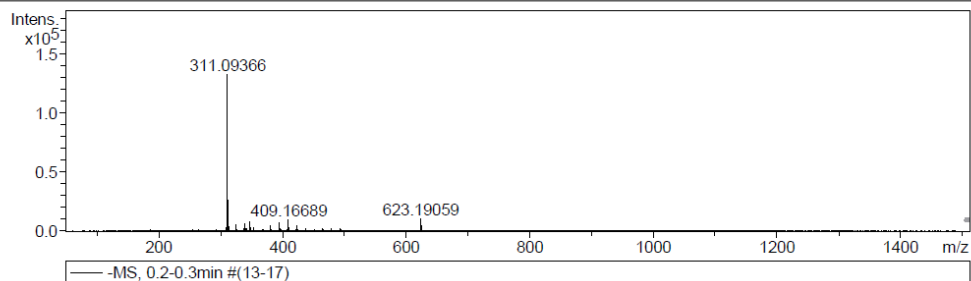


Figure A6. HRESIMS spectrum of cylindroxanthone D (GC1) in MeCN

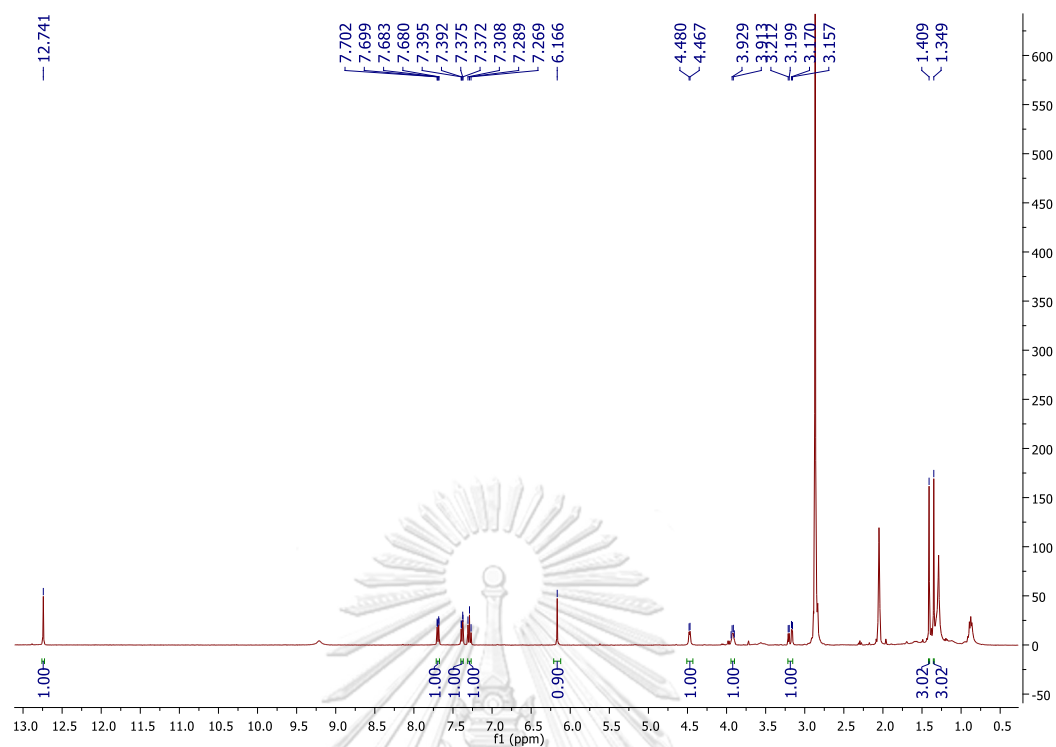


Figure A7.  $^1\text{H}$  NMR spectrum of cylindroxanthone E (GC2) in acetone- $d_6$

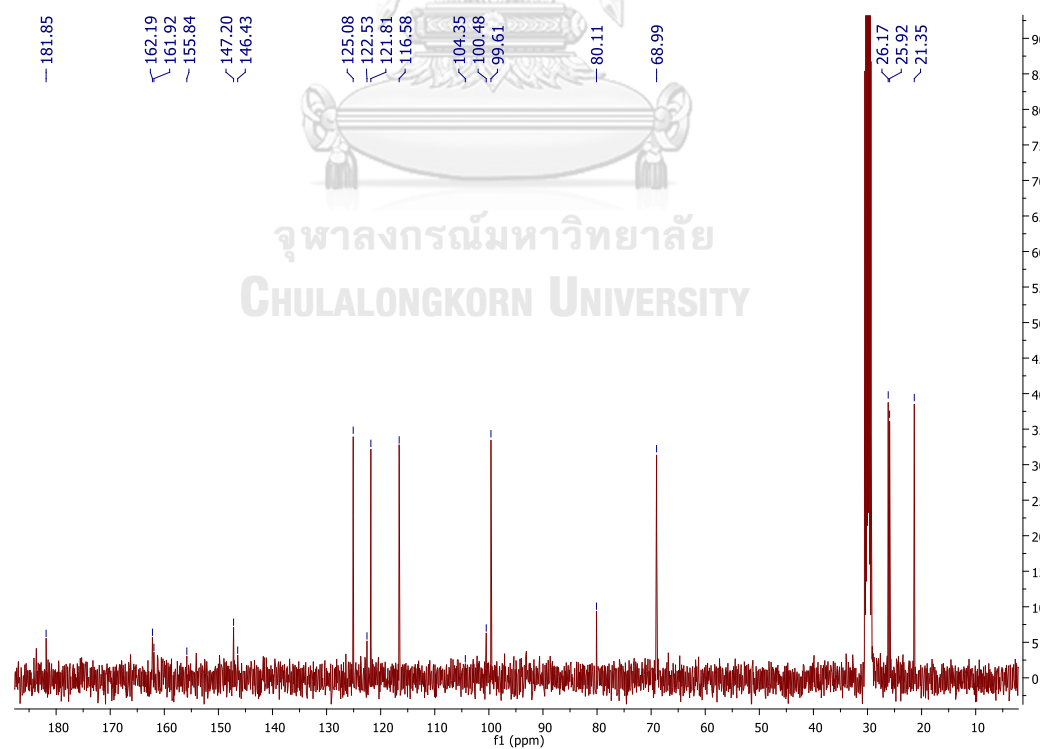
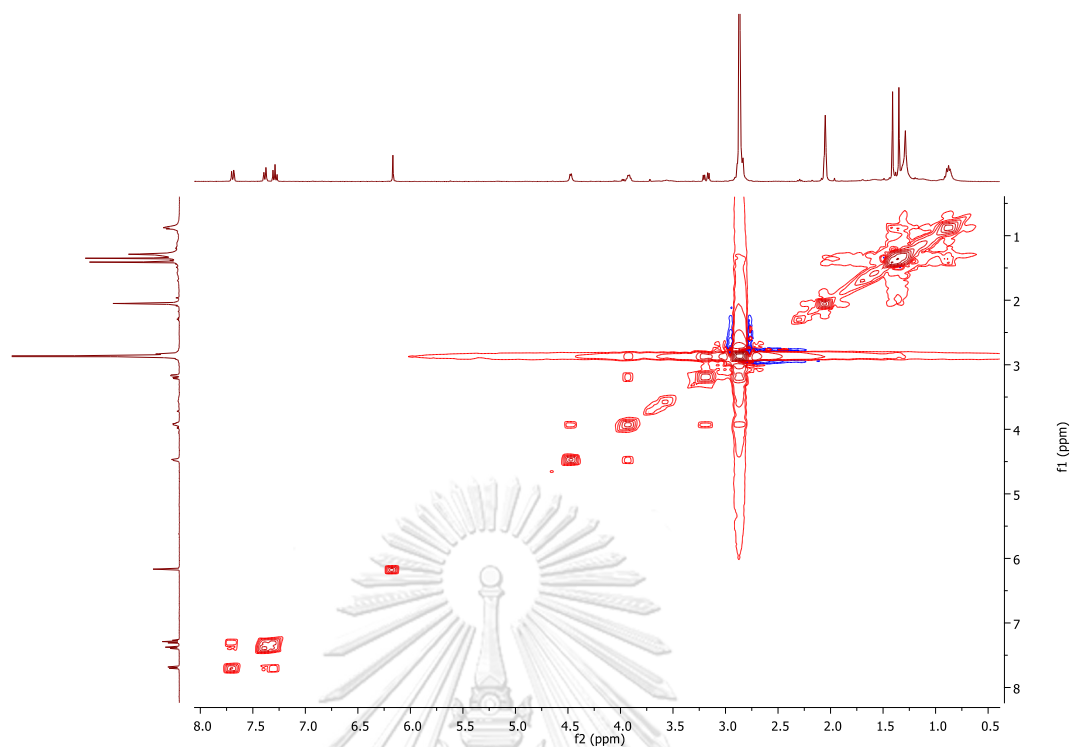
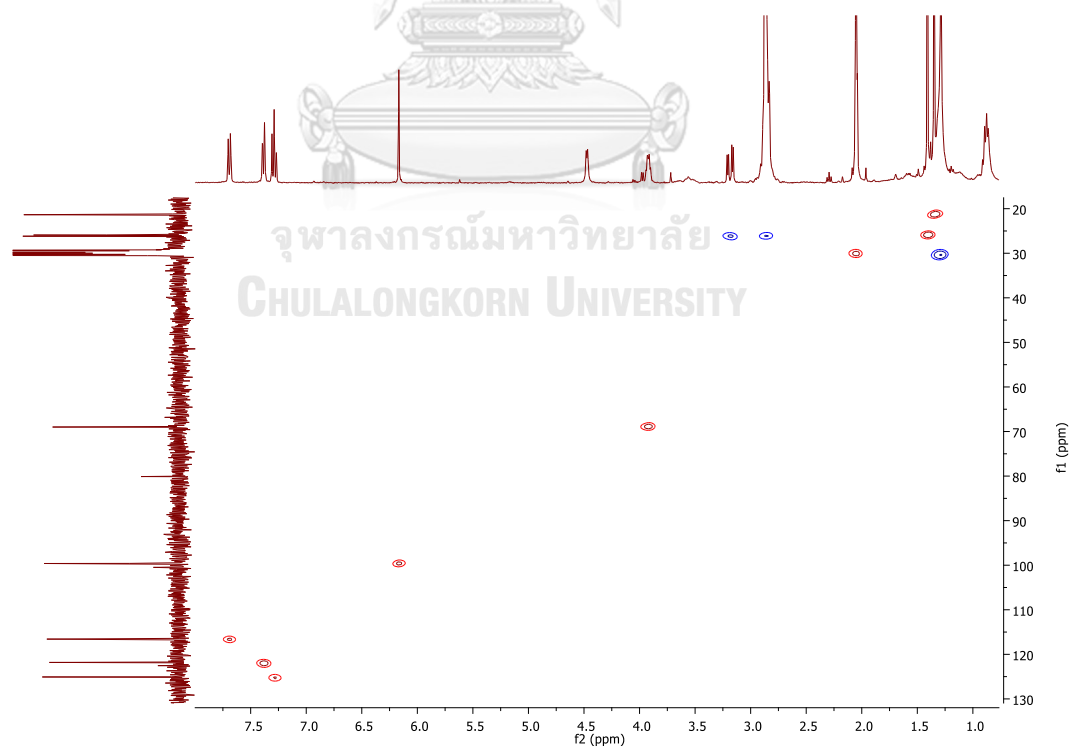
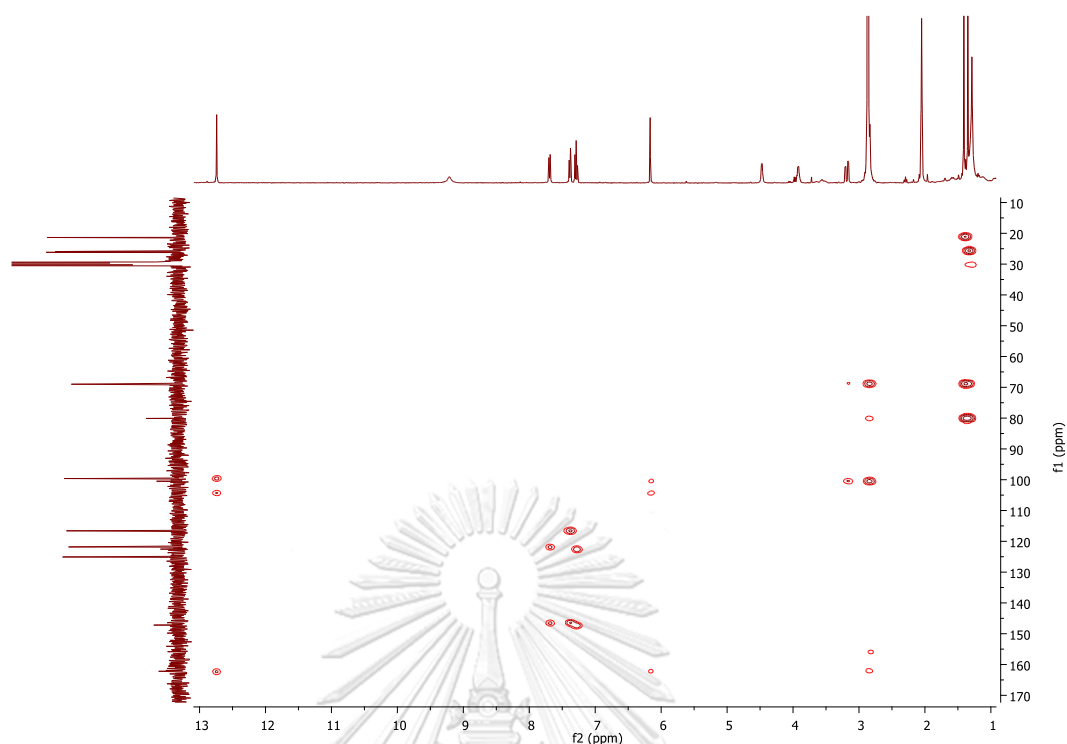


Figure A8.  $^{13}\text{C}$  NMR spectrum of cylindroxanthone E (GC2) in acetone- $d_6$

Figure A9. COSY spectrum of cylindroxanthone E (GC2) in acetone- $d_6$ Figure A10. HSQC spectrum of cylindroxanthone E (GC2) in acetone- $d_6$

Figure A11. HMBC spectrum of cylindroxanthone E (GC2) in acetone- $d_6$ 

### Mass Spectrum List Report

<b>Analysis Info</b>		Acquisition Date	3/16/2018 12:29:17 PM
Analysis Name	D:\Data\Data Service\180316_neg_R8-2.d	Operator	CU.
Method	NV_neg_0.3min_profile_1segment_lowNbulizerDrygas(2).m	Instrument / Ser#	micrOTOF-Q II 10335
Sample Name	180316_neg_R8-2		
Comment			

#### Acquisition Parameter

Source Type	ESI	Ion Polarity	Negative	Set Nebulizer	0.4 Bar
Focus	Not active	Set Capillary	4000 V	Set Dry Heater	200 °C
Scan Begin	50 m/z	Set End Plate Offset	-500 V	Set Dry Gas	4.0 l/min
Scan End	1500 m/z	Set Collision Cell RF	150.0 Vpp	Set Divert Valve	Waste

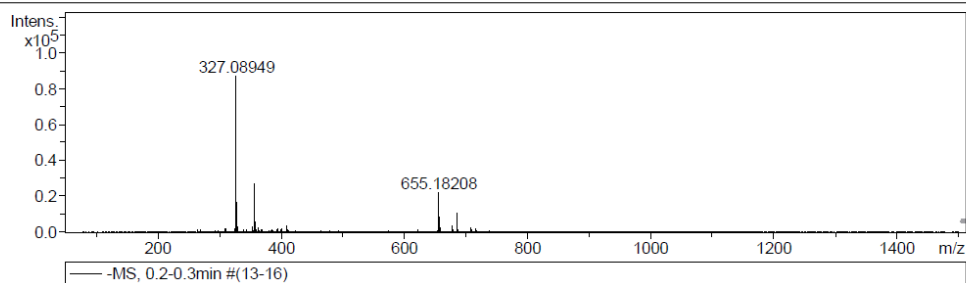


Figure A12. HRESIMS spectrum of cylindroxanthone E (GC2) in MeCN



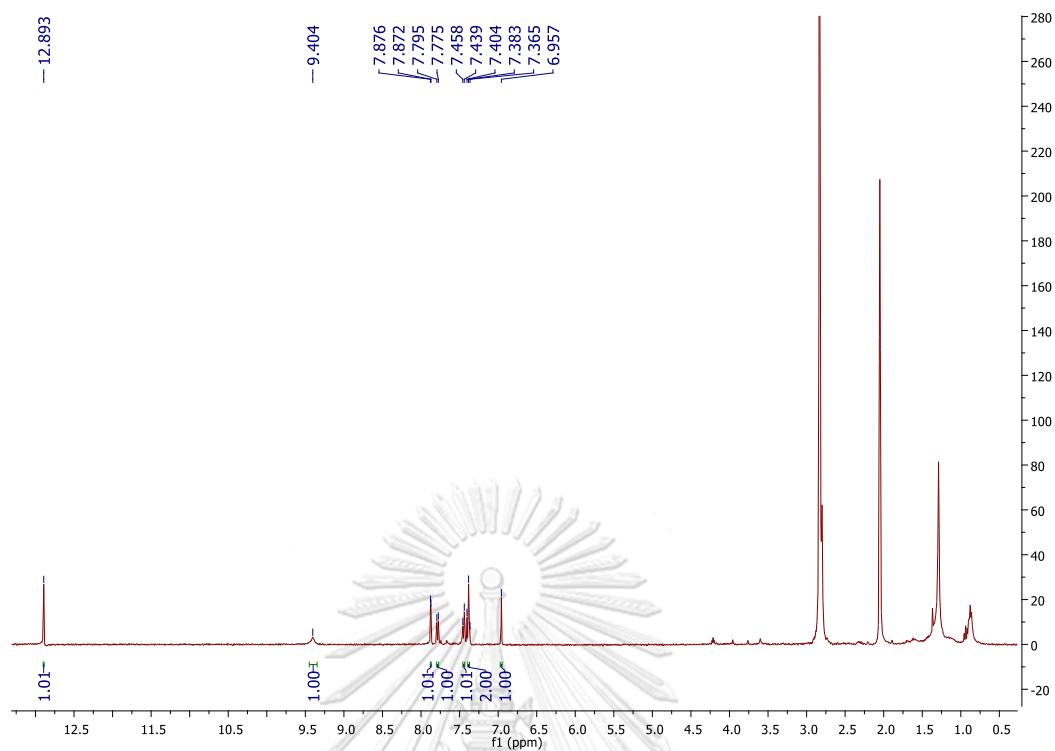


Figure A13.  $^1\text{H}$  NMR spectrum of cylindroxanthone F (GC3) in acetone- $d_6$

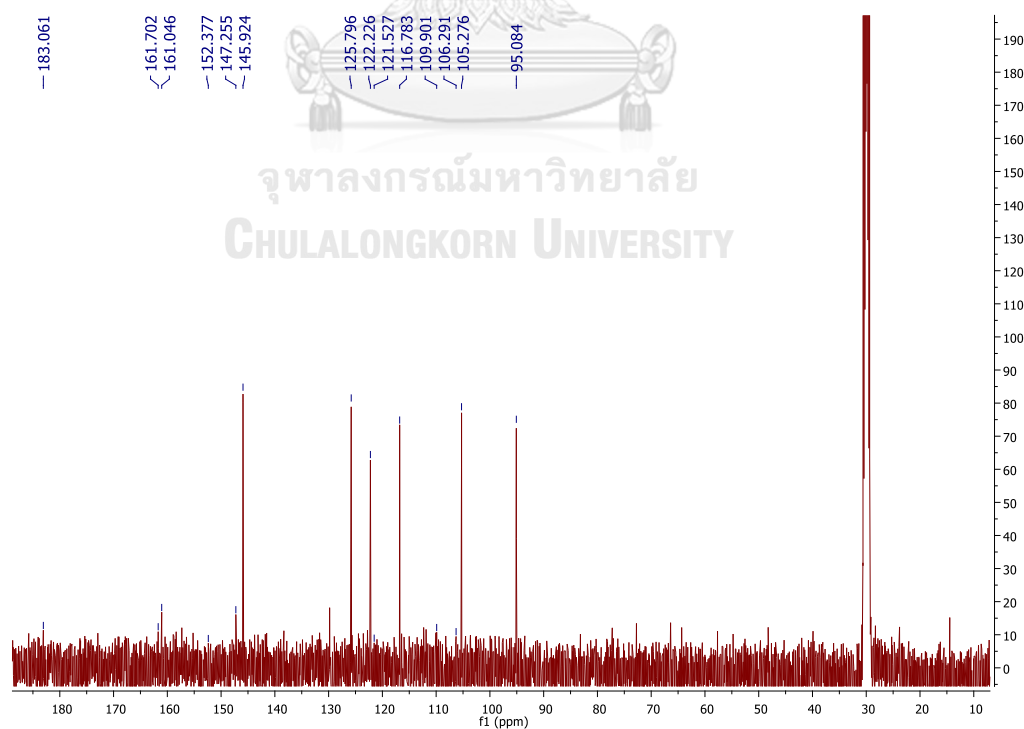


Figure A14.  $^{13}\text{C}$  NMR spectrum of cylindroxanthone F (GC3) in acetone- $d_6$

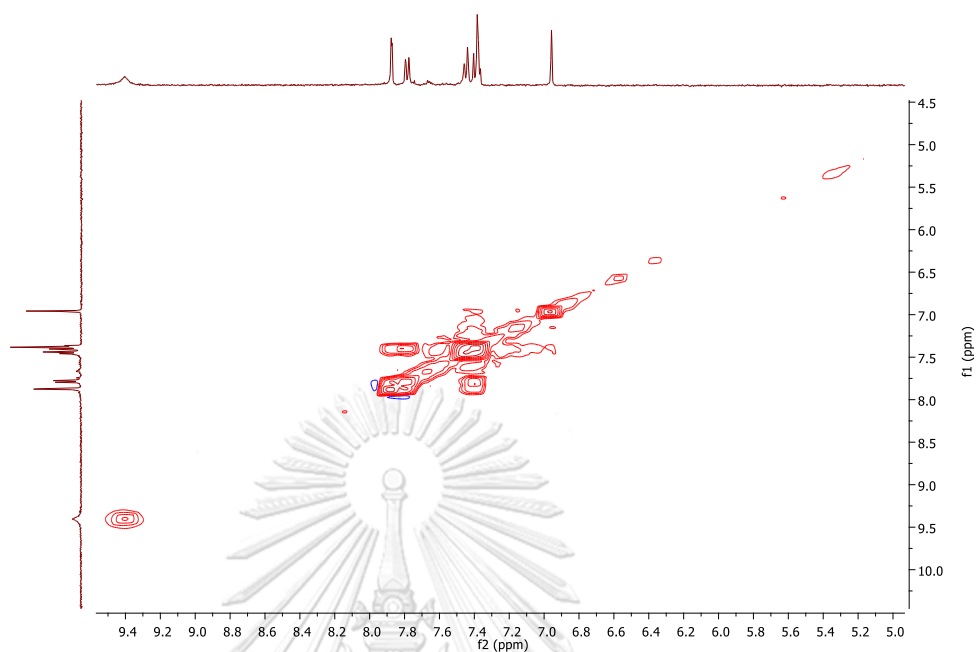


Figure A15. COSY spectrum of cylindroxanthone F (**GC3**) in acetone- $d_6$

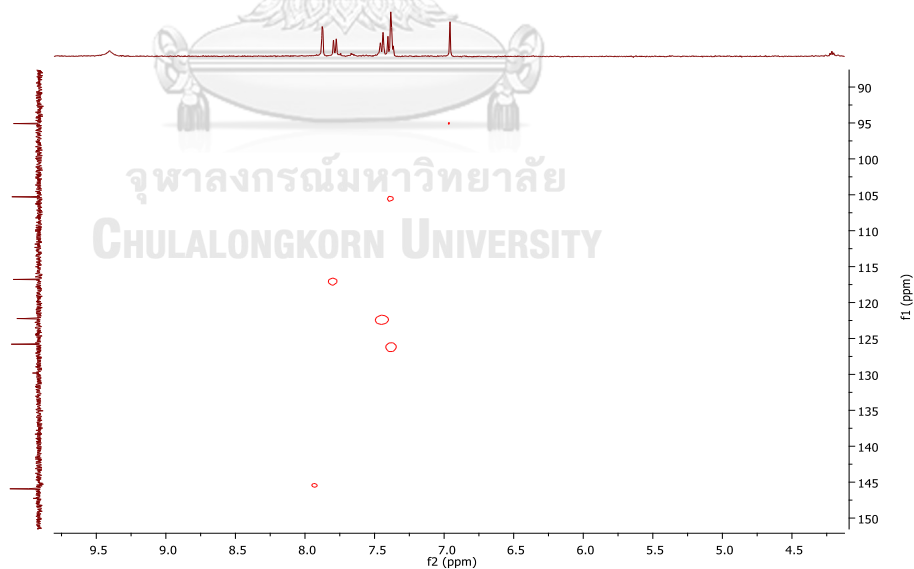


Figure A16. HSQC spectrum of cylindroxanthone F (**GC3**) in acetone- $d_6$

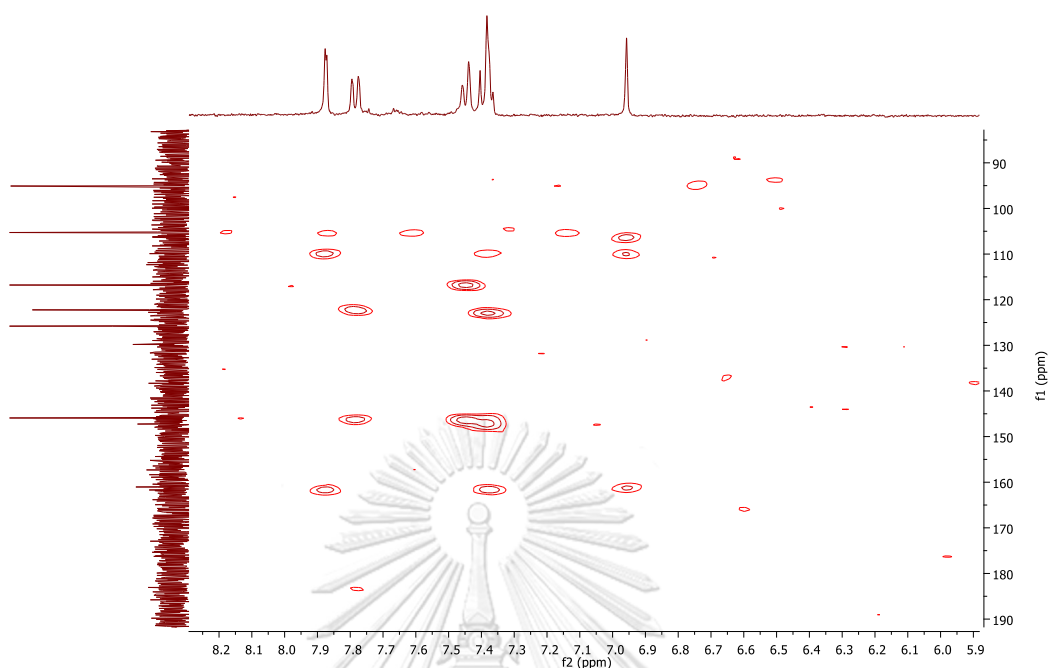


Figure A17. HMBC spectrum of cylindroxanthone F (**GC3**) in acetone- $d_6$

### Mass Spectrum List Report

<b>Analysis Info</b>		Acquisition Date	3/16/2018 1:52:52 PM
Analysis Name	D:\Data\Data Service\180316_neg_GCD-19.d	Operator	CU
Method	NV_neg_0.3min_profile_1segment_lowNubulizerDrygas(2).m	Instrument / Ser#	micrOTOF-Q II 10335
Sample Name	180316_neg_GCD-19		
Comment			

#### Acquisition Parameter

Source Type	ESI	Ion Polarity	Negative	Set Nebulizer	0.4 Bar
Focus	Not active	Set Capillary	4000 V	Set Dry Heater	200 °C
Scan Begin	50 m/z	Set End Plate Offset	-500 V	Set Dry Gas	4.0 l/min
Scan End	1500 m/z	Set Collision Cell RF	150.0 Vpp	Set Divert Valve	Waste

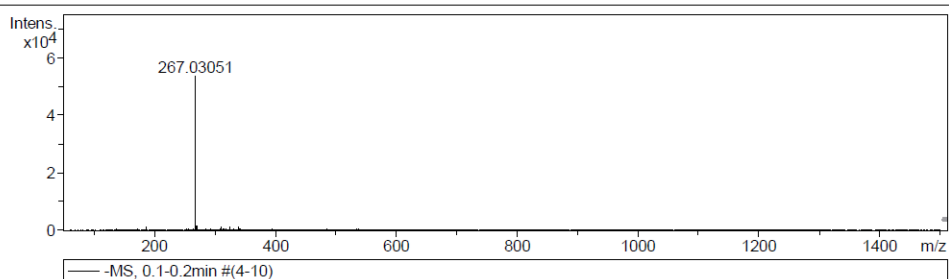


Figure A18. HRESIMS spectrum of cylindroxanthone F (**GC3**) in MeCN

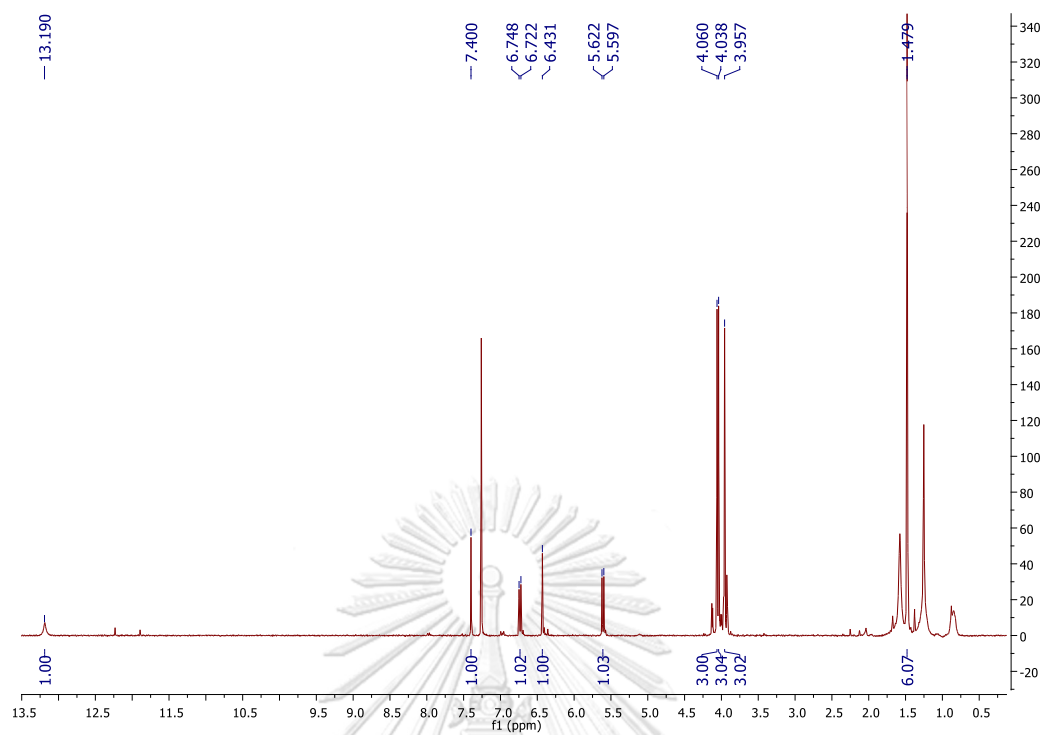


Figure A19.  $^1\text{H}$  NMR spectrum of cylindroxanthone G (**GC4**) in  $\text{CDCl}_3$

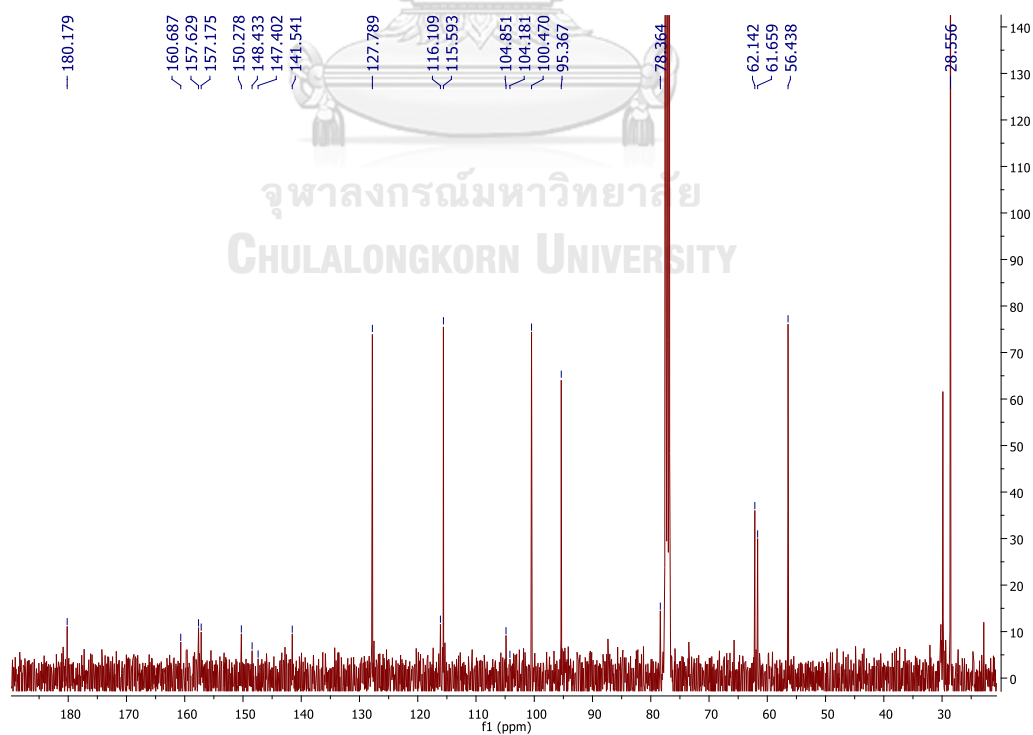


Figure A20.  $^{13}\text{C}$  NMR spectrum of cylindroxanthone G (**GC4**) in  $\text{CDCl}_3$

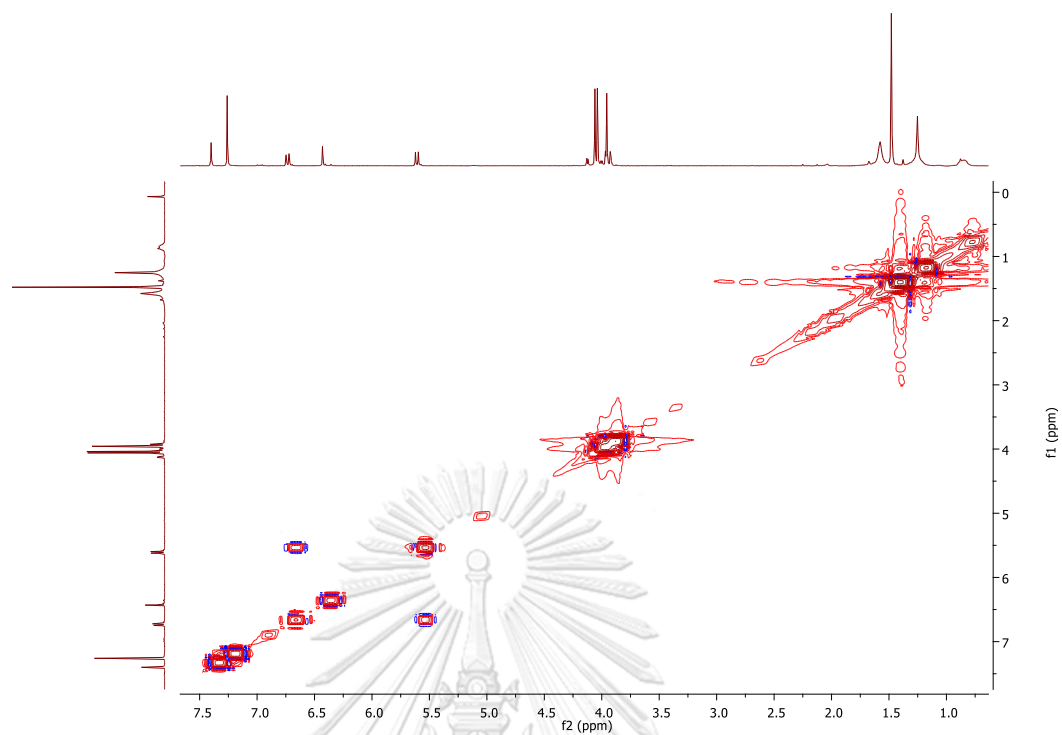


Figure A21. COSY spectrum of cylindroxanthone G (**GC4**) in  $\text{CDCl}_3$

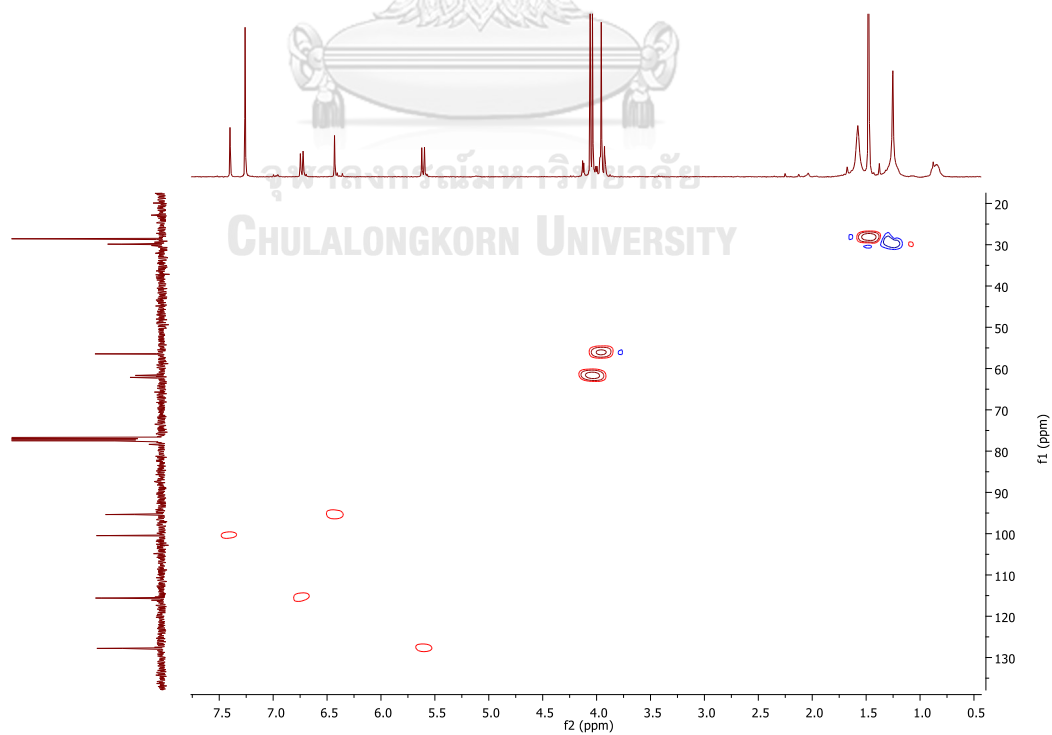
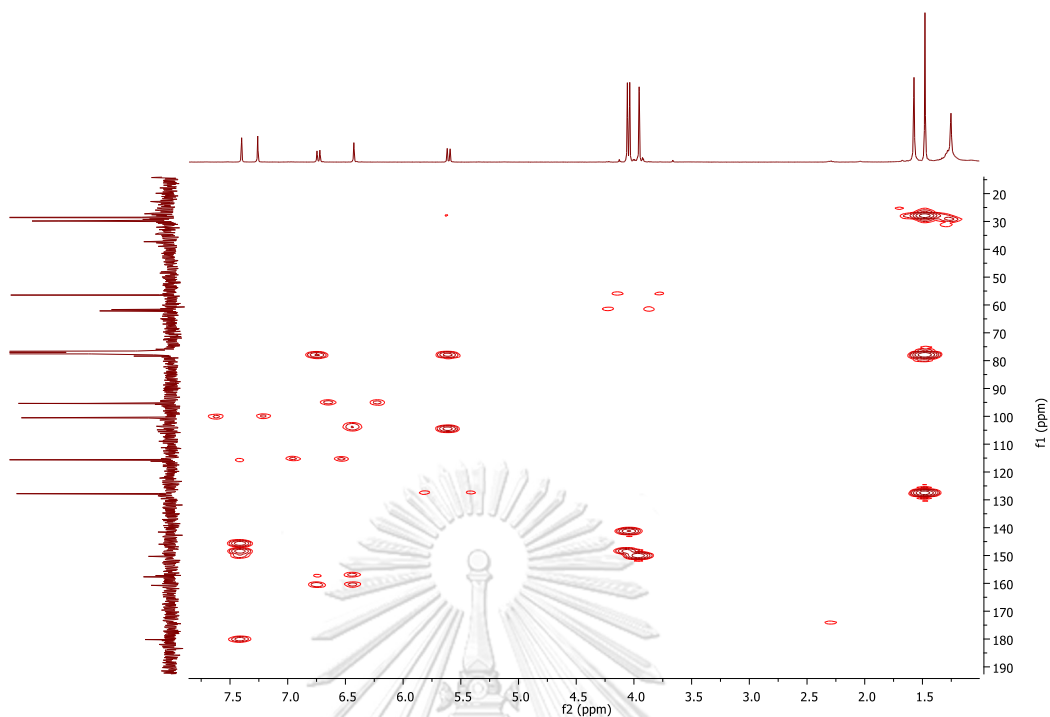


Figure A22. HSQC spectrum of cylindroxanthone G (**GC4**) in  $\text{CDCl}_3$

Figure A23. HMBC spectrum of cylindroxanthone G (**GC4**) in  $\text{CDCl}_3$ 

### Mass Spectrum List Report

#### Analysis Info

Analysis Name OSCUHF590307001.d  
 Method MKE\_tune\_wide\_20130204.m  
 Sample Name GCy-2  
 GCy-2

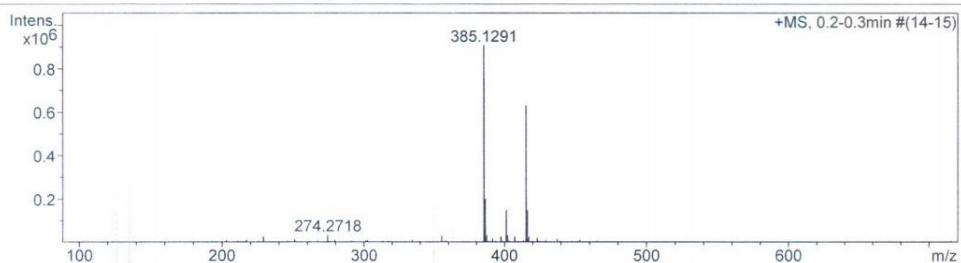
Acquisition Date 3/7/2016 1:00:09 PM  
 Operator Administrator  
 Instrument micrOTOF 72

#### Acquisition Parameter

Source Type ESI  
 Scan Range n/a  
 Scan Begin 50 m/z  
 Scan End 3000 m/z

Ion Polarity Positive  
 Capillary Exit 100.0 V  
 Hexapole RF 150.0 V  
 Skimmer 1 45.0 V  
 Hexapole 1 24.3 V

Set Corrector Fill 50 V  
 Set Pulsar Pull 337 V  
 Set Pulsar Push 337 V  
 Set Reflector 1300 V  
 Set Flight Tube 9000 V  
 Set Detector TOF 2295 V

Figure A24. HRESIMS spectrum of cylindroxanthone G (**GC4**) in  $\text{CH}_2\text{Cl}_2$

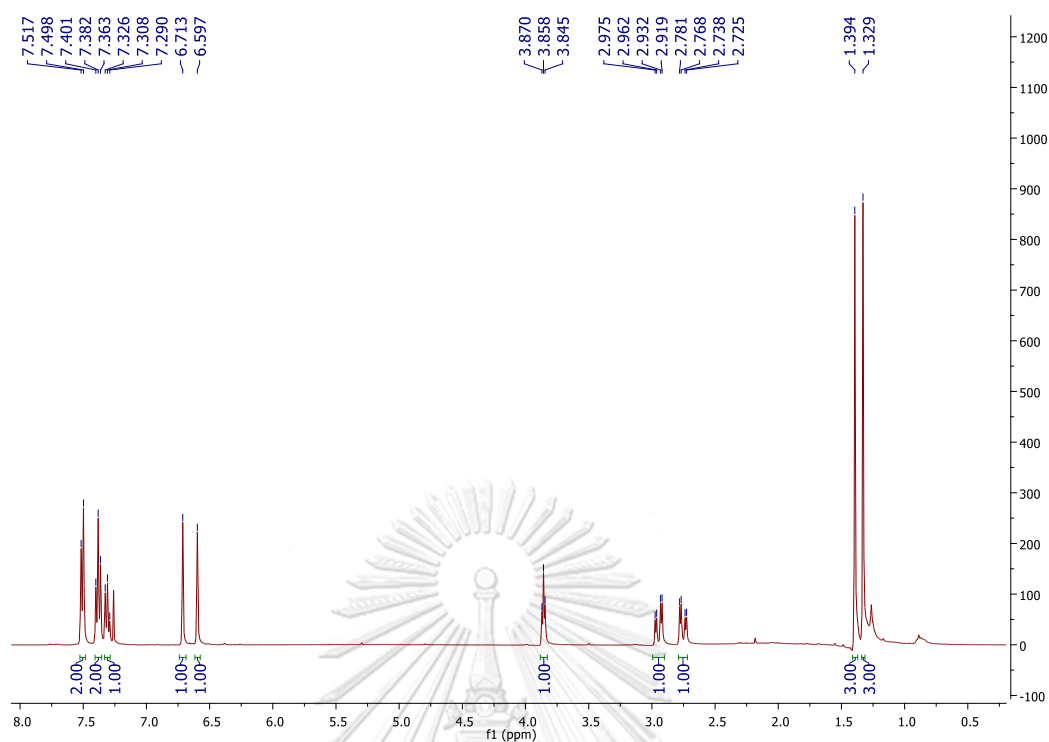


Figure A25.  $^1\text{H}$  NMR spectrum of cylindrobiphenyl A (GC5) in  $\text{CDCl}_3$

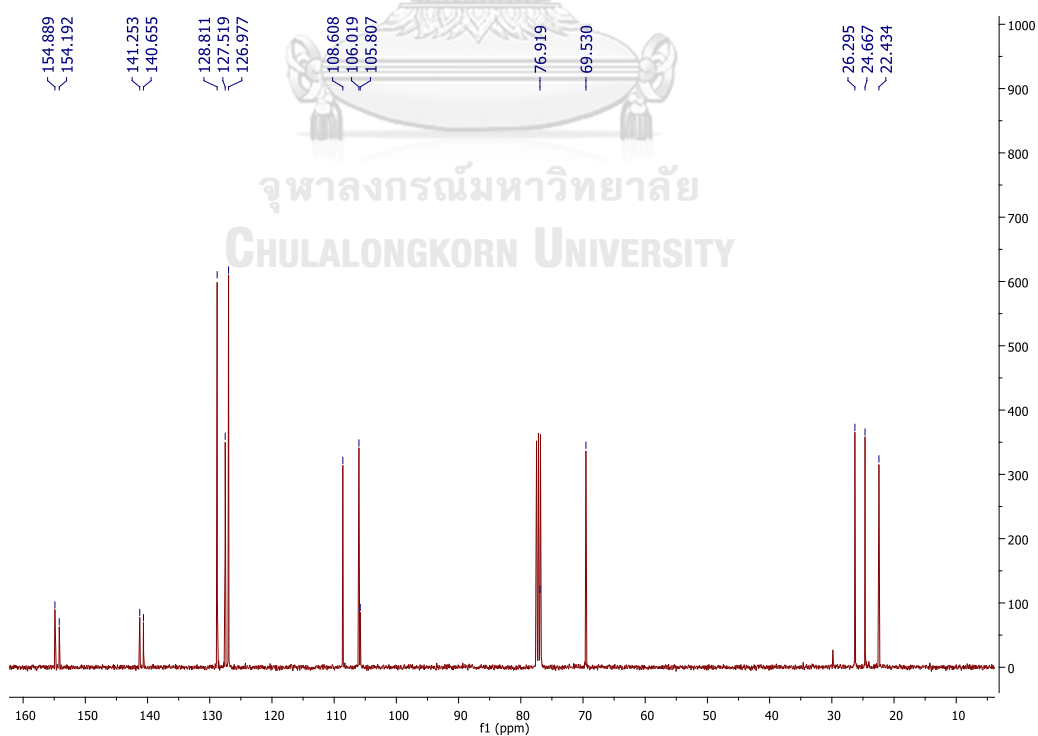


Figure A26.  $^{13}\text{C}$  NMR spectrum of cylindrobiphenyl A (GC5) in  $\text{CDCl}_3$

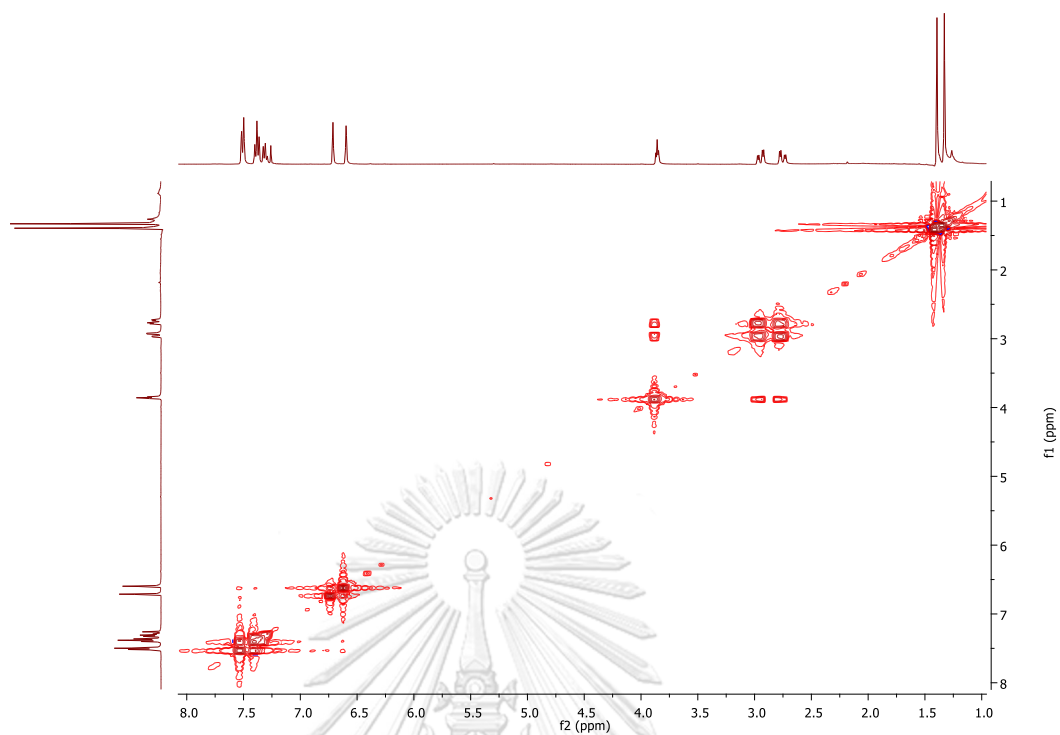


Figure A27. COSY spectrum of cylindrobiphenyl A (**GC5**) in  $\text{CDCl}_3$

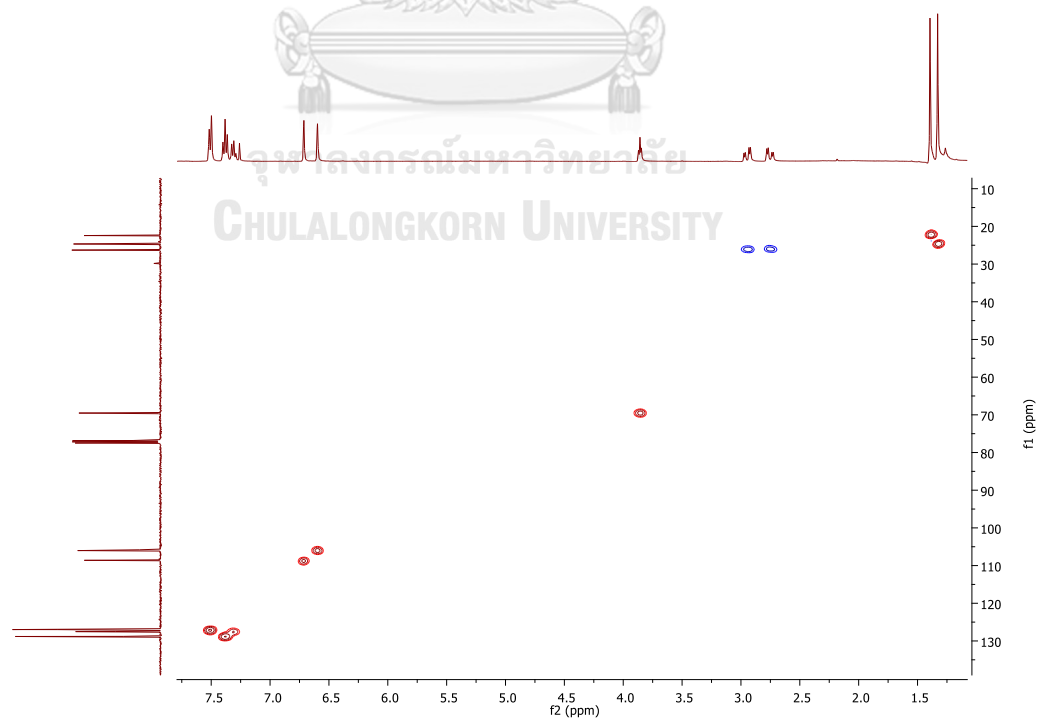
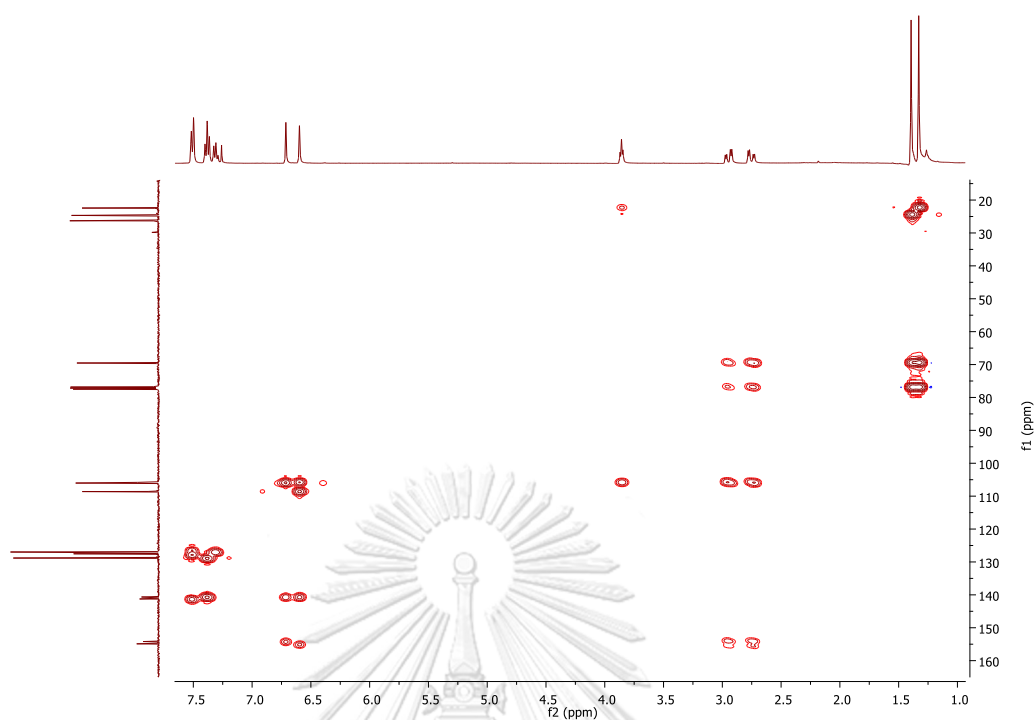


Figure A28. HSQC spectrum of cylindrobiphenyl A (**GC5**) in  $\text{CDCl}_3$



Figure A29. HMBC spectrum of cylindrobiphenyl A (GC5) in  $\text{CDCl}_3$ 

### Mass Spectrum List Report

<b>Analysis Info</b>		Acquisition Date	3/16/2018 1:57:15 PM	
Analysis Name	D:\Data\Data Service\180316_neg_R5-1-7-1.d		Operator	CU.
Method	NV_neg_0.3min_profile_1segment_lowNubulizerDrygas(2).m		Instrument / Ser#	micrOTOF-Q II 10335
Sample Name	180316_neg_R5-1-7			
Comment				

#### Acquisition Parameter

Source Type	ESI	Ion Polarity	Negative	Set Nebulizer	0.4 Bar
Focus	Not active	Set Capillary	4000 V	Set Dry Heater	200 °C
Scan Begin	50 m/z	Set End Plate Offset	-500 V	Set Dry Gas	4.0 l/min
Scan End	1500 m/z	Set Collision Cell RF	150.0 Vpp	Set Divert Valve	Waste

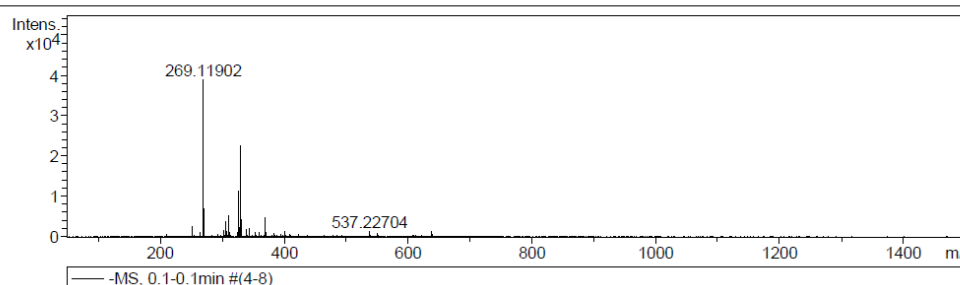


Figure A30. HRMSIMS spectrum of cylindrobiphenyl A (GC5) in MeCN

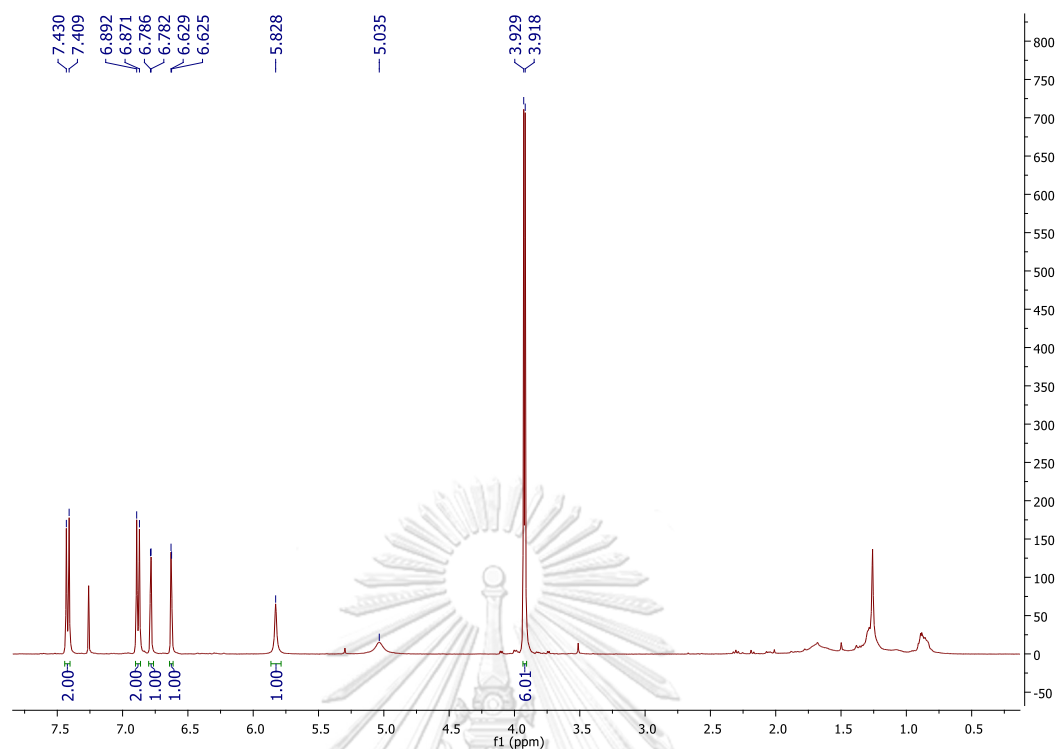


Figure A31. <sup>1</sup>H NMR spectrum of cylindrobiphenyl B (GC6) in CDCl<sub>3</sub>

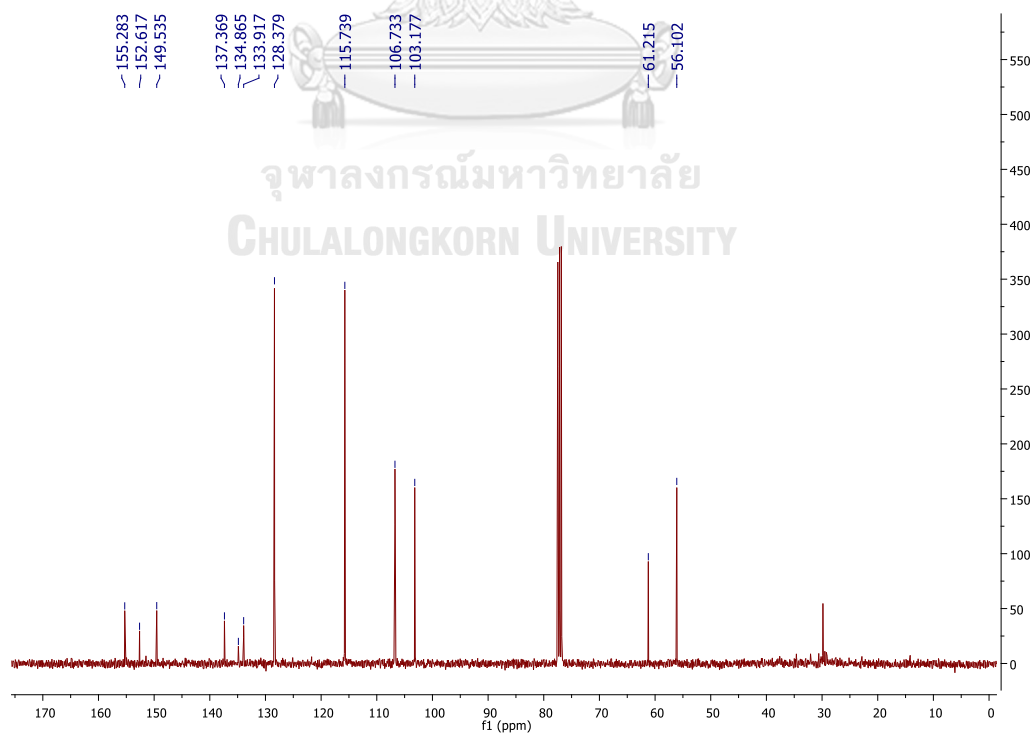


Figure A32. <sup>13</sup>C NMR spectrum of cylindrobiphenyl B (GC6) in CDCl<sub>3</sub>

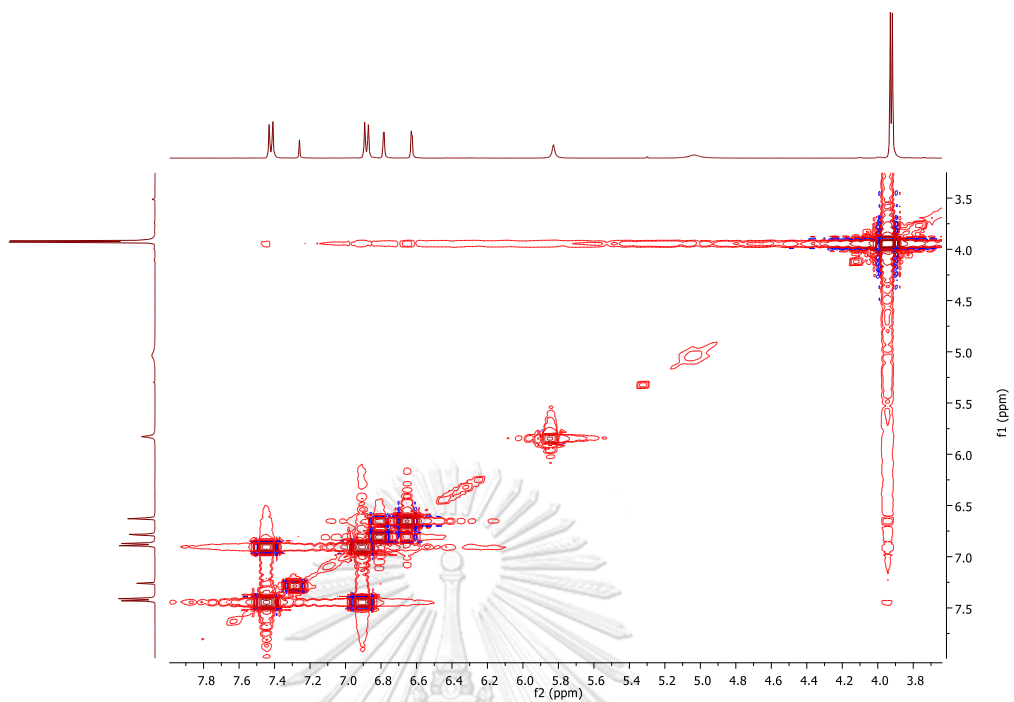


Figure A33. COSY spectrum of cylindrobiphenyl B (**GC6**) in CDCl<sub>3</sub>

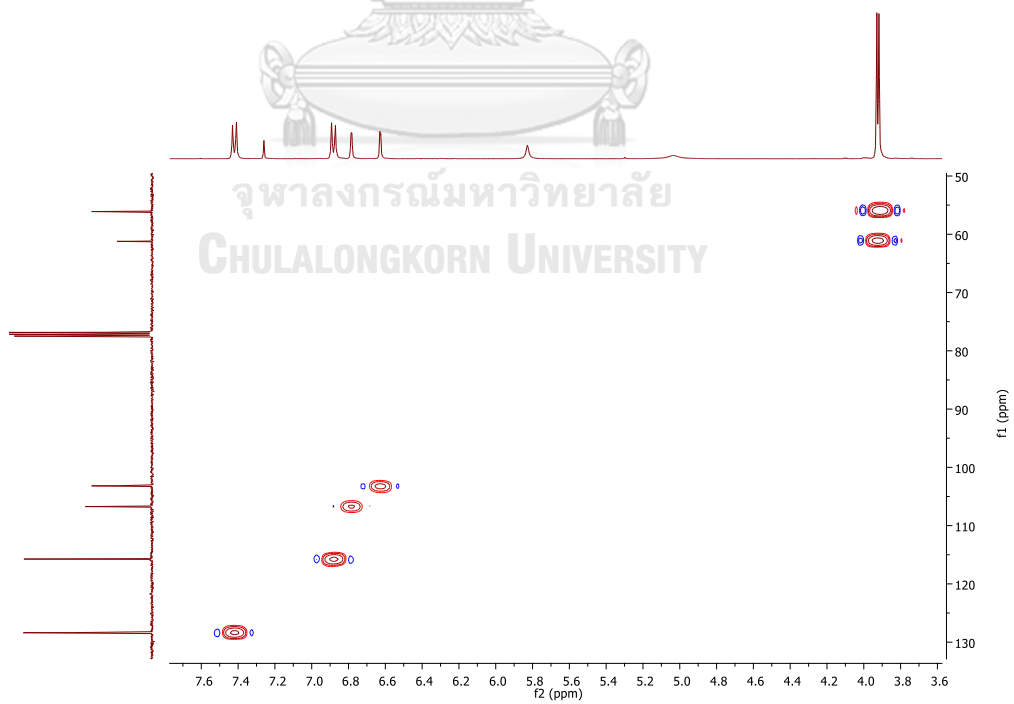
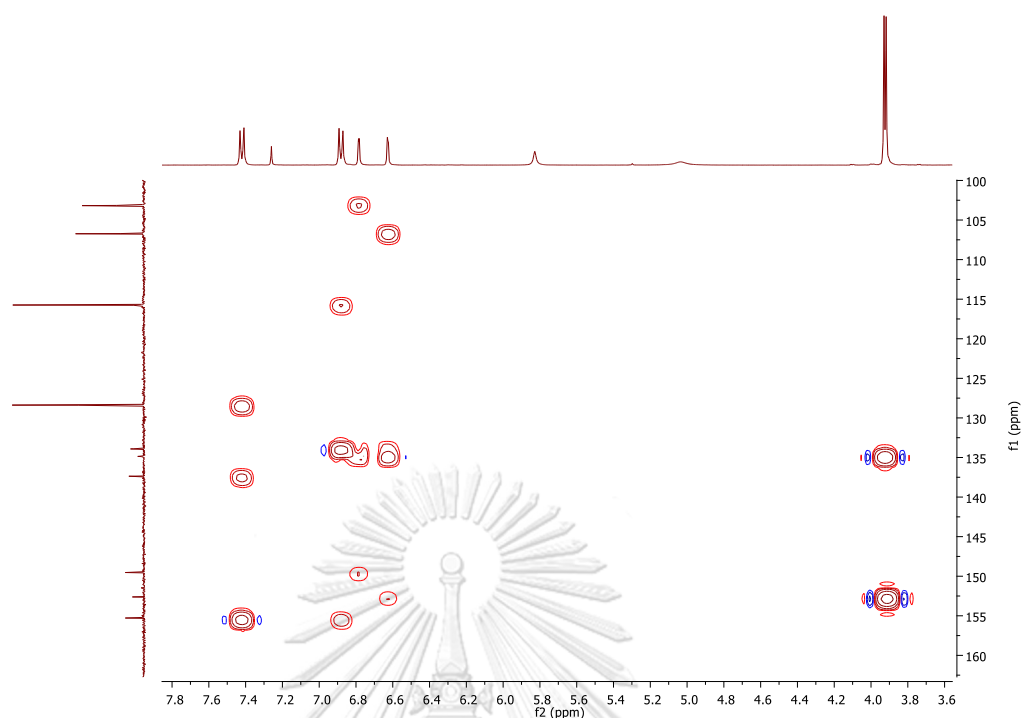


Figure A34. HSQC spectrum of cylindrobiphenyl B (**GC6**) in CDCl<sub>3</sub>

Figure A35. HMBC spectrum of cylindrobiphenyl B (GC6) in CDCl<sub>3</sub>

### Mass Spectrum List Report

<b>Analysis Info</b>		Acquisition Date	3/16/2018 12:41:39 PM
Analysis Name	D:\Data\Data Service\180316_neg_R5-1-5.d	Operator	CU.
Method	NV_neg_0.3min_profile_1segment_lowNubulizerDrygas(2).m	Instrument / Ser#	micrOTOF-Q II 10335
Sample Name	180316_neg_R5-1-5-2		
Comment			

#### Acquisition Parameter

Source Type	ESI	Ion Polarity	Negative	Set Nebulizer	0.4 Bar
Focus	Not active	Set Capillary	4000 V	Set Dry Heater	200 °C
Scan Begin	50 m/z	Set End Plate Offset	-500 V	Set Dry Gas	4.0 l/min
Scan End	1500 m/z	Set Collision Cell RF	150.0 Vpp	Set Divert Valve	Waste

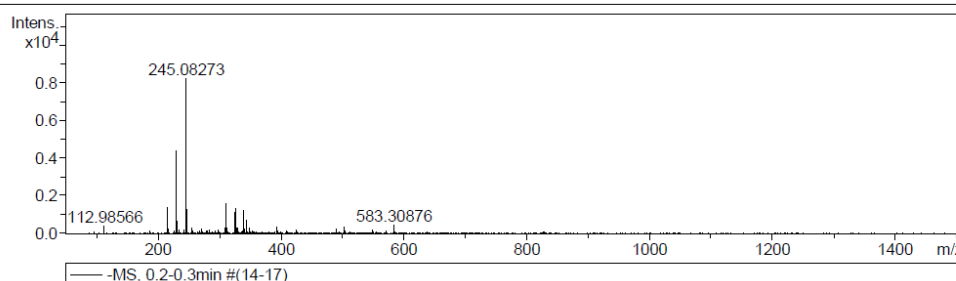


Figure A36. HRMSIMS spectrum of cylindrobiphenyl B (GC6) in MeCN

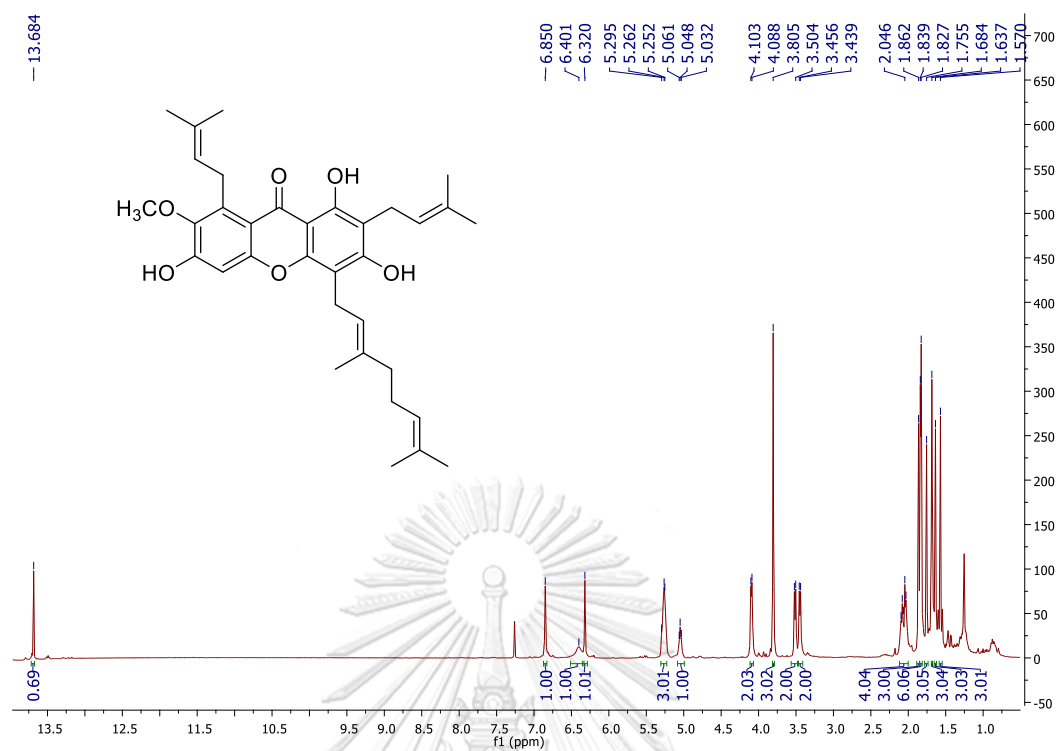


Figure B1.  $^1\text{H}$  NMR spectrum of tetrandraxanthone A (GT1) in  $\text{CDCl}_3$

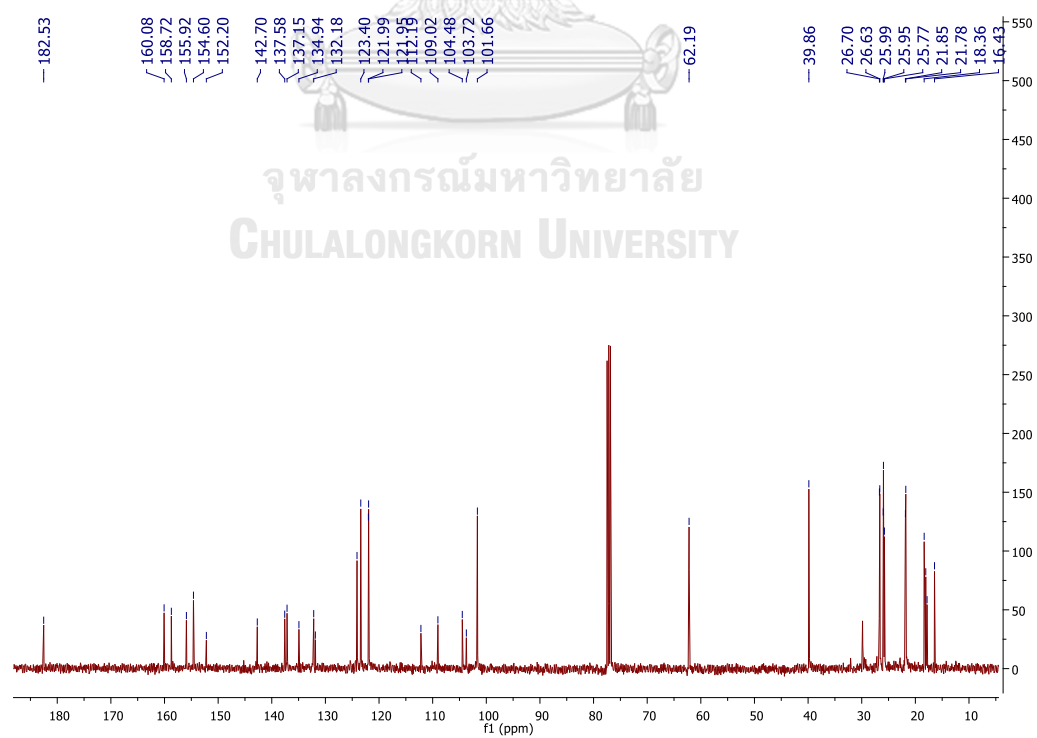


Figure B2.  $^{13}\text{C}$  NMR spectrum of tetrandraxanthone A (GT1) in  $\text{CDCl}_3$

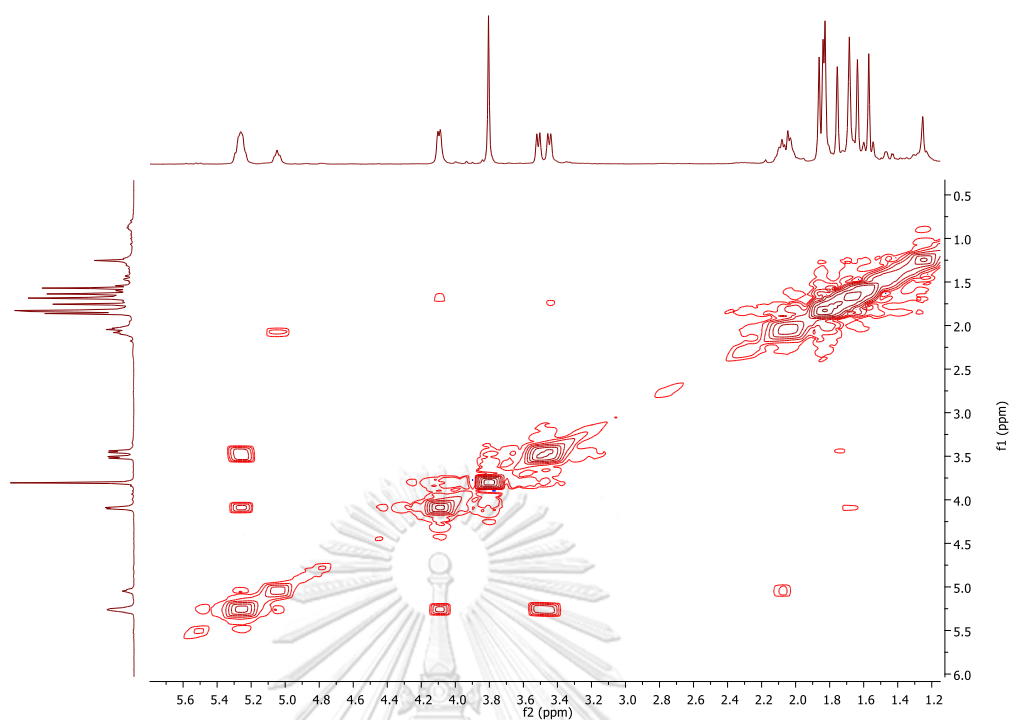


Figure B3. COSY spectrum of tetrandraxanthone A (**GT1**) in  $\text{CDCl}_3$

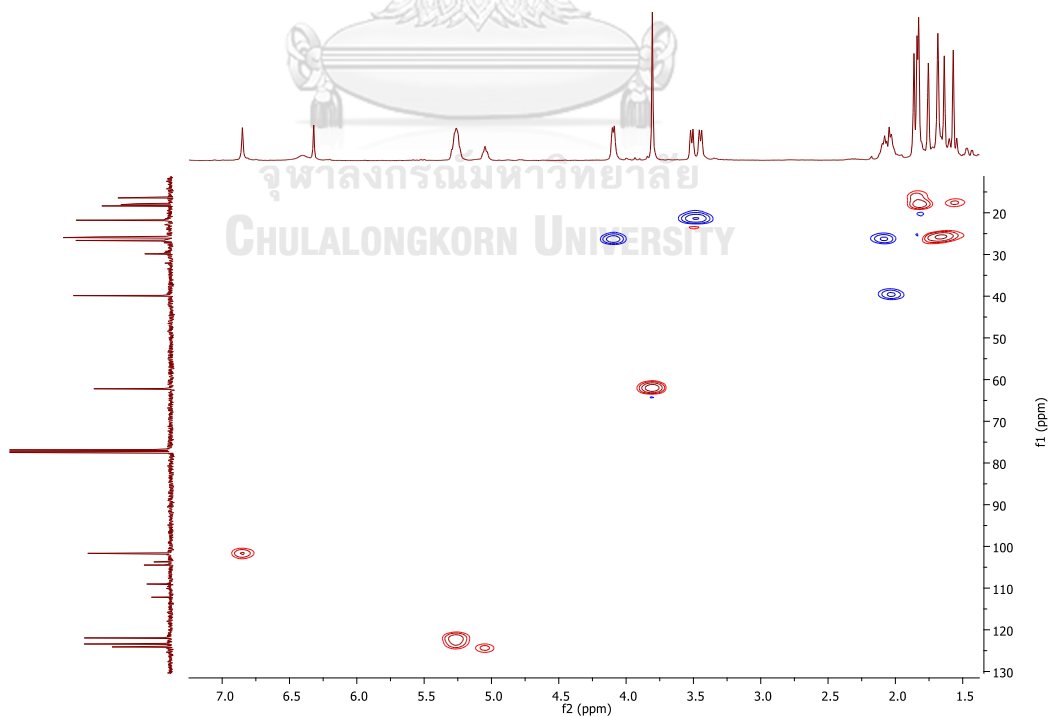
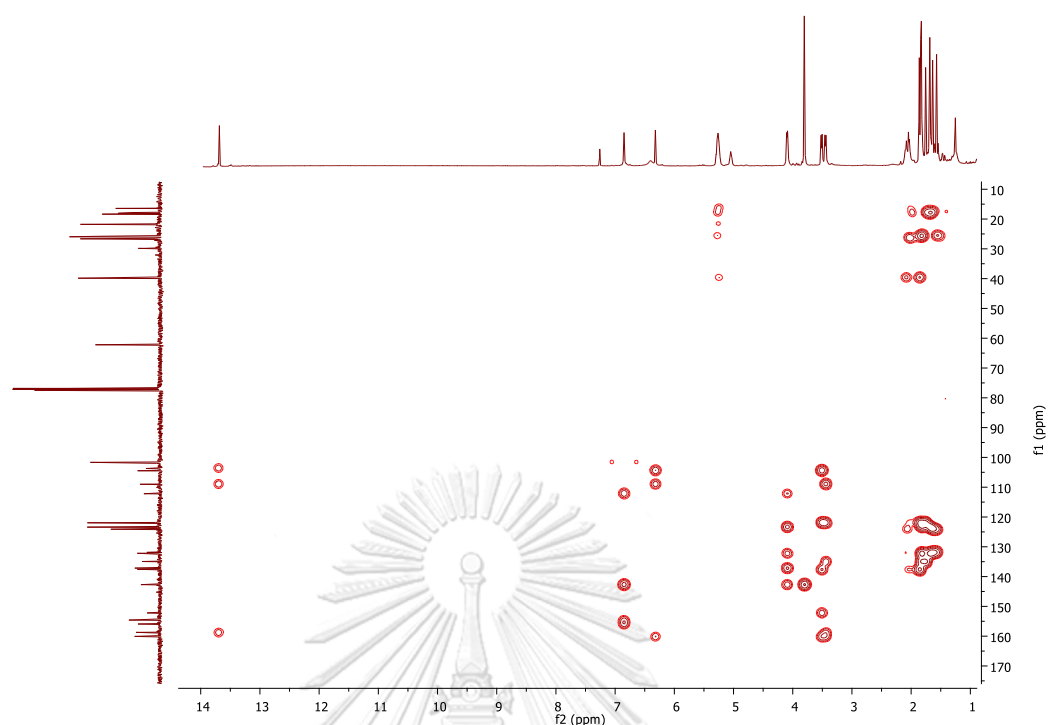
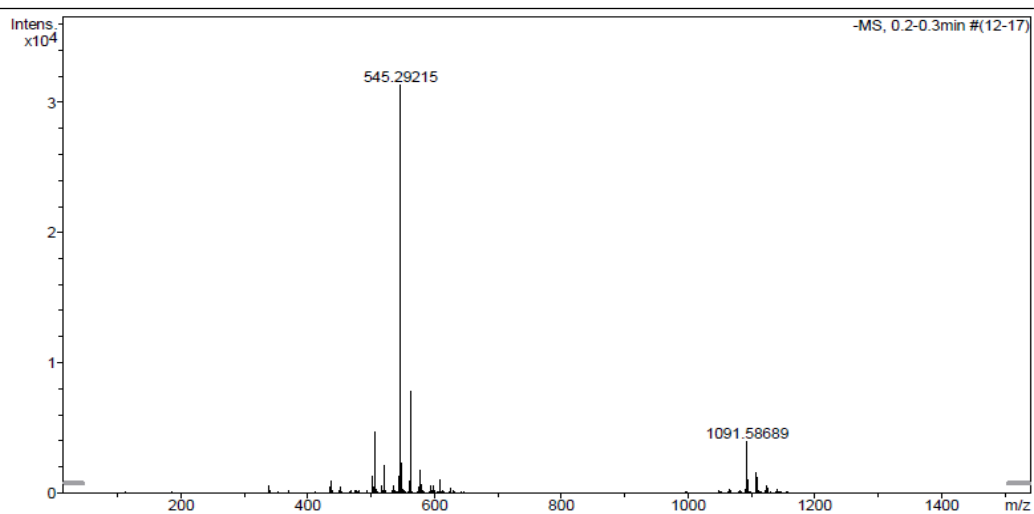


Figure B4. HSQC spectrum of tetrandraxanthone A (**GT1**) in  $\text{CDCl}_3$

Figure B5. HMBC spectrum of tetrandraxanthone A (**GT1**) in CDCl<sub>3</sub>

## Generic Display Report

Analysis Info		Acquisition Date	2/23/2018 3:55:49 PM
Analysis Name	D:\Data\Data Service\180223_pos_GTH-2.d	Operator	CU
Method	NV_neg_0.3min_profile_1segment_lowNubulizerDrygas(2).m	Instrument	microTOF-Q II
Sample Name	180223_pos_GTH-2		
Comment			

Figure B6. HRESIMS spectrum of tetrandraxanthone A (**GT1**) in MeCN

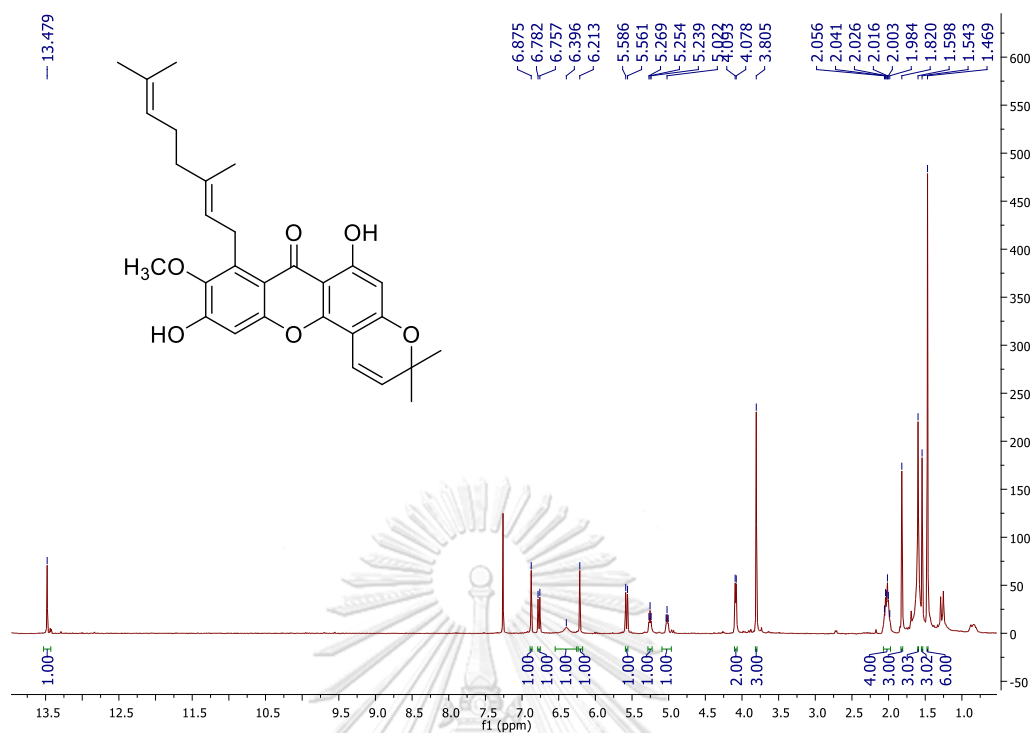


Figure B7. <sup>1</sup>H NMR spectrum of tetrandraxanthone B (GT2) in CDCl<sub>3</sub>

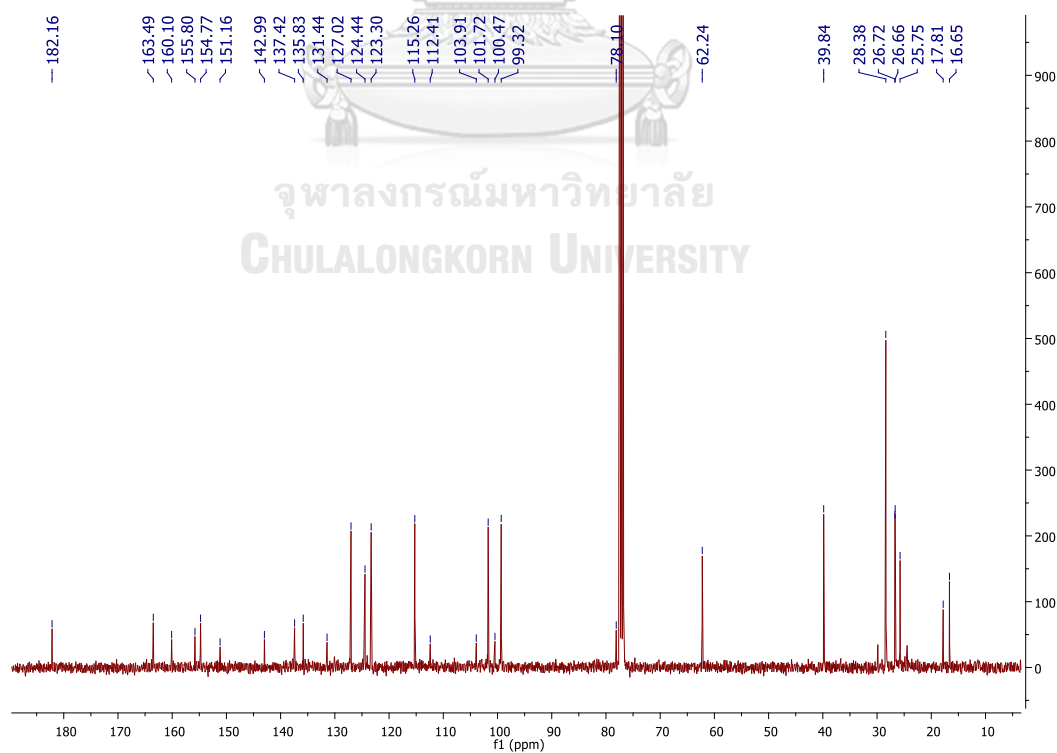


Figure B8. <sup>13</sup>C NMR spectrum of tetrandraxanthone B (GT2) in CDCl<sub>3</sub>



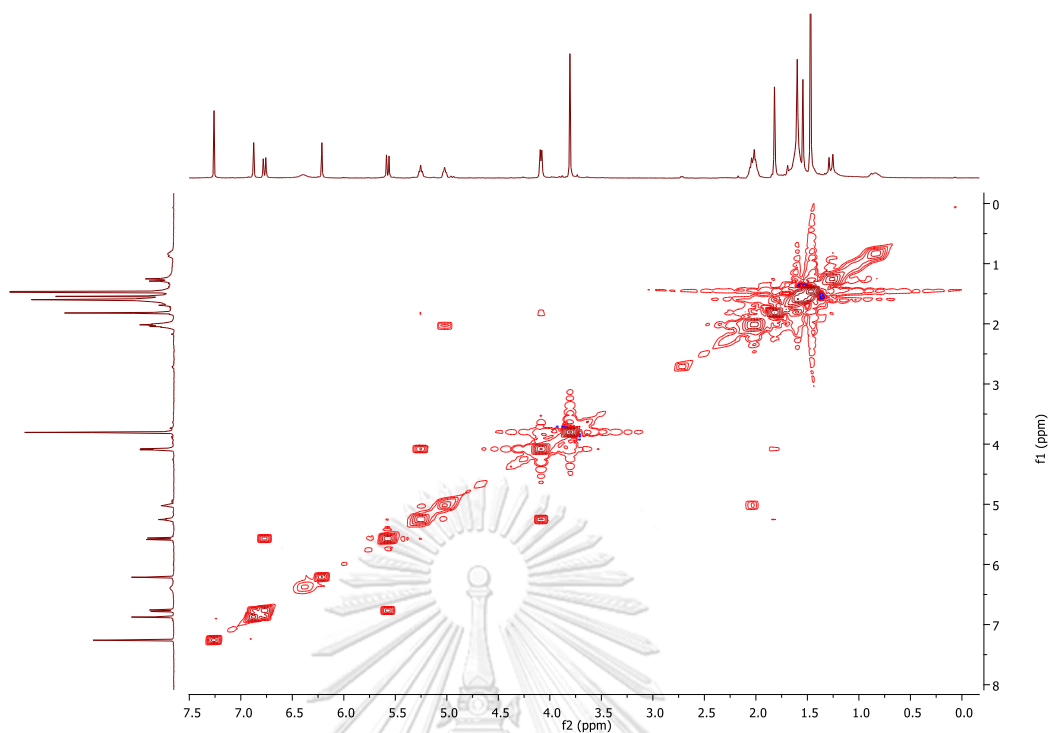


Figure B9. COSY spectrum of tetrandraxanthone B (**GT2**) in  $\text{CDCl}_3$

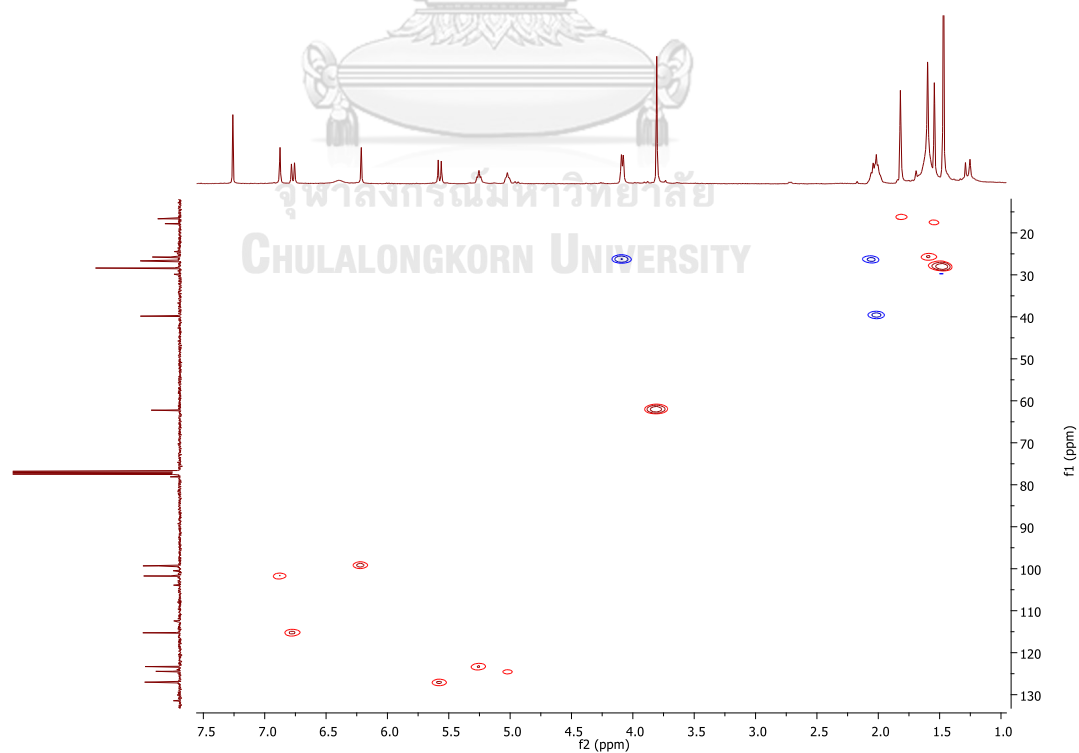
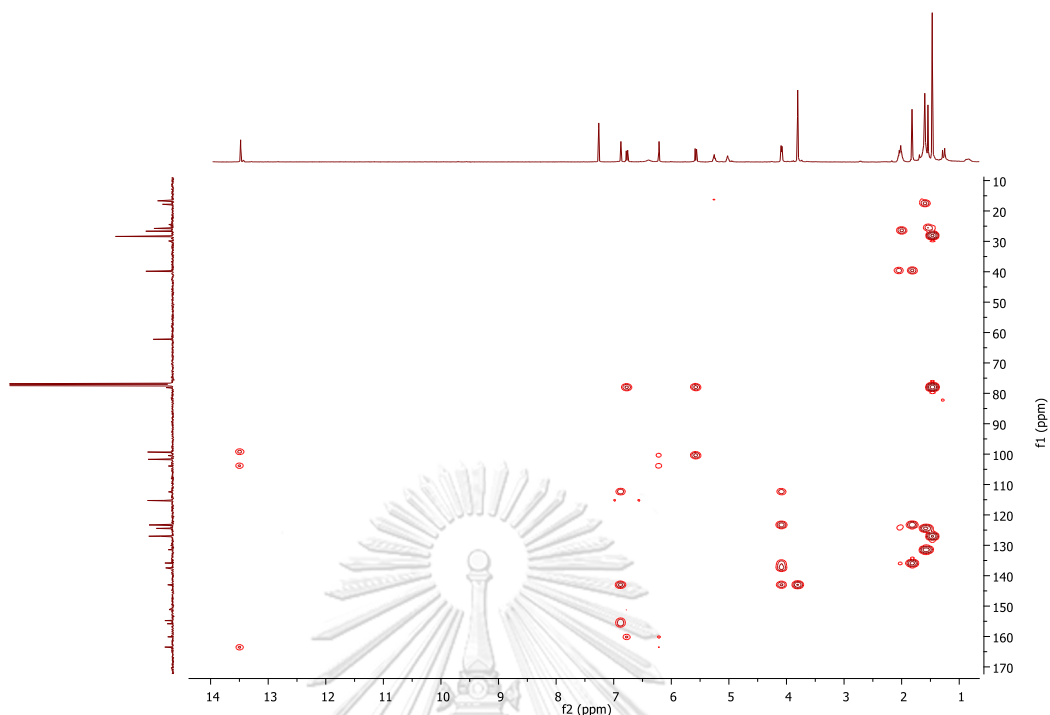


Figure B10. HSQC spectrum of tetrandraxanthone B (**GT2**) in  $\text{CDCl}_3$

Figure B11. HMBC spectrum of tetrandraxanthone B (GT2) in CDCl<sub>3</sub>

## Generic Display Report

<b>Analysis Info</b>	Acquisition Date	2/23/2018 4:06:00 PM	
Analysis Name	D:\Data\Data Service\180223_pos_GTH-3A.d		
Method	NV_neg_0.3min_profile_1segment_lowNubulizerDrygas(2).m	Operator	CU.
Sample Name	180223_pos_GTH-3A	Instrument	microTOF-Q II
Comment			

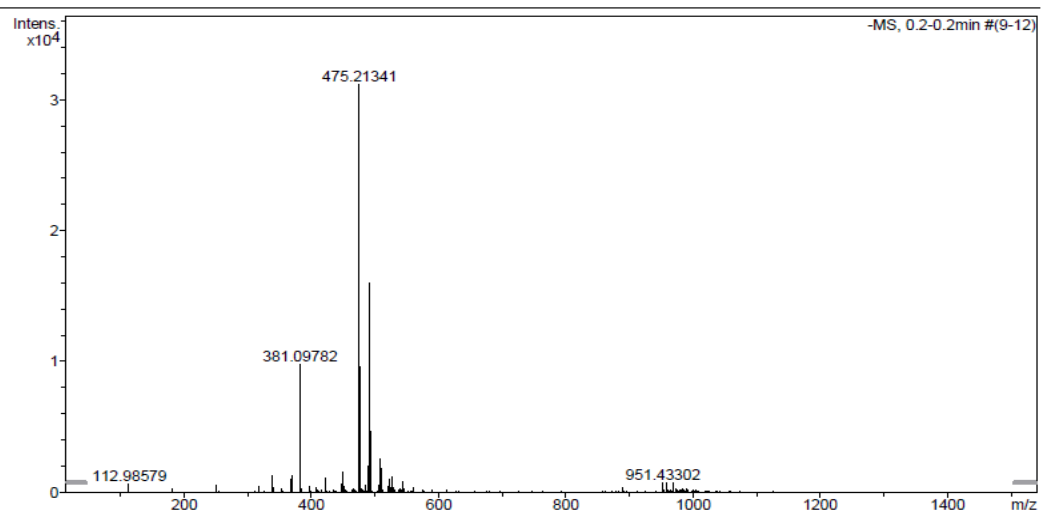


Figure B12. HRESIMS spectrum of tetrandraxanthone B (GT2) in MeCN

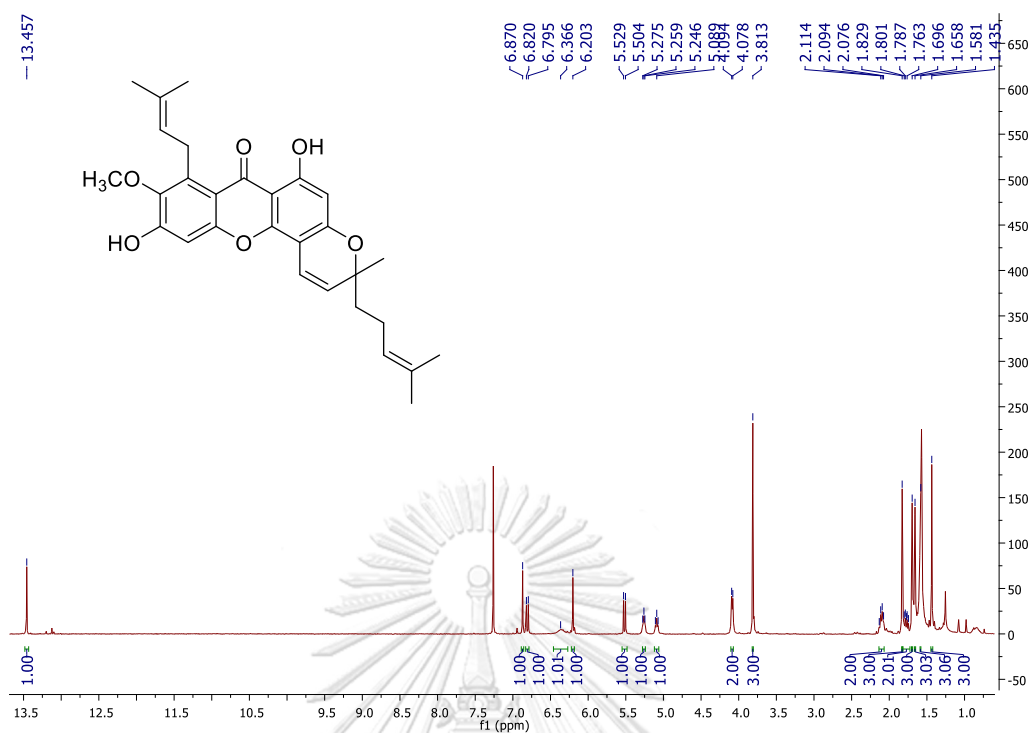


Figure B13.  $^1\text{H}$  NMR spectrum of tetrandraxanthone C (GT3) in  $\text{CDCl}_3$

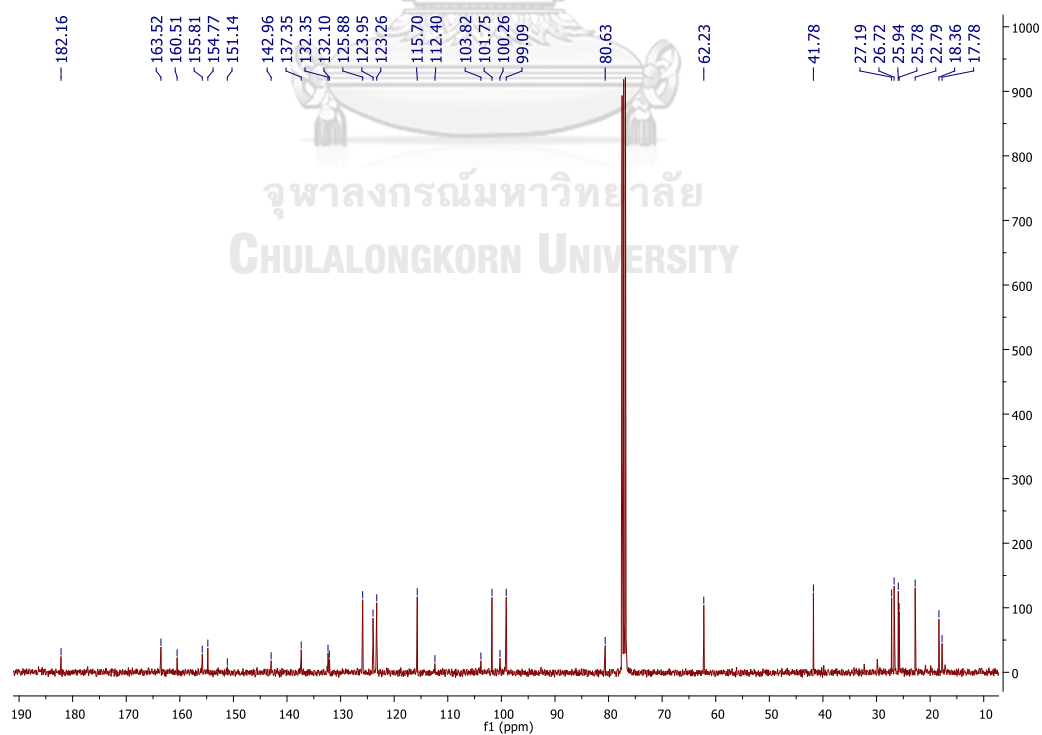


Figure B14.  $^{13}\text{C}$  NMR spectrum of tetrandraxanthone C (GT3) in  $\text{CDCl}_3$

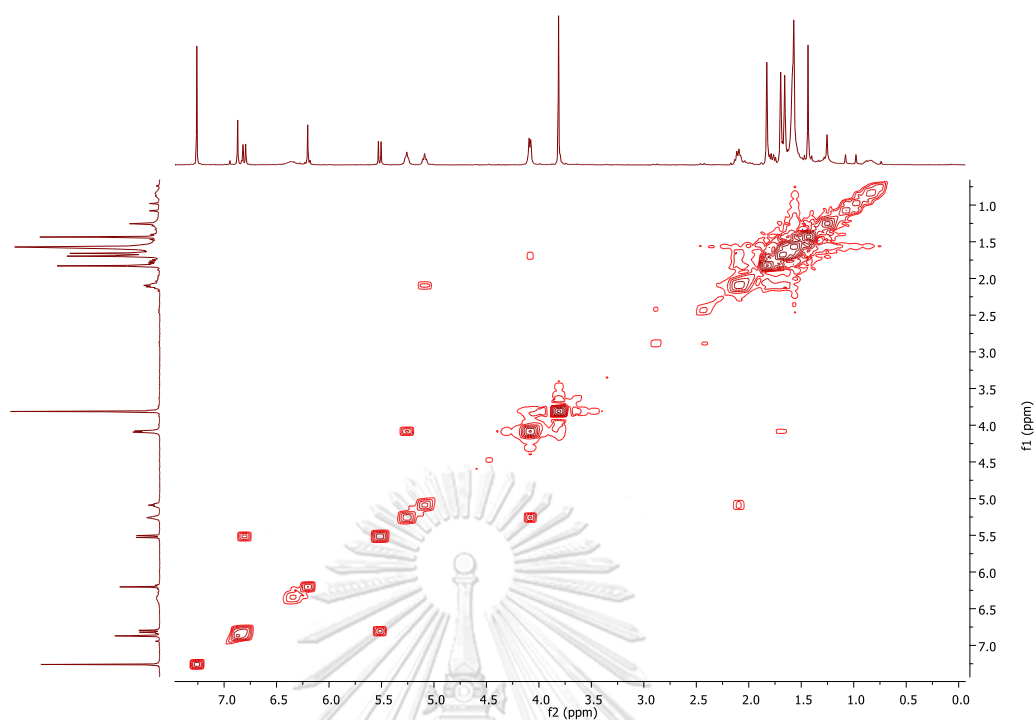


Figure B15. COSY spectrum of tetrandraxanthone C (**GT3**) in  $\text{CDCl}_3$

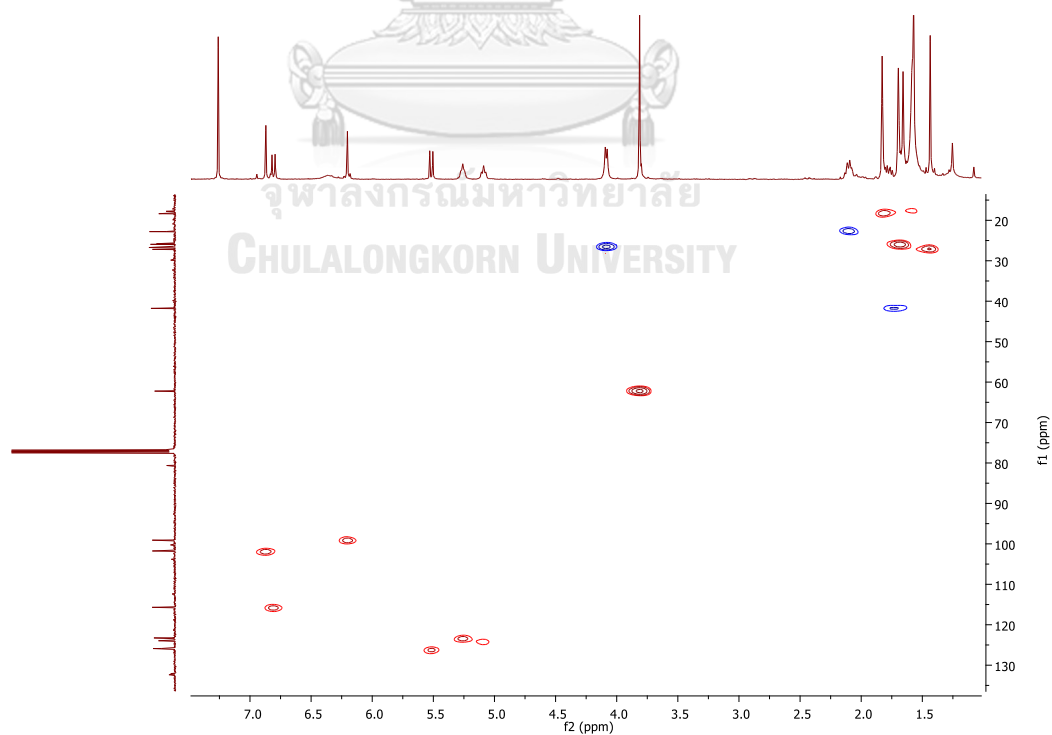
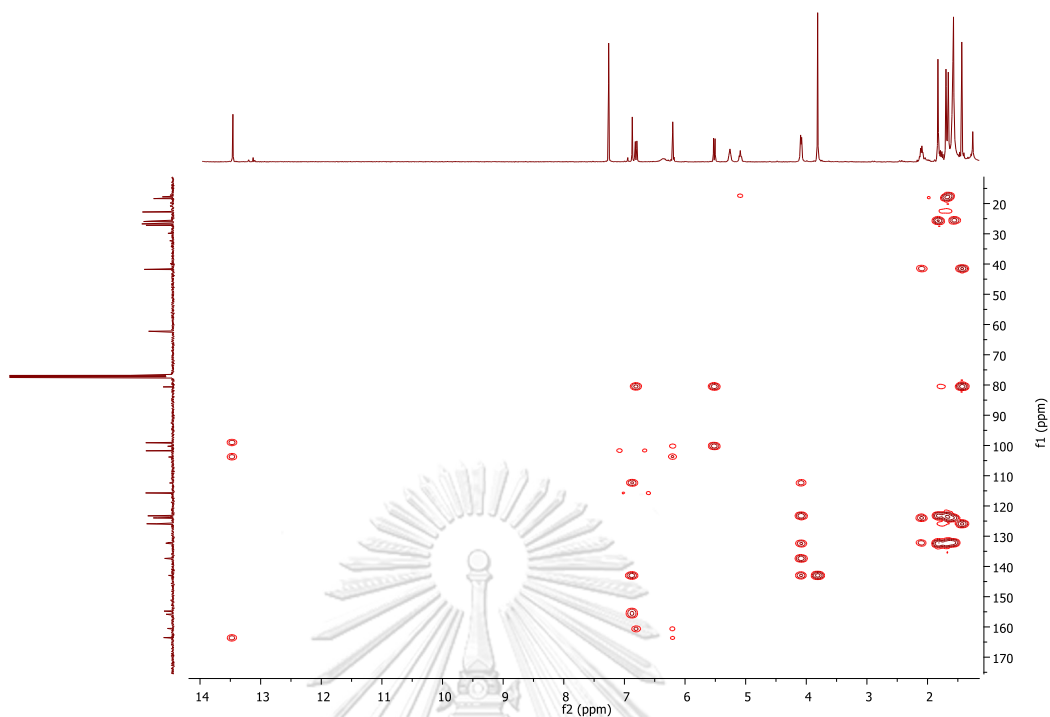
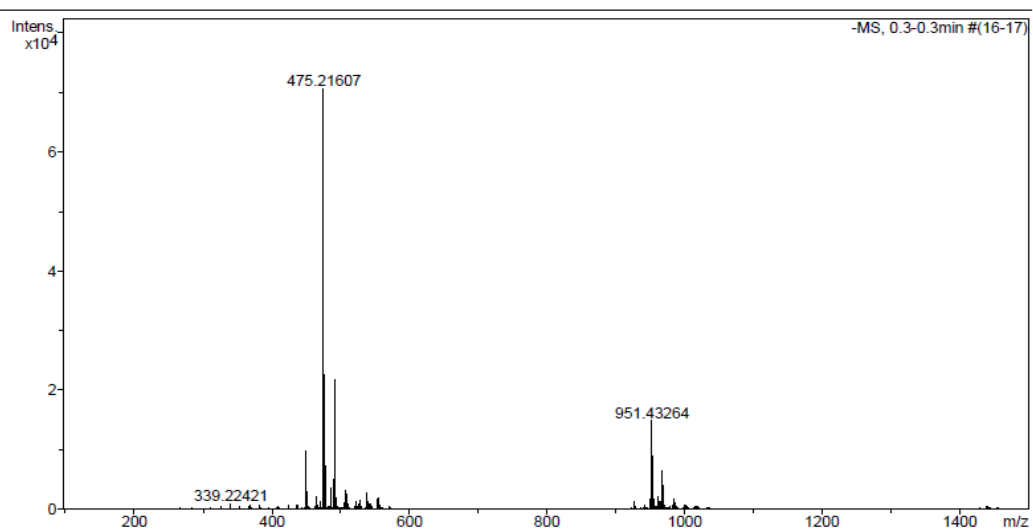


Figure B16. HSQC spectrum of tetrandraxanthone C (**GT3**) in  $\text{CDCl}_3$

Figure B17. HMBC spectrum of tetrandraxanthone C (**GT3**) in CDCl<sub>3</sub>

## Generic Display Report

<b>Analysis Info</b>	Acquisition Date	3/16/2018 11:12:24 AM	
Analysis Name	D:\Data\Data Service\180316_neg_GTH-3B.d		
Method	NV_neg_0.3min_profile_1segment_lowNubulizerDrygas(2).m	Operator	CU
Sample Name	180316_neg_GTH-3B	Instrument	microTOF-Q II
Comment			

Figure B18. HRESIMS spectrum of tetrandraxanthone C (**GT3**) in MeCN

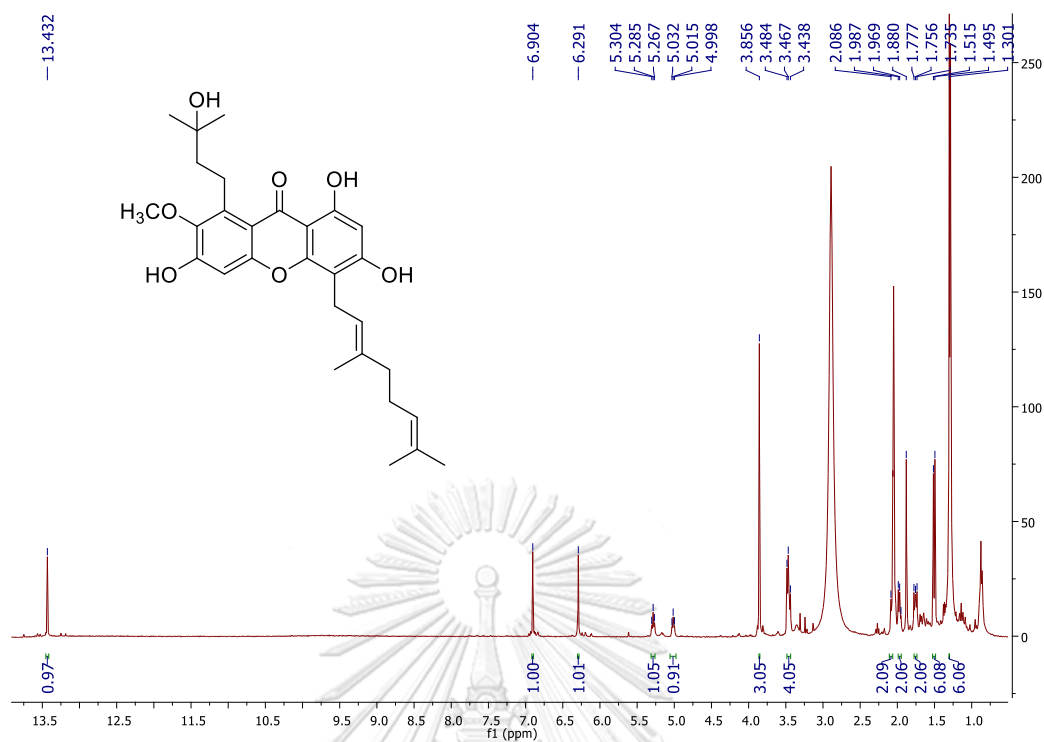


Figure B19.  $^1\text{H}$  NMR spectrum of tetrandraxanthone D (GT4) in acetone- $d_6$

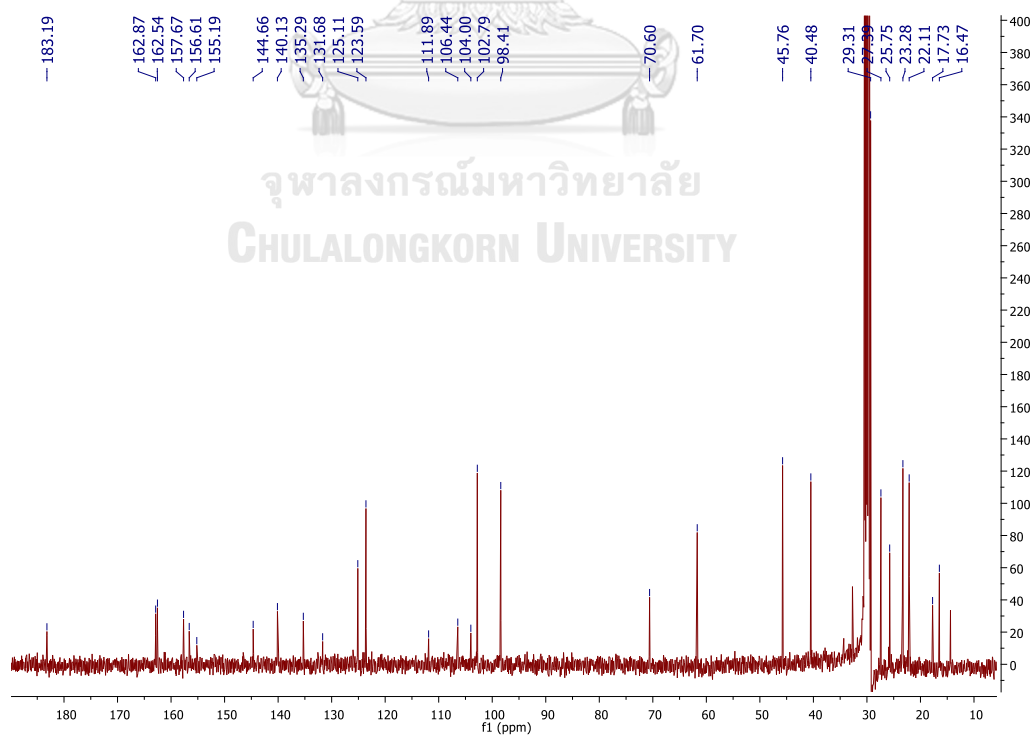


Figure B20.  $^{13}\text{C}$  NMR spectrum of tetrandraxanthone D (GT4) in acetone- $d_6$

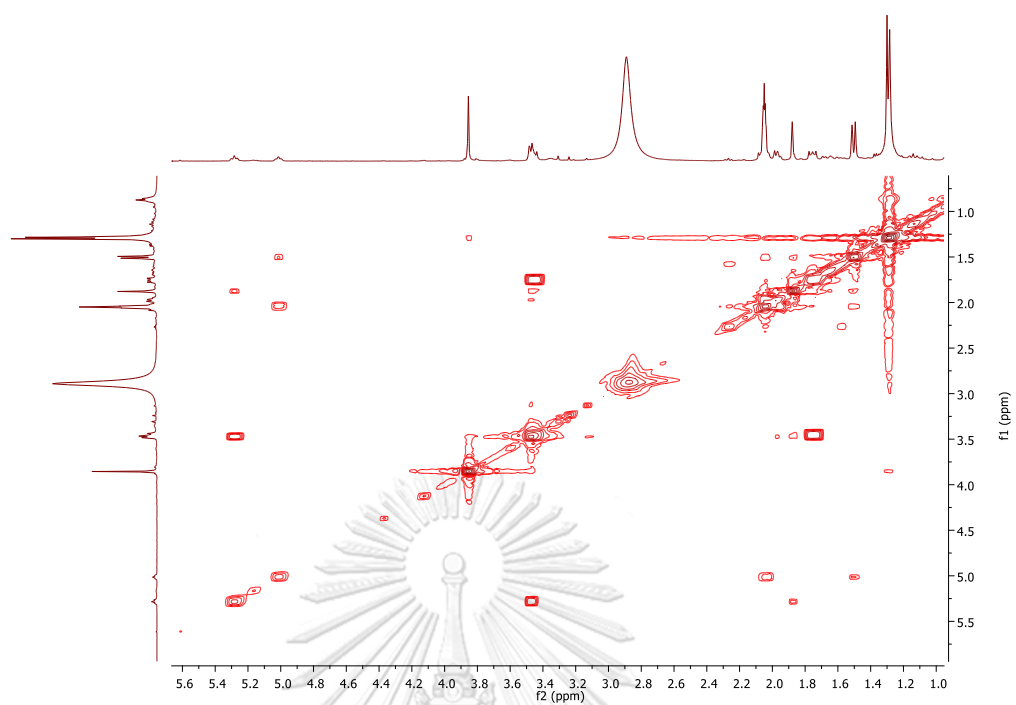


Figure B21. COSY spectrum of tetrandraxanthone D (**GT4**) in acetone- $d_6$

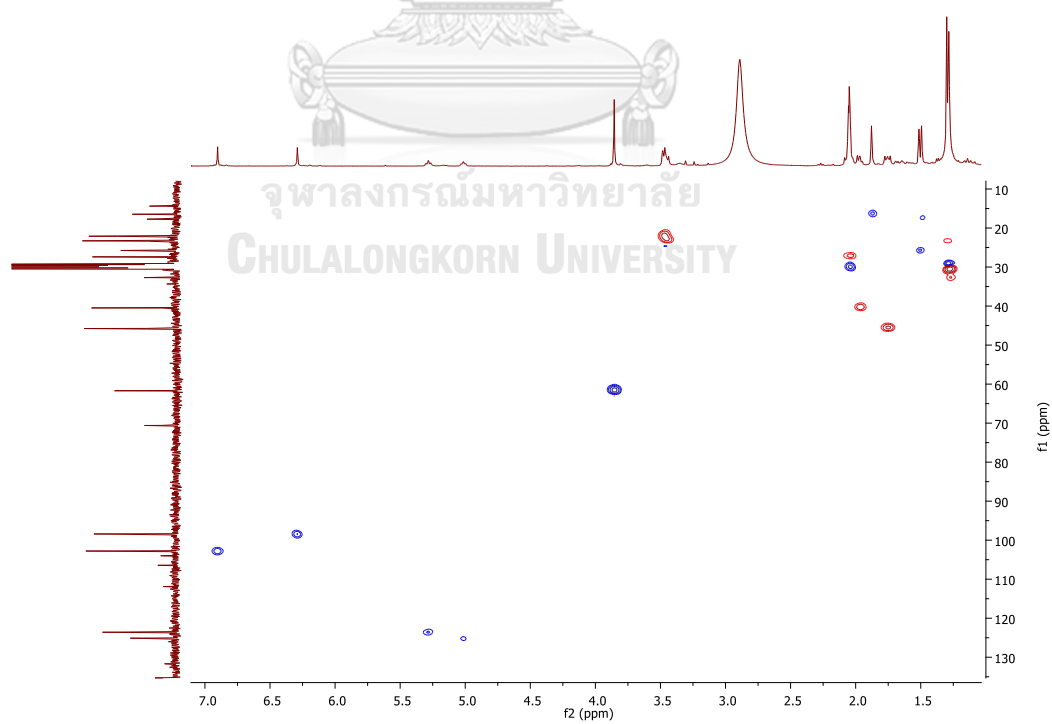


Figure B22. HSQC spectrum of tetrandraxanthone D (**GT4**) in acetone- $d_6$

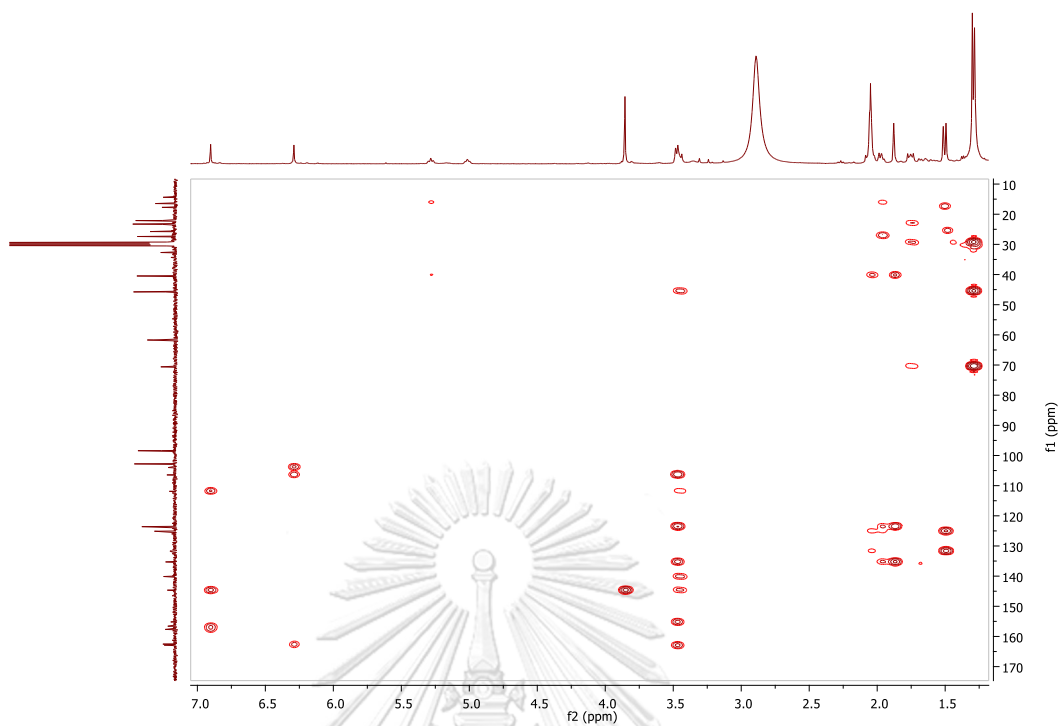


Figure B23. HMBC spectrum of tetrandraxanthone D (GT4) in acetone- $d_6$

### Generic Display Report

Analysis Info		Acquisition Date	
Analysis Name	D:\Data\Data Service\180316_neg_GTH-20.d	3/16/2018	11:19:21 AM
Method	NV_neg_0.3min_profile_1segment_lowNubulizerDrygas(2).m	Operator	CU.
Sample Name	180316_neg_GTH-20-2	Instrument	micrOTOF-Q II
Comment			

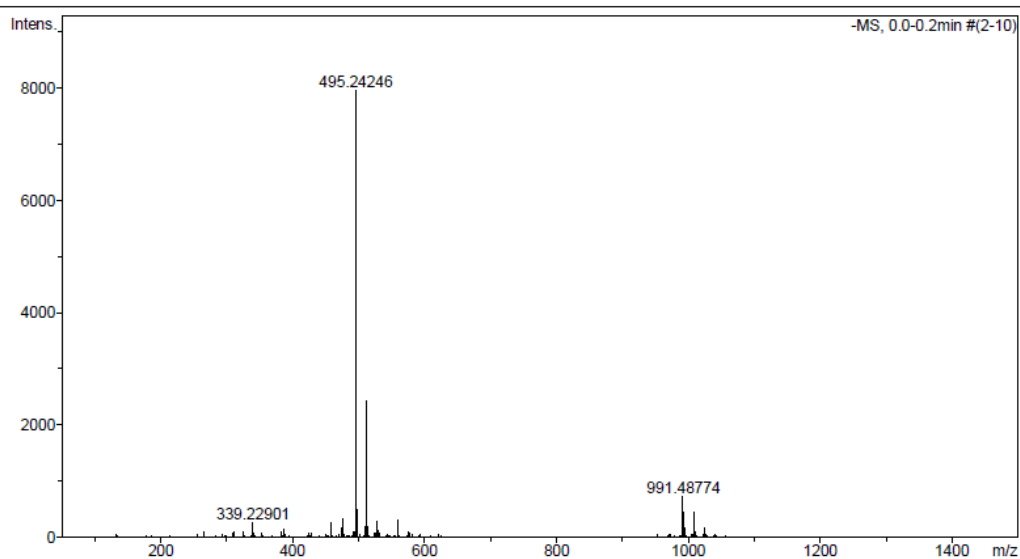


Figure B24. HRESIMS spectrum of tetrandraxanthone D (GT4) in MeCN



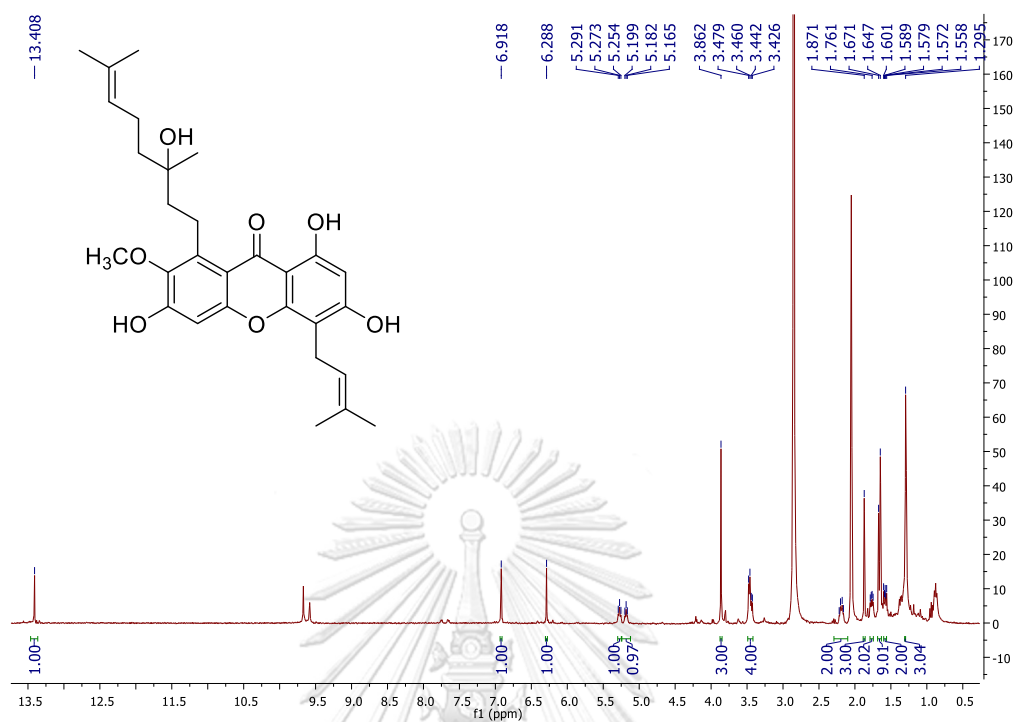


Figure B25. <sup>1</sup>H NMR spectrum of tetrandraxanthone E (GT5) in acetone-*d*<sub>6</sub>

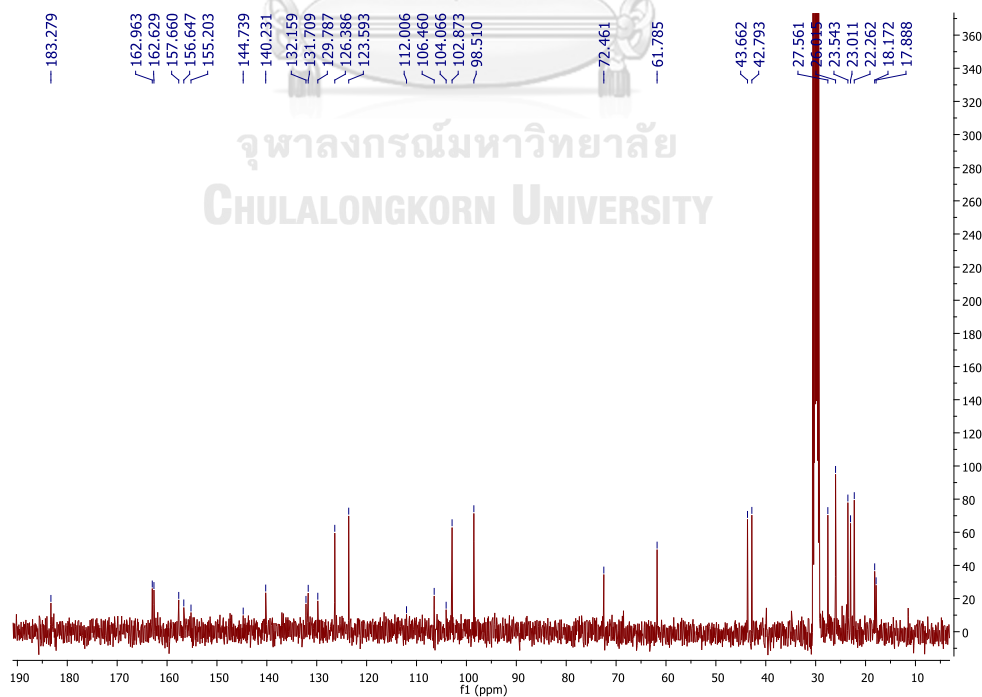


Figure B26. <sup>13</sup>C NMR spectrum of tetrandraxanthone E (GT5) in acetone-*d*<sub>6</sub>

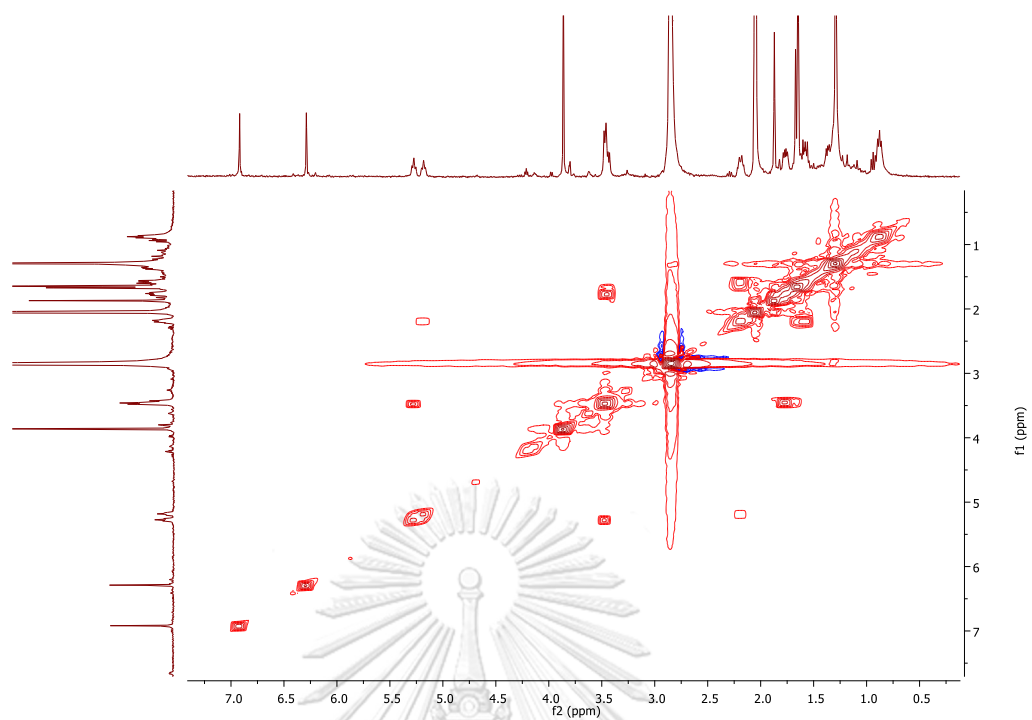


Figure B27. COSY spectrum of tetrandraxanthone E (GT5) in acetone- $d_6$

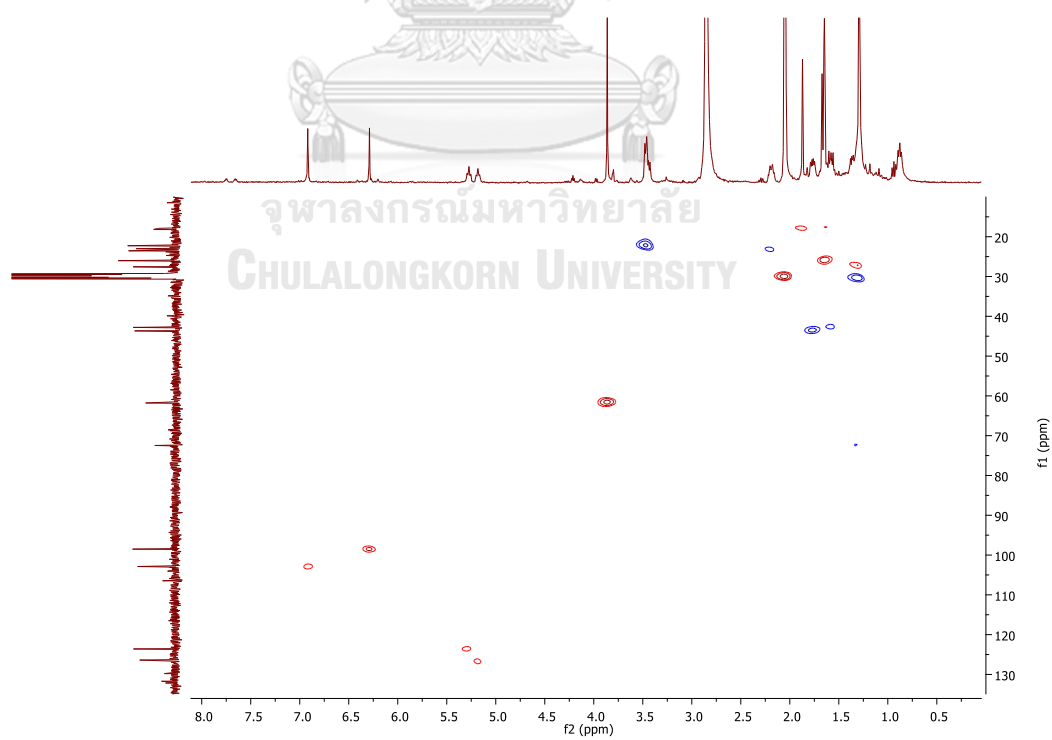


Figure B28. HSQC spectrum of tetrandraxanthone E (GT5) in acetone- $d_6$

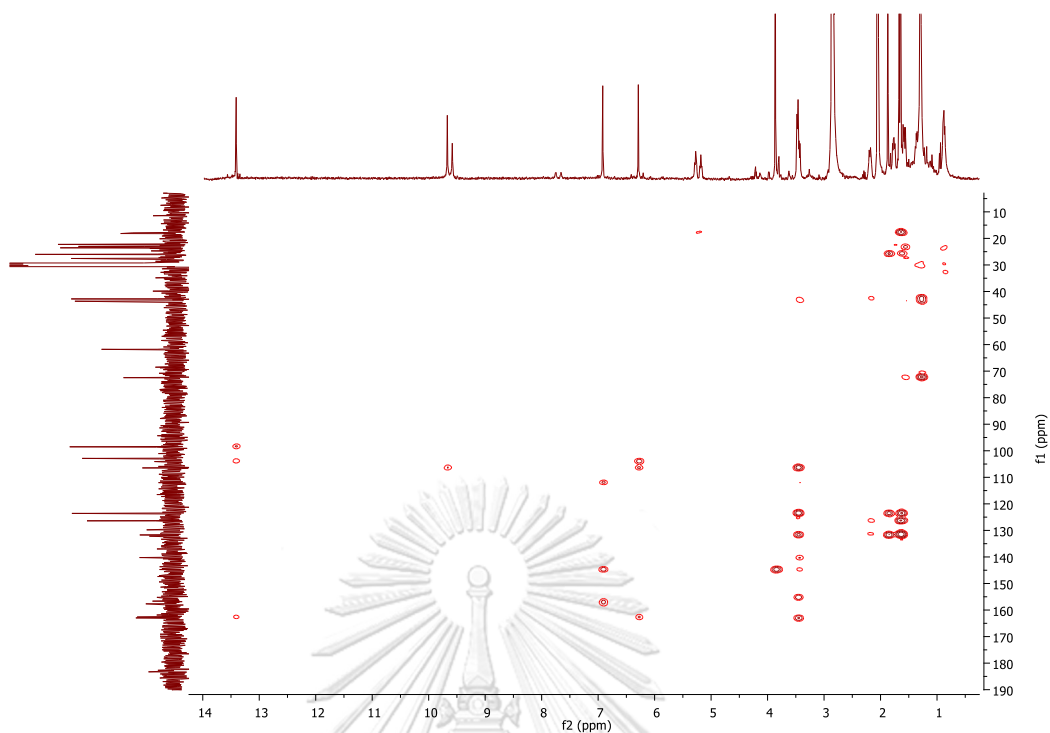


Figure B29. HMBC spectrum of tetrandraxanthone E (GT5) in acetone- $d_6$

### Generic Display Report

Analysis Info		Acquisition Date	
Analysis Name	D:\Data\Data Service\180316_neg_P6B1-1.d	3/16/2018	11:06:26 AM
Method	NV_neg_0.3min_profile_1segment_lowNubulizerDrygas(2).m	Operator	CU.
Sample Name	180316_neg_P6B1-1	Instrument	microTOF-Q II
Comment			

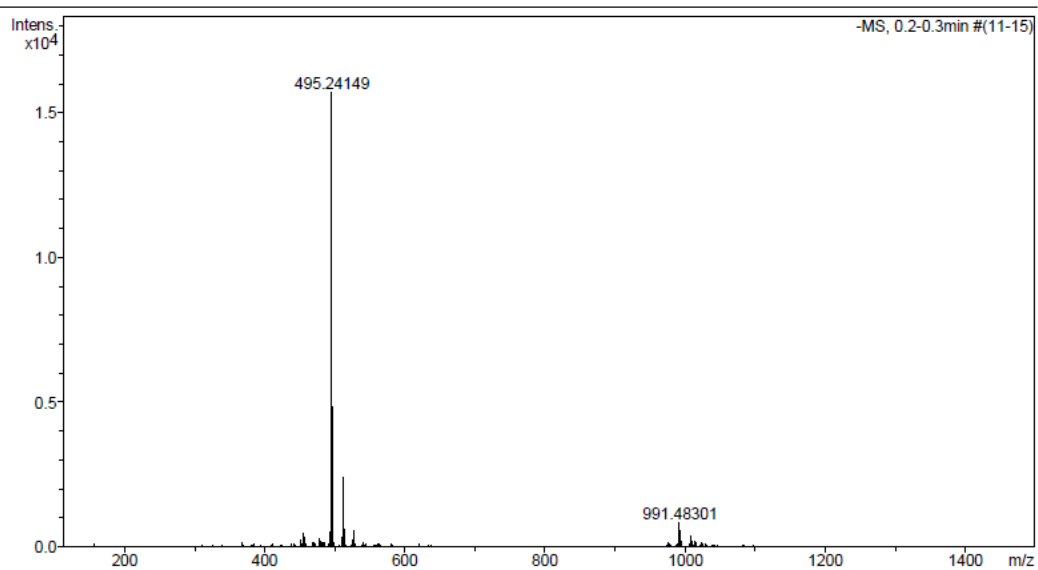


Figure B30. HRESIMS spectrum of tetrandraxanthone E (GT5) in MeCN

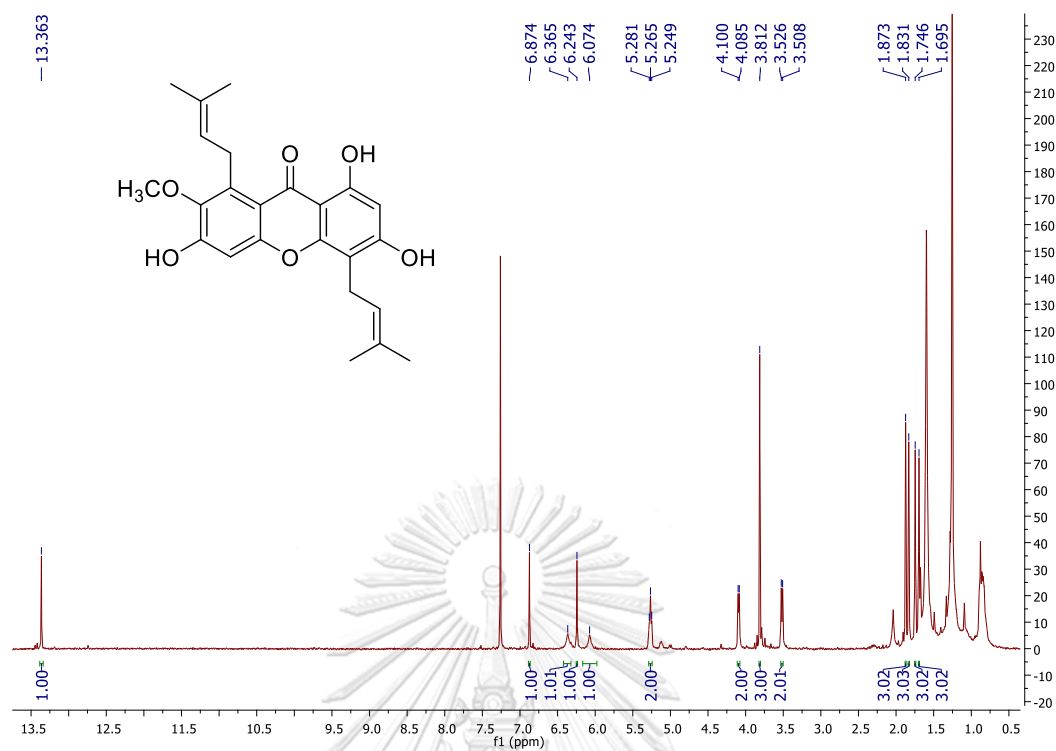


Figure B31. <sup>1</sup>H NMR spectrum of tetrandraxanthone F (GT6) in CDCl<sub>3</sub>

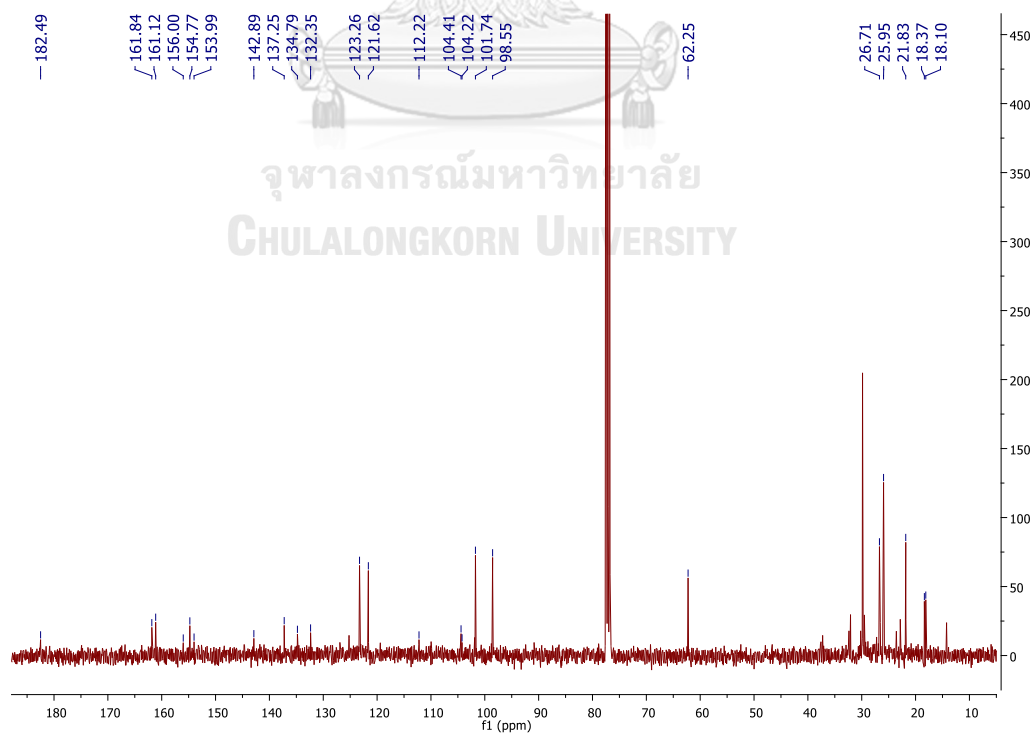


Figure B32. <sup>13</sup>C NMR spectrum of tetrandraxanthone F (GT6) in CDCl<sub>3</sub>

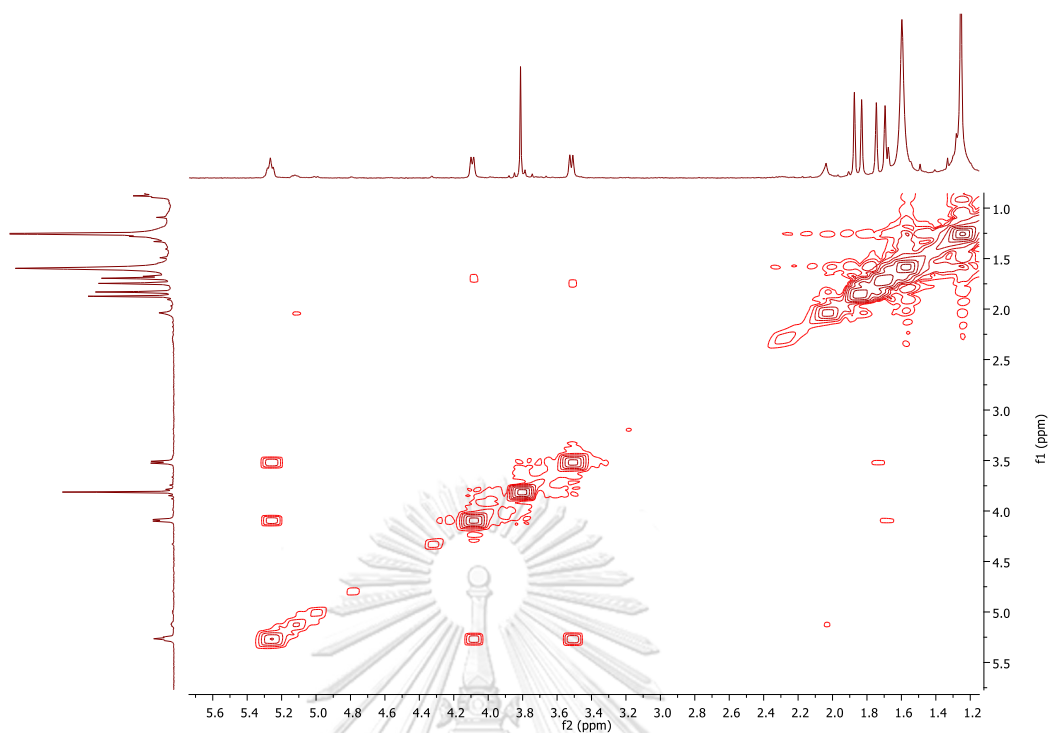


Figure B33. COSY spectrum of tetrandraxanthone F (GT6) in CDCl<sub>3</sub>

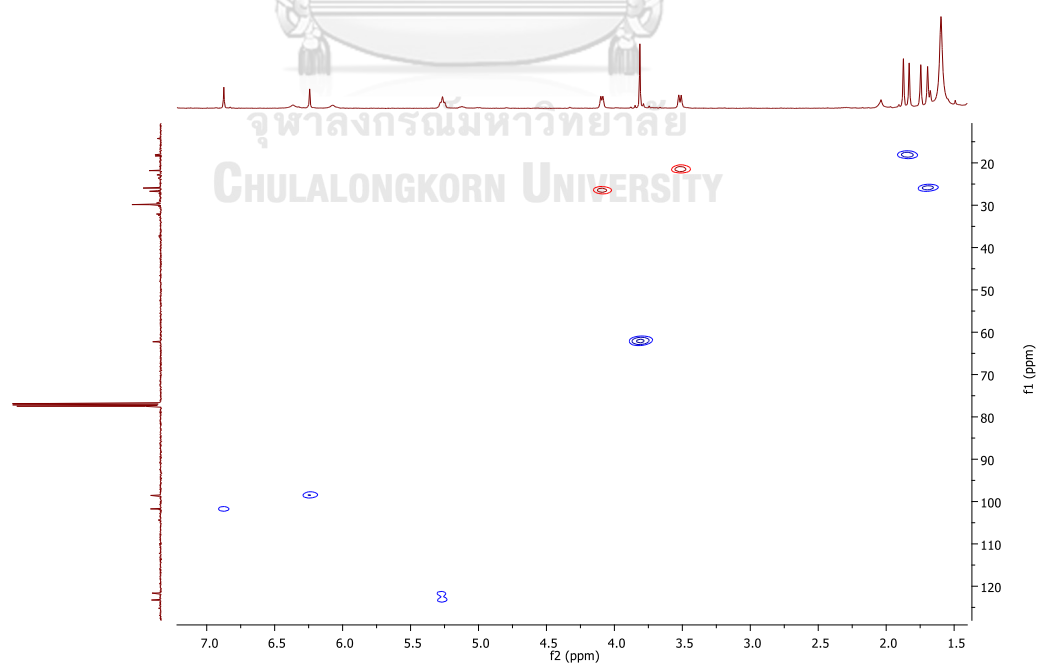
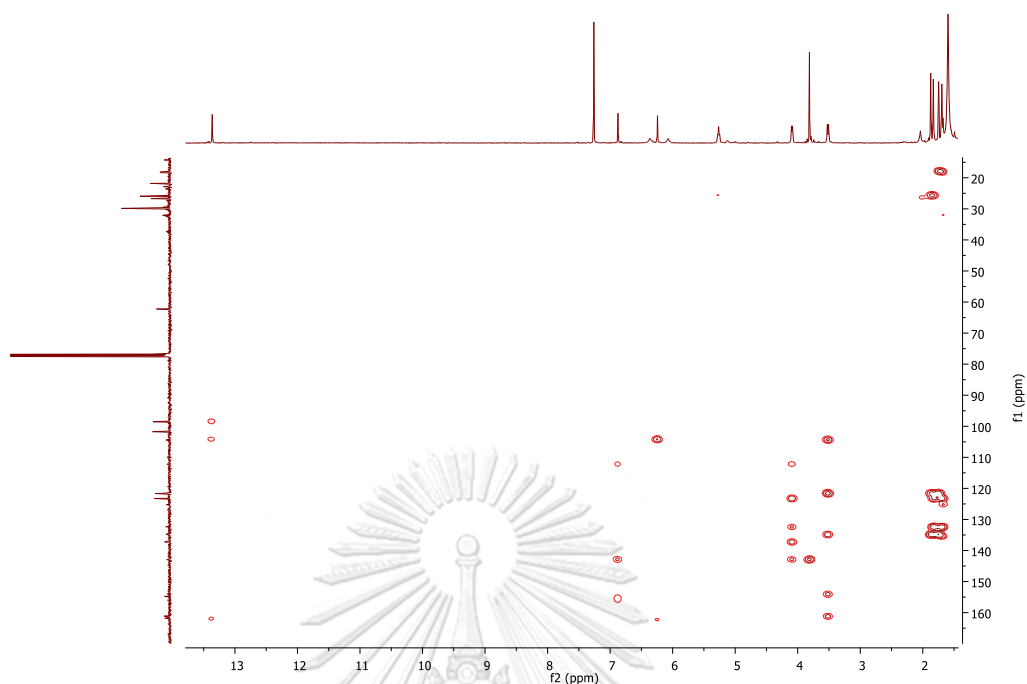


Figure B34. HSQC spectrum of tetrandraxanthone F (GT6) in CDCl<sub>3</sub>

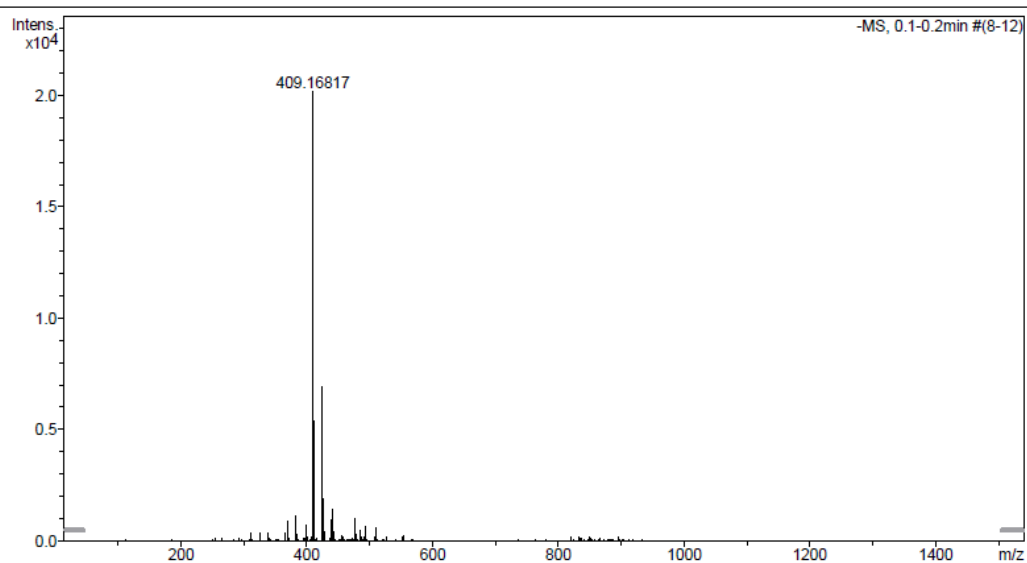
Figure B35. HMBC spectrum of tetrandraxanthone F (**GT6**) in CDCl<sub>3</sub>

---

### Generic Display Report

---

<b>Analysis Info</b>	Acquisition Date	3/16/2018 10:47:03 AM	
Analysis Name	D:\Data\Data Service\180316_neg_GTH-28.d		
Method	NV_neg_0.3min_profile_1segment_lowNubulizerDrygas(2).m	Operator	CU.
Sample Name	180316_neg_GTH-28	Instrument	microTOF-Q II
Comment			

Figure B36. HRESIMS spectrum of tetrandraxanthone F (**GT6**) in MeCN

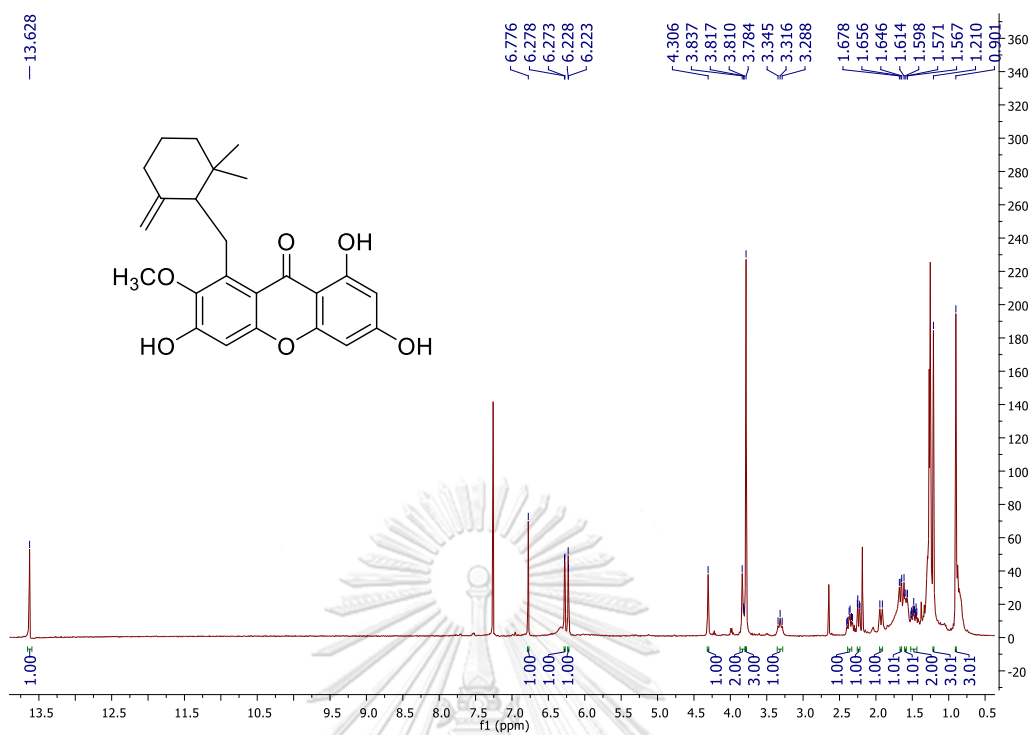


Figure B37.  $^1\text{H}$  NMR spectrum of tetrandraxanthone G (GT7) in  $\text{CDCl}_3$

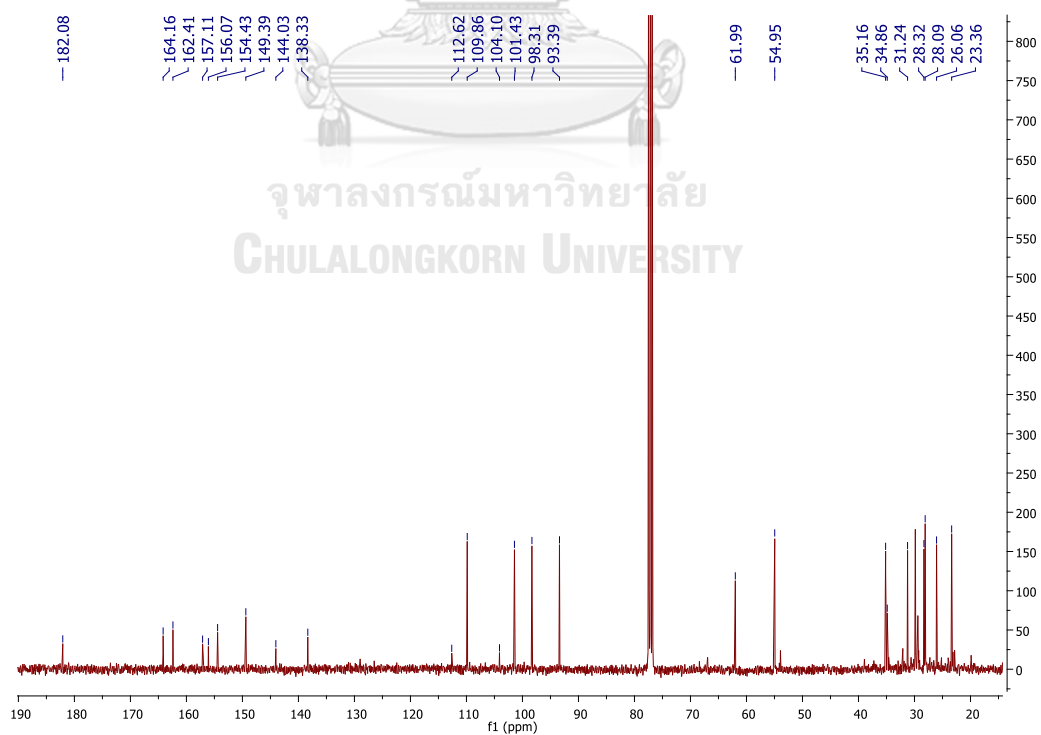


Figure B38.  $^{13}\text{C}$  NMR spectrum of tetrandraxanthone G (GT7) in  $\text{CDCl}_3$

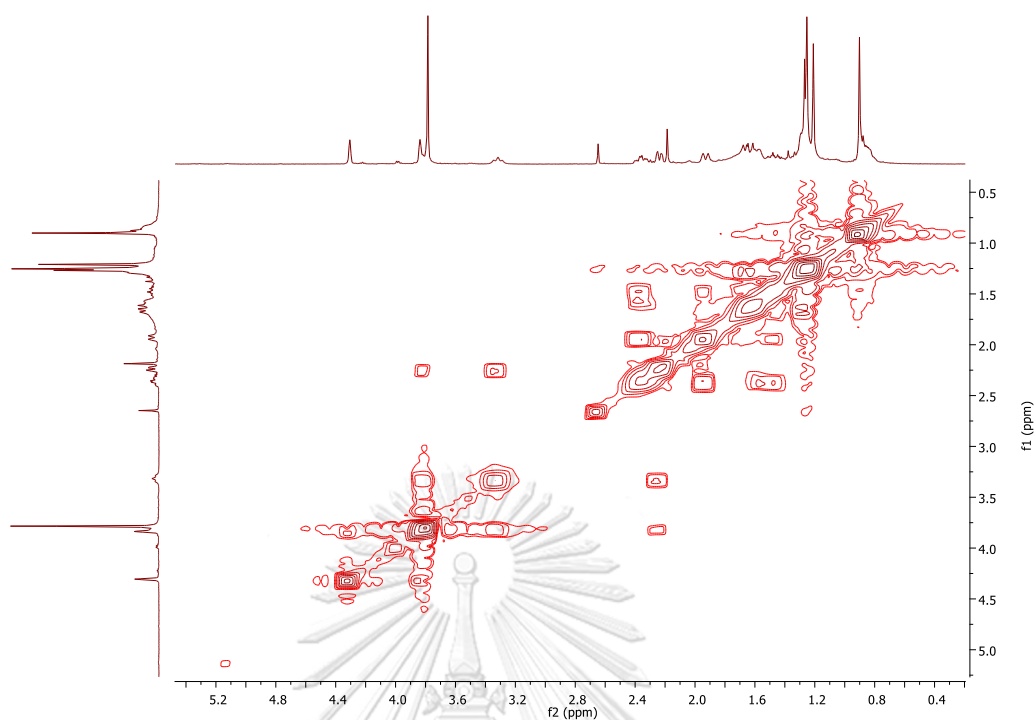


Figure B39. COSY spectrum of tetrandraxanthone G (**GT7**) in  $\text{CDCl}_3$

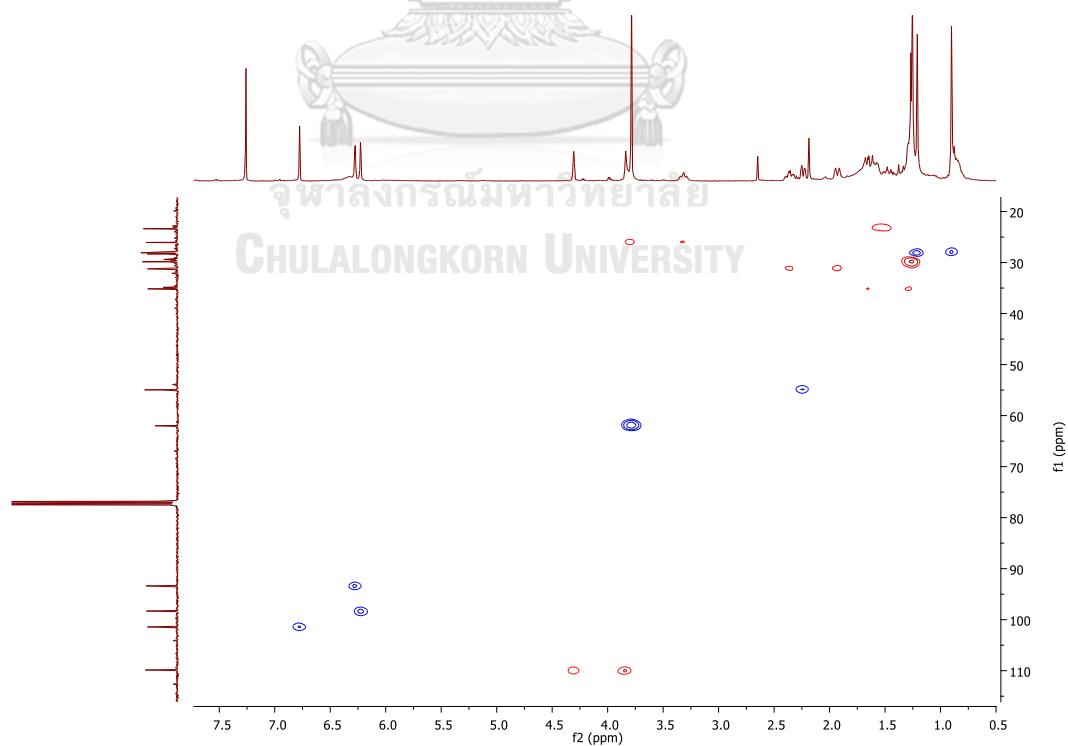
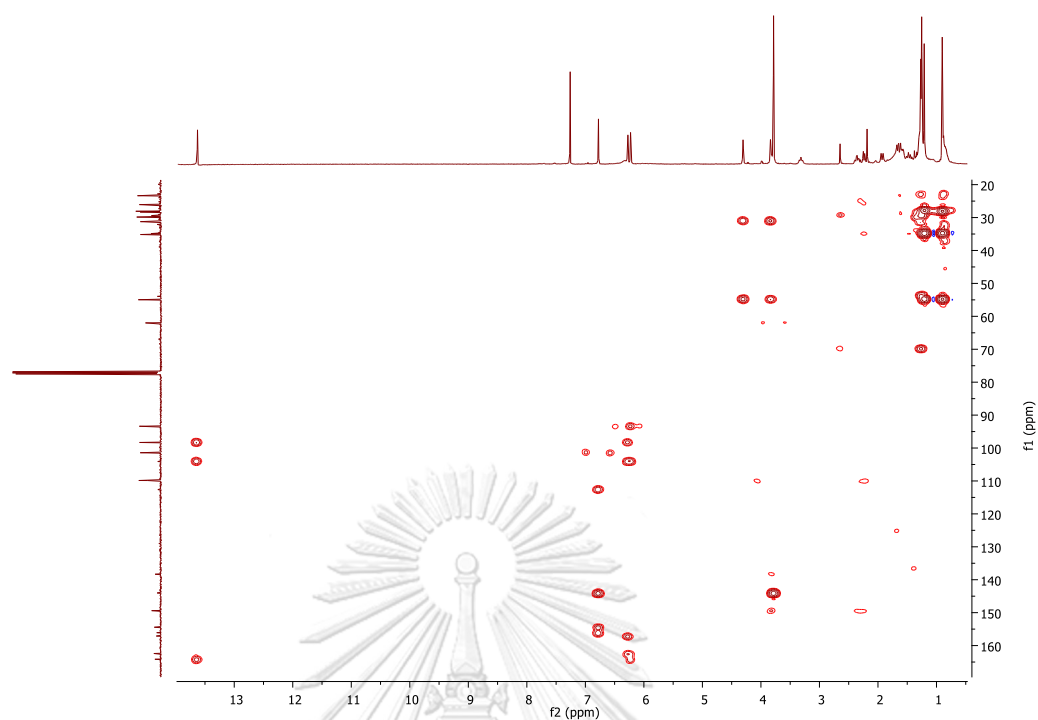


Figure B40. HSQC spectrum of tetrandraxanthone G (**GT7**) in  $\text{CDCl}_3$



Figure B41. HMBC spectrum of tetrandraxanthone G (**GT7**) in CDCl<sub>3</sub>

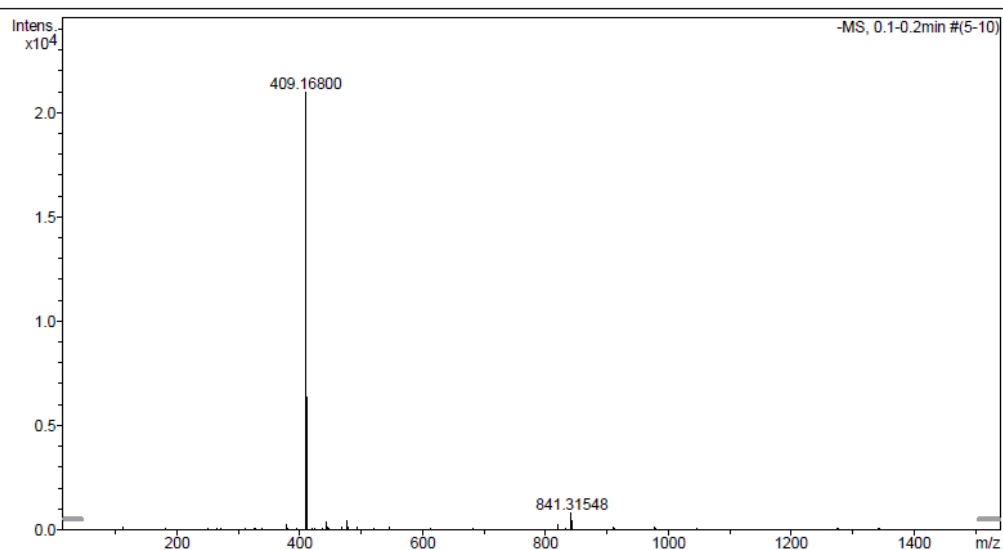
---

### Generic Display Report

---

<b>Analysis Info</b>	Acquisition Date	3/16/2018 12:23:54 PM	
Analysis Name	D:\Data\Data Service\180316_neg_GTH-25.d		
Method	NV_neg_0.3min_profile_1segment_lowNubulizerDrygas(2).m	Operator	CU.
Sample Name	180316_neg_GTH-25	Instrument	micrOTOF-Q II
Comment			

---

Figure B42. HRESIMS spectrum of tetrandraxanthone G (**GT7**) in MeCN

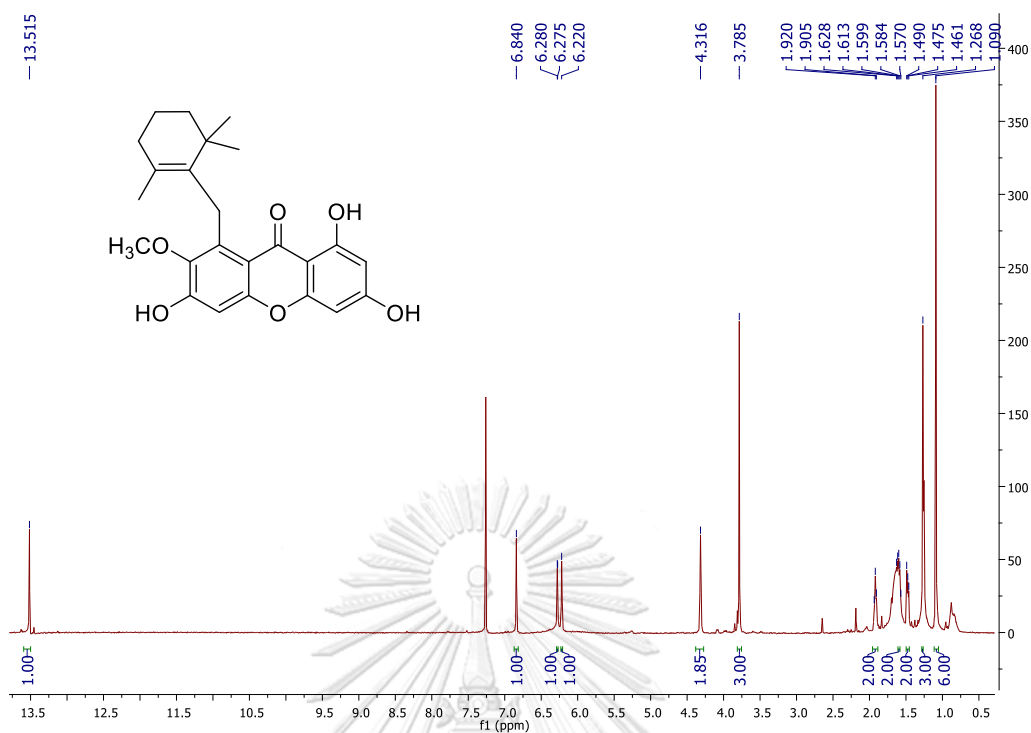


Figure B43.  $^1\text{H}$  NMR spectrum of tetrandraxanthone H (GT8) in  $\text{CDCl}_3$

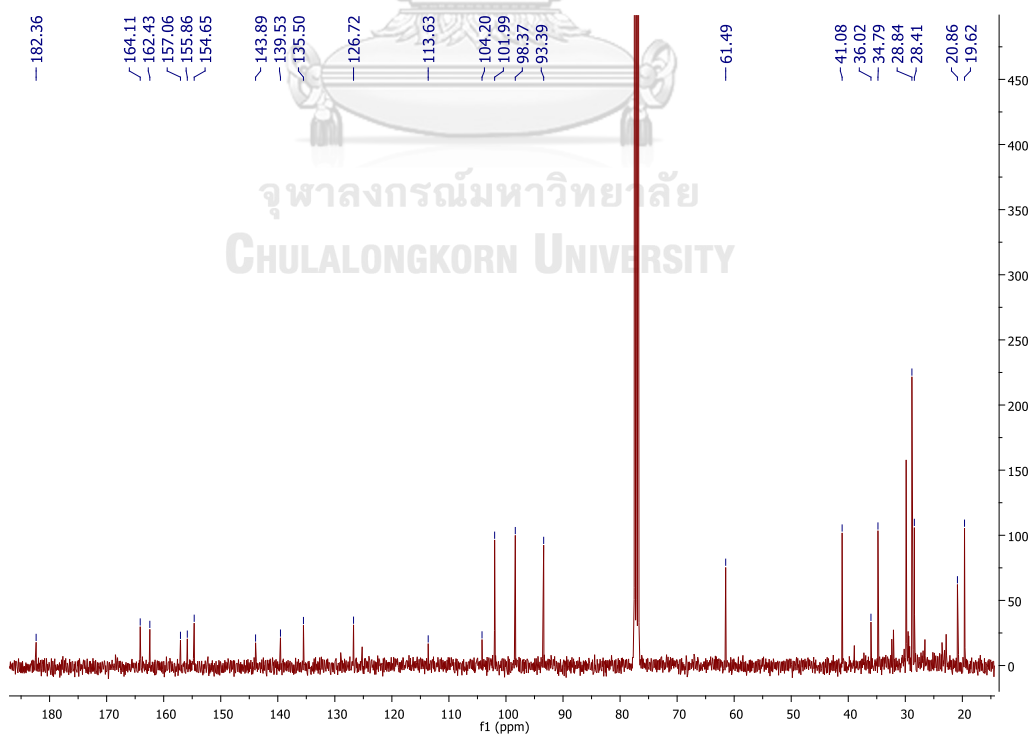


Figure B44.  $^{13}\text{C}$  NMR spectrum of tetrandraxanthone H (GT8) in  $\text{CDCl}_3$

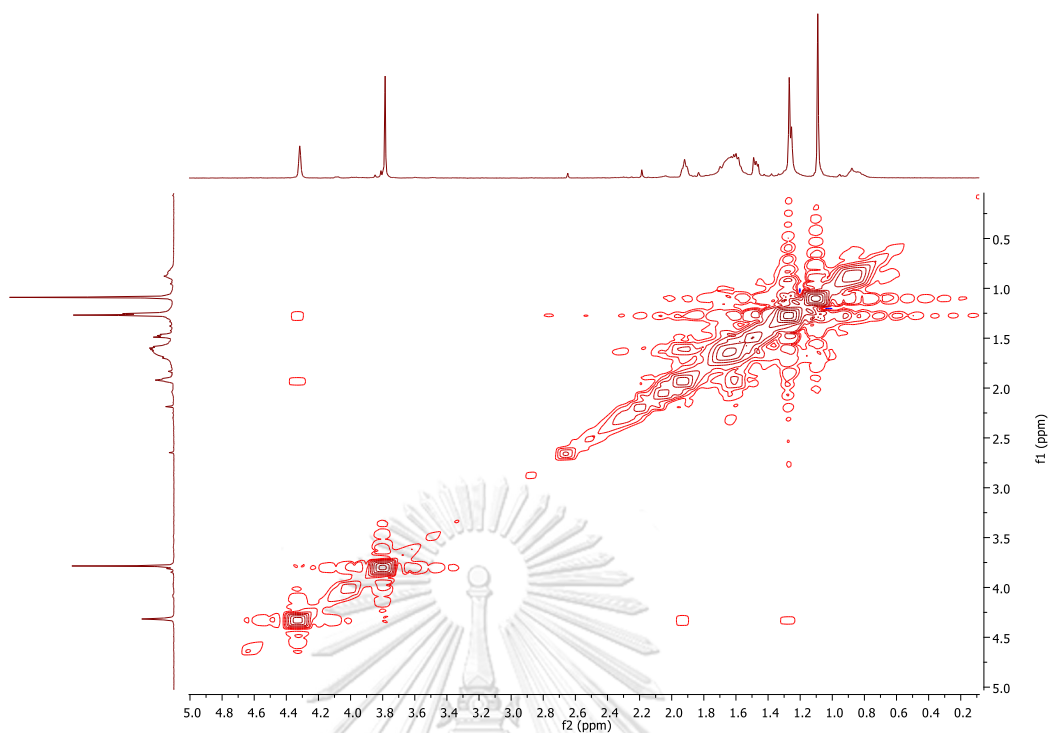


Figure B45. COSY spectrum of tetrandraxanthone H (**GT8**) in  $\text{CDCl}_3$

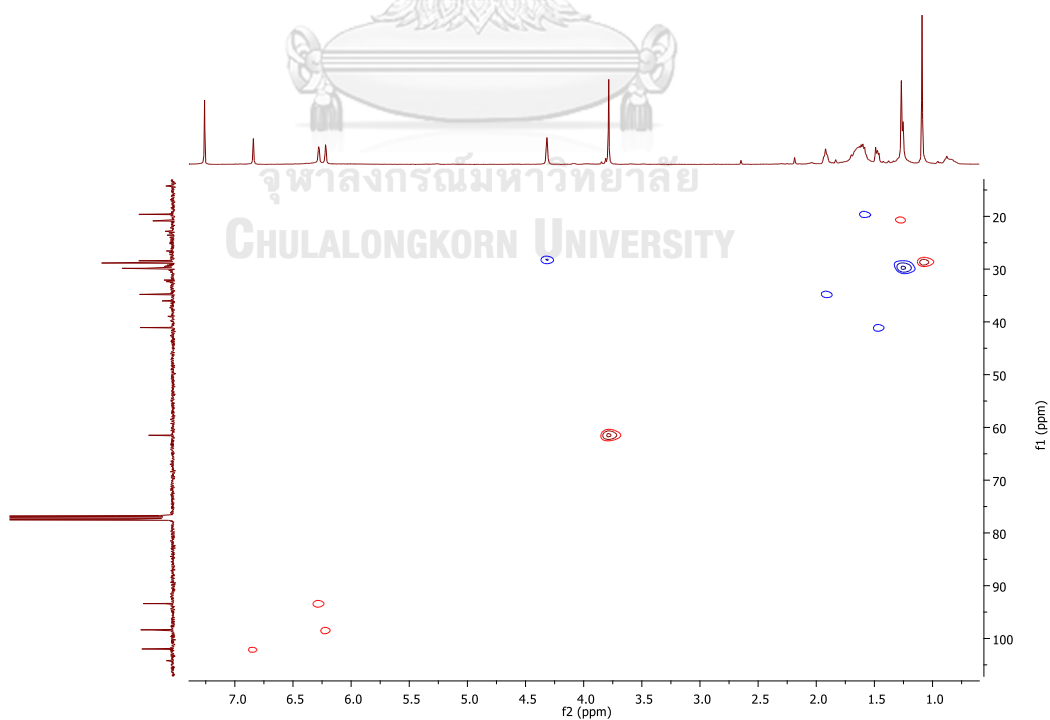
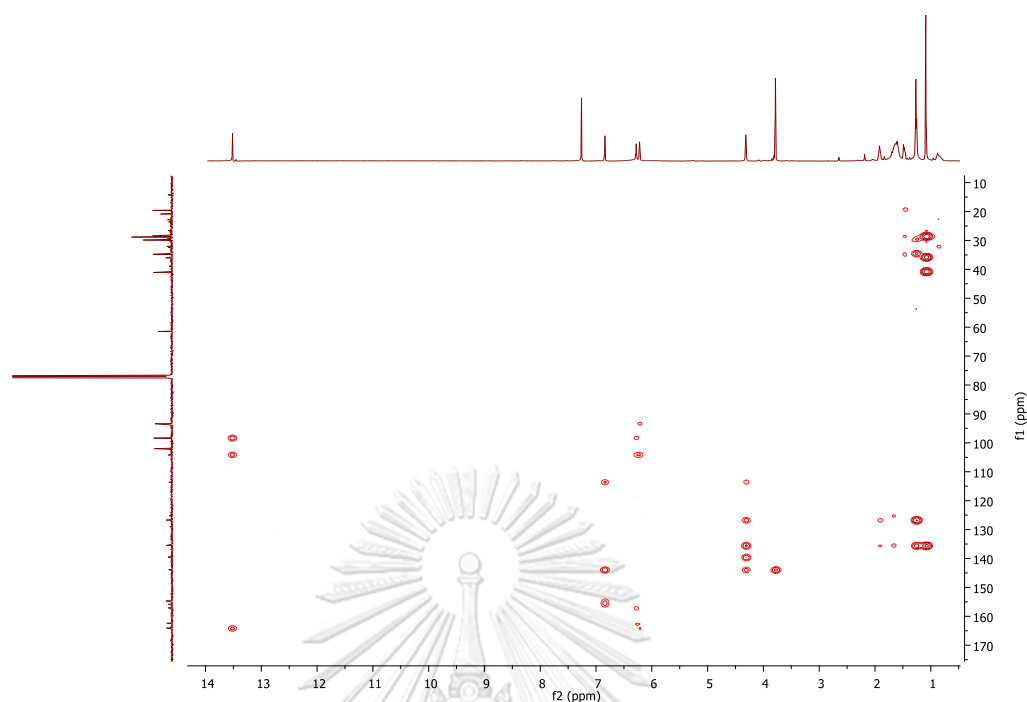


Figure B46. HSQC spectrum of tetrandraxanthone H (**GT8**) in  $\text{CDCl}_3$

Figure B47. HMBC spectrum of tetrandraxanthone H (GT8) in CDCl<sub>3</sub>

## Generic Display Report

<b>Analysis Info</b>	Acquisition Date	3/18/2018 11:54:01 AM	
Analysis Name	D:\Data\Data Service\180316\180316_neg_GTH-26.d	Operator	CU.
Method	NV_neg_0.3min_profile_1segment_lowNubulizerDrygas(2).m	Instrument	micrOTOF-Q II
Sample Name	180316_neg_GTH-26		
Comment			

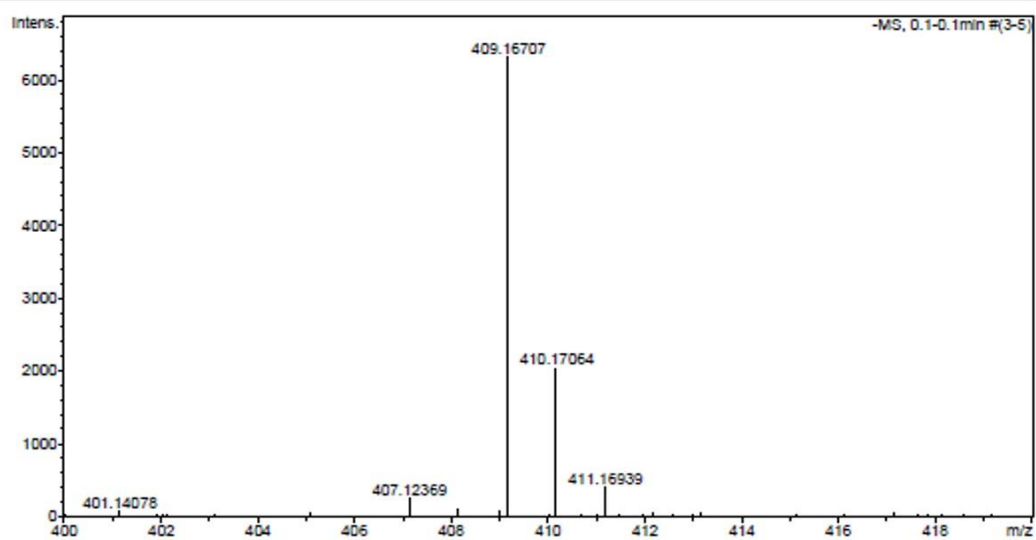


Figure B48. HRESIMS spectrum of tetrandraxanthone H (GT8) in MeCN

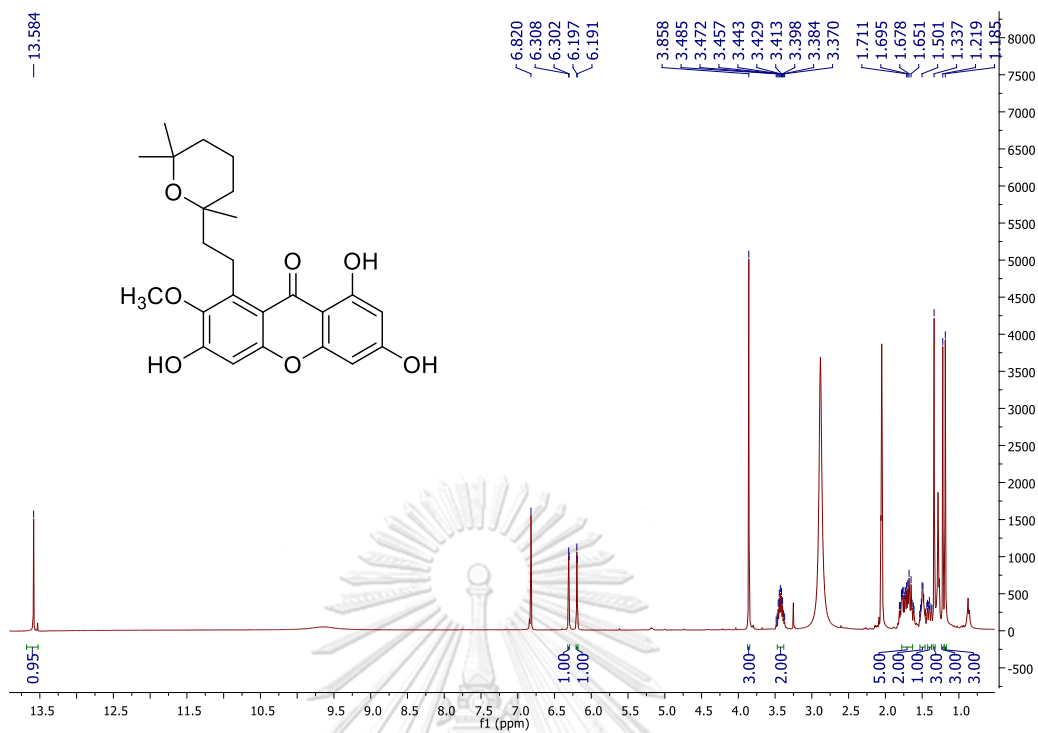


Figure B49.  $^1\text{H}$  NMR spectrum of tetrandraxanthone I (GT9) in acetone- $d_6$

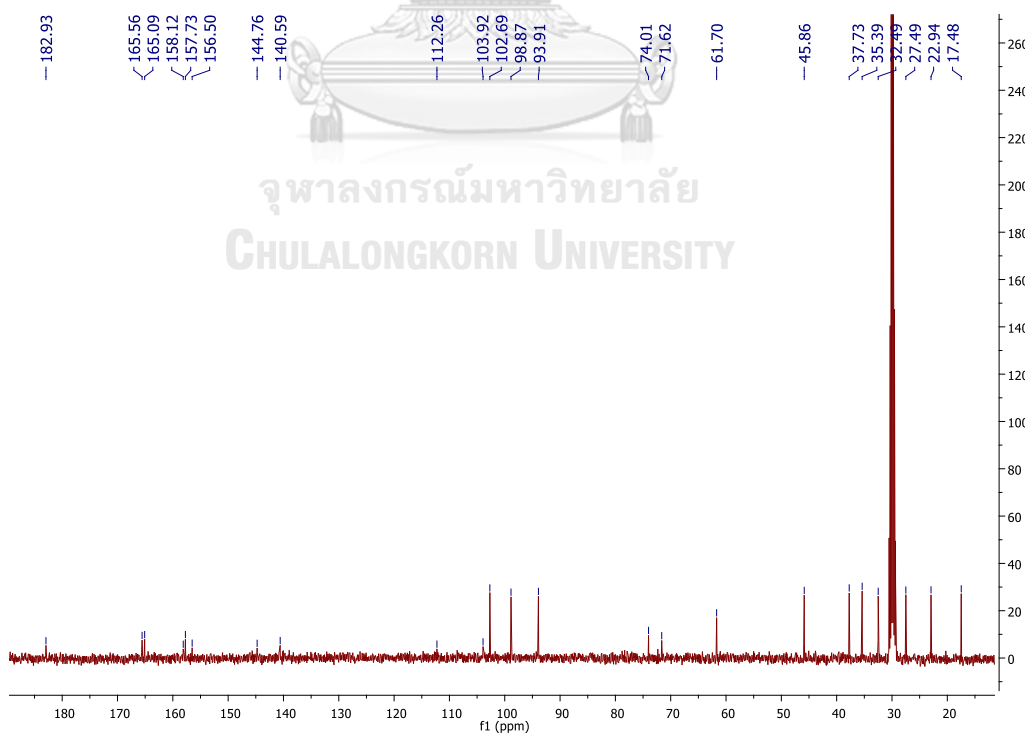


Figure B50.  $^{13}\text{C}$  NMR spectrum of tetrandraxanthone I (GT9) in acetone- $d_6$

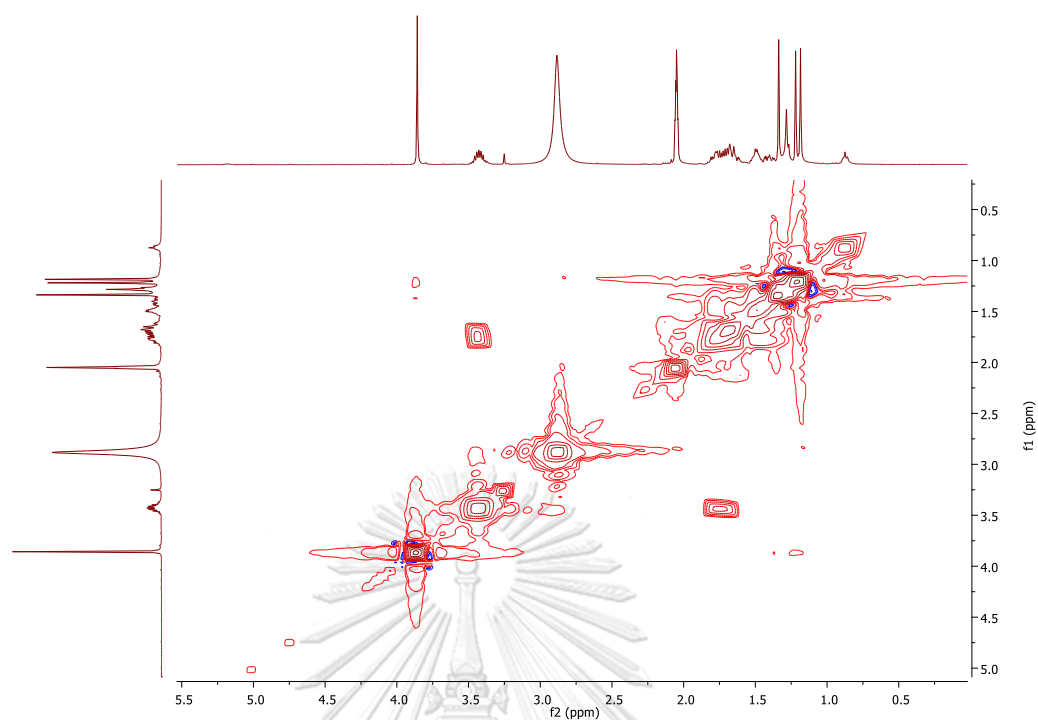


Figure B51. COSY spectrum of tetrandraxanthone I (GT9) in acetone- $d_6$

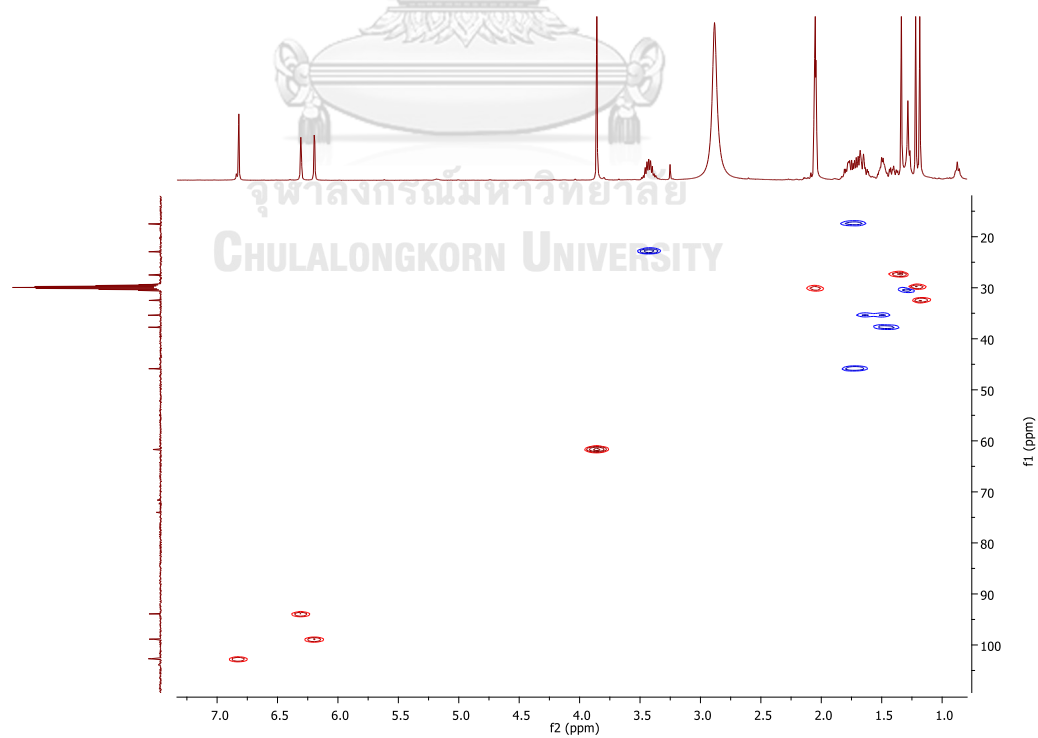


Figure B52. HSQC spectrum of tetrandraxanthone I (GT9) in acetone- $d_6$

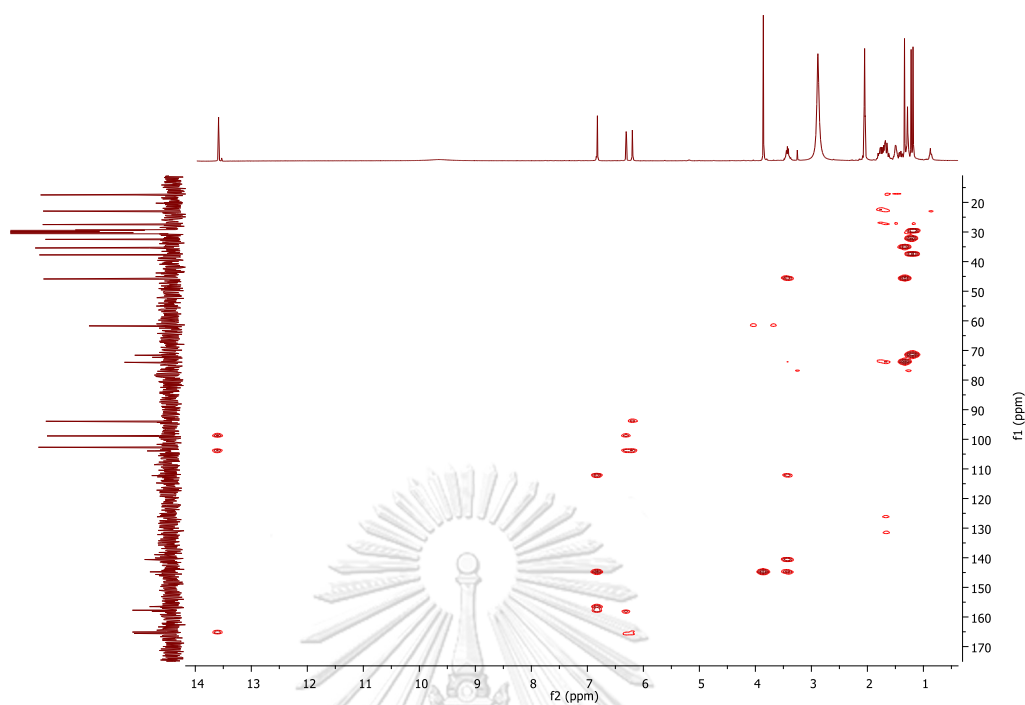


Figure B53. HMBC spectrum of tetrandraxanthone I (GT9) in acetone- $d_6$

### Generic Display Report

Analysis Info		Acquisition Date	3/16/2018 11:21:39 AM
Analysis Name	D:\Data\Data Service\180316_neg_GTH-21.d	Operator	CU.
Method	NV_neg_0.3min_profile_1segment_lowNubulizerDrygas(2).m	Instrument	micrOTOF-Q II
Sample Name	180316_neg_GTH-21		
Comment			

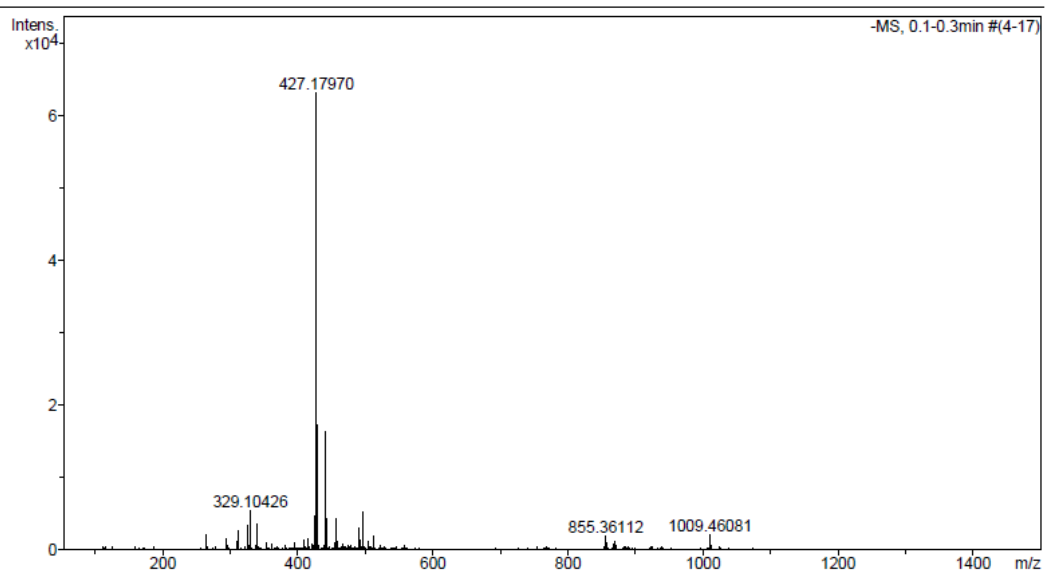


Figure B54. HRESIMS spectrum of tetrandraxanthone I (GT9) in MeCN

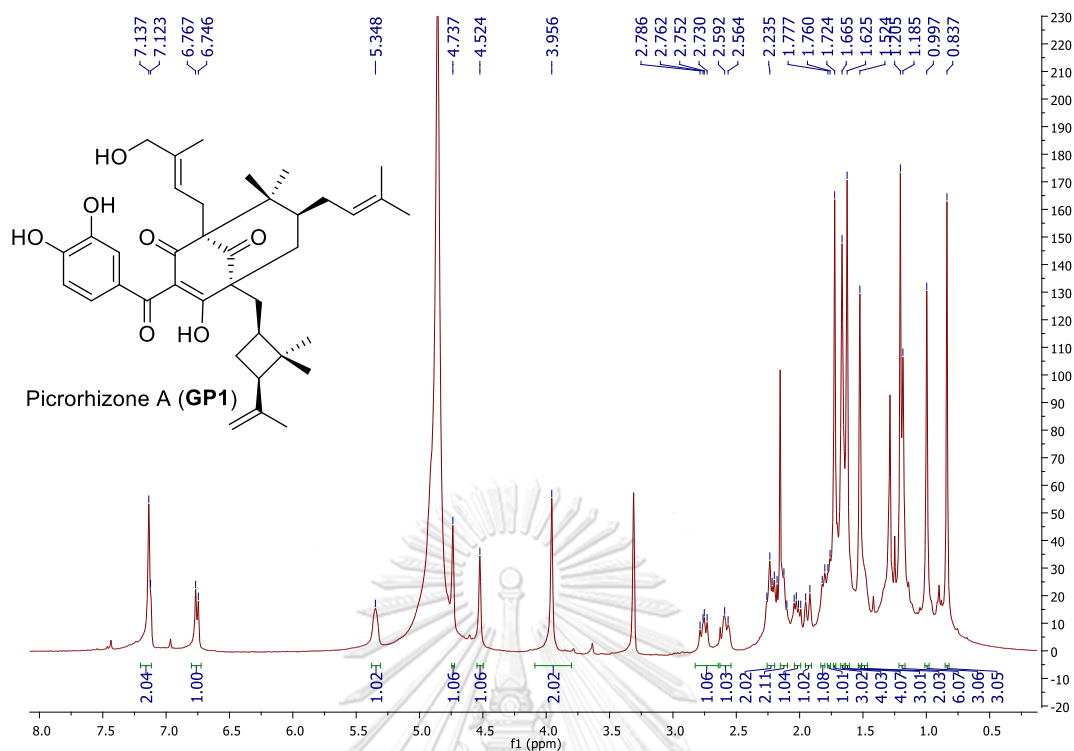


Figure C1.  $^1\text{H}$  NMR spectrum of picrorhizone A (GP1) in methanol- $d_4$

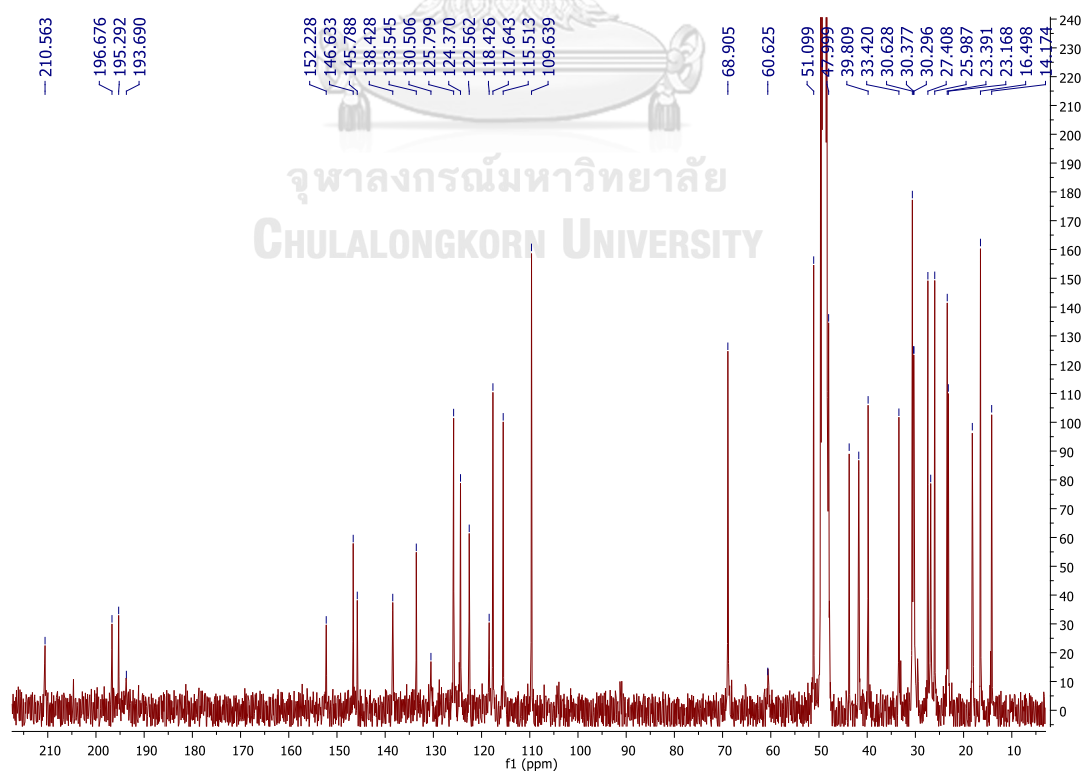


Figure C2.  $^{13}\text{C}$  NMR spectrum of picrorhizone A (GP1) in methanol- $d_4$



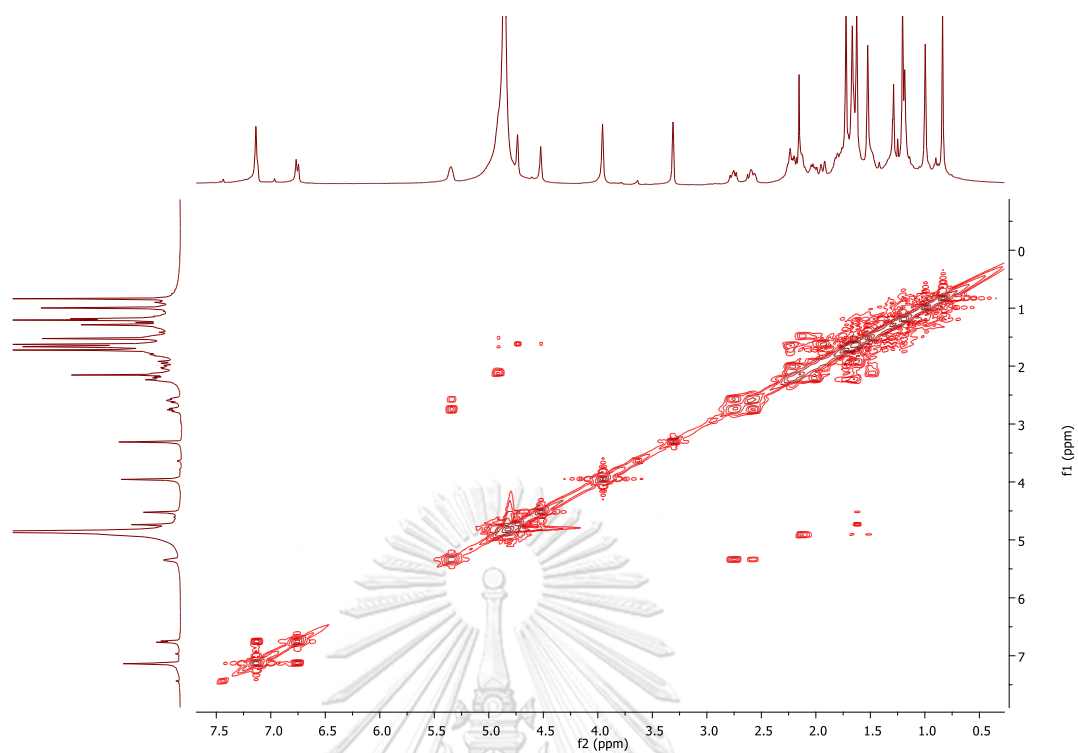


Figure C3. COSY spectrum of picrorhizone A (GP1) in methanol- $d_4$

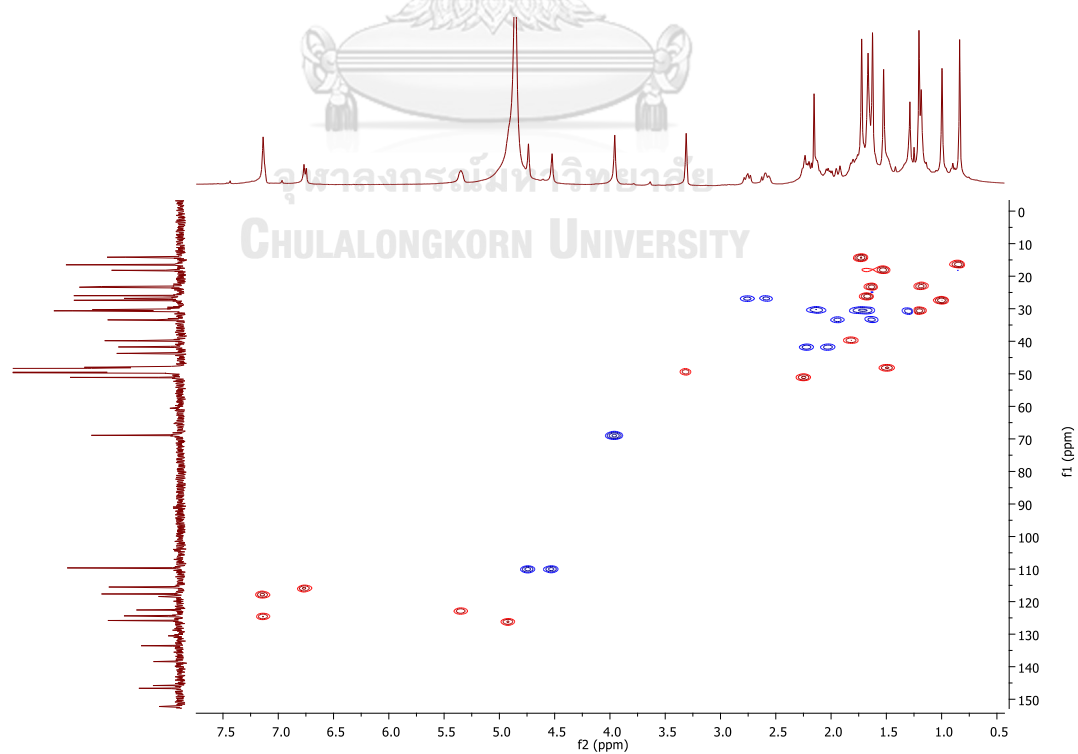


Figure C4. HSQC spectrum of picrorhizone A (GP1) in methanol- $d_4$

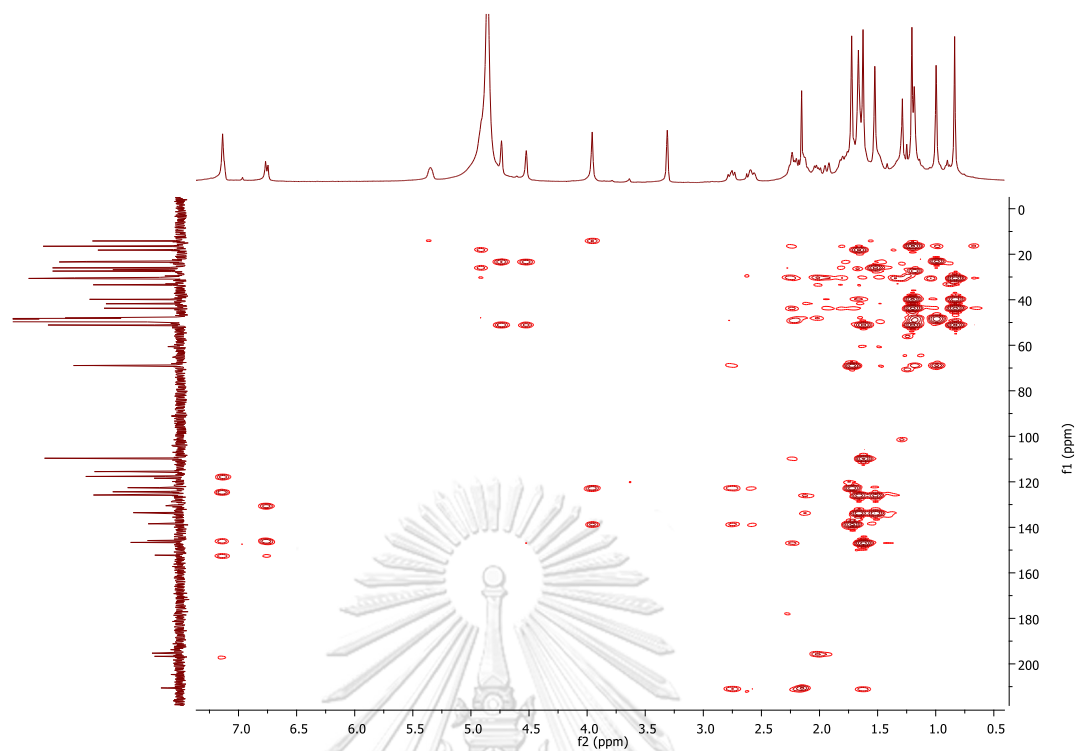


Figure C5. HMBC spectrum of picrorhizone A (GP1) in methanol- $d_4$

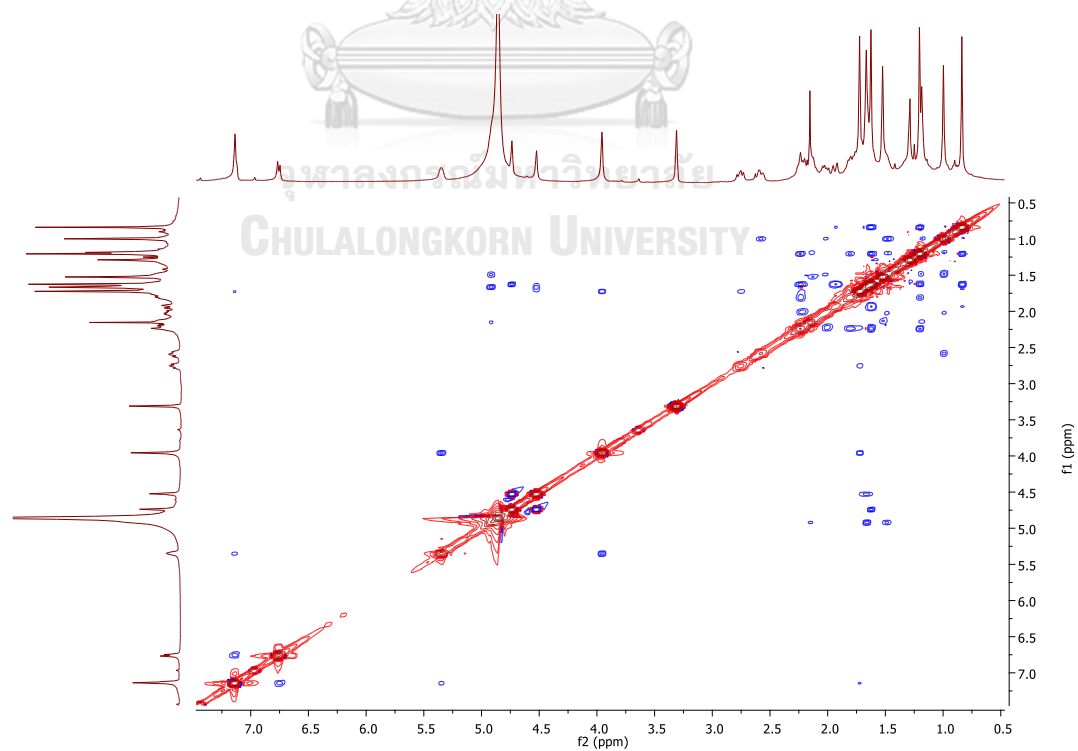


Figure C6a. NOESY spectrum of picrorhizone A (GP1) in methanol- $d_4$

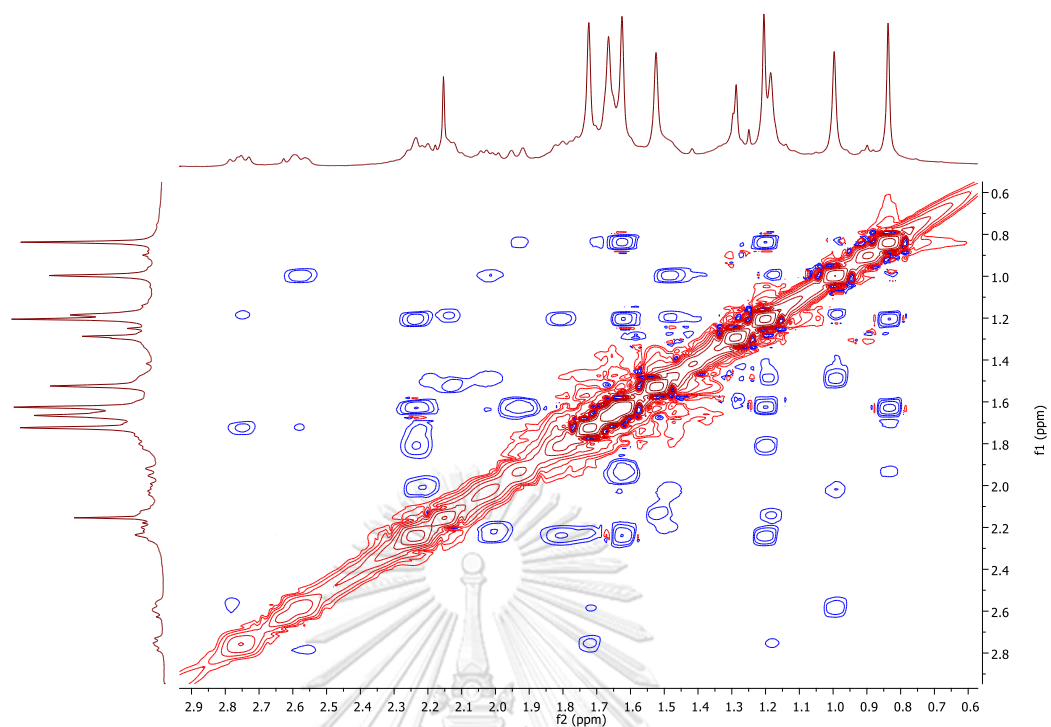


Figure C6b. Expanded NOESY spectrum of picrorhizone A (**GP1**) in methanol- $d_4$

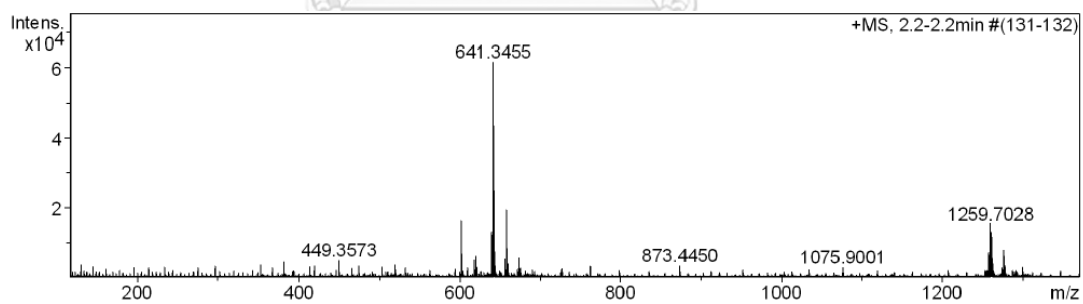


Figure C7. HRESIMS spectrum of picrorhizone A (**GP1**) in methanol

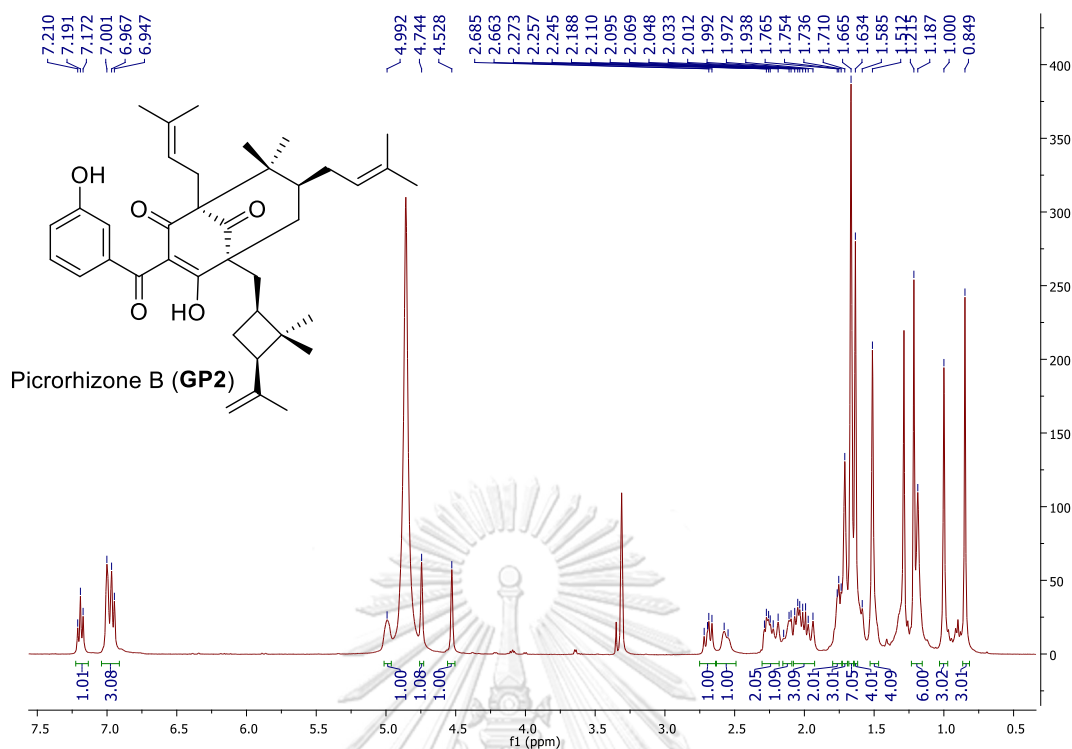


Figure C8.  $^1\text{H}$  NMR spectrum of picrorhizone B (GP2) in methanol- $d_4$

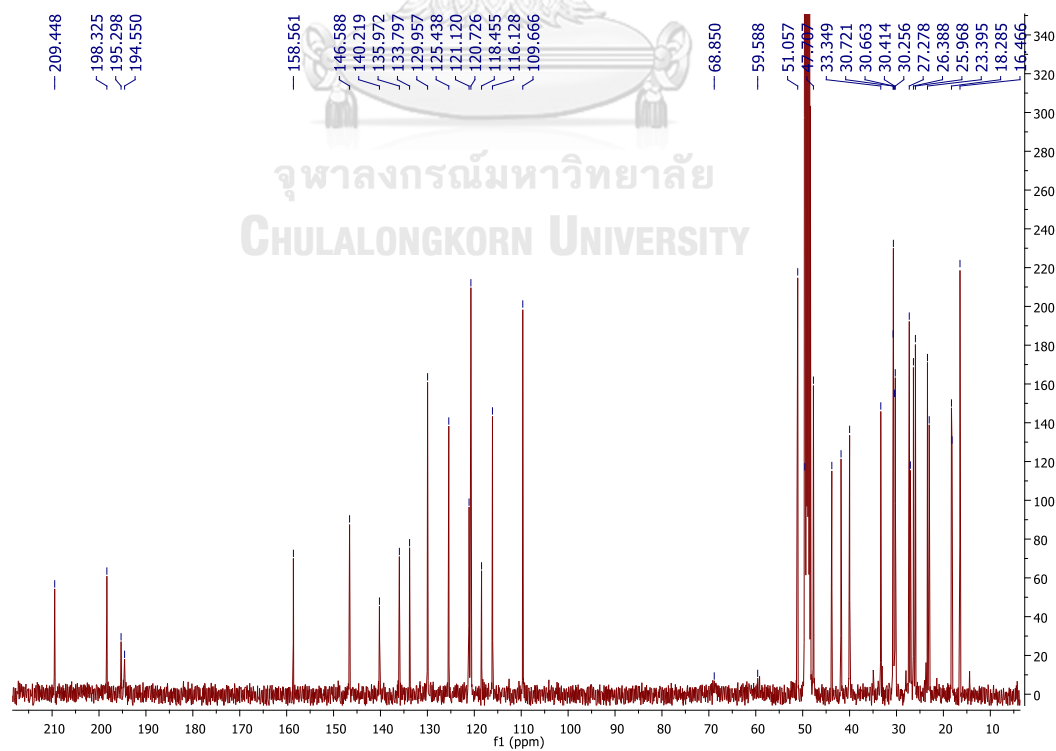


Figure C9.  $^{13}\text{C}$  NMR spectrum of picrorhizone B (GP2) in methanol- $d_4$

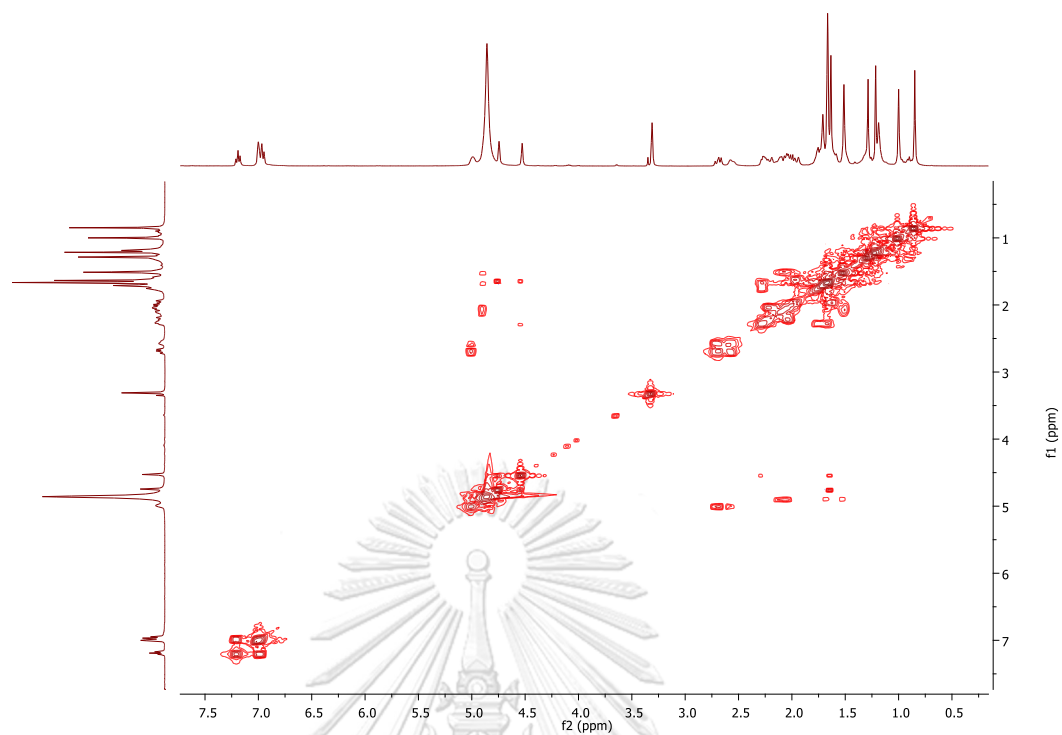


Figure C10. COSY spectrum of picrorhizone B (GP2) in methanol- $d_4$

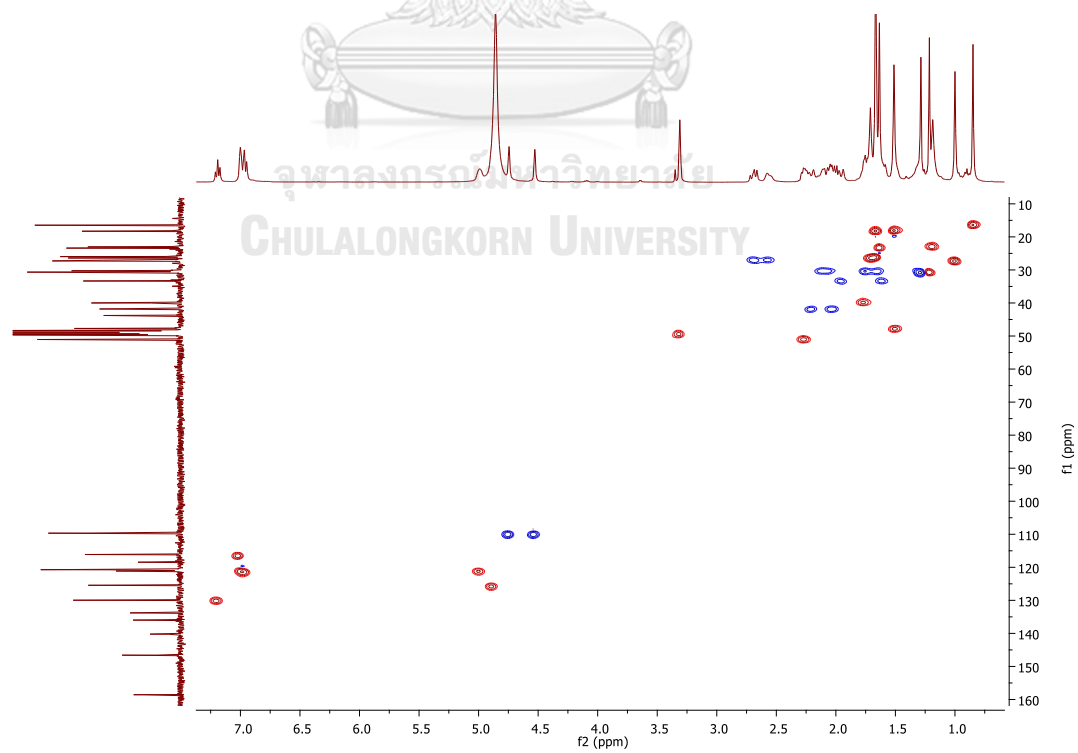
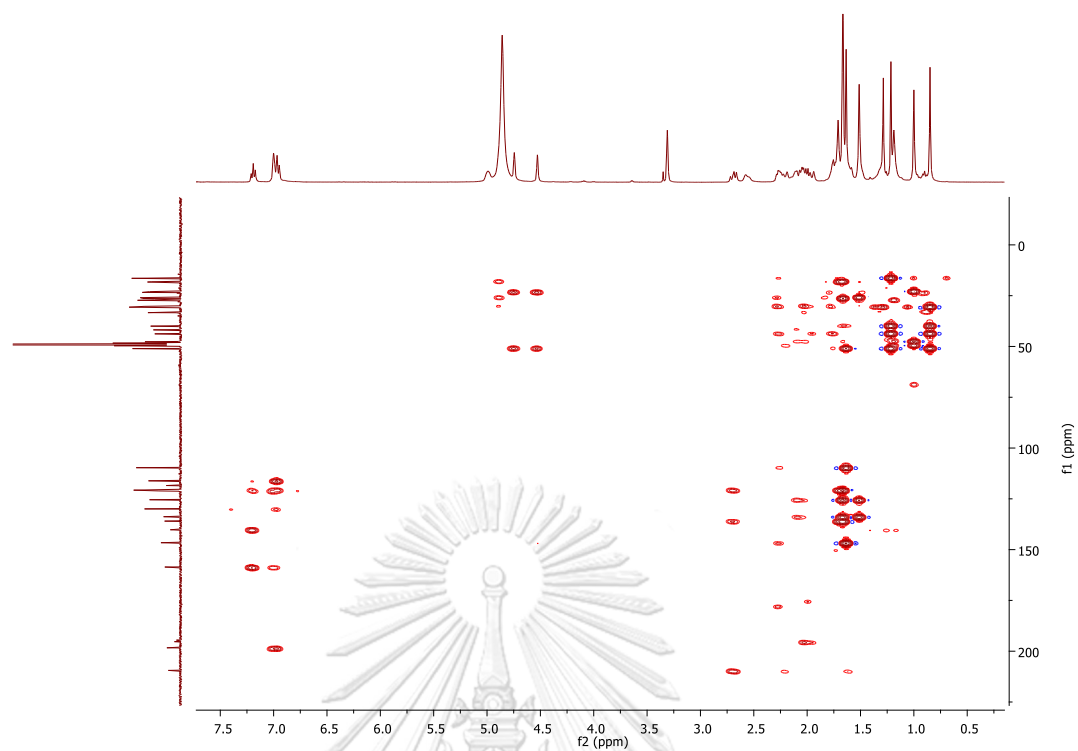
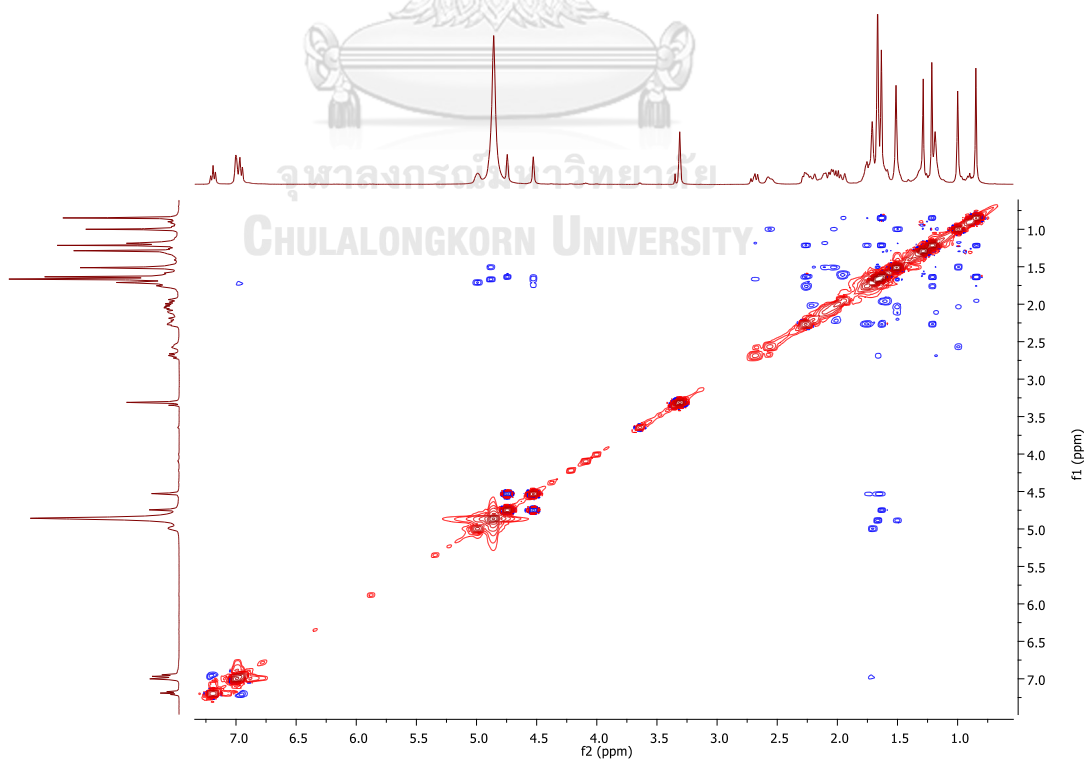


Figure C11. HSQC spectrum of picrorhizone B (GP2) in methanol- $d_4$

Figure C12. HMBC spectrum of picrorhizone B (GP2) in methanol- $d_4$ Figure C13. NOESY spectrum of picrorhizone B (GP2) in methanol- $d_4$

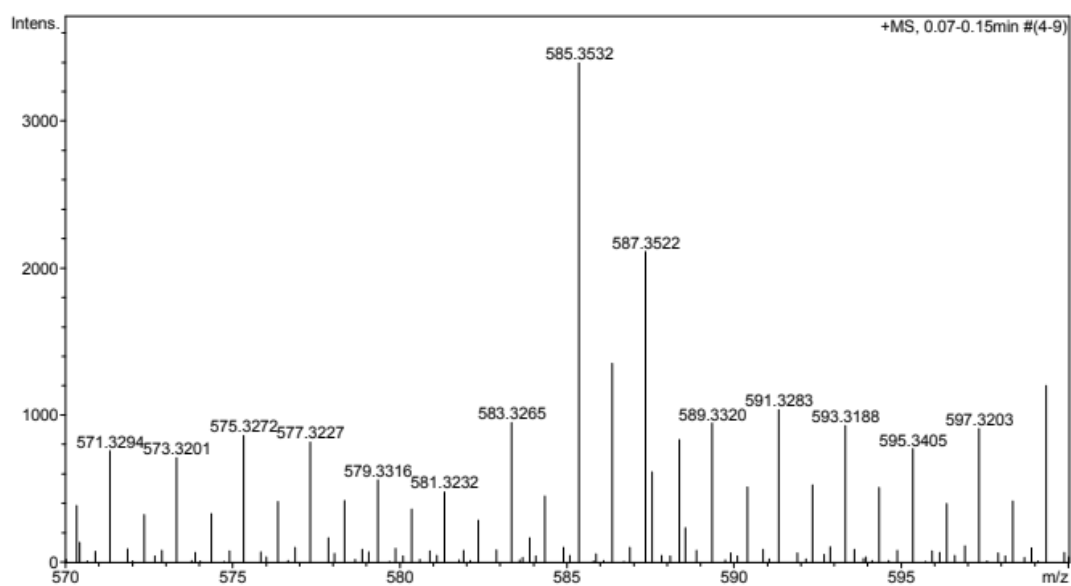


Figure C14. HRESIMS spectrum of picrorhizone B (GP2) in methanol- $d_4$



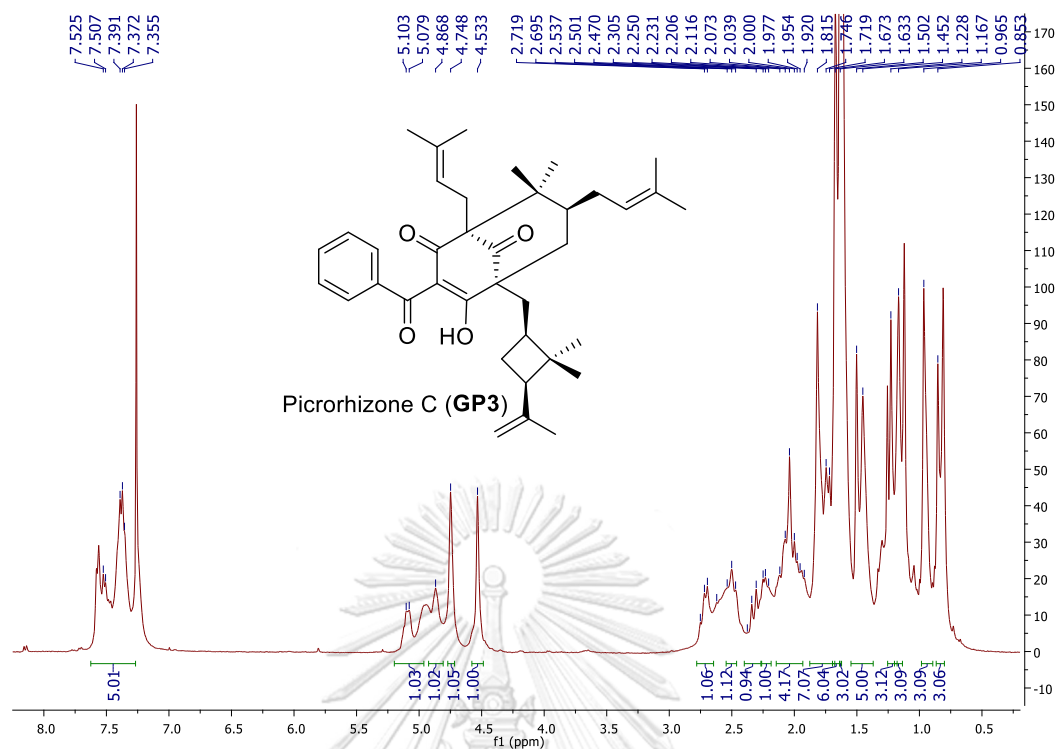


Figure C15.  $^1\text{H}$  NMR spectrum of picrorhizone C (GP3) in  $\text{CDCl}_3$

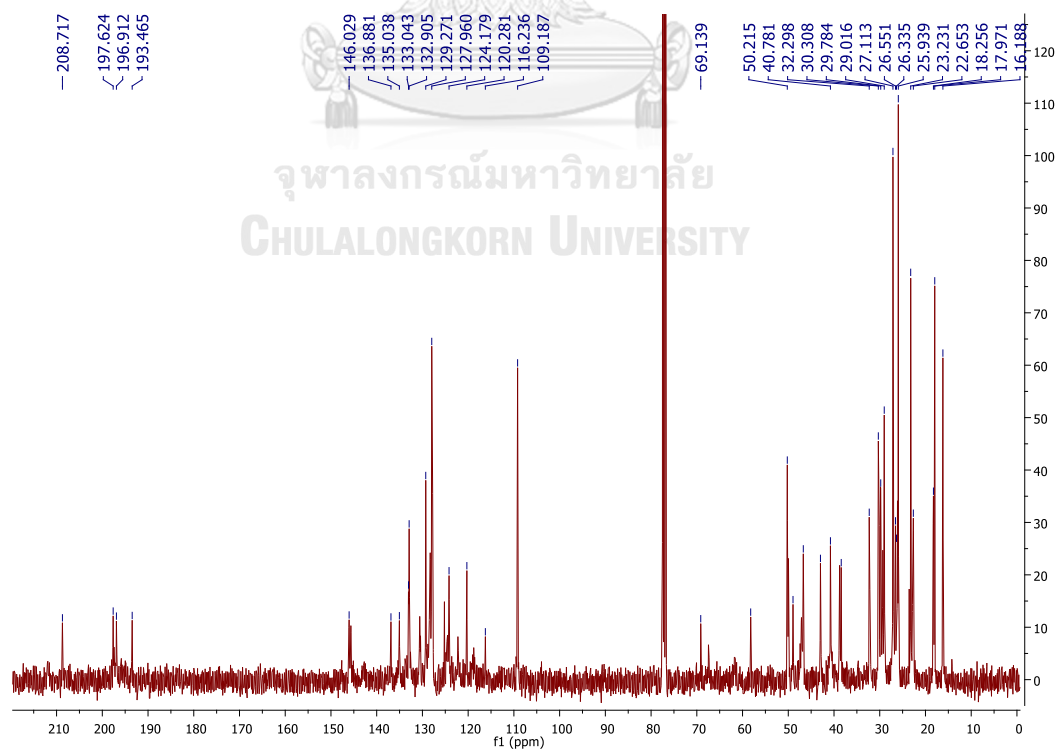


Figure C16.  $^{13}\text{C}$  NMR spectrum of picrorhizone C (GP3) in  $\text{CDCl}_3$



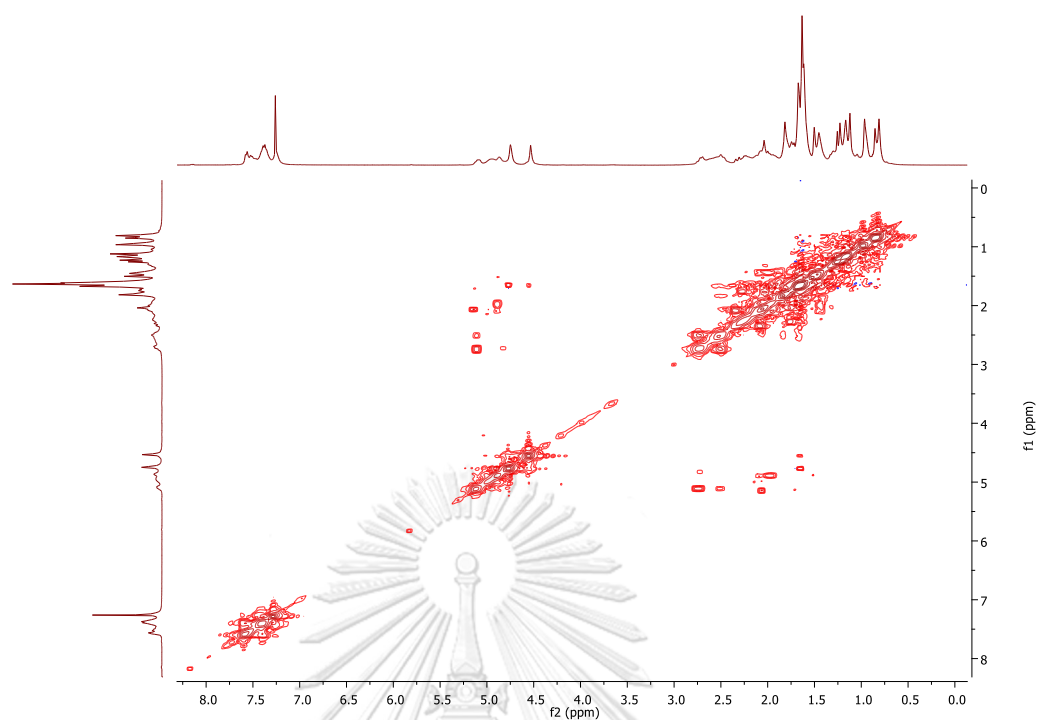


Figure C17. COSY spectrum of picrorhizone C (GP3) in  $\text{CDCl}_3$

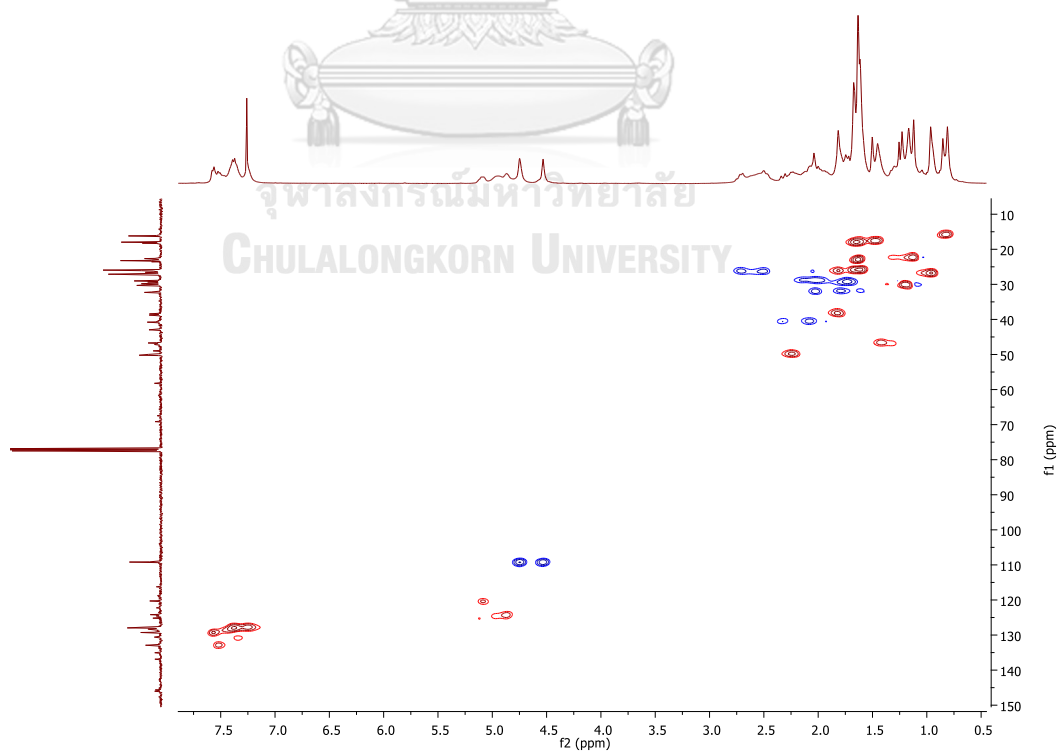


Figure C18. HSQC spectrum of picrorhizone C (GP3) in  $\text{CDCl}_3$

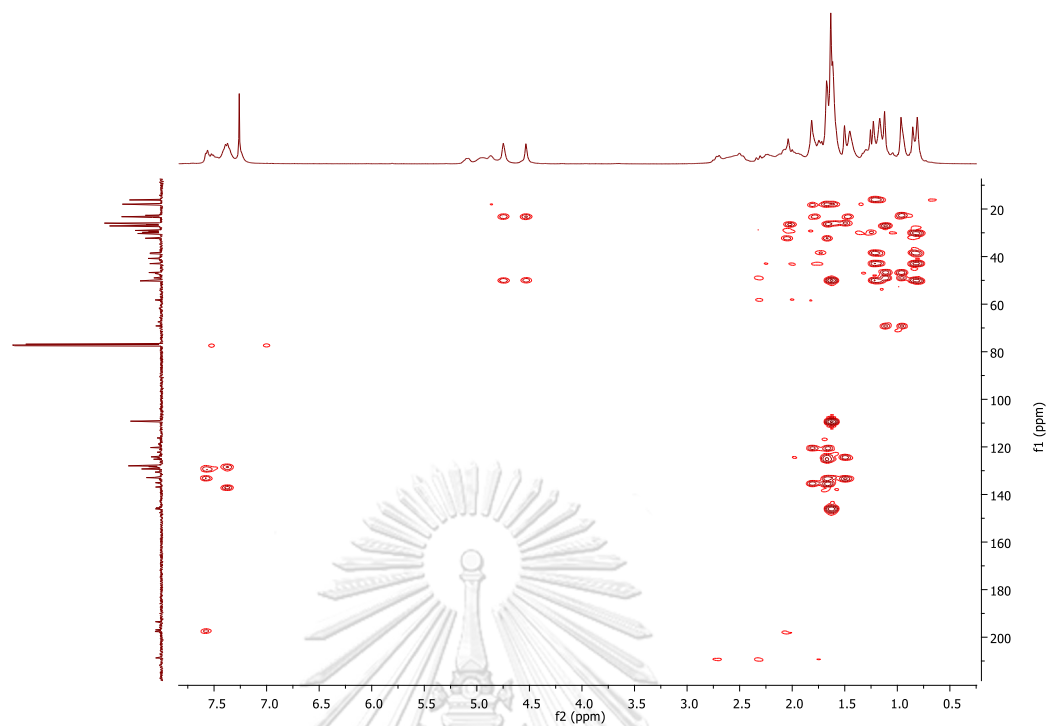


Figure C19. HMBC spectrum of picrorhizone C (**GP3**) in CDCl<sub>3</sub>

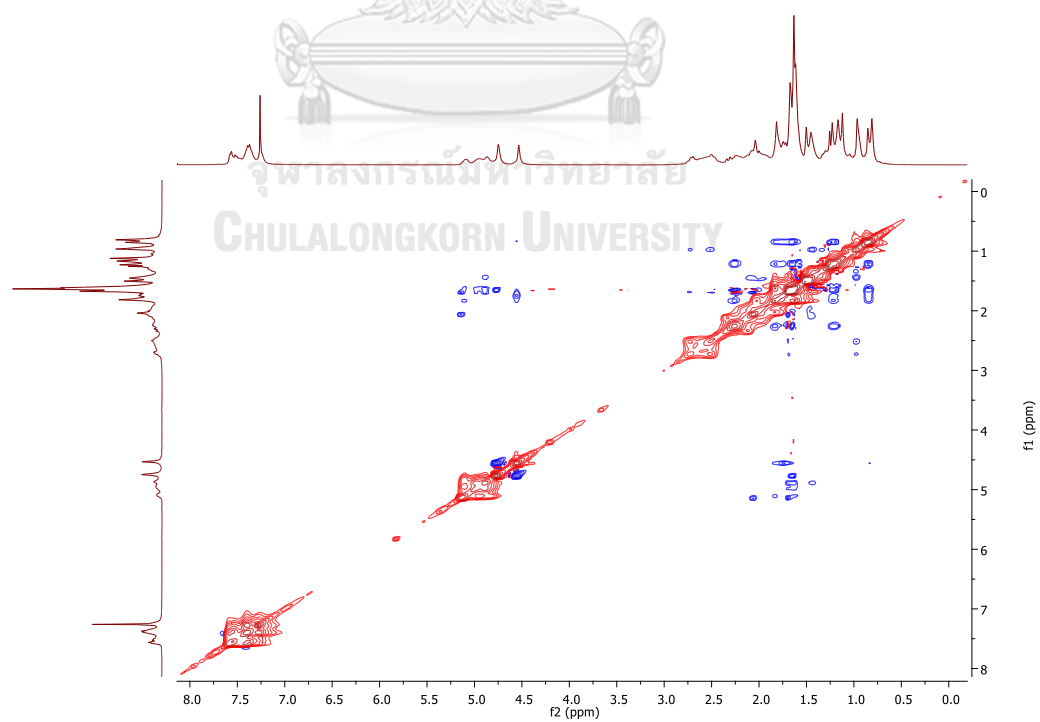


Figure C20. NOESY spectrum of picrorhizone C (**GP3**) in CDCl<sub>3</sub>

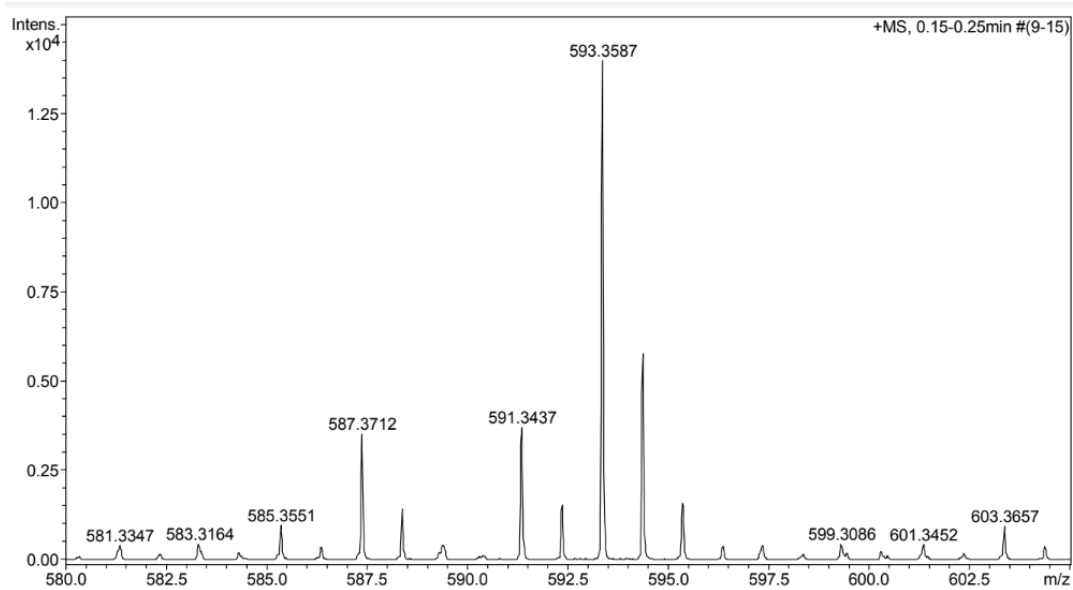


Figure C21. HRESIMS spectrum of picrorhizone C (GP3) in MeCN



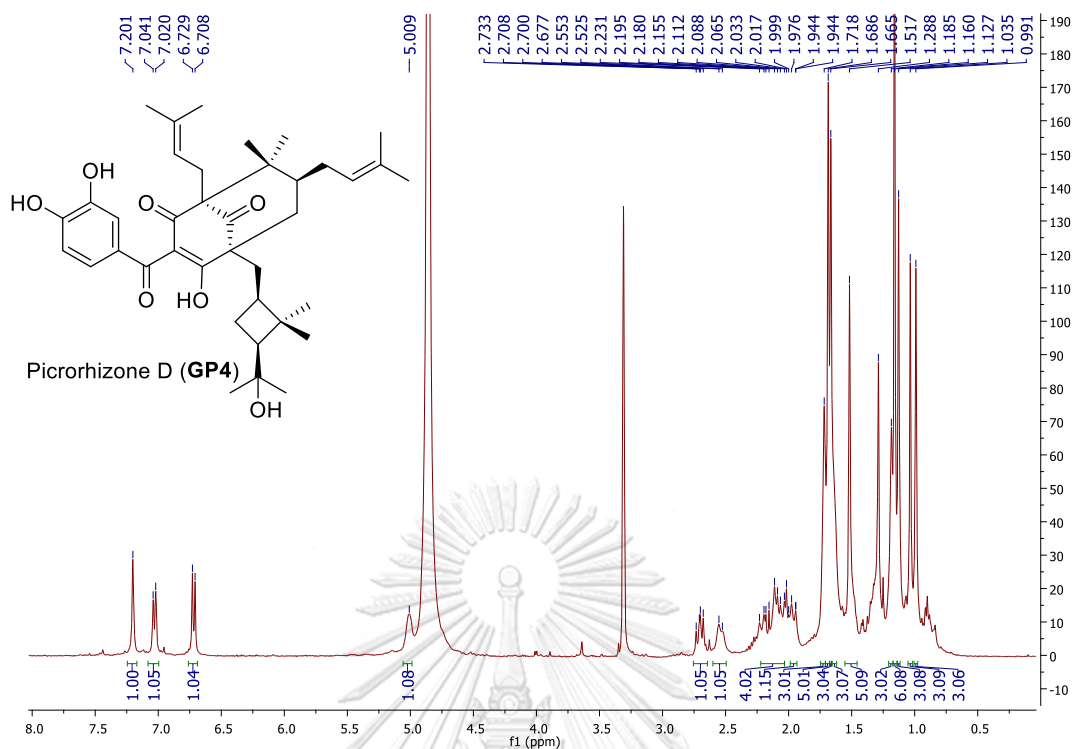


Figure C22.  $^1\text{H}$  NMR spectrum of picrorhizone D (GP4) in methanol- $d_4$

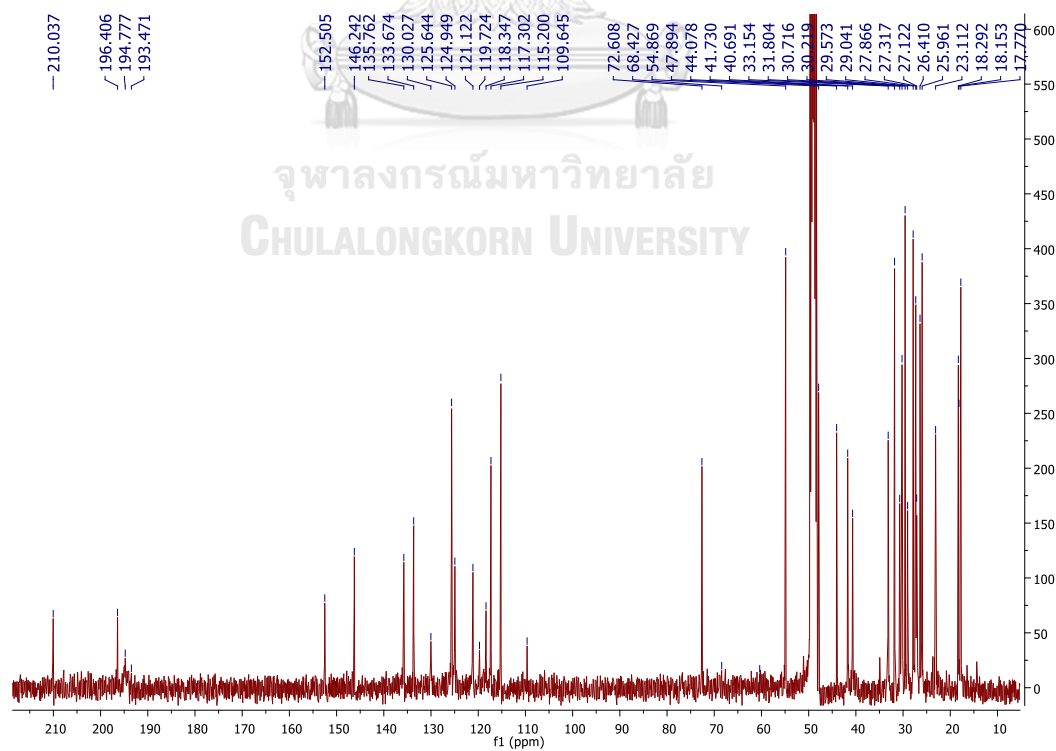


Figure C23.  $^{13}\text{C}$  NMR spectrum of picrorhizone D (GP4) in methanol- $d_4$

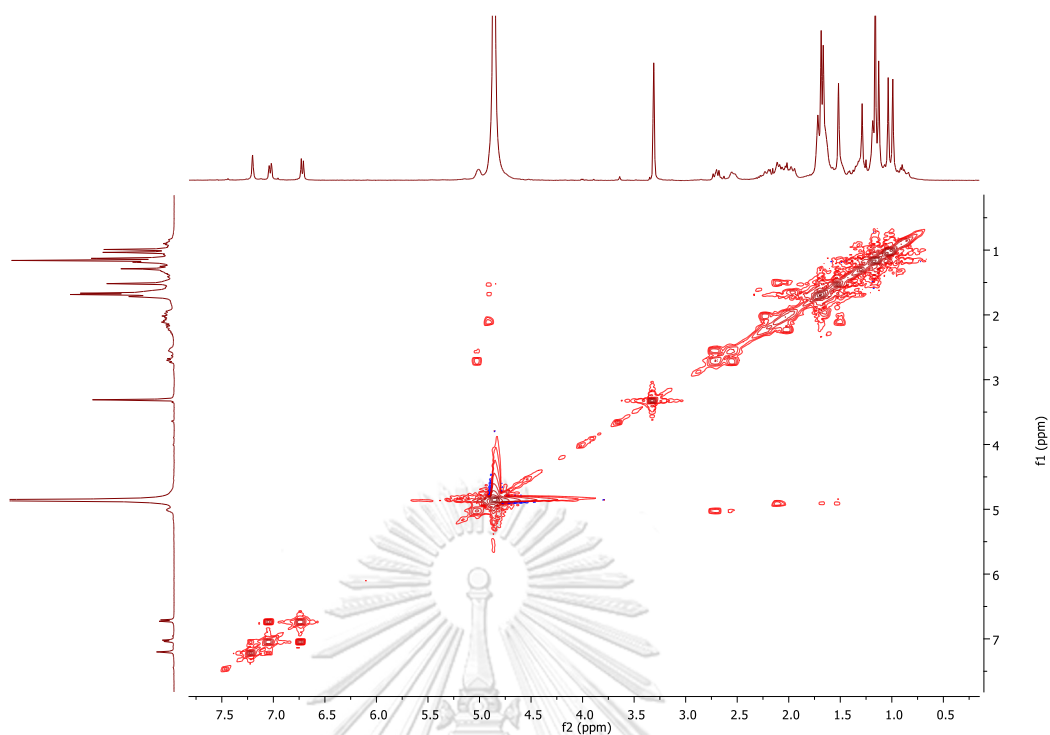


Figure C24. COSY spectrum of picrorhizone D (GP4) in methanol- $d_4$

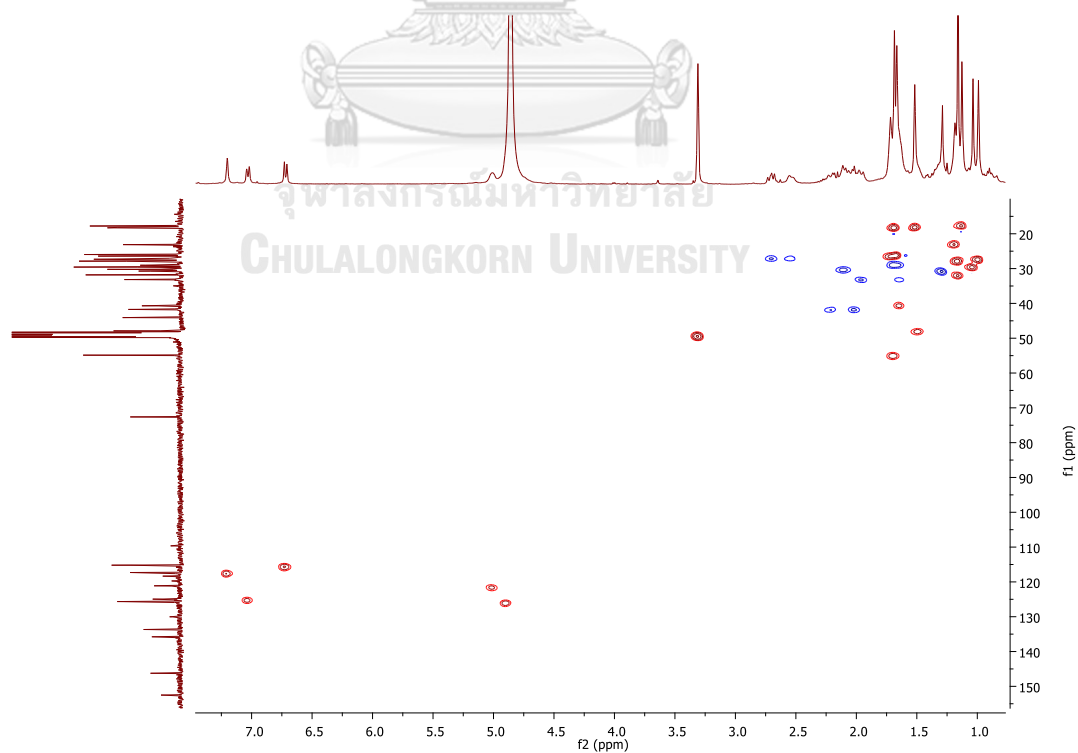


Figure C25. HSQC spectrum of picrorhizone D (GP4) in methanol- $d_4$

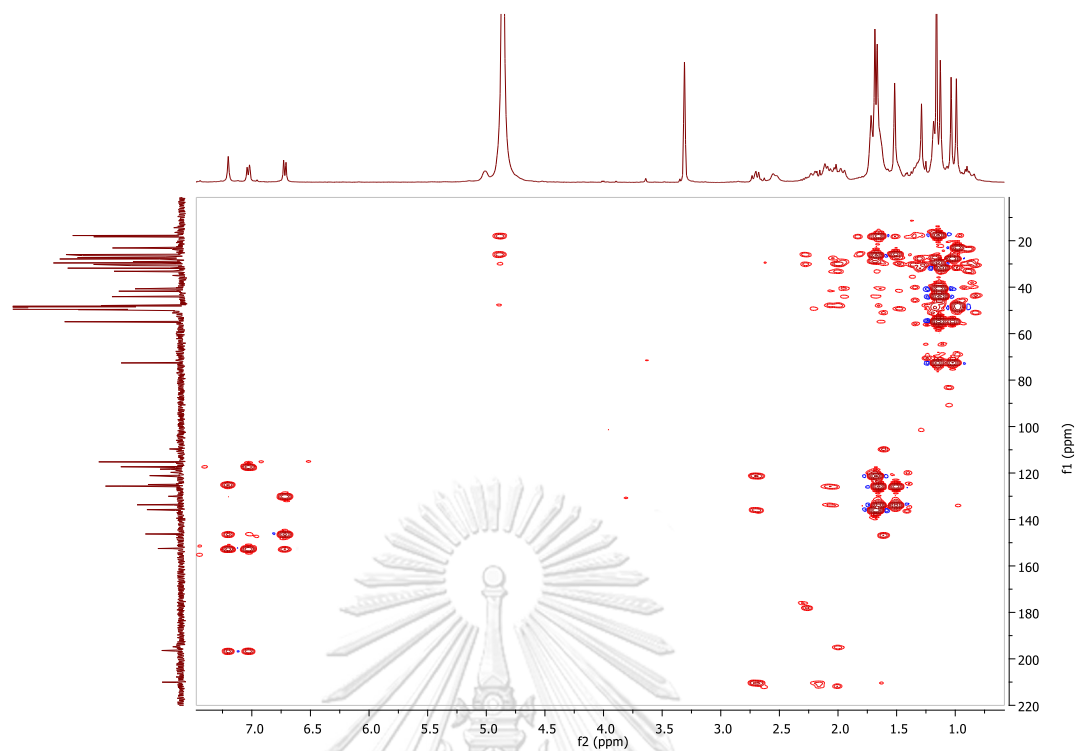


Figure C26. HMBC spectrum of picrorhizone D (GP4) in methanol- $d_4$

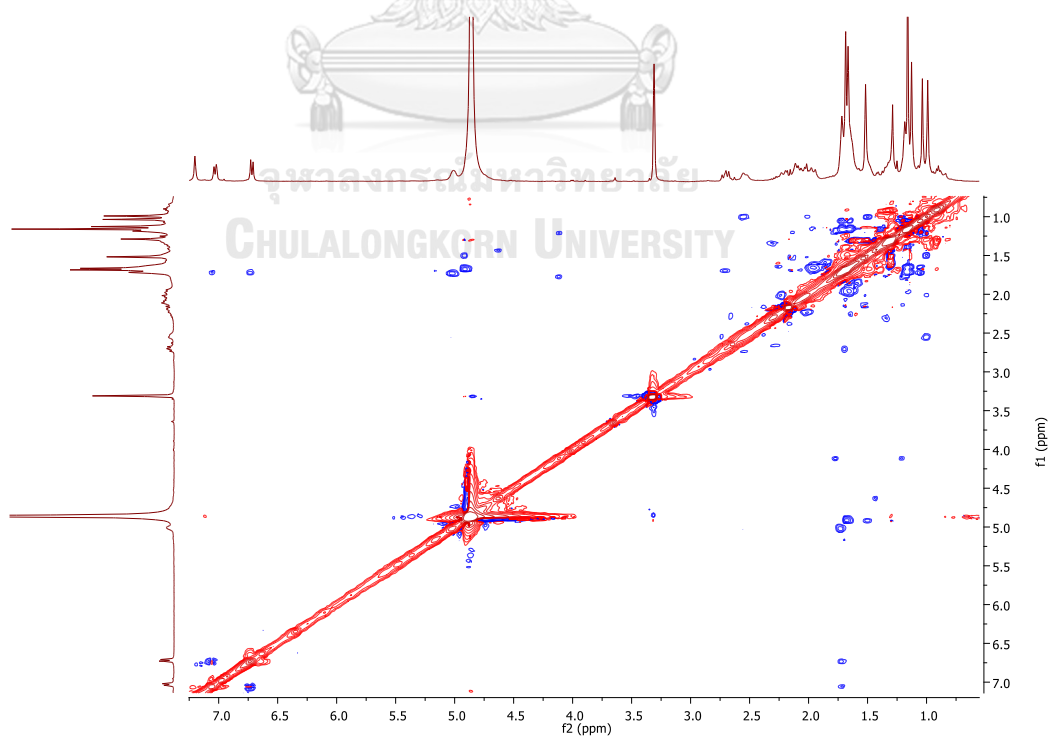


Figure C27. NOESY spectrum of picrorhizone D (GP4) in methanol- $d_4$

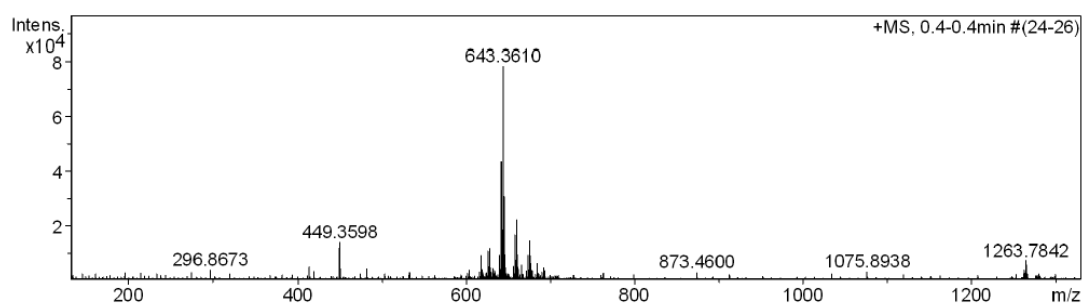


Figure C28. HRESIMS spectrum of picrorhizone D (GP4) in methanol



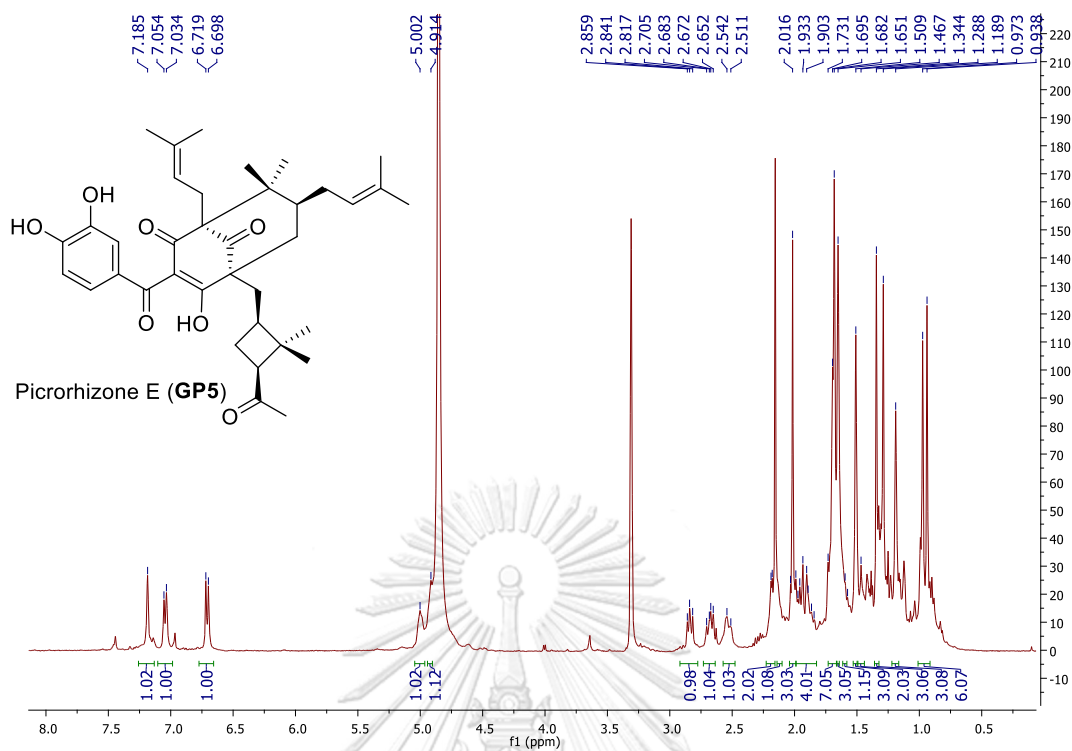


Figure C29.  $^1\text{H}$  NMR spectrum of picrorhizone E (GP5) in methanol- $d_4$

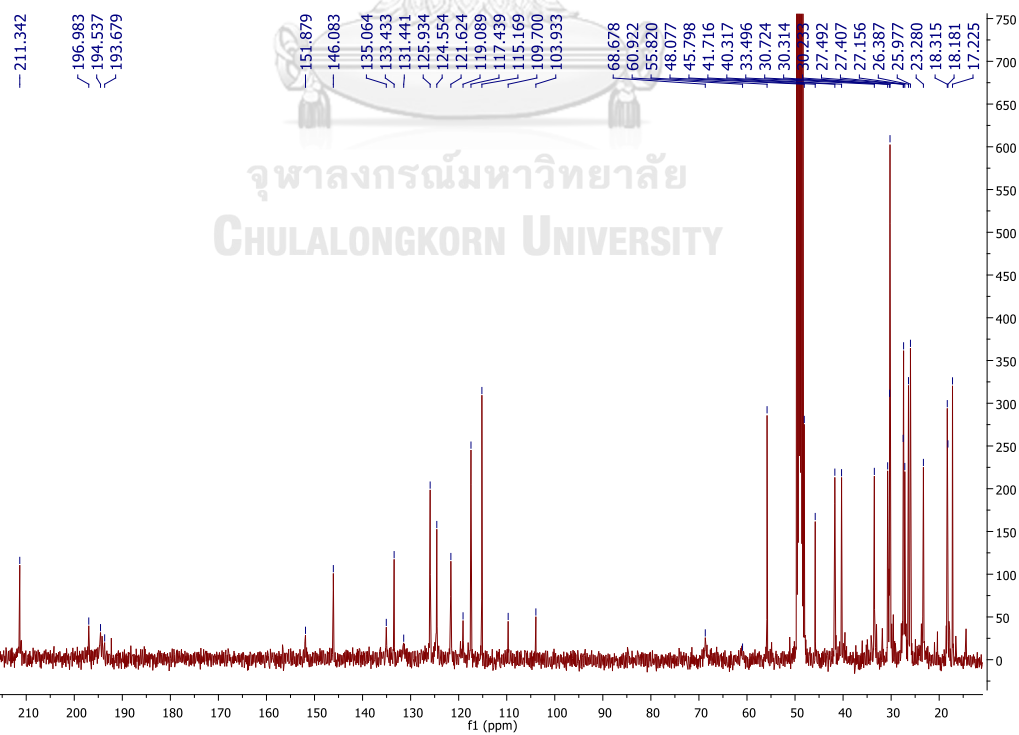


Figure C30.  $^{13}\text{C}$  NMR spectrum of picrorhizone E (GP5) in methanol- $d_4$



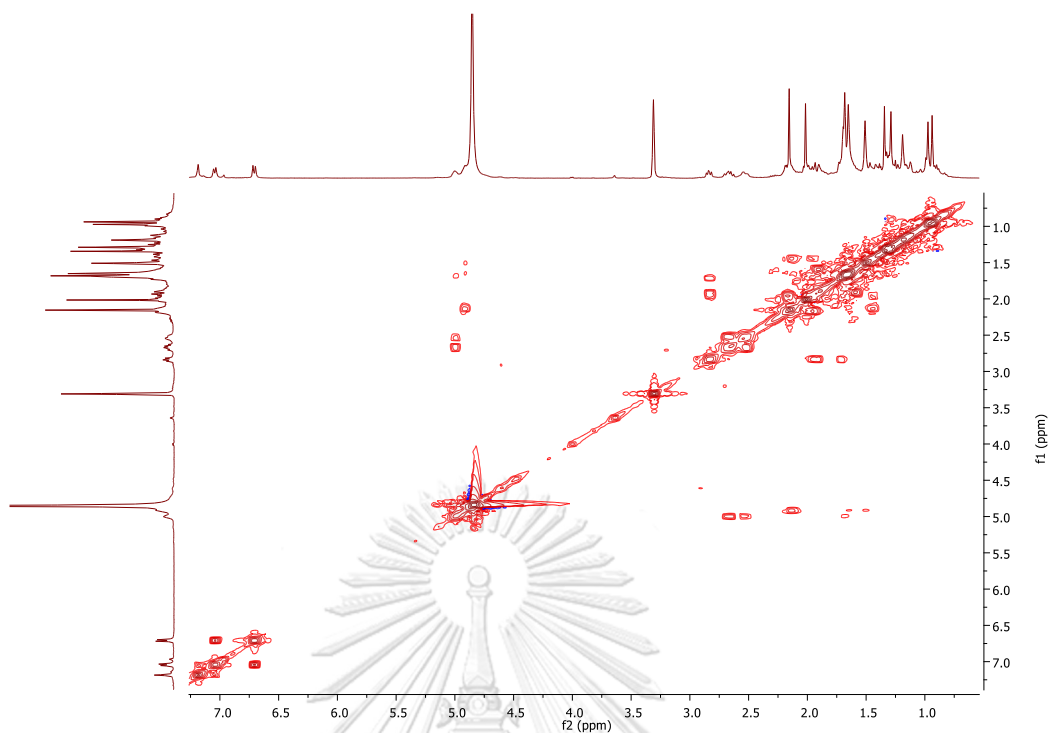


Figure C31. COSY spectrum of picrorhizone E (GP5) in methanol- $d_4$

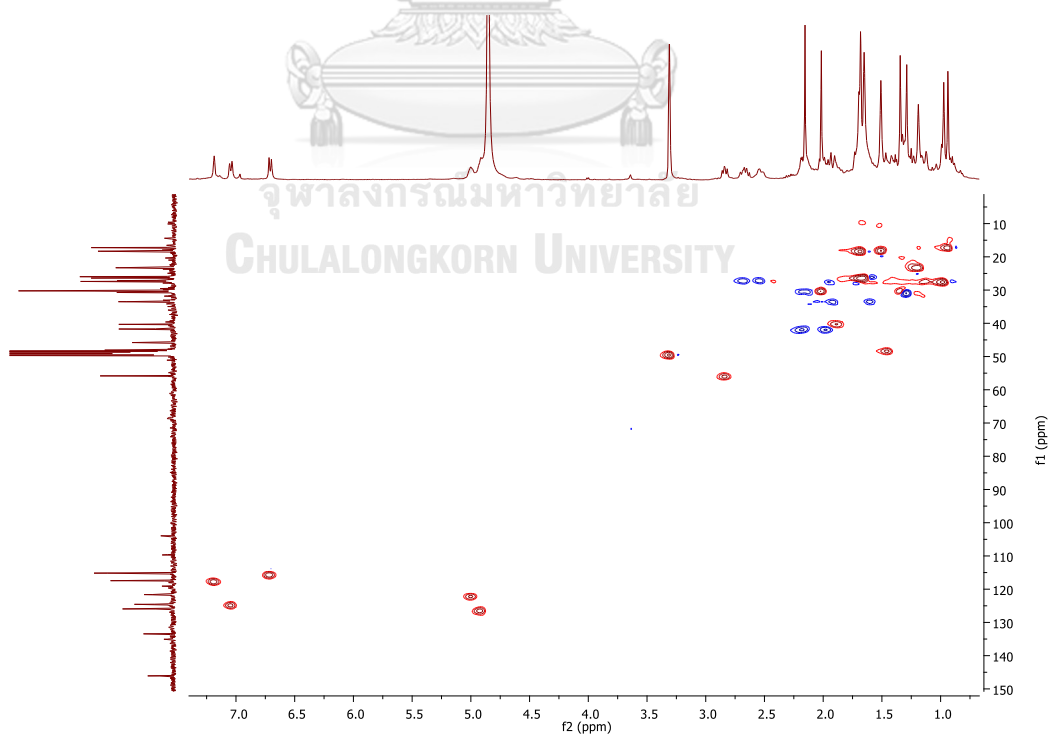
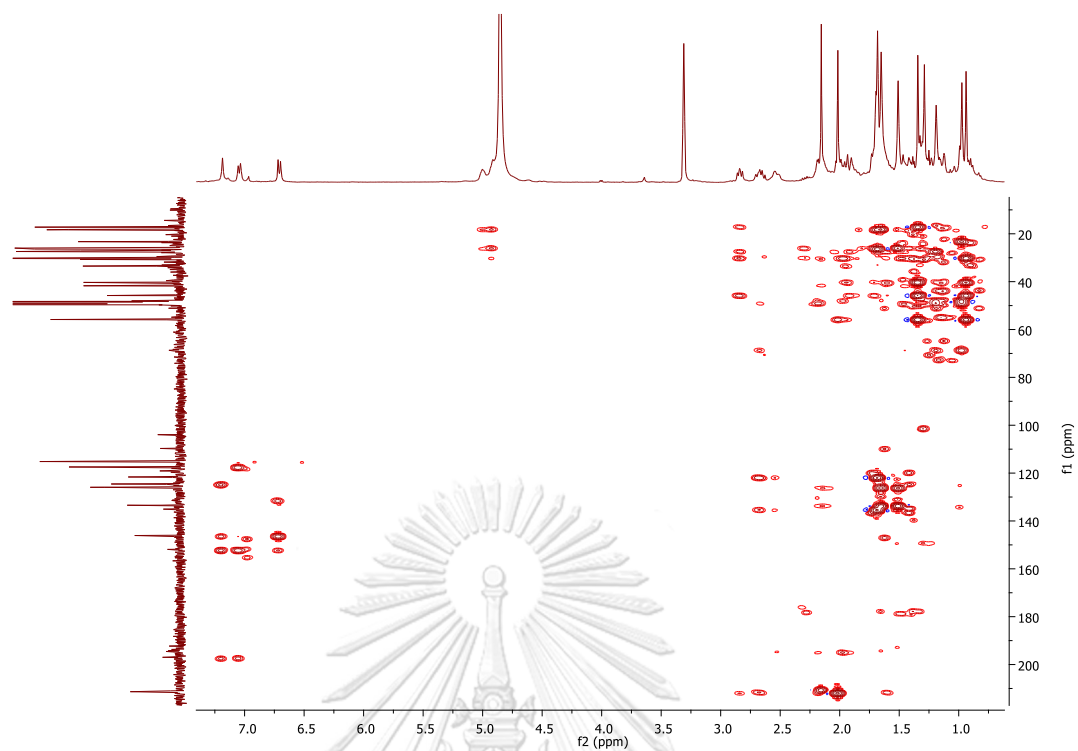
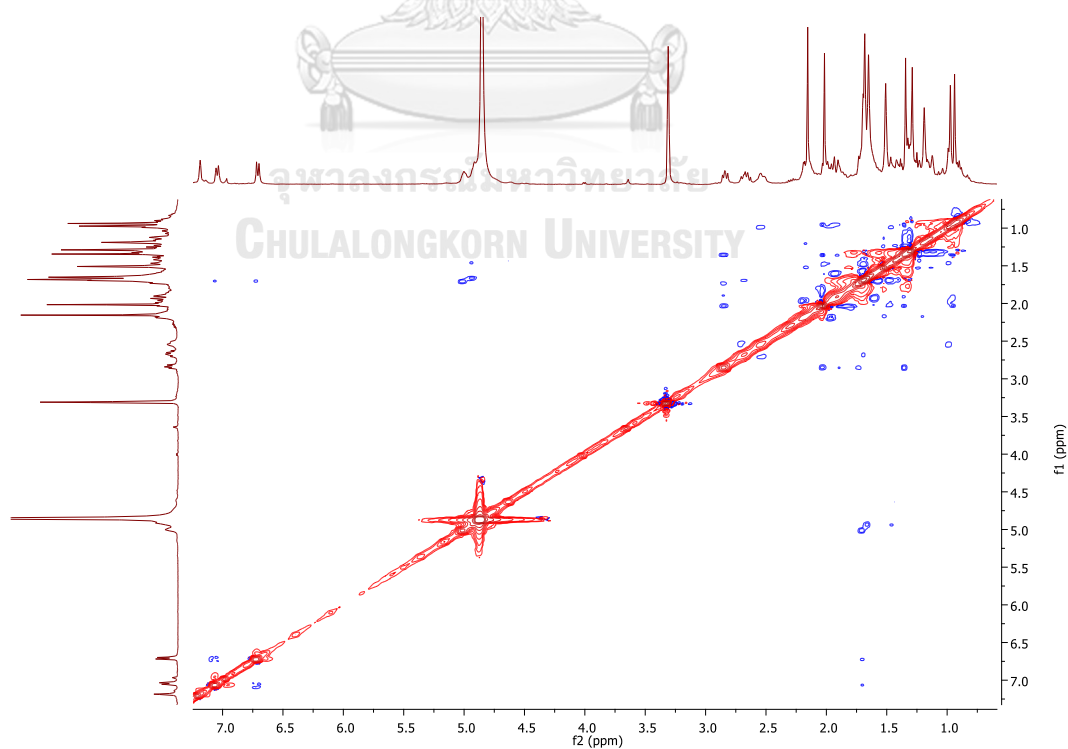


Figure C32. HSQC spectrum of picrorhizone E (GP5) in methanol- $d_4$

Figure C33. HMBC spectrum of picrorhizone E (GP5) in methanol- $d_4$ Figure C34. NOESY spectrum of picrorhizone E (GP5) in methanol- $d_4$

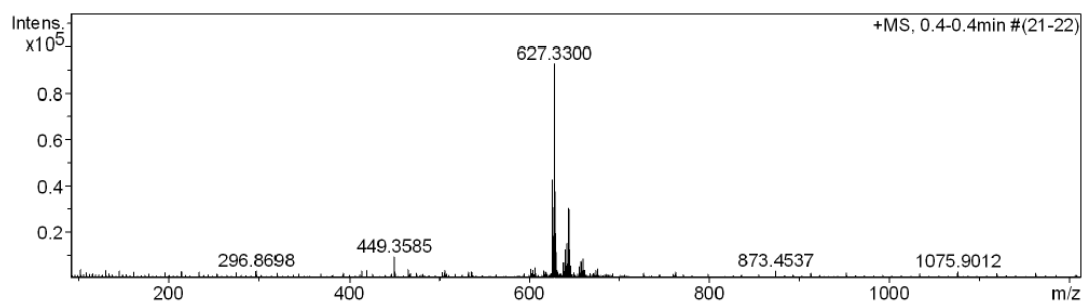


Figure C35. HRESIMS spectrum of picrorhizone E (GP5) in methanol



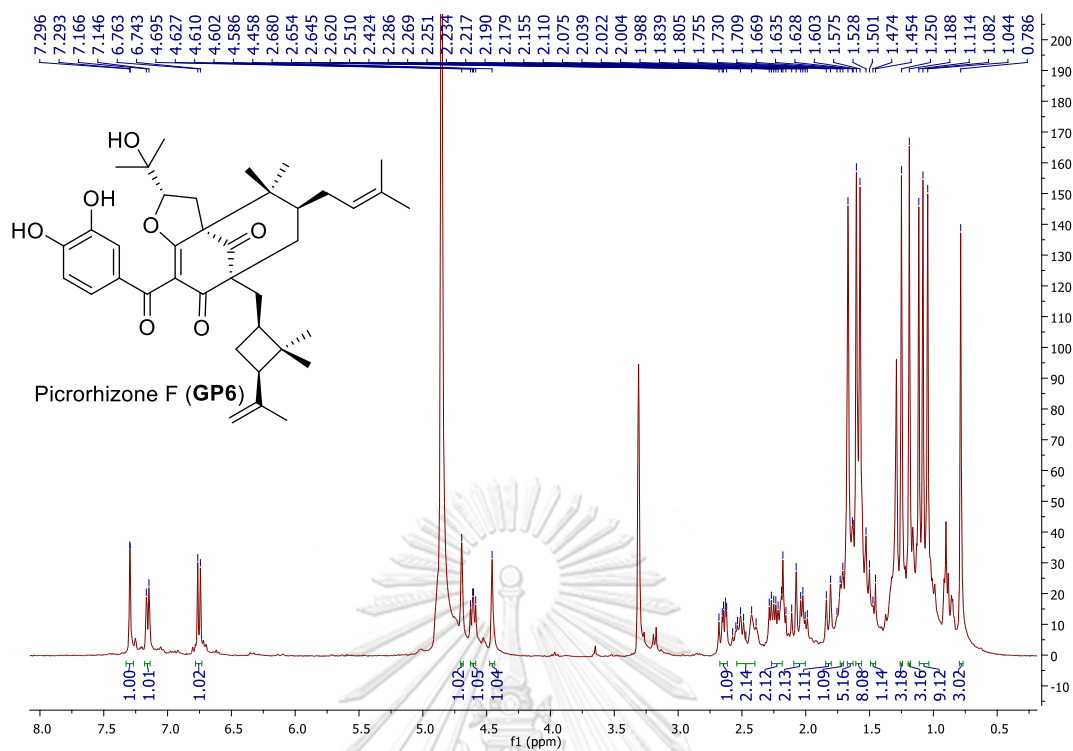


Figure C36.  $^1\text{H}$  NMR spectrum of picrorhizone F (GP6) in methanol- $d_4$

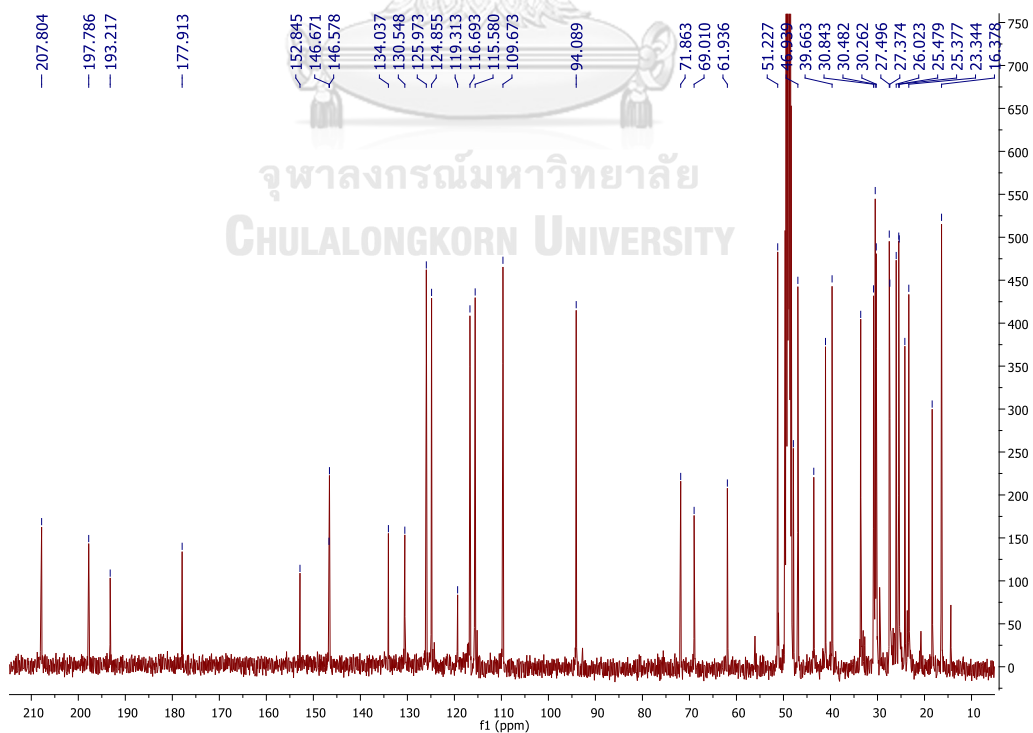
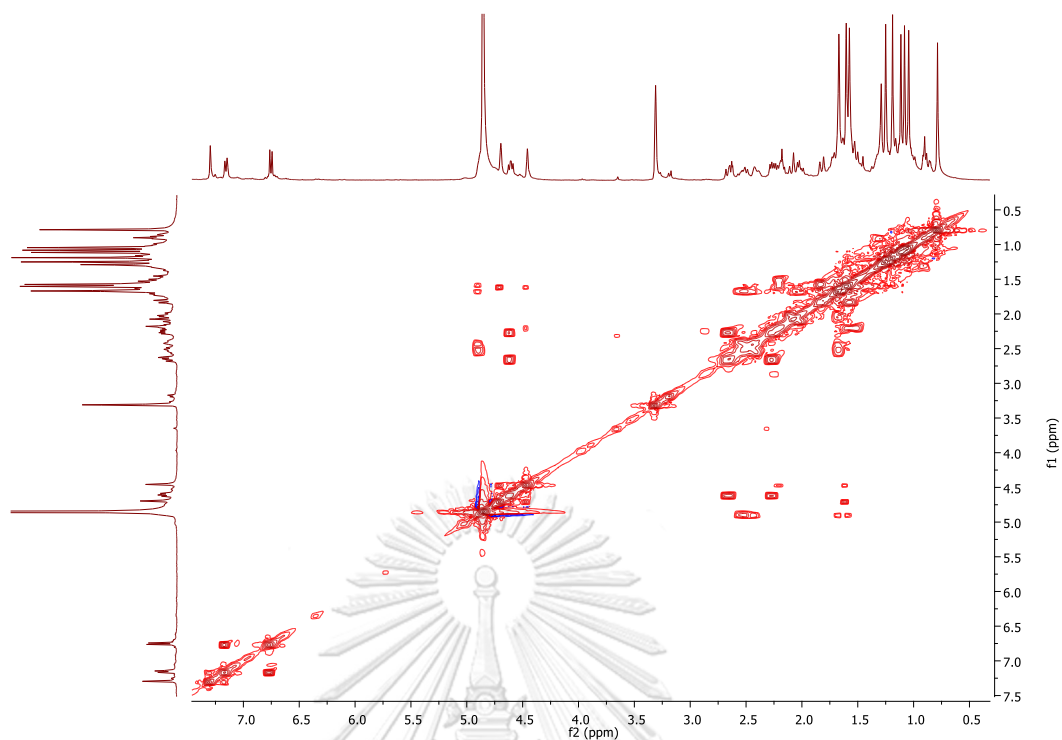
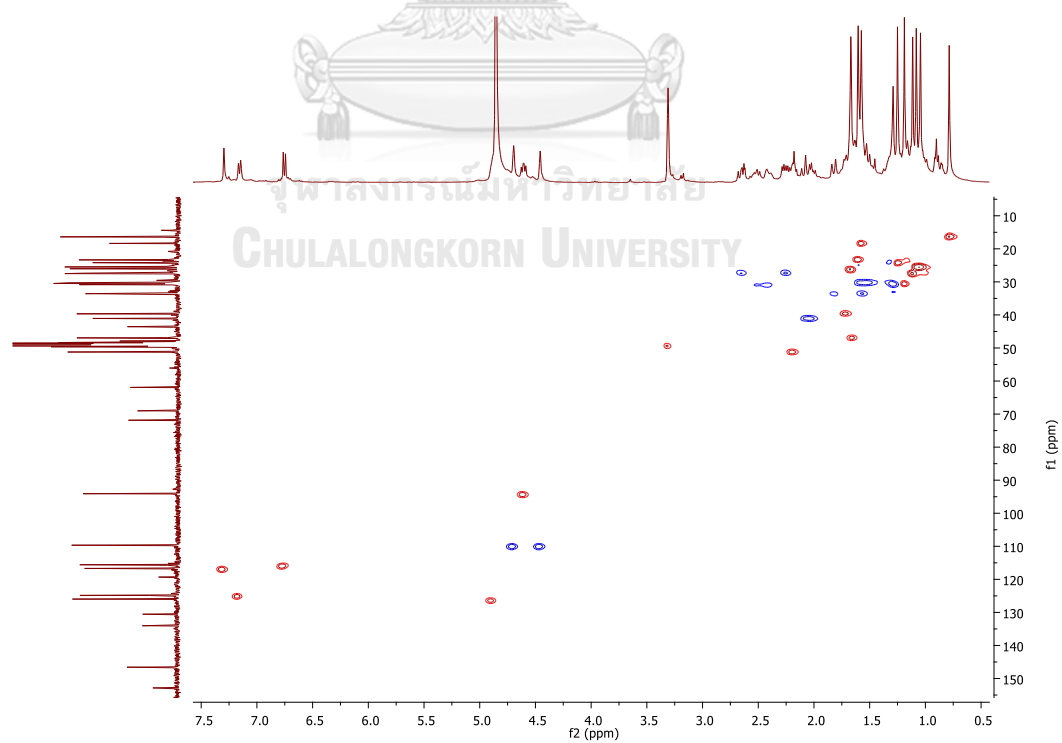


Figure C37.  $^{13}\text{C}$  NMR spectrum of picrorhizone F (GP6) in methanol- $d_4$

Figure C38. COSY spectrum of picrorhizone F (GP6) in methanol- $d_4$ Figure C39. HSQC spectrum of picrorhizone F (GP6) in methanol- $d_4$

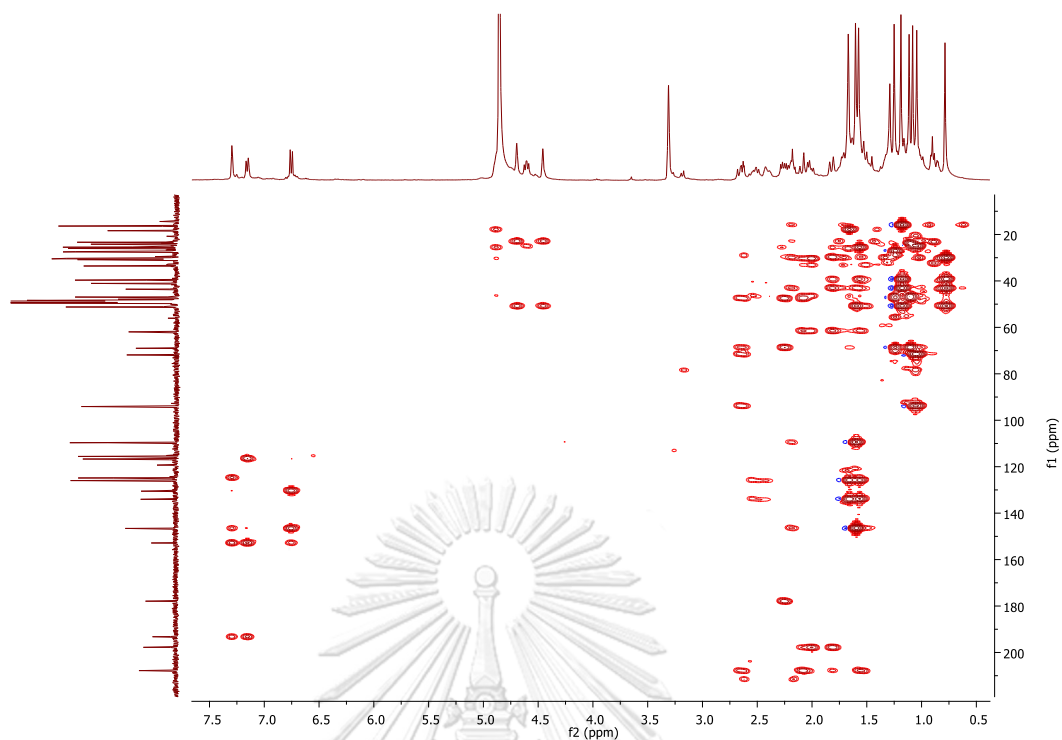


Figure C40. HMBC spectrum of picrorhizone F (GP6) in methanol- $d_4$

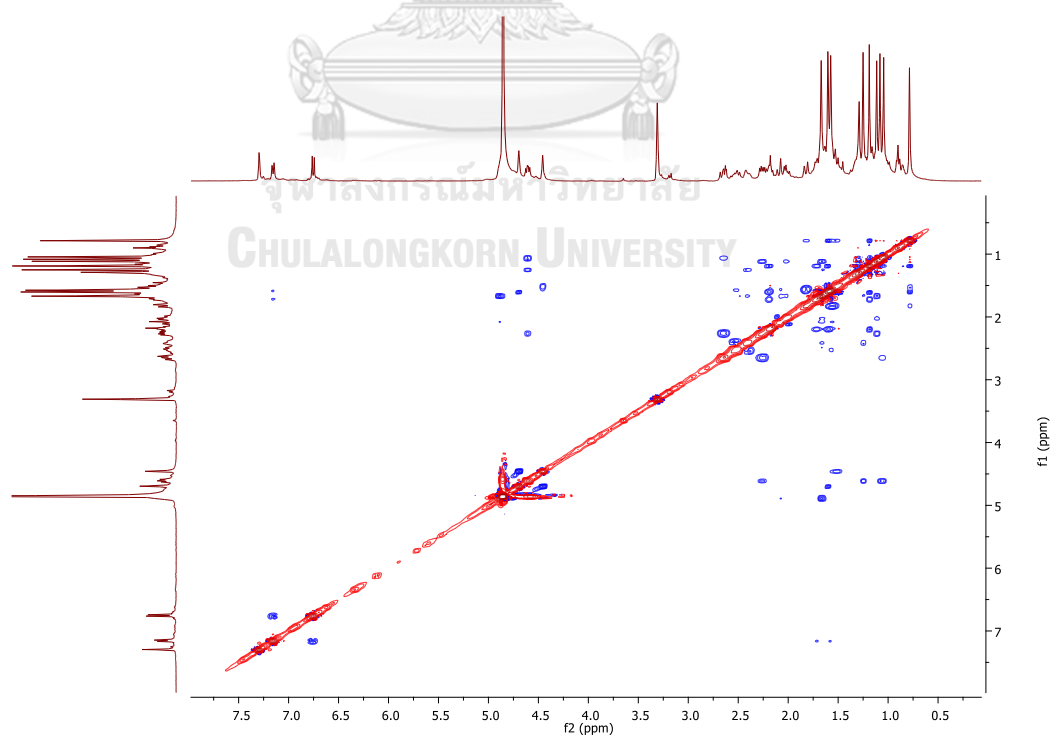


Figure C41. NOESY spectrum of picrorhizone F (GP6) in methanol- $d_4$

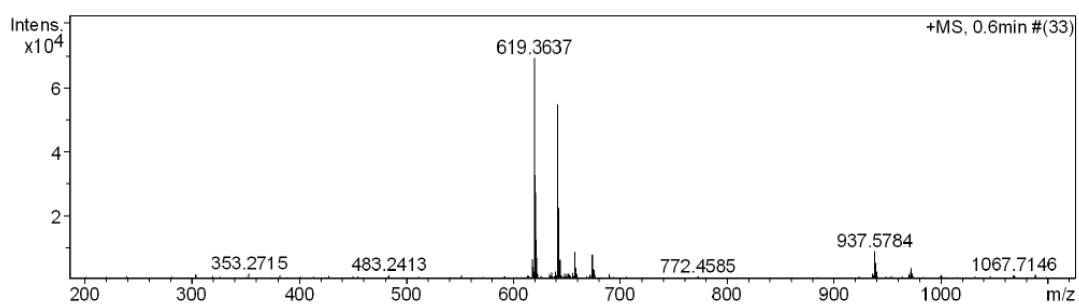


Figure C42. HRESIMS spectrum of picrorhizone F (GP6) in methanol



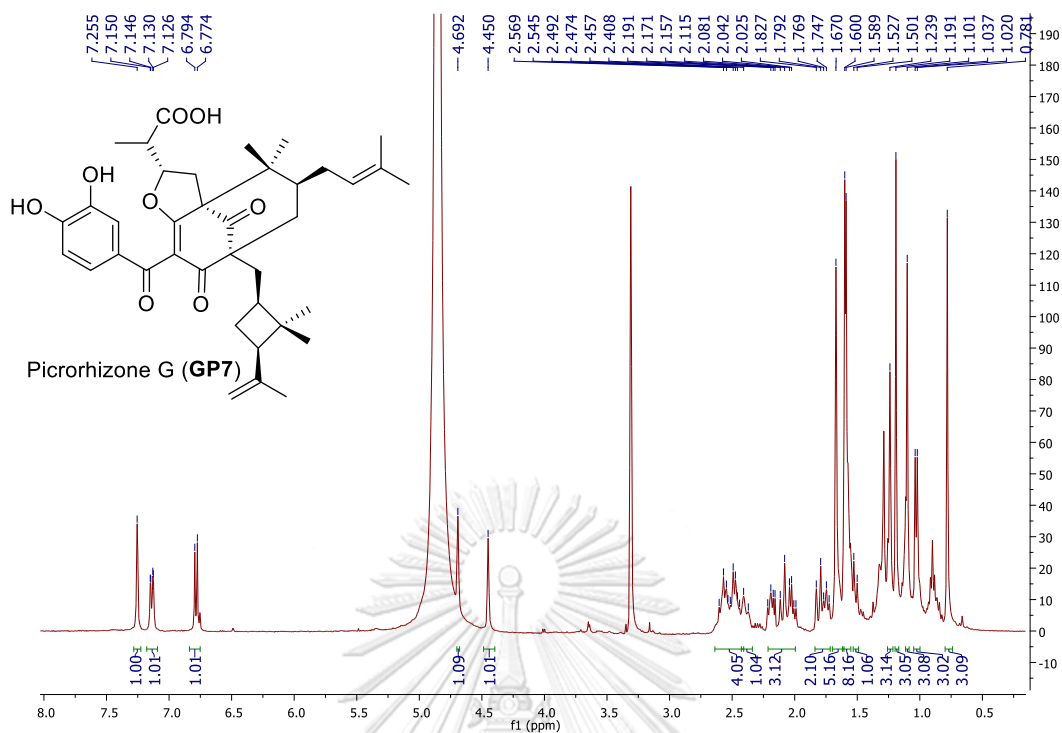


Figure C43.  $^1\text{H}$  NMR spectrum of picrorhizone G (GP7) in methanol- $d_4$

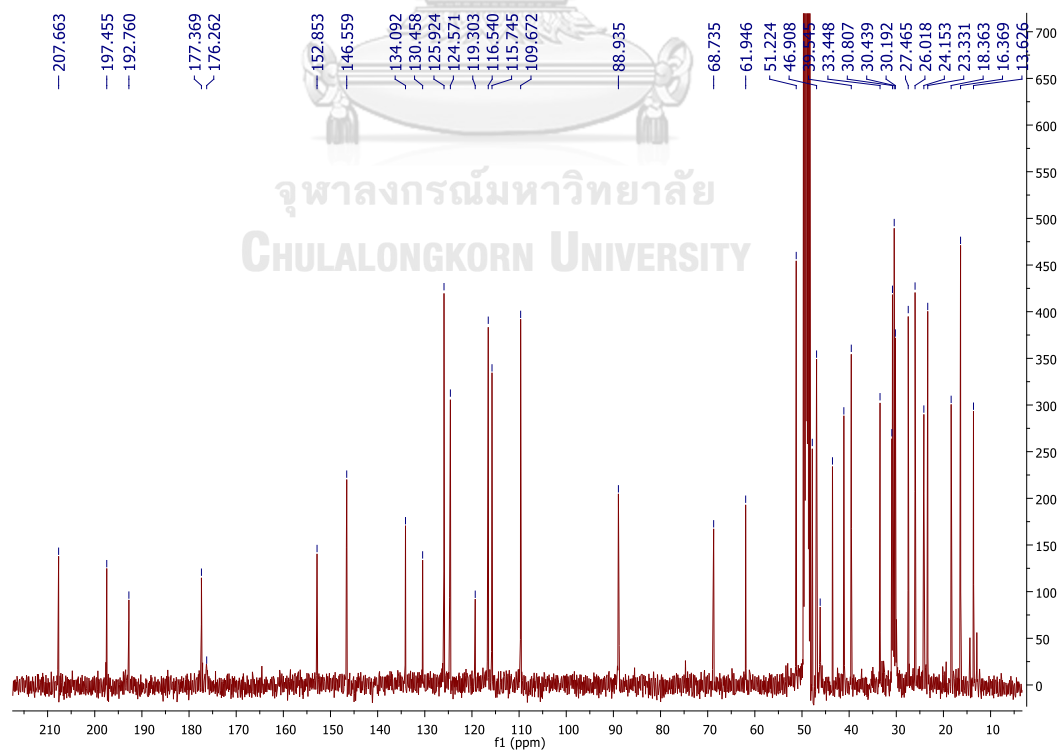
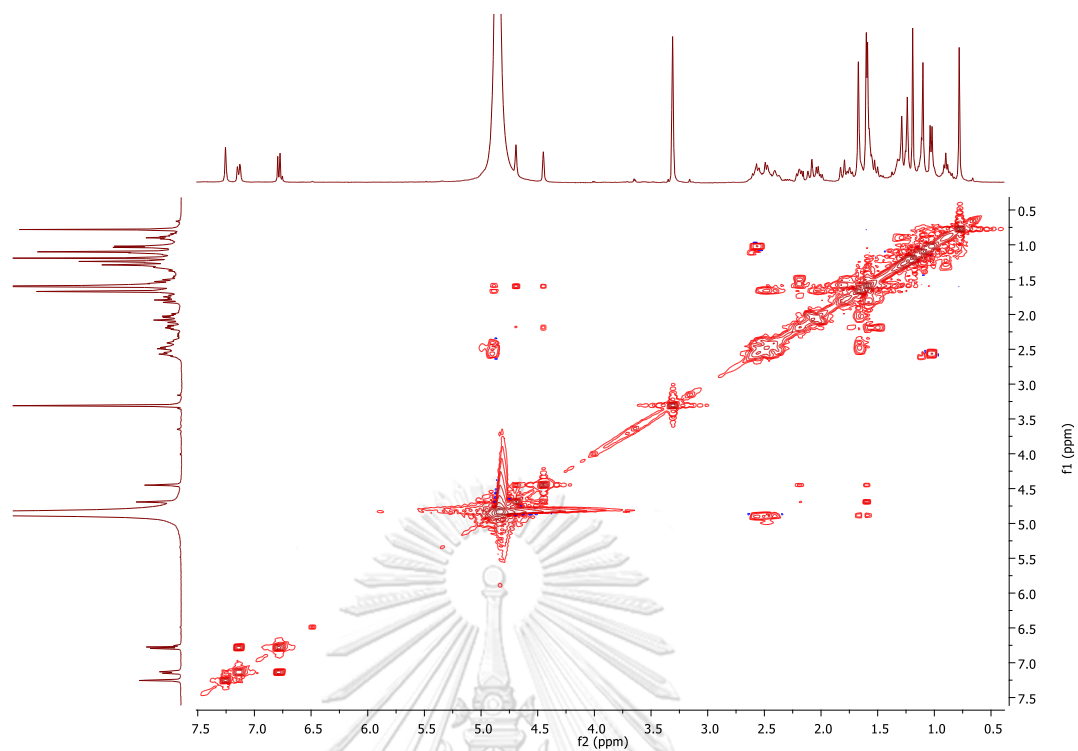
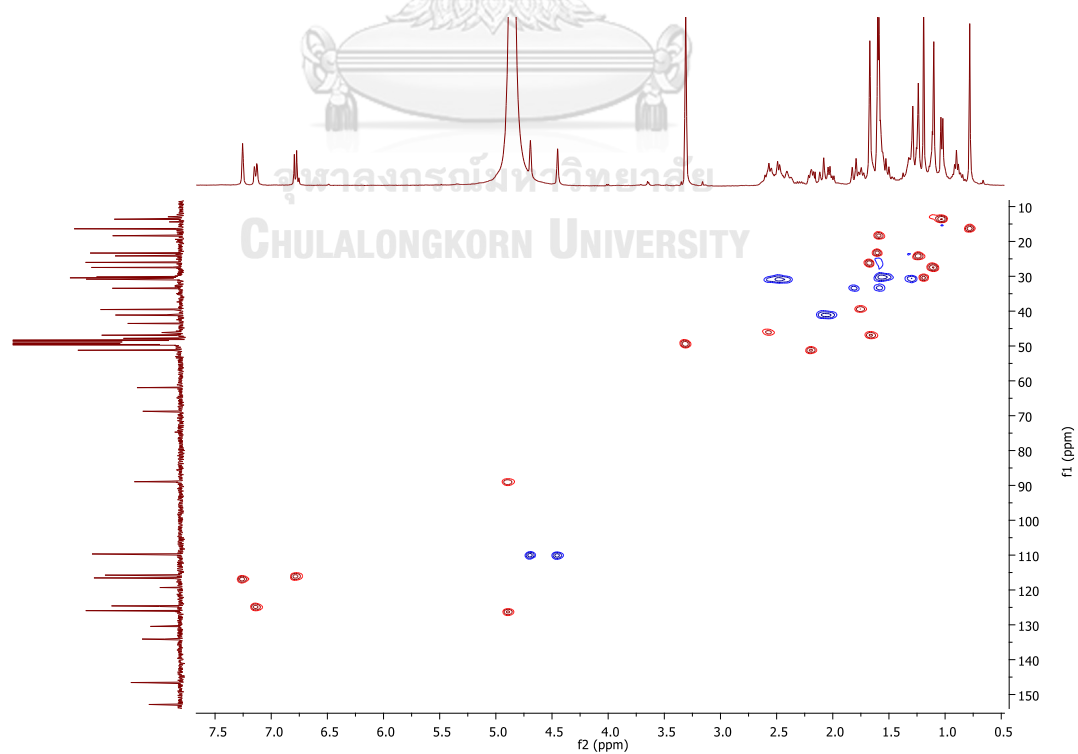
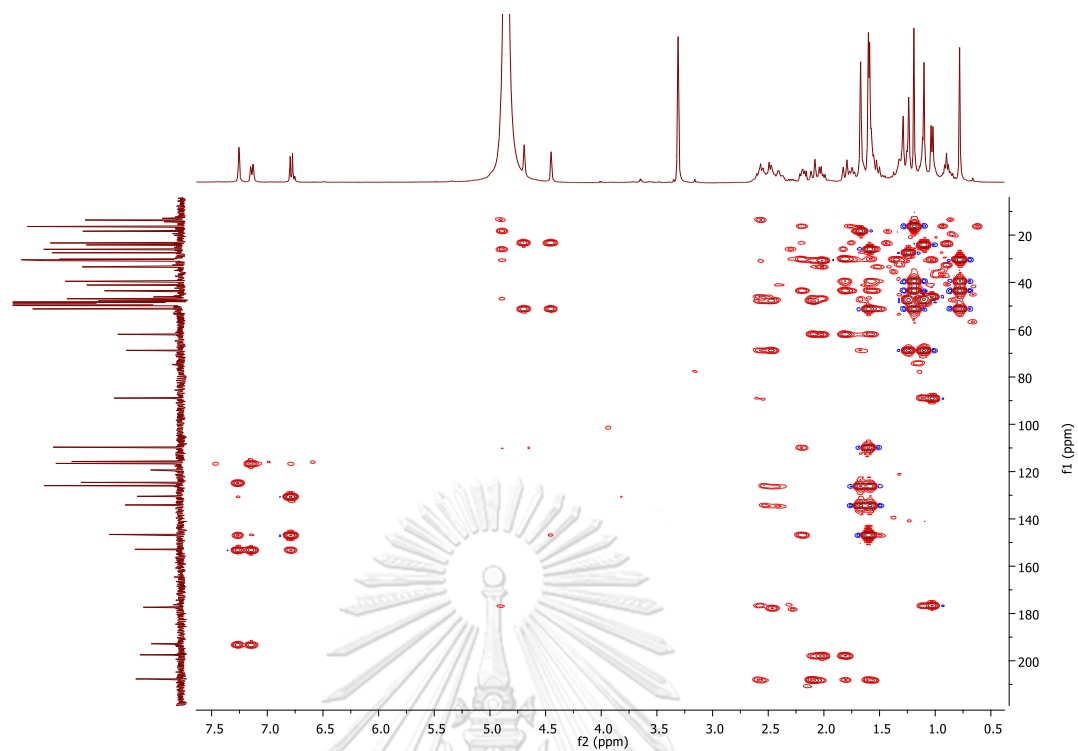
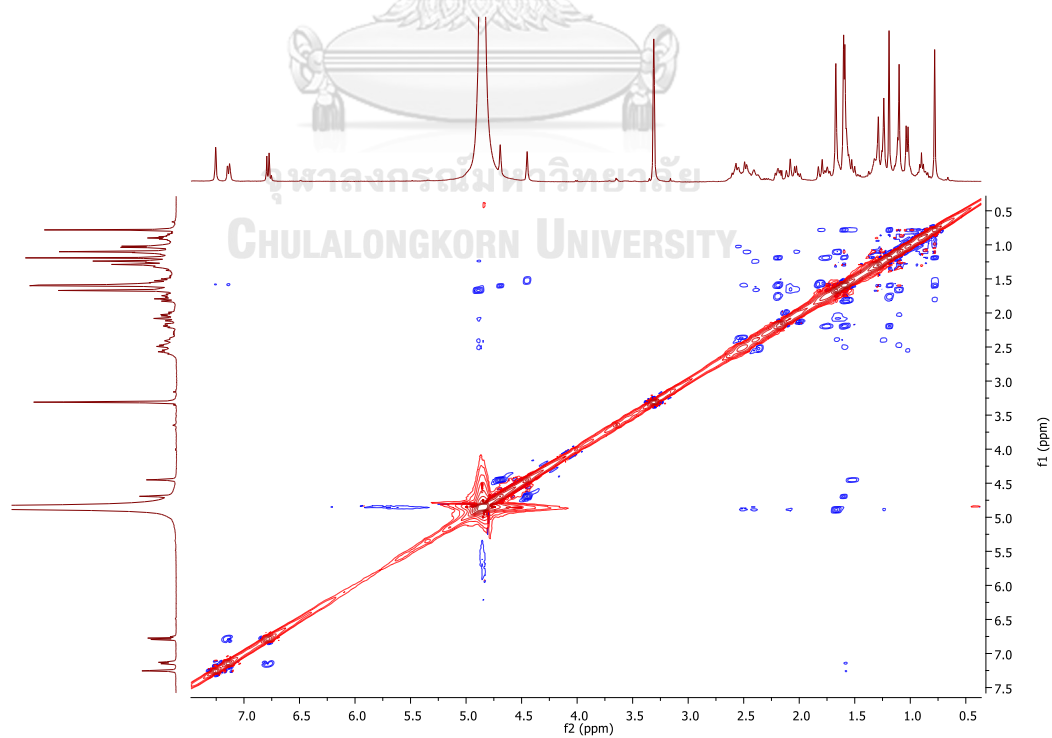


Figure C44.  $^{13}\text{C}$  NMR spectrum of picrorhizone G (GP7) in methanol- $d_4$



Figure C45. COSY spectrum of picrorhizone G (GP7) in methanol-*d*<sub>4</sub>Figure C46. HSQC spectrum of picrorhizone G (GP7) in methanol-*d*<sub>4</sub>

Figure C47. HMBC spectrum of picrorhizone G (GP7) in methanol- $d_4$ Figure C48. NOESY spectrum of picrorhizone G (GP7) in methanol- $d_4$

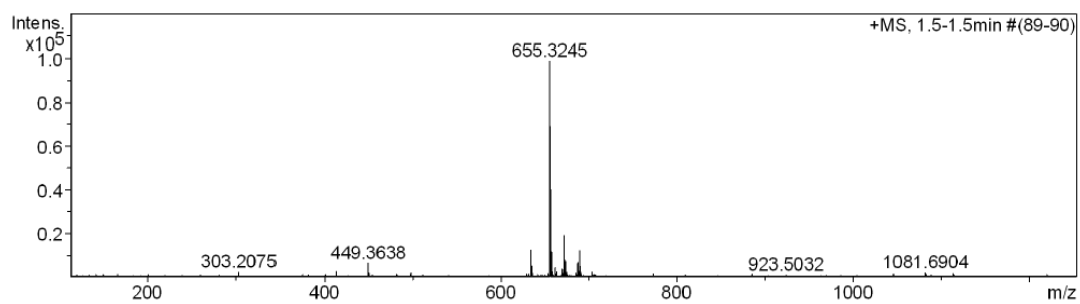


Figure C49. HRESIMS spectrum of picrorhizone G (GP7) in methanol



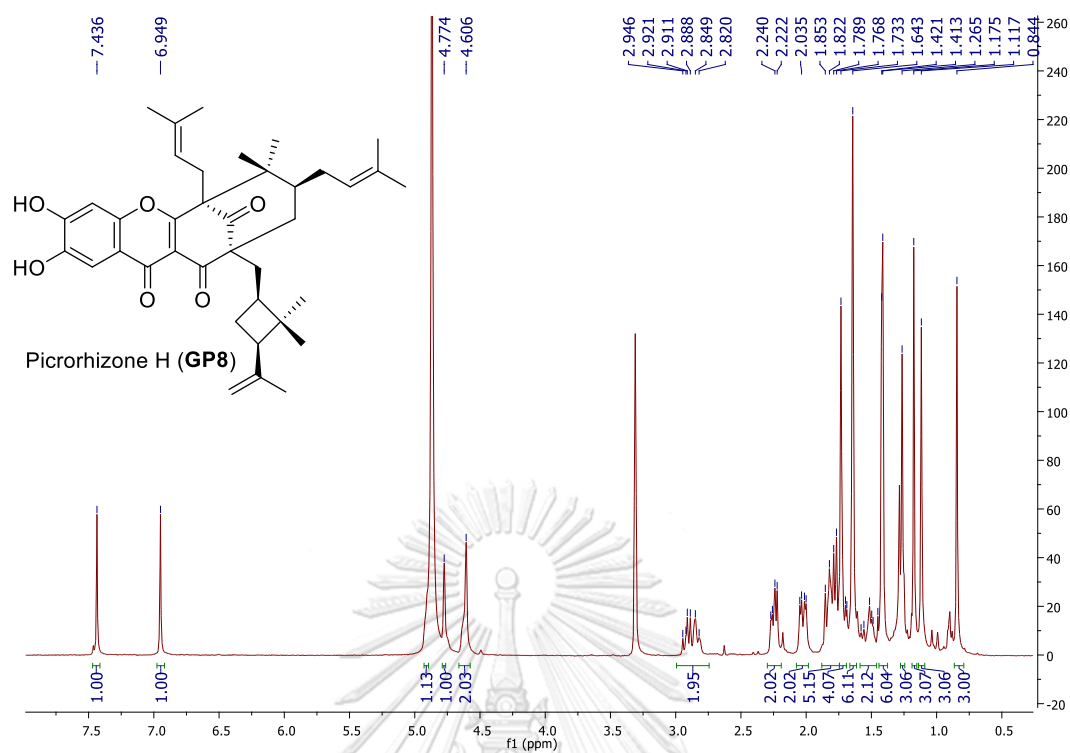


Figure C50.  $^1\text{H}$  NMR spectrum of picrorhizone H (GP8) in methanol- $d_4$

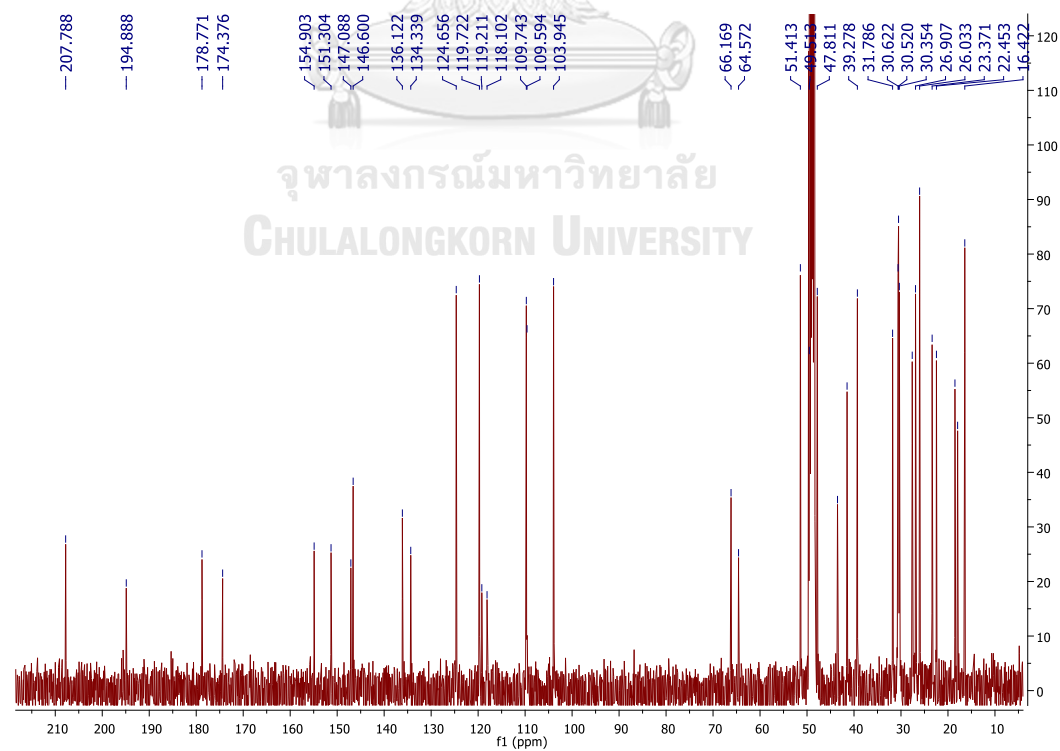
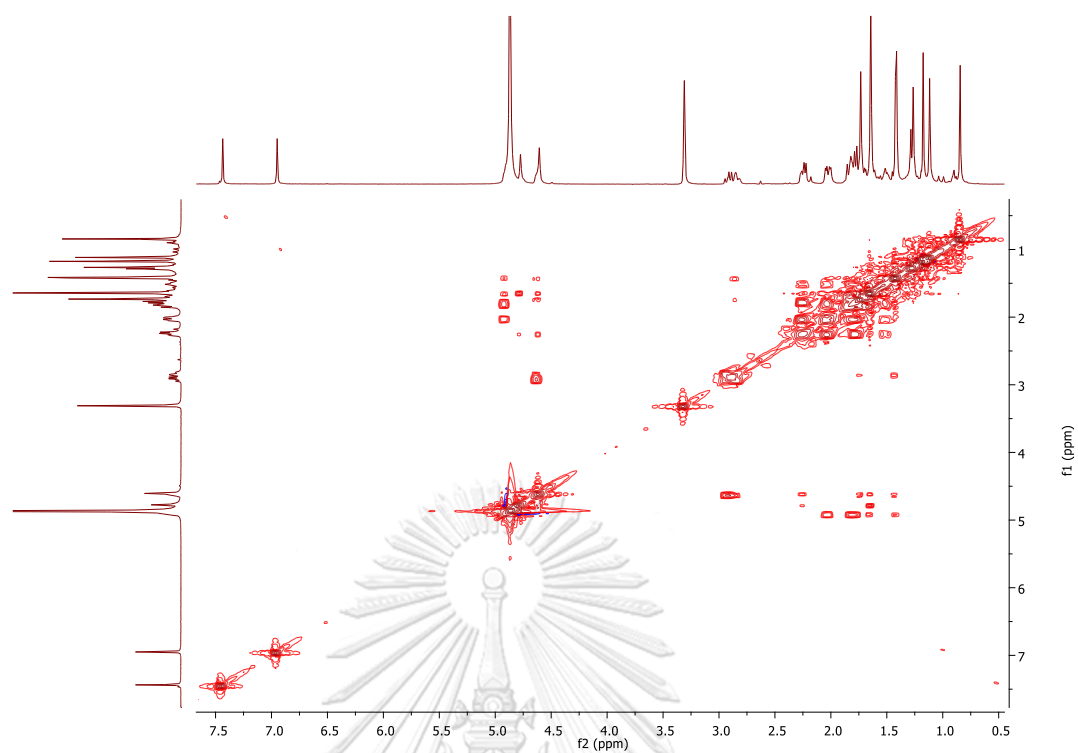
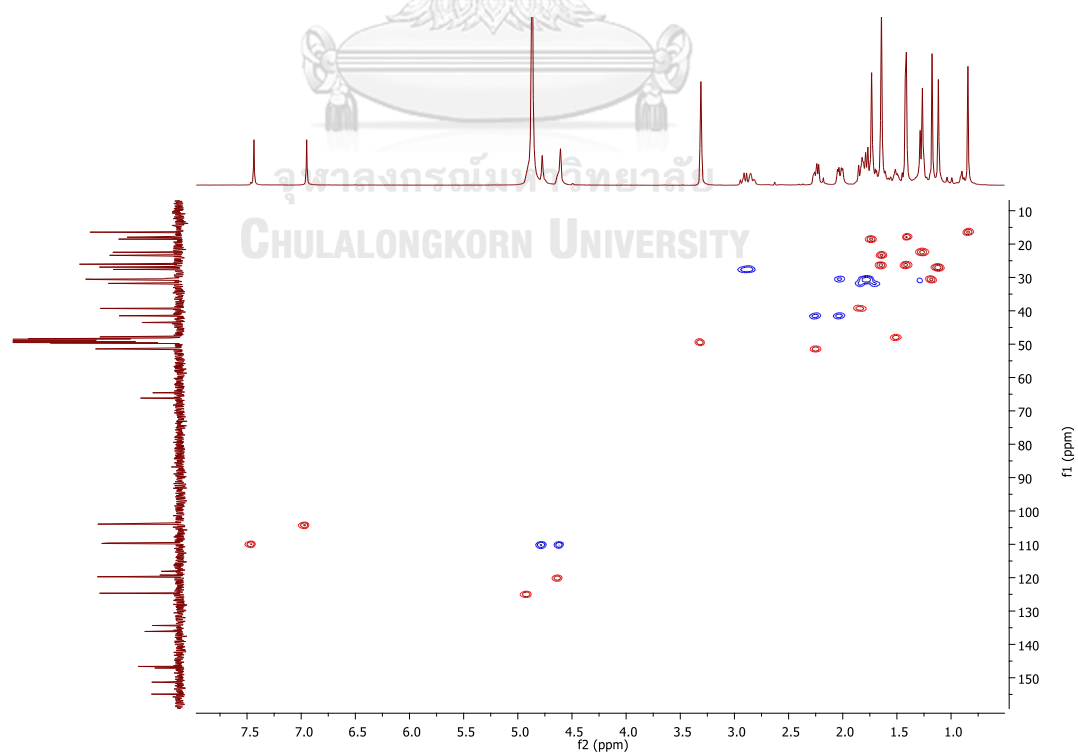
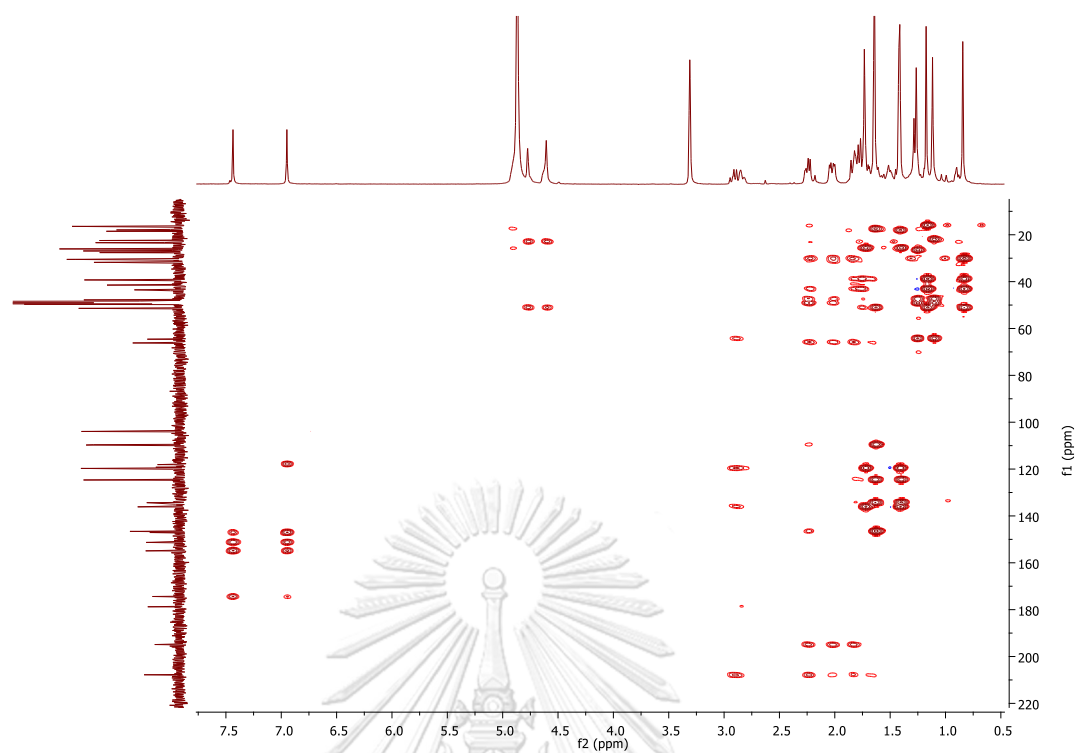
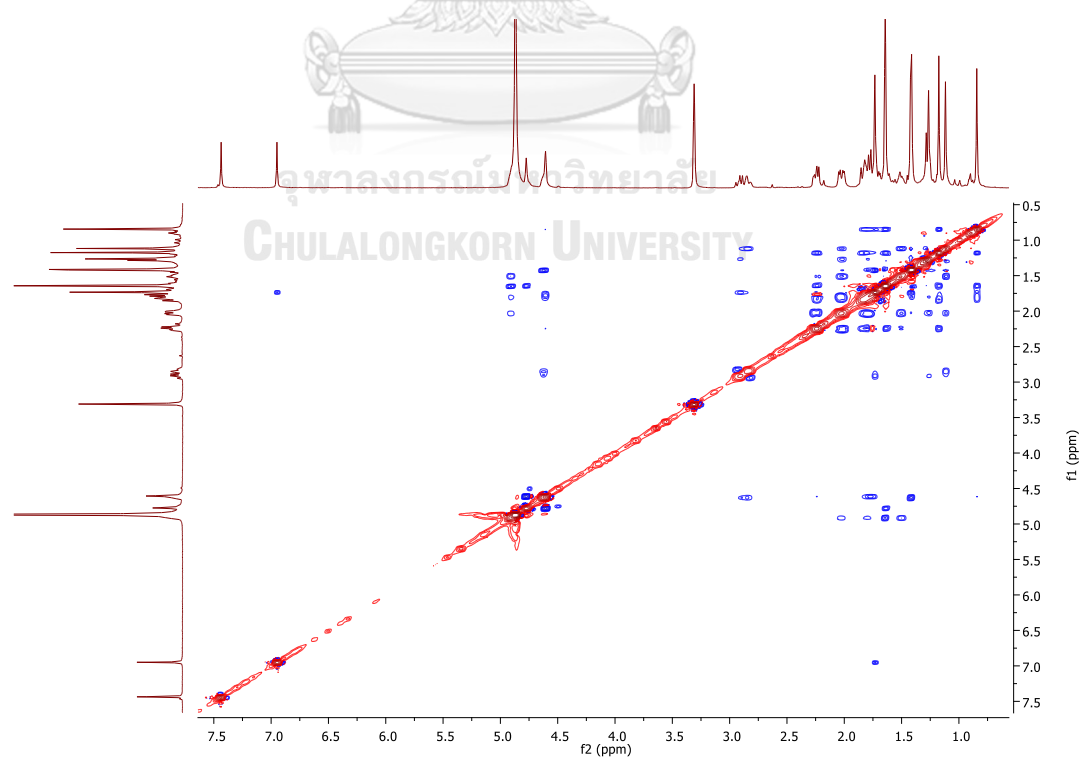


Figure C51.  $^{13}\text{C}$  NMR spectrum of picrorhizone H (GP8) in methanol- $d_4$

Figure C52. COSY spectrum of picrorhizone H (GP8) in methanol- $d_4$ Figure C53. HSQC spectrum of picrorhizone H (GP8) in methanol- $d_4$

Figure C54. HMBC spectrum of picrorhizone H (GP8) in methanol- $d_4$ Figure C55. NOESY spectrum of picrorhizone H (GP8) in methanol- $d_4$

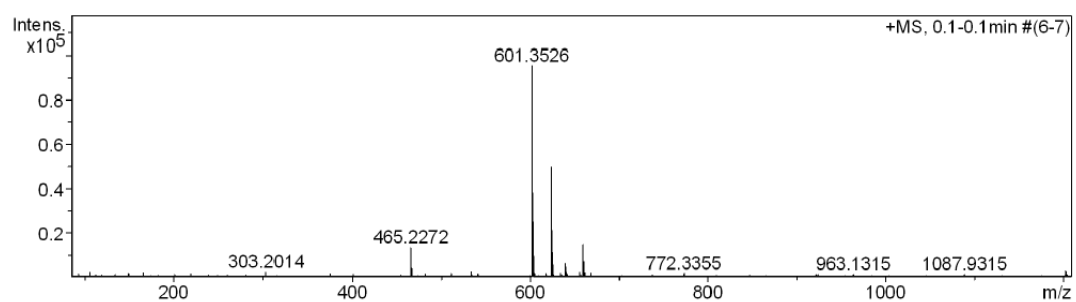


Figure C56. HRESIMS spectrum of picrorhizone H (GP8) in methanol



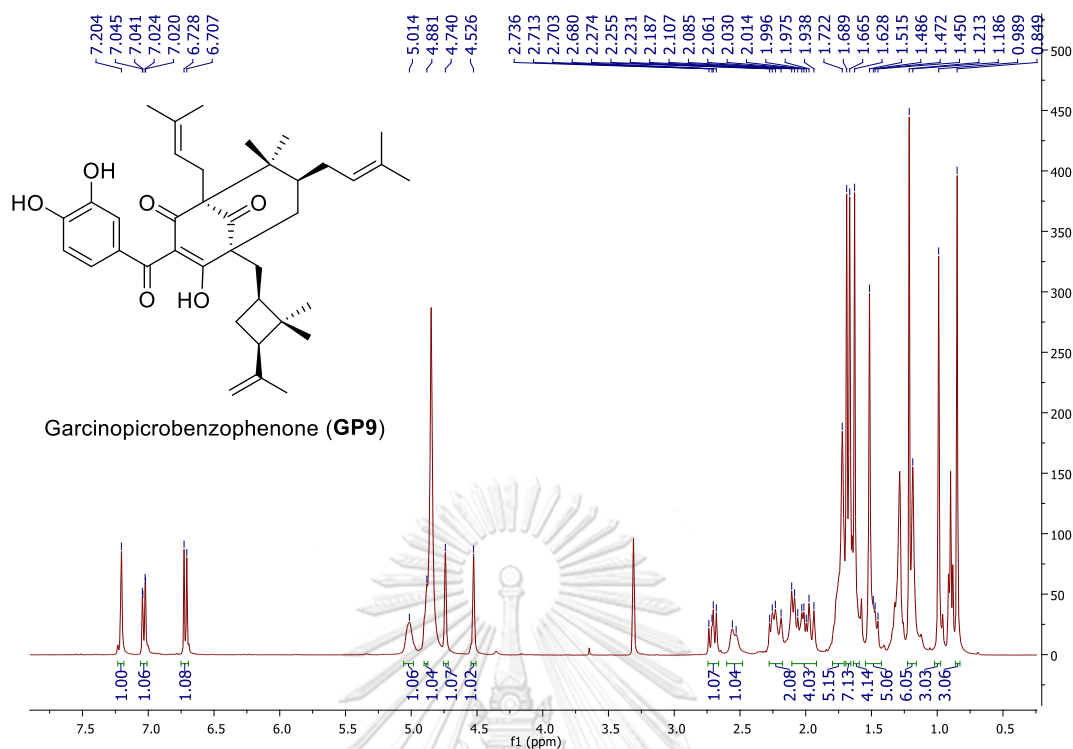


Figure C57.  $^1\text{H}$  NMR spectrum of garcinopicrobenzophenone (GP9) in methanol- $d_4$

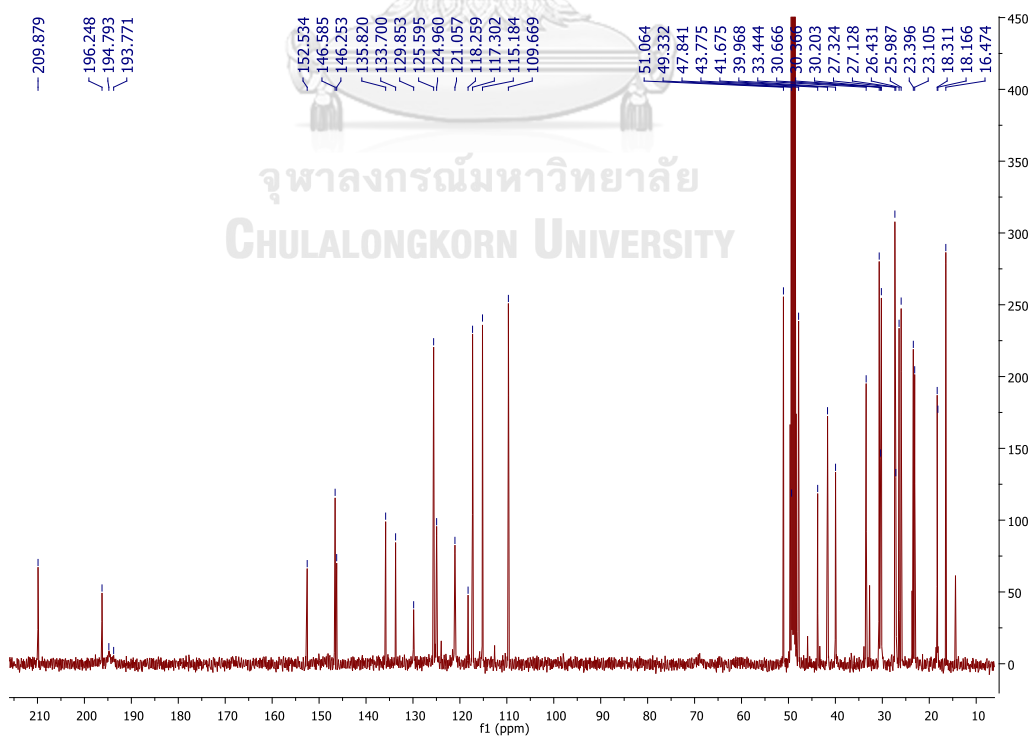


Figure C58.  $^{13}\text{C}$  NMR spectrum of garcinopicrobenzophenone (GP9) in methanol- $d_4$



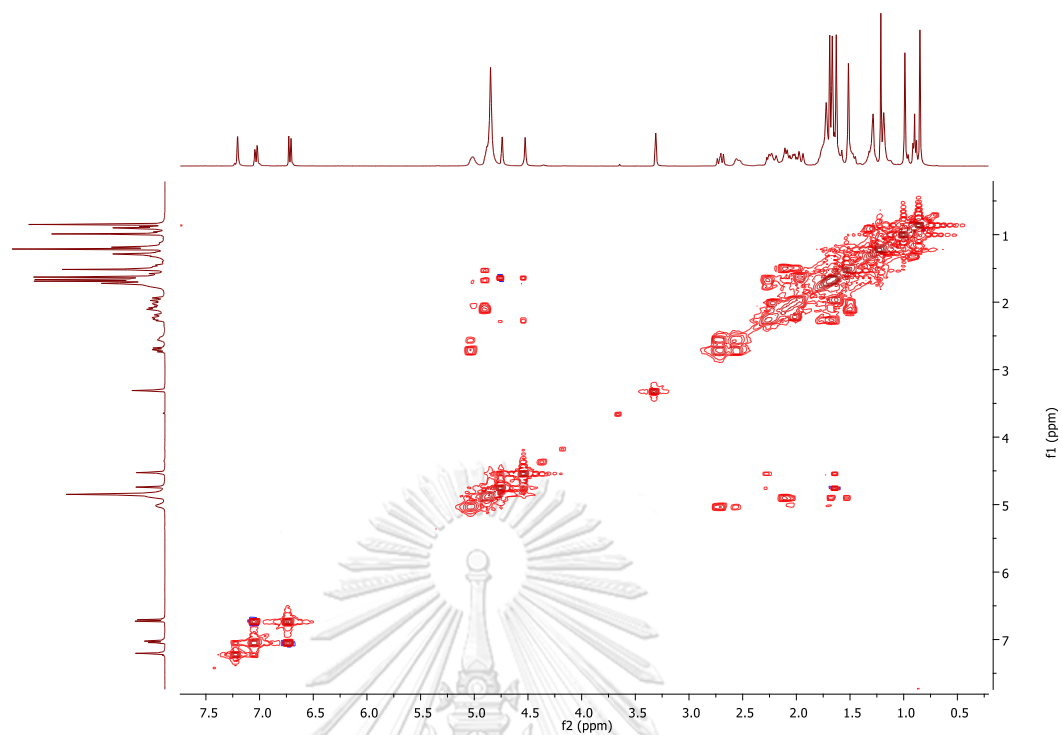


Figure C59. COSY spectrum of garcinopicrobenzophenone (GP9) in methanol- $d_4$

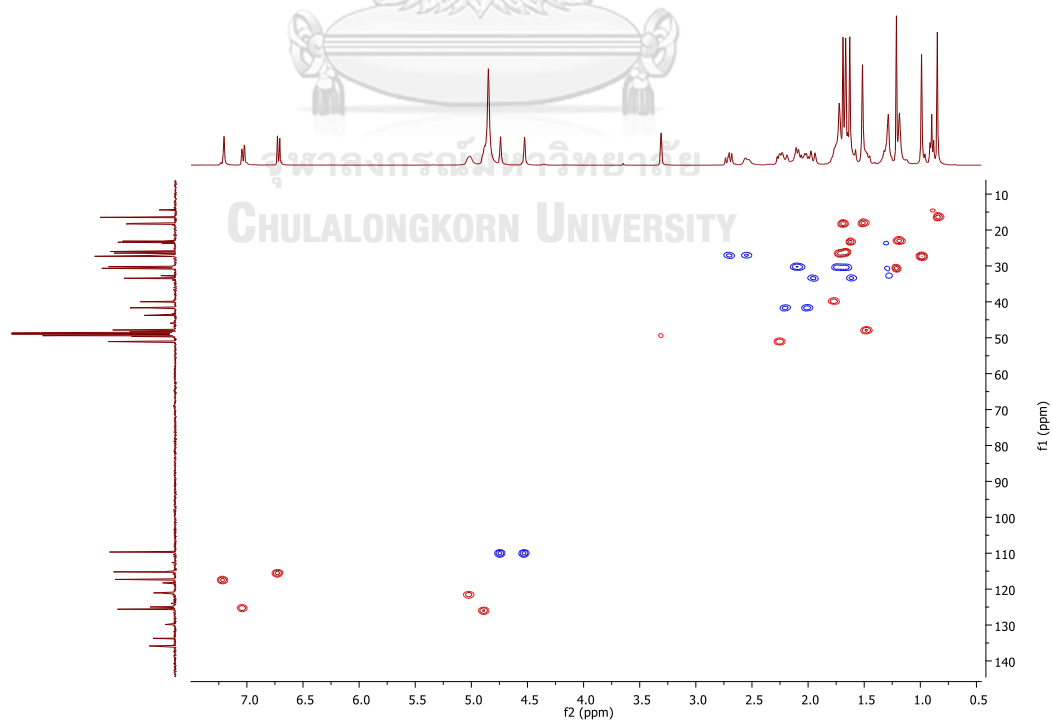


Figure C60. HSQC spectrum of garcinopicrobenzophenone (GP9) in methanol- $d_4$

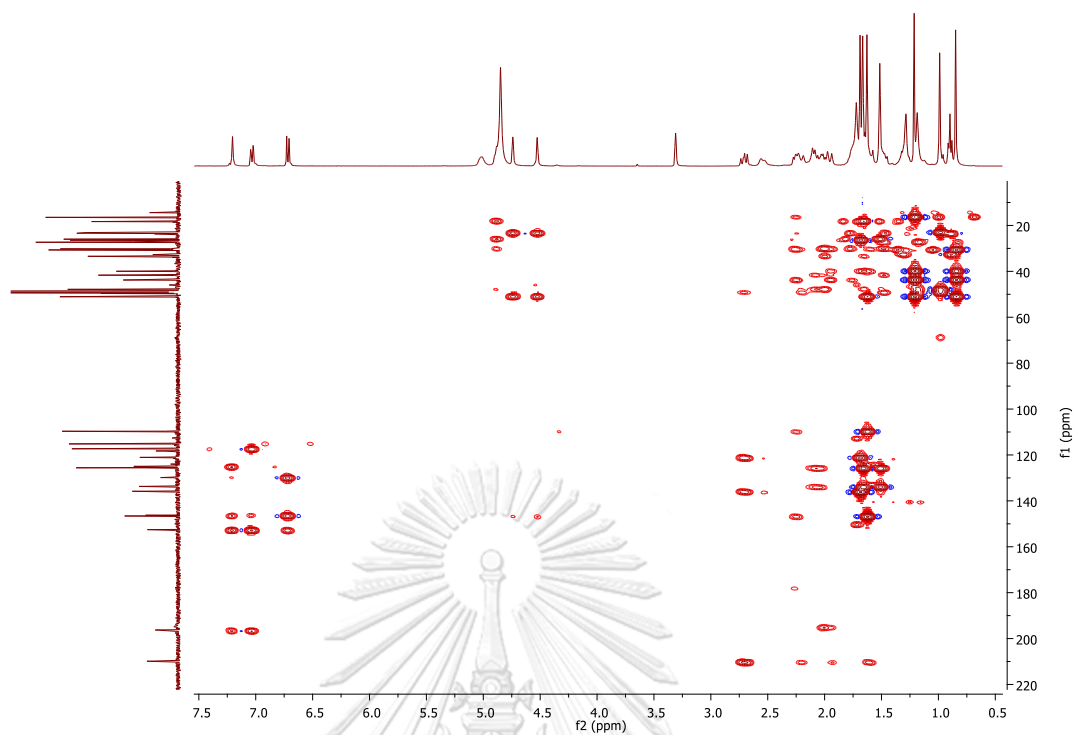


Figure C61. HMBC spectrum of garcinopicrobenzophenone (GP9) in methanol- $d_4$

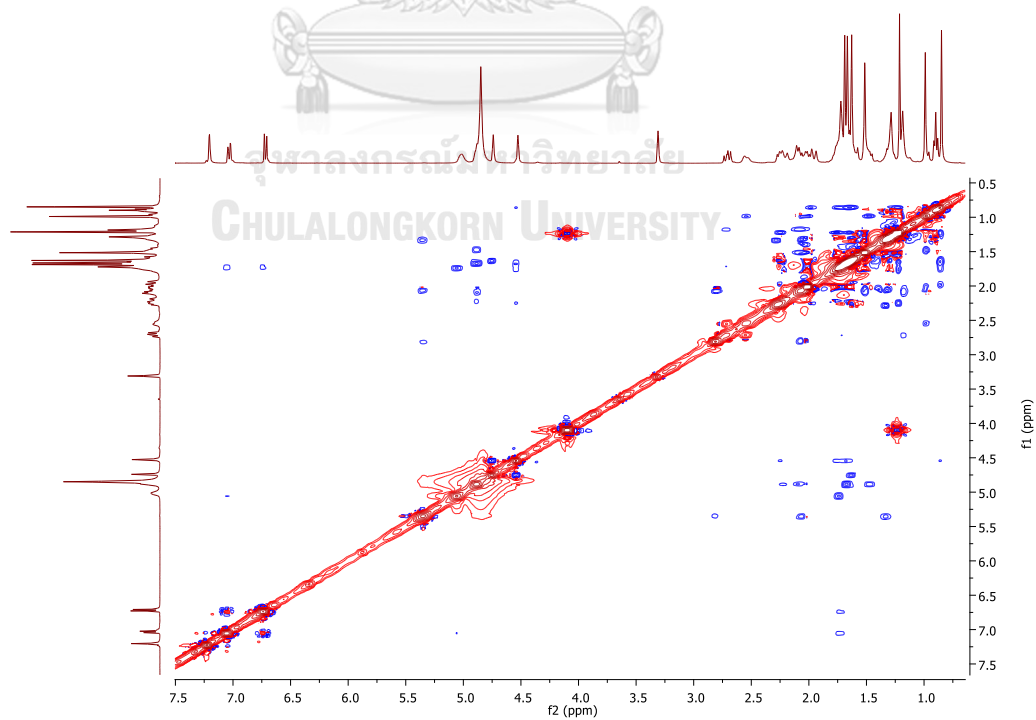


Figure C62. NOESY spectrum of garcinopicrobenzophenone (GP9) in methanol- $d_4$

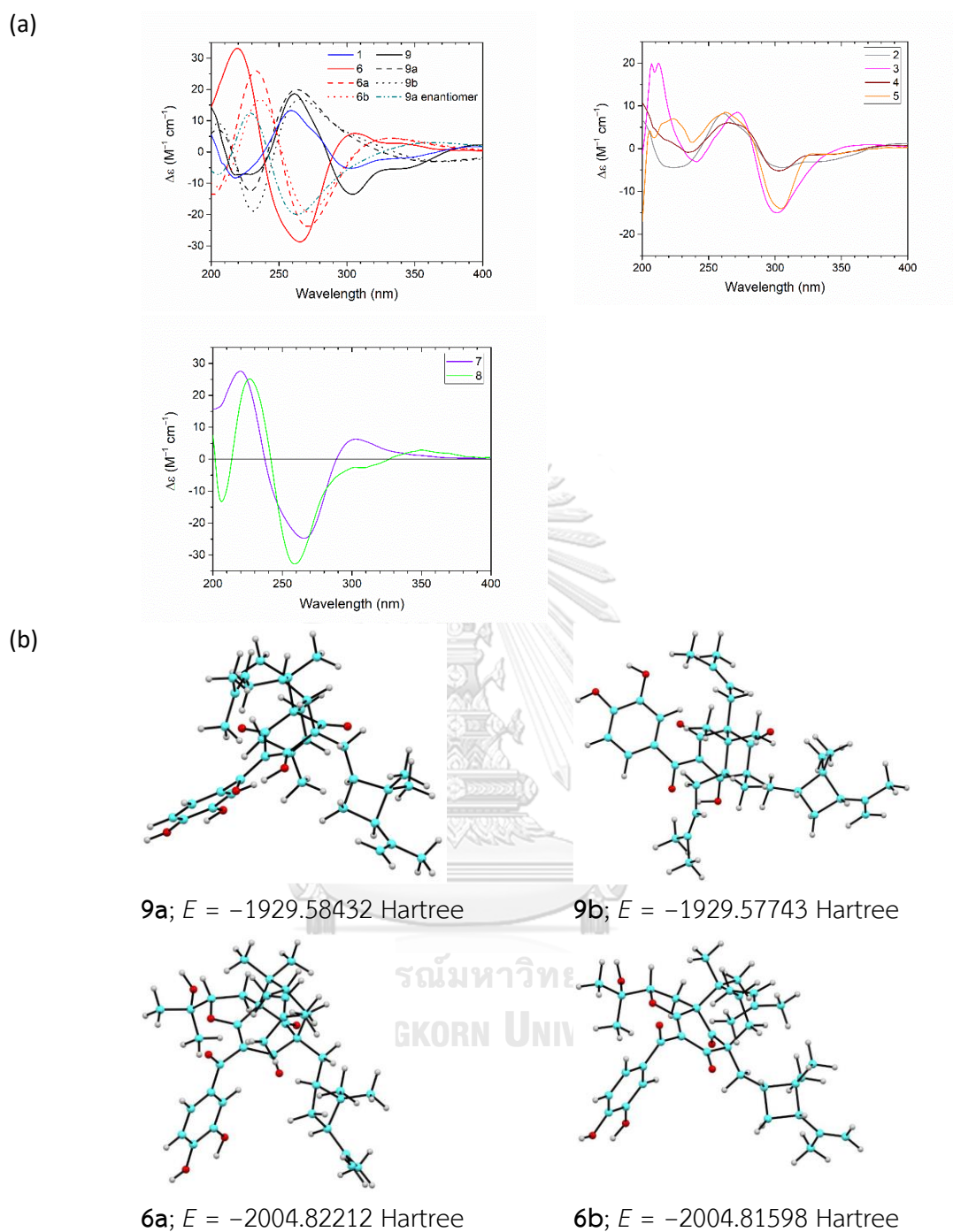
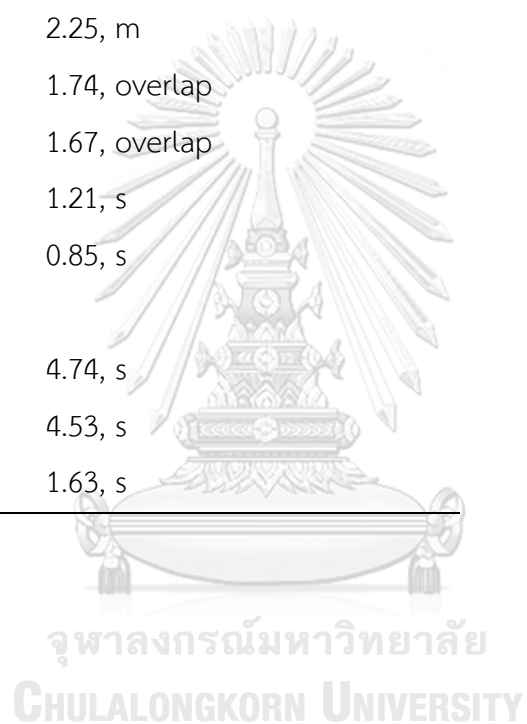


Figure C63. (a) Calculated (**6a**, **6b**, **9a**, **9a** enantiomer, **9b**) and experimental ECD spectra (**1–9**) of **GP1–GP9** and (b) Optimized structures and molecular energies ( $E$ ) from ECD calculation using TD-DFT method for diastereomeric models **9a** and **9b**, as well as **6a** and **6b**.

Table C1.  $^1\text{H}$  (400 MHz) and  $^{13}\text{C}$  (100 MHz) NMR spectroscopic data of **GP9** in methanol- $d_4$

position	<b>GP9</b>	
	$\delta_{\text{C}}$	$\delta_{\text{H}}$ ( $J$ in Hz)
1	194.8	
2	118.3	
3	193.8	
4	68.8	
5	49.3	
6	47.8	1.48, overlap
7eq	41.7	2.20, d (14.0)
7ax		2.01, dd (14.0, 6.8)
8	61.3	
9	209.9	
10	196.3	
11	129.9	
12	117.3	7.20, d (1.6)
13	146.3	
14	152.5	
15	115.2	6.72, d (8.4)
16	125.0	7.03, dd (8.4, 1.6)
17a	27.1	2.70, dd (13.2, 9.2)
17b		2.55, br d (13.2)
18	121.1	5.01, br t (9.2)
19	135.8	
20	26.4	1.72, s
21	18.3	1.69, s
22	23.1	1.19, s
23	27.3	0.99, s
24a	30.2	2.10, overlap
24b		2.03, overlap

25	125.6	4.88, overlap
26	133.7	
27	26.0	1.67, s
28	18.2	1.52, s
29a	33.4	1.95, d (14.8)
29b		1.61, overlap
30	40.0	1.77, overlap
31	43.8	
32	51.1	2.25, m
33a	30.4	1.74, overlap
33b		1.67, overlap
34	30.7	1.21, s
35	16.5	0.85, s
36	146.6	
37a	109.4	4.74, s
37b		4.53, s
38	23.4	1.63, s



## VITA

**NAME** Edwin Risky Sukandar

**DATE OF BIRTH** 15 November 1993

**PLACE OF BIRTH** Surabaya, Indonesia

**INSTITUTIONS ATTENDED**

- > 2017.08 — 2020.07 Ph.D Program in Chemistry  
Department of Chemistry, Faculty of Science,  
Chulalongkorn University, Thailand
- > 2014.08 – 2016.07 M.Sc Program in Chemistry  
Department of Chemistry, Faculty of Science,  
Chulalongkorn University, Thailand
- > 2010.09 – 2014.03 B.Sc Program in Chemistry  
Department of Chemistry, Faculty of Science, Sepuluh  
Nopember Institute of Technology, Indonesia

**HOME ADDRESS**

Jalan Karah I-B No.26  
Kelurahan Karah, Kecamatan Jambangan  
Kota Surabaya 60232, Jawa Timur, Indonesia

**PUBLICATION**

(1) Sukandar, E. R.; Kaennakam, S.; Aree, T.; Nost, X.;  
Rassamee, K.; Bauer, R.; Siripong, P.; Ersam, T.; Tip-pyang,  
S. “Picrorhizones A–H, polyprenylated  
benzoylphloroglucinols from the stem bark of *Garcinia  
picrorhiza*”, *Journal of Natural Products* 2020. DOI:  
10.1021/acs.jnatprod.9b01106

(2) Kaennakam, S.; Sukandar, E. R.; Hongnak, S.; Rassamee,  
K.; Siripong, P.; Tip-pyang, S. “Velucarpin D, a new  
pterocarpan from the stems of *Dalbergia velutina* and its  
cytotoxicity”, *Natural Product Research* 2020. DOI:  
10.1080/14786419.2020.1749613

(3) Sukandar, E. R.; Kaennakam, S.; Rassamee, K.; Ersam, T.;

Siripong, P.; Tip-pyang, S. “Tetrandraxanthone A–I, prenylated and geranylated xanthenes from the stem bark of *Garcinia tetrandra*”, *Journal of Natural Products* 2019, 82, 1312–1318.

(4) Kaennakam, S.; Sukandar, E. R.; Siripong, P.; Rassamee, K.; Tip-pyang, S. “Cytotoxic chalcones and isoflavones from the stems of *Dalbergia velutina*”, *Phytochemistry letters* 2019, 31, 187–191.

(5) Kaennakam, S.; Sukandar, E. R.; Siripong, P.; Rassamee, K.; Tip-pyang, S. “Veluflavanones A–P, cytotoxic geranylated flavanones from *Dalbergia velutina* stems”, *Journal of Natural Products* 2019, 82, 276–282.

(6) Sukandar, E. R.; Kaennakam, S.; Rassamee, K.; Siripong, P.; Fatmawati, S.; Ersam, T.; Tip-pyang, S. “Xanthenes and biphenyls from the stems of *Garcinia cylindrocarpa* and their cytotoxicity”, *Fitoterapia* 2018, 130, 112–117.

(7) Sukandar, E. R.; Siripong, P.; Khumkratok, S.; Tip-pyang, S. “New depsidones and xanthone from the roots of *Garcinia schomburgkiana*”, *Fitoterapia* 2016, 111, 73–77.

(8) Sukandar, E. R.; Ersam, T.; Fatmawati, S.; Siripong, P.; Aree, T.; Tip-pyang, S. “Cylindroxanthenes A–C, three new xanthenes and their cytotoxicity from the stem bark of *Garcinia cylindrocarpa*”, *Fitoterapia* 2016, 108, 62–65.

#### AWARD RECEIVED

> 2017 –2020 ASEAN Scholarship Recipient,  
Chulalongkorn University, Thailand

> 2014 – 2016 ASEAN Scholarship Recipient,  
Chulalongkorn University, Thailand

> 2014 Bank Central Asia (BCA)  
Scholarship Recipient, Sepuluh Nopember Institute of  
Technology, Indonesia

> 2014 University's List, Academic  
Performance Award, Sepuluh Nopember Institute of  
Technology, Indonesia

